Bench Scale Study of the Vacuum Freezing Ejector Absorption Process

United States Department of the Interior

Office of Saline Water • Research and Development Progress Report No. 744

Int-OSW-RDPR-71-744

Research and Development Progress Report No. 744 • November 1971
Int-OSW-RDPR-71-744

Bench Scale Study of the Vacuum Freezing Ejector Absorption Process

By J. Koretchko, G. Hajela, Colt Industries, Inc., Beloit, Wisconsin, for Office of Saline Water, J. W. O'Meara, Acting Director; W. F. Savage, Assistant Director, Engineering and Development; W. W. Rinne, Chief, Special Projects Division; C. L. Gransee, Project Engineer.

Contract 14-30-2679

United States Department of the Interior • Rogers C. B. Morton, Secretary
James R. Smith, Assistant Secretary for Water and Power Resources

For sale by the Superintendent of Documents, U.S. Government Printing Office, Washington, D.C. 20402 - Price $3.50
Stock Number 2400-0702

As the Nation's principal conservation agency, the Department of the Interior has basic responsibilities for water, fish, wildlife, mineral, land, park, and recreational resources. Indian Territorial affairs are other major concerns of America's "Department of Natural Resources".

The Department works to assure the wisest choice in managing all our resources so each will make its full contribution to a better United States—now and in the future.

FOREWORD

This is one of a continuing series of reports designed to present accounts of progress in saline water conversion and the economics of its application. Such data are expected to contribute to the long-range development of economical processes applicable to low-cost demineralization of sea and other saline water.

Except for minor editing, the data herein are as contained in a report submitted by the contractor. The data and conclusions given in the report are essentially those of the contractor and are not necessarily endorsed by the Department of the Interior.

TABLE OF CONTENTS

LIST OF FIGURES

LIST OF FIGURES

LIST OF TABLES

ABSTRACT

Koretchko J. + Dr. Hajela . . . . . Colt Industries
Dr's. Mixon F. + Orcutt J. . . . . Research Triangle Institute
Dr's. Loth J. + Phillips B. . . . . Consultants

A BENCH SCALE STUDY OF THE VACUUM FREEZING EJECTOR ABSORPTION (VFEA) PROCESS.

Colt Industries; Power Systems Division;
Water and Waste Management Operation.

OSW Contract No. 14-30-2679.

The work effort consisted of: bench scale testing of Ejector and Absorber system components, and a mathematical process and system study.

Ejector development was conducted at the Aerospace Lab, University of West Virginia under the direction of Dr. John Loth. This effort consisted of an analytical evaluation and a model test program. A 6,000 gpd equivalent bench size ejector test facility was erected at Colt's desalting laboratory at Beloit, Wisconsin. Performance tests showed the ejector to be free of any operating difficulties and projected* mass ratios were obtained. A 6,000 gpd absorption system test loop was also erected at Beloit. An absorber mass transfer coefficient of 6#/hr-ft^2-mmHg was obtained during testing. The coefficient was found to be a strong function of the NaOH viscosity. Studies conducted indicated that NaOH was the most suitable absorbent for the process. The Research Triangle Institute was retained by subcontract to conduct a mathematical study of the VFEA process. The optimal cost of water produced by the VFEA process has been estimated at 30.46 cents per K gal. at the 1 Mgd level, exclusive of labor costs. This cost was not strongly sensitive to changes in operating conditions. A preliminary design of a 60,000 gpd pilot plant was completed.

* lb. primary steam/lb. secondary vapor.

I. INTRODUCTION

Colt Industries, through its Power Systems Division, Water and Waste Management Operation, has conducted extensive work in developing the Vacuum-Freezing Desalting Process.

The Vacuum-Freezing process is based on several well established physical phenomena:

1. When seawater is boiled, the vapor produced is pure water.

2. When seawater is frozen, the individual ice crystals consist of pure water.

3. The freezing point of seawater is unaffected by reductions in pressure.

4. The boiling point of seawater varies with pressure. By reducing the pressure the boiling point is reduced until the triple point is reached, (that point where a substance is in equilibrium in all three phases; vapor, liquid, and solid.

5. To convert one pound of water into vapor about 1070 Btu of heat must be applied.

6. To convert one pound of water into ice about 144 Btu of heat must be removed.

Colt's development work started in 1959 under private financing. The effort began with the study of the basic process and techniques for freezing ice crystals, compressing water vapor, cleaning ice crystals of residual brine, and melting ice crystals with compressed water vapor. Equipment was designed at the Beloit, Wisconsin Research Center and a test unit was built. The unit had a design capacity of 60,000 gpd. This unit underwent constant modification throughout this test period in order to improve the performance of all components.

In February of 1965, Colt Industries and the Office of Saline Water concluded a contract for transfer of the VFVC pilot plant at Beloit to the O.S.W. test station at Wrightsville Beach,North Carolina, for the purpose of evaluating the freezing process in an actual seawater environment.

Operation of this pilot plant was extremely successful. The plant capacity was nearly doubled to 111,000 gpd and power consumption reduced by a third to 47 KW-HR/1000 gal. Substantial improvements were made in the vapor compressor, carryover separator, brine drainage system, and heat removal system. Operation of this pilot plant successfully demonstrated a lack of corrosion and scaling, and an ease of operation (the control system was designed for unattended operation).

Also under O.S.W. sponsored contract Colt designed, constructed, and tested a 15,000 gpd portable pilot plant on brackish feed water at the O.S.W. test station at Roswell, New Mexico. The operation of the Roswell pilot plant had considerable significance because it showed that the freezing process could desalt waters which were high in calcium sulphate without any evidence of scale deposit.

A flex blade compressor was used to compress the vapor from the freezer to the melter. The compressor for the Wrightsville Beach pilot plant was ten feet in diameter and had a fairly high moment of inertia for starting. Larger compressors were contemplated for a 250,000 gpd plant and even possibly 500,000 gpd plants. For larger desalting plants of perhaps five million gpd and upward no practical compressor combination could be foreseen.

Hence, in order to apply the advantages of freeze desalting to larger plants, it was necessary to seek a different solution. This search resulted in a new freezing process, hereafter called the Vacuum Freezing Ejector Absorption Process (VFEA).

Schematic diagrams were prepared by Colt's desalting engineers showing a freeze desalting system with an ejector for accomplishing the compression of water vapor. The ejector had the advantage of no moving parts and was capable of being designed for larger plants. The real novelty was in the fact that the water vapor, or low pressure steam, was recycled through the system to act as primary steam for the ejector. The addition of heat, through the use of external steam, was completely separated from the process cycle and was a heat source only.

For a media to absorb water vapor, a solution of sodium hydroxide was chosen as being most appropriate to the pressures and temperatures in the new process.

It was also an inexpensive chemical in comparison to alternate choices and was readily available in quantities.

Continued engineering effort on the VFEA process reinforced opinions of the process advantages. Up to this point, however, the evaluation done had been primarily in house. Therefore, several consultants were engaged to make an impartial evaluation of the process.

Foremost of these was Professor Thomas E. Sherwood, former Chairman of Chemical Engineering at M.I.T. He was an active member of the Office of Saline Water team for evaluation of freeze desalting.

The recommendations of Professor Sherwood were pertinent since they pointed out the areas in VFEA where state of the art did not provide information; namely, the large low pressure ejector, the design of internally cooled absorbers for sodium hydroxide solutions. These recommendations formed the basis of Colt's projected development plans for the VFEA process.

In April of 1970, Colt Industries and the Office of Saline Water concluded a contract (14-30-2679) for a bench scale study of the VFEA process.

II. SUMMARY

The Bench Scale Development of the Vacuum Freezing Ejector Absorption Process can be divided into the following areas:

1. Ejector Development

   Dr. John Loth was retained as the principal ejector designer and consultant. Dr. Loth is Director of the Propulsion Laboratory, Aerospace Dept., University of West Virginia.

   A subcontract for ejector development was awarded to the Aerospace Lab., University of West Virginia. The subcontract had these objectives:

   a. The theoretical feasibility of an ejector was analyzed using only quasi-one dimensional conservation of mass, momentum, and energy equations, and estimated effects of wall shear and wall pressure forces.

   b. An ejector model test was conducted to obtain experimental coefficient required for design of large size ejector. West Virginia University has only a small vacuum capability of 240 lbs. per day of noncondensible gas, but corrosive gases like steam could not be handled. However, it was anticipated that by electrically heating nitrogen gas the proper velocities and pressure levels of a steam ejector could be simulated. It turned out that the nozzle total temperature required in order to simulate the steam nozzle exit velocity created some unexpected side effects. The small size of the model creates a high ratio of surface area to volume ratio and the heat transfer from the driving nozzle supply pipe to the secondary flow was very large so that the secondary flow density decreased in order of magnitude and invalidated the predicted performance.

   c. The third aspect of the subcontract was to write a numerical program for the entire ejector flow field, so that the behavior of the ejector could be computed for a given geometry.

An equivalent 6,000 gpd bench size test ejector was designed, constructed and tested at Colt's Power Systems Division laboratories in Beloit, Wisconsin. The test loop enabled testing the ejector at process conditions, using the same media (water vapor) as in the VFEA process. The loop was designed such that the primary steam pressure and temperature could be varied, as well as, the suction and discharge pressure of the secondary vapor flow. The test loop schematic is shown below:

EJECTOR LOOP TEST

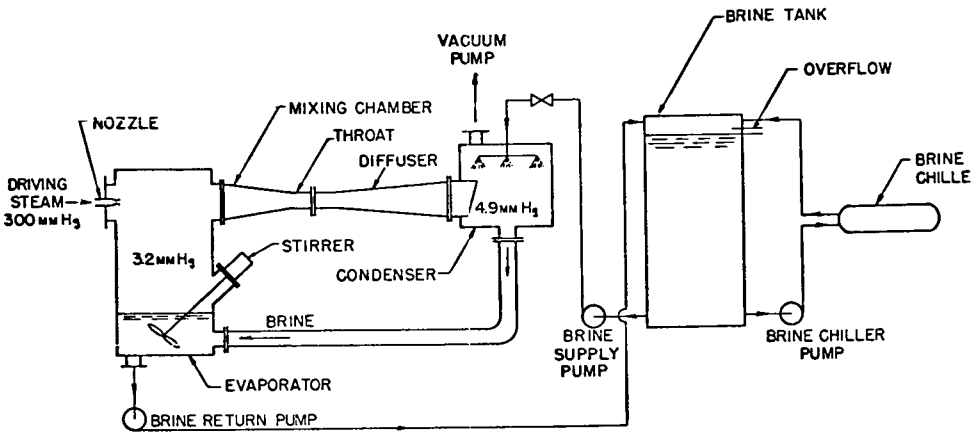

Experimental testing was conducted with the primary purpose to obtain minimum mass ratio. Testing was also conducted to determine the operating characteristics of the ejector at varying process conditions.

Results and Conclusions

a. Mass Ratio

The ejector mass ratio was found to increase as the outlet pressure increased by a relationship as shown by the figure on the following page.

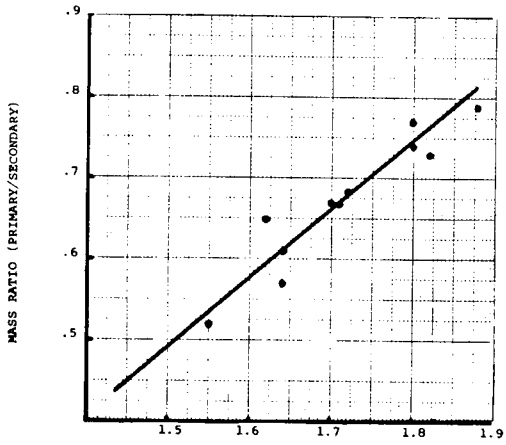

b. Nozzle Efficiency

The nozzle efficiency was found to be 96%.

c. Diffuser Efficiency

The diffuser efficiency was found to be 95%.

d. Ejector Operation

The test ejector was extremely stable with no back flow or stall over the operating range.

No special procedures were needed for start-up.

The ejector operated without any appreciable noise.

There was no freezing during testing.

2. Absorber Development

The objective of the development program was to determine the optimum heat transfer coefficient and design configuration for the absorber. A considerable background of experience exists in the absorption field; however, very little work has been done at the low pressure contemplated for the VFEA process, and at high capacities of water absorption required for large plants.

Dr. Ben Phillips was retained as an absorption system consultant. Dr. Phillips has had considerable experience in the development of heat operated cooling units for buildings and was eminently qualified to give direction to the development program.

An equivalent 6,000 gpd bench scale absorption cycle test loop was erected at Colt's desalting laboratories at Beloit, Wisconsin. The bench scale test loop operated at actual VFEA process conditions and component requirements. The loop was designed for both open and closed loop testing such that both component and system evaluations could be accomplished.

The test loop schematic is shown below:

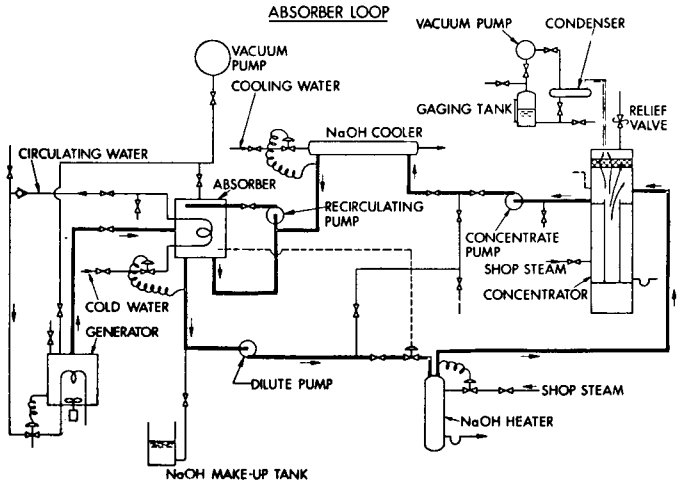

Test Results and Conclusions

a. Heat Transfer Coefficients

The heat transfer coefficient was found to be dependent on the NaOH viscosity by a relationship of the form:

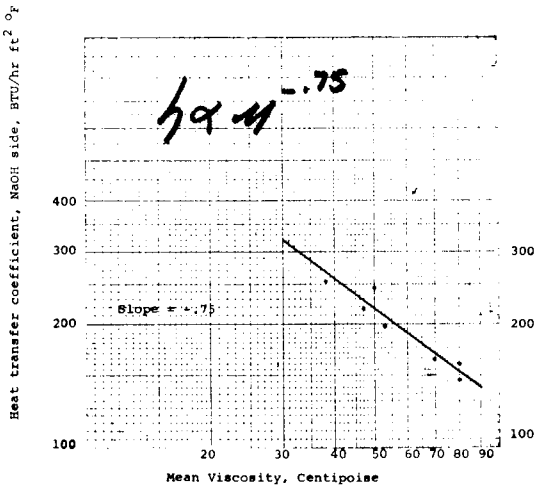

The heat transfer coefficient was independent on the NaOH recirculation rate, providing all tube surfaces were wet. A recirculation rate of 5 gpm/ft^2 of top cross-sectional area was found adequate to assure tube wetness.

Vertical tube spacing had no effect on the coefficient.

Horizontal tube spacing was critical if the distance between tubes was less than 1/2".

b. Mass Transfer Coefficient

Vapor side mass transfer coefficient of up to 6#/hr-Ft^2-mm Hg have been obtained during bench scale testing. The mass transfer coefficient was found to be dependent on the

viscosity by a relationship of the form:

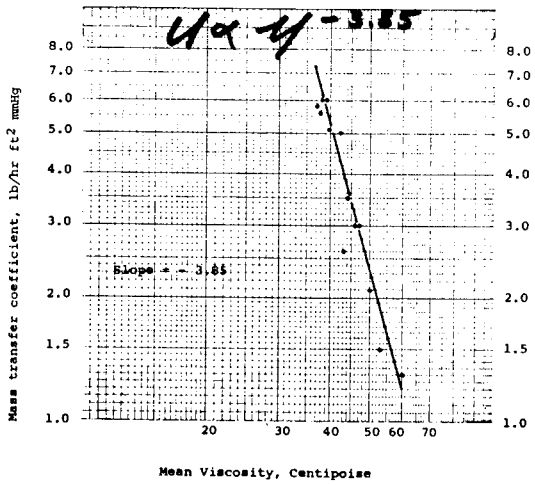

The mass transfer coefficient was independent on the NaOH recirculation rate providing all tube surfaces were wet.

c. There was no carryover of NaOH solution from the concentrator into the product condenser during the entire testing period.

d. Carbon steel tubing was found to be adequate for the absorber, while the concentrator required either stainless or 70/30 Cu Ni tubing.

NaOH was found to be the most suitable absorbent for this process. If improvements are necessary, chemical additives, properly selected, could improve the heat transfer coefficient by as much as 25%.

3. Process Study

The Research Triangle Institute was retained by subcontract to conduct a mathematical process study. The work effort was conducted by Dr's. Mixon and Orcutt of the RTI staff. Because of the large number of variables involved in the process, it was not feasible to make a optimization without the use of computer programs. This study included both steady state and dynamic analysis of each individual process component.

451-332 O - 71 - 2

A program for design optimization by digital computer has been developed that searches over possible design parameters to find the design corresponding to minimum cost of water. Results of computations using the program indicate that the cost of water

a) decreases with increasing conversion from 20 percent to 50 percent conversion,

THE EFFECT OF CONVERSION

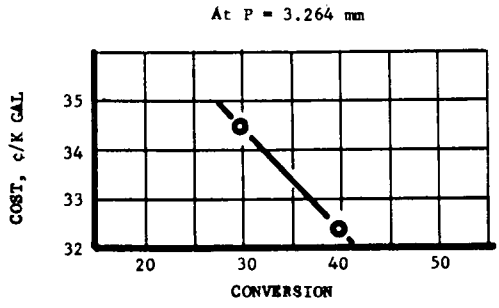

b) increases, but only very slightly, with increasing freezer pressure from 3.1 to 3.25 mm Hg,

THE EFFECT OF PRESSURE

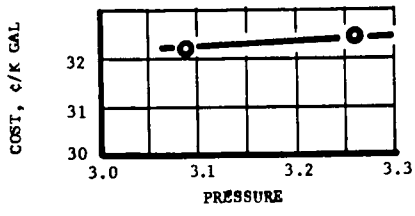

c) decreases with increasing feed temperature to the freezer from 31° to 33°F, with an optimal point occurring slightly above 33°F.

THE EFFECT OF FEED TEMPERATURE INTO THE FREEZER

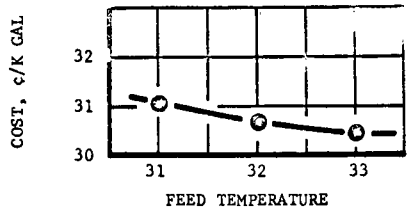

d) increases significantly with increased ejector ratio, and

THE EFFECT OF EJECTOR PRIMARY TO SECONDARY RATIO

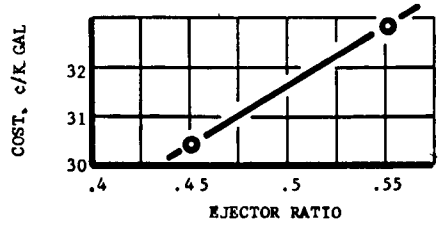

e) decreases with increasing plant capacity.

THE EFFECT OF PLANT SIZE

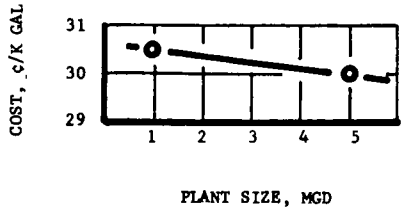

The optimal cost of water produced by the VFEA process has been estimated at 30.46 cents per k gal at the 1 Mgd level, exclusive of labor costs. This cost is not strongly sensitive to changes in operating conditions.

A simulation by analog computer of the dynamics of the integrated process has indicated that the process is well behaved and should be amenable to relatively simple control techniques. No inherent instabilities were discovered.

4. Pilot Plant Design

A preliminary design of a 60,000 gpd pilot plant was completed. The purpose of the pilot plant is to evaluate the VFEA process more completely, and to develop it to be commercially feasible such that it produces water at a lower cost than current desalting processes. The drawing on the following page is a pictorial flow diagram of the pilot plant.

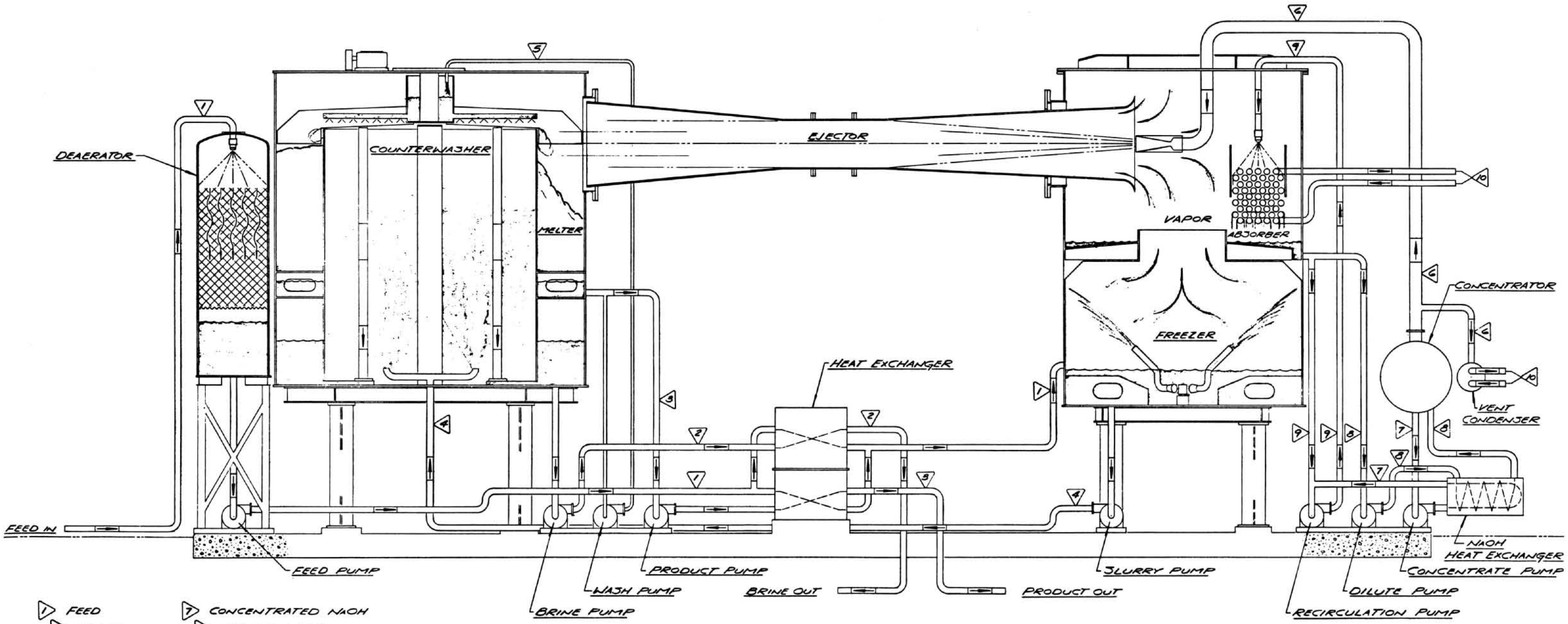

VFEA
PILOT PLANT DESIGN
PROCESS FLOW SCHEMATIC

FIG. 1

III. PROCESS DESCRIPTION

The VFEA (Vacuum Freezing Ejector Absorption) Process is a freezing process in which the vapor is compressed by a combination steam ejector and absorber loop, and the primary energy source is heat rather than mechanical energy.

The absorber loop raises a portion of the vapor evolved in the freezer to a level sufficient to drive the steam ejector. The work done in the ejector is, thus, reduced by the amount of primary steam used. Further, the primary steam need not be removed from the system because it, along with the secondary steam, is stoichiometrically in balance with the melted ice.

The absorber, in raising the freezer vapor from a level of slightly more than 3 mmHg, performs the function of a compressor with less work input than would be required for adiabatic compression.

The VFEA Process thus retains the advantages of the freezing process; low corrosion; low energy consumption; and minimal scaling.

Functional Description:

Sea water feed from a suitable intake system is first pumped to a cold water vacuum deaerator of the packed column type where the bulk of the dissolved air and other gases are removed leaving a low residual oxygen content in the sea water.

This deaerated sea water is then pumped from the deaerator through a heat exchanger where the sea water is cooled by outflowing cold brine and product water. The heat exchanger has sufficient capacity and performance to enable low approach temperatures to be realized. From the heat exchanger the cold deaerated sea water flows into the freezer where it encounters a vacuum. Air is continually purged from process vessels to maintain the required vacuum. Here a portion of the sea water is evaporated and as this heat of evaporation is released from the sea water itself, ice crystals are formed in the sea water. Ideally seven and one half pounds of ice are produced for each pound of vapor formed. The vapor is continuously removed from the freezer enabling continuous vacuum freezing to take place. The slurry of ice crystals and sea water brine is continuously removed from the freezer and pumped to a counterwasher where ice/brine separation takes place. In the counterwasher the ice is accumulated into an ice bed and

the brine is extracted through drain tubes immersed in the bed. The flow of brine through the ice bed creates a piston-like force on the bed causing the ice-bed to be supported out of the brine where gravity drainage of brine from the upper portion of the ice bed takes place enabling relatively brine free ice to appear at the top of the column. Here, a small flow of cold product water is sprinkled as wash water onto the ice displacing the remaining brine film from the ice enabling brine free ice to be removed from the top of the column by means of a mechanical scraper. In displacing the adherring brine film from the ice a portion of the wash water permeates the ice bed and is extracted with the outflowing brine. The harvested ice passes from the counterwasher to the melter while the cold brine is pumped through the heat exchanger and the absorber where it is used for cooling incoming sea water and the sodium hydroxide absorbent.

A portion of the water vapor which was formed in the freezer passes to the absorber where it is absorbed on a concentrated solution of sodium hydroxide which is sprayed over cooling coils. Outgoing brine and product water as well as supplementary sea water passing through these coils remove the heat of absorption from the sodium hydroxide absorbent. The average vapor pressure of the absorbent is maintained below the freezer pressure to provide the driving force for vapor absorption.

The dilute sodium hydroxide from the absorber is pumped through an absorbent heat exchanger where it is heated by the concentrated sodium hydroxide and introduced into the concentrator. In the concentrator the dilute sodium hydroxide is indirectly heated by steam. The water vapor absorbed in the freezer is now boiled off. Concentrated sodium hydroxide which accumulates in the concentrator is recycled back to the absorber.

A portion of the vapor boiled off in the concentrator is excess water vapor generated from mechanical and thermal process inefficiencies. This vapor must be removed to maintain the process in thermal equilibrium. The excess vapor is condensed by outflowing product water in a direct contact condenser where the vapor is recovered as additional product water. The remainder of the water vapor boiled off in the concentrator flows as primary steam to a steam ejector nozzle.

In the ejector the remaining portion of the water vapor evolved in the freezer enters as secondary steam and is entrained by the primary steam flow and compressed. From the steam ejector this combined vapor mixture flows to the melter where direct contact condensing of this vapor takes place by impingement onto the ice which is accumulated in the melter from the counterwasher. The resulting continuous melting and condensing of the ice and vapor produces cold product water having a salinity less than 500 ppm total dissolved solids. This cold product water is pumped from the melter through the heat exchanger to cool incoming sea water and through the absorber and direct contact condenser for cooling, then is discharged from the process.

The following page contains a VFEA diagrammatic drawing. The temperature, pressure, and concentration are typical for a desalting plant with a 65°F feed temperature.

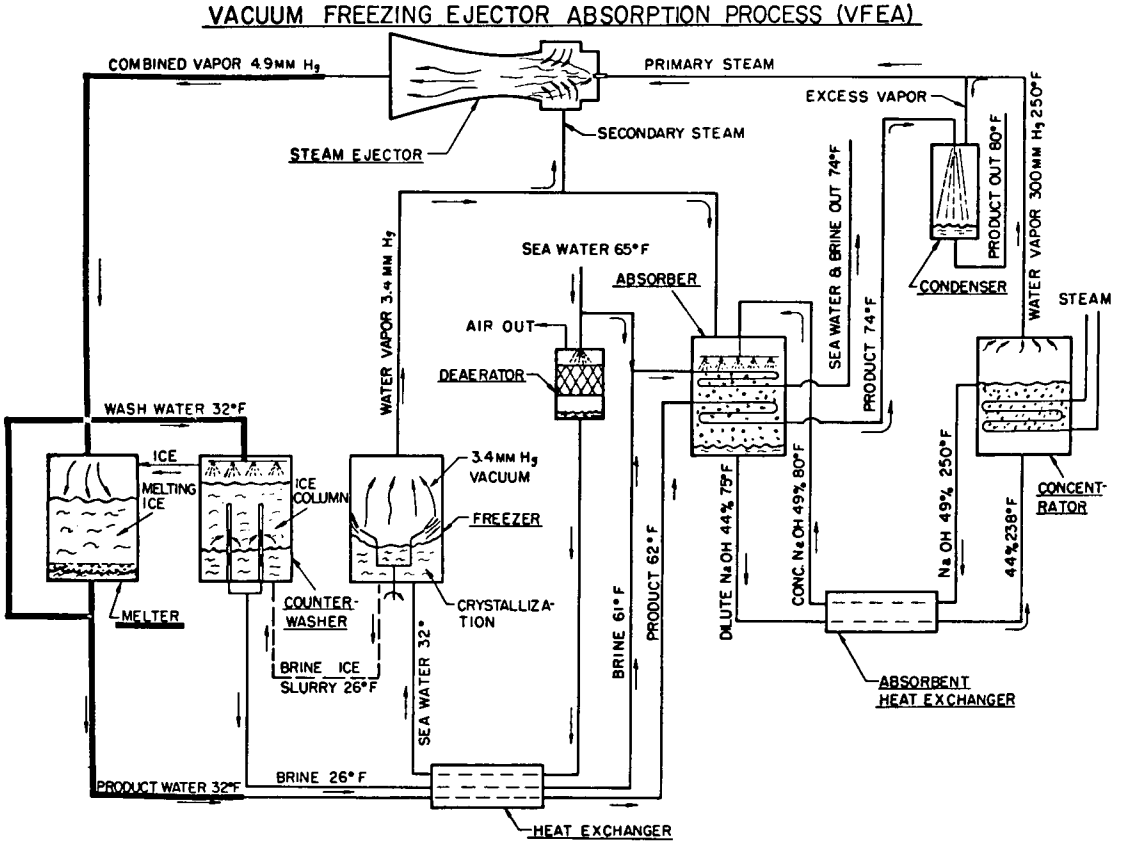

VFEA PROCESS DIAGRAMMATIC
FIG. 1

IV. EJECTOR DESIGN AND DEVELOPMENT

The subcontract on ejector development with the University of West Virginia, Aero Space Laboratory, had three objectives, First, the theoretical feasibility of an economic ejector was analyzed using only quasi-one dimensional conservation of mass, momentum, and energy equations, and estimated effects of wall shear and wall pressure forces. These equations were used to show the theoretical feasibility.

Second, an Ejector Model test was conducted to obtain experimental coefficient required for design of large size ejector. West Virginia University has only a small vacuum capability of 240 lbs. per day of noncondensible gas, but corrosive gases like steam could not be handled. However, it was anticipated that by electrically heating nitrogen gas the proper velocities and pressure levels of a steam ejector could be simulated. It turned out that the nozzle total temperature required in order to simulate the steam nozzle exit velocity, created some unexpected side effects. The small scale of the model creates a high ratio of surface area to volume ratio and the heat transfer from the driving nozzle supply pipe to the secondary flow was very large so that the secondary flow density decreased in order of magnitude and invalidated the predicted performance.

Without electrical heating this problem was eliminated, but then the nozzle exit velocity was only 1/4 of the required value and the obtainable mass flow ratio only 1 to 1 which corresponds to the predictions of the theoretical model. Using different gases like helium and argon one can simulate the proper velocities and pressures, but not the densities and a true ejector performance could not be simulated.

The third aspect of the subcontract was to write a numerical program for the entire ejector flow field including a detailed analysis of the mixing zone growth rate and the local turbulent shear stress so that the behavior of the ejector can be computed for a given geometry under varying operating conditions. This program uses an emperical constant for the shear stress on the mass dividing streamline. The value of the emperical constant was chosen to simulate the observed behavior of the bench scale test ejector in Wisconsin.

General Ejector Characteristics

Ejectors are used for a wide range of industrial processes where large volumes of gas or liquid need to be handled. The isentropic compression efficiency is usually less than that of a mechanical compressor.

However, the installation, operating and maintenance cost is usually lower than for mechanical compressions. This depends on the availability of an inexpensive high-pressure driving fluid. The absence of moving parts greatly reduces the installation and maintenance costs.

The performance of most ejector configurations can be accurately estimated using a quasi-one dimensional control volume analysis which extends between the inlet and the exit of the mixing duct. Conventional forms of the continuity, momemtum and energy equations are used for the performance analysis and the equation of state can be used when one deals with compressible fluids. Estimates of the wall shear stresses and nozzle losses are sufficient when one deals with a constant area ejector. In case one deals with more efficient converging mixing ducts, one has to make an assumption for the wall pressure distribution which is often done by assuming it to vary linearly with changes in cross-sectional area or linearly with distance along the axis. A detailed analysis of the mixing process is usually not required unless one operates with very small or very large mass flow ratios. If the velocities of the primary and secondary flows are indicated by V_p and V_s and that of the ejector exit flow by V_e, then the kinetic energy loss in the ejector is given by:

$$\Delta E = 1/2 \left[(\dot{W}_p + \dot{W}_s) V_e^2 - (\dot{W}_p V_p^2 + \dot{W}_s V_s^2) \right]$$

The momentum equation for an ideal constant area ejector with isothermal incompressible flow gives:

$$V_e = \frac{\dot{W}_p V_p + \dot{W}_s V_s}{\dot{W}_p + \dot{W}_s}$$

$$\text{or} \quad \Delta E = -1/2 \left[\frac{\dot{m}}{1+\dot{m}} (V_p - V_s)^2 \right]$$

The kinetic energy loss reduces with a reduction in mass flow ratio and with a reduction in the velocity difference $V_p - V_s$. Convergence of the mixing duct also reduces this loss, but this is partially offset by increased diffuser losses. The achievement of a maximum compression ratio $r = P_{te}/P_{ts}$ is usually the objective in an ejector design for given inlet conditions. Some general statements can be made: The lower the mass flow ratio the higher the compression ratio. The higher the pressure ratio P_{tp}/P_s the higher the compression ratio. Lowering the back

pressure P_{te} usually increases the mass flow ratio until the break-off point is reached which occurs when the secondary flow becomes sonic at the maximum expansion diameter of the primary flow. At this point the secondary flow is choked and will not increase further.

All ejectors operate with subsonic secondary inlet velocity. The primary flow can either be subsonic, sonic, or supersonic and the maximum efficiency is obtained with sonic or supersonic nozzles when the flow is fully expanded or $P_p = P_s$. The growth rate of the mixing zone is a maximum when the primary flow is subsonic. Then any local reduction in the primary stream tube acts as a venturi and lowers the pressure there locally which increases the disturbance causing a rapid turbulent mixing.

The higher the Mach number of the supersonic stream the more stable the core is, and the slower the mixing rate. This can be seen by considering a local restriction in a supersonic streamtube, which will create oblique shocks and a pressure rise which tends to eliminate the disturbance.

The pressure ratio in an ejector can be achieved several ways. When the mass flow ratio is zero and the primary flow is supersonic, then the pressure ratio is close to that obtained in a normal shock. As the mass flow ratio increases, the angle through which the supersonic flow deflects reduces and the pressure ratio comes close to the pressure rise in the oblique shock. Further increases in the mass flow ratio results in shock-free subsonic compression and the pressure ratios are obtained accurately from the three conservation equations. For very large mass flow ratios the application of the quasi-one dimensional equations may be very incorrect due to the large flow nonuniformity at the cross-sections where the equations are applied.

If a converging mixing duct is used at high mass flow ratios then a constant pressure mixing would be optimum if the diffuser losses are ignorable. However, in an actual geometry optimization, the diffuser performance has to be included and one will find the optimum configuration to be a constant pressure converging duct followed by a constant area throat in which the pressure rises.

Ejector Design

The economical justification of the VFEA process depends strongly on the ejector efficiency. The in- and outlet pressures of the ejector are controlled at all times by the evaporator and condensor conditions and the optimization consists in maximizing the mass flow ratio $\dot{m}$.

Method of Calculations :

The desired ejector inlet conditions are specified. Then for a chosen geometry, the exit pressure is computed. Then the inlet mass flow rates must be adjusted in order to obtain the desired exit pressure. The geometry can be changed in order to minimize the required mass flow ratio.

The secondary flow is the cold-saturated vapor flowing at subsonic velocity and which has specified:

mass flow rate $\dot{m}_s$

velocity V_s

static temperature T_s

saturation pressure P_s

density ρ_s

total enthalpy h_{ts}

The density is found from the steam tables which is much more accurate than using the perfect gas equation of state to compute the density. The energy equation with a constant specific heat should not be used to find the total enthalpy, because the steam tables are more accurate.

The primary flow is the driving steam, which is hot and superheated in the stagnation condition, but when expanded at the nozzle exit it is saturated with moisture and flowing at high supersonic velocity. Its static pressure P_p equals P_s and the static temperature T_p almost equals T_s if the flow is close to thermal equilibrium. The primary flow inlet conditions are specified as:

mass flow rate $\dot{m}_p$

velocity of the vapor V_p

velocity of the condensate V_c

percentage moisture $\%m$

static temperature T_p

static pressure $P_p = P_s$

density ρ_p

total enthalpy h_{tp}

The same reasons as mentioned before explain the specification of the density and total enthalpy of the nozzle exit flow.

The convergence angles of the mixing regions I, II, and III, Fig. 1 are specified as: Θ_I, Θ_{II}, Θ_{III}, and the length over diameter is specified for the constant area region IV, also called the ejector throat. The pressure and the average velocity is computed at the exit of the throat and is used together with an empirical diffuser performance equation, to compute the resulting diffuser static exit pressure. Several angles Θ_I and Θ_{II} are tried until the pressure at region I and II is nearly constant. Next the angle Θ_{III} is decreased until the resulting rate of static pressure rise becomes so high, that the boundary layer might separate. The convergence of section III is continued for an as short as possible distance, but not until the following constant area duct, region IV, can be used without causing boundary layer separation. The length of region IV is selected such that the average velocity approaches closely to the maximum center line velocity.

Assumptions made to simplify the analysis:

a) a profile similarity will be used for all mixing areas in regions I through IV of the type

$$\frac{\rho - \rho_i}{\rho_o - \rho_i} = F_1(\eta) \quad \text{and} \quad \frac{u - u_i}{u_o - u_i} = F_2(\eta)$$

where η is a dimensionless coordinate of a point r as given by $\eta = \frac{r - r_i}{r_o - r_i}$ such that $\eta_i = 0$ and $\eta_o = 1.0$. The density profile is assumed rather than the usual temperature profile because the density gradients are large and enter directly in the continuity and momentum equations. The usually estimated temperature profile cannot be used to find the density because the equation of state does not apply with moisture in the flow as it comes out of the nozzle. Also, temperature gradients are neglible with $T_s = T_p$ at the ejector inlet, because both flows are saturated at the same vapor pressure $P_p = P_s$. The velocity $U = U_{(r,x)}$ and the centerline velocity $U_c = U_{i(x)}$, the radia $r_i = r_{i(x)}$ and $r_o = r_{o(x)}$ define the inner and outer boundaries of the mixing zone respectively. The mixing zone is also defined by the dimensionless coordinates η_i and η_o. The dividing stream line coordinate η_D located at r_D

is defined such that the mass flowing inside the area $r < r_D$ equals the mass flow rate from the nozzle $\dot{m}_p$. The velocity and the velocity gradient at r_D define the shear stress τ_D along the dividing streamline. It is the magnitude of this shear stress τ_D which controls the spreading rate of the mixing zone. The angles θ_I, θ_{II}, and θ_{III} can be used to compute the radius of the wall $r_w = r_{w(x)}$. All flow angles are assumed so small that the radial components of velocity, the shear stress, and the pressure can be ignored.

The computer calculation is a step by step procedure, starting at the known ejector inlet conditions and computing the flow parameters downstream. Starting at the crossection located at x_j and computing those at location x_{j+1}, etc. In each step the pressure $P_{(j+1)}$ is first assumed equal to $P_{(j)}$ then the area $Ax_{(j+1)}$ is computed and compared with the required value from the specified wall contour. If the specified area is different, then change the pressure $P_{(j+1)}$ by adding P_{static} as shown:

$$\Delta P_{required} = \left[1 - \left(\frac{A_{x(j+1)\ obtained}}{A_{x(j+1)\ required}} \right)^2 \right] \times P_{dynamic\ obtained\ at\ r_{reference}} \quad (1)$$

This is derived by assuming only small changes in pressure and negligible changes in density so that the incompressible Bernouilli equation applies. This method is only used in regions I and II where the pressure should remain nearly constant.

$$\text{Constant} = P_{static} + P_{dynamic}$$

By adding ΔP_{static} to $P_{(j+1)}$ the $P_{dynamic}$ is reduced by

$$\Delta P_{required} = (1/2 \rho V^2)_{j+1\ obtained} - (1/2 \rho V^2)_{j+1\ required}$$

$$\text{or} \quad \frac{V(j+1)required}{V(j+1)obtained} = \sqrt{1 - \frac{P_{required}}{(1/2\rho V^2)_{j+1\ obtained}}}$$

$$\text{from continuety find} \quad \frac{\dot{m}_{required}}{\dot{m}_{obtained}} = 1 = \frac{(\rho VA)_{j+1\ required}}{(\rho VA)_{j+1\ obtained}}$$

$$\text{or} \quad \frac{A_{x\ (j+1)\ obtained}}{A_{x\ (j+1)\ required}} = \frac{V_{(j+1)\ required}}{V_{(j+1)\ obtained}} = \sqrt{1 - \frac{\Delta P\ required}{(1/2\rho V^2)_{j+1\ obt.}}}$$

solving for

$$\Delta P_{required} = \left[1 - \left(\frac{A_{x(j+1)\ obtained}}{A_{x(j+1)\ required}}\right)^2\right] x\ (1/2\rho V^2)_{j+1\ obtained\ at\ r_{ref}}$$

This dynamic pressure $(1/2\rho V^2)_{j+1} = P_{dynamic\ (j+1)}$

should be computed at a radial location r_{ref}. where the flow is subsonic and the iteration converges most rapidly. A suitable location seems to be the radius which divides the tube into two equal areas or $\pi r_{ref}^2 = 1/2 \pi r_w^2$

$$\text{or} \quad r_{ref} = r_w \sqrt{1/2} \qquad (2)$$

Basic Equations, using only x components of velocities and shear stresses.

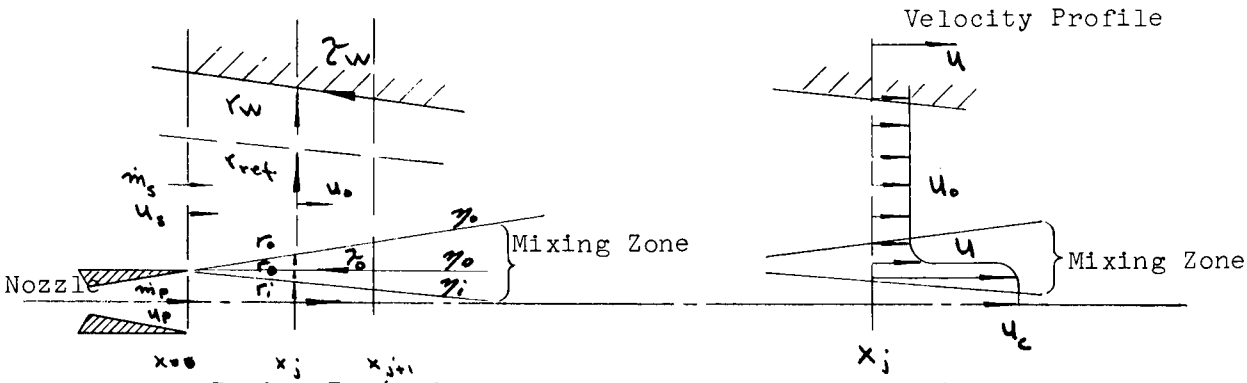

Region I (left-hand side of equations contain known flow parameters at section x_j)

Continuity

$$\dot{m}_p = \left[\int_0^{r_i} \rho_p u_c 2\pi r dr + \int_{r_i}^{r_d} \rho u 2\pi r dr \right] \qquad (3)$$

$$\dot{m}_s = \left[\int_{r_D}^{r_o} \rho u 2\pi r dr + \int_{r_o}^{r_w} \rho_s u_o 2\pi r dr \right] \qquad (4)$$

Momentum

$$\left[\int_0^{r_i} \rho_p u_c^2 2\pi r dr + \int_{r_i}^{r_D} \rho u^2 2\pi r dr \right] - \tau_D 2\pi r_{Dj} dx = \left[\int_0^{r_i} \rho_p u_c^2 2\pi r dr + \int_{r_i}^{r_D} \rho u^2 2\pi r dr \right] + \frac{P_{j+1} - P_j}{2} \times \pi \left(r_{Dj}^2 + r_{Dj+1}^2 \right) \qquad (5)$$

$$\left[\int_{r_D}^{r_o} \rho u^2 2\pi r dr + \int_{r_o}^{r_w} \rho_s u_o^2 2\pi r dr \right] + \tau_D 2\pi r_{Dj} dx - \tau_w 2\pi r dx = \left[\int_{r_D}^{r_o} \rho u^2 2\pi r dr + \int_{r_o}^{r_w} \rho_s u_o^2 2\pi r dr \right] + \frac{P_{j+1} - P_j}{2} \times \pi \left[\left(r_w^2 - r_D^2 \right)_j + \left(r_w^2 - r_D^2 \right)_{j+1} \right] \qquad (6)$$

Energy

$$\int_0^{r_w} \rho u h_t 2\pi dr = \dot{m}_s h_{ts} + \dot{m}_p h_{tp} \qquad (7)$$

This equation will not be used inside region I, because the mixing zone represents such a small region that an error in the total enthalpy there can have little effect on the overall energy balance. However this equation is used in the other regions in order to determine the flow centerline density ρ_c and velocity U_c to be used in the density and velocity profiles.

Integrate the equations by substituting the proper velocity profile functions $\rho = (\rho_o - \rho_i) F_1(\eta) + \rho_i$ &

$$u = (u_o - u_i) F_2(\eta) + u_i$$

For the shear stress one has to insert the proper function of the velocity and its first and second derivative on the dividing streamline. The temperature effect is given by the local density ρ_D

$$\tau_D = F_3(u_o, u_o', u_o'', \rho_o) = F_3(F_1, F_2, F_2', F_2'')_D$$

The wall shear stress is given by a friction coefficient based on the local Reynolds number

$$\tau_w = C_{fw} \tfrac{1}{2} \rho_w u_w^2$$

The pressure term is:

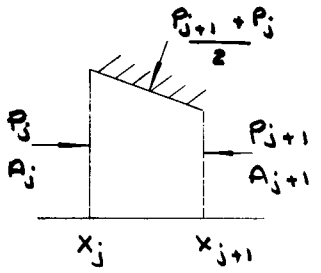

Momentun at $j + P_j A_j$ = Momentum at $j+1 +$

$$\frac{P_{j+1} + P_j}{2}(A_j - A_{j+1})$$

or Momentum at j = Momentum at $j + 1 +$

$$\frac{(P_{j+1} - P_j)(A_j + A_{j+1})}{2}$$

451-332 O - 71 - 3

Continuity Equation

$$\frac{\dot{m}_p}{\pi} = \left[\rho_p u_c r_i^2 + 2b \int_0^{\eta_0} (F_1 F_2 \bar{u}\bar{\rho} + F_1 \bar{\rho} u_i + F_2 \bar{u} \rho_i + u_i \rho_i)(b\eta\, d\eta + r_i\, d\eta) \right]_{j+1} \quad (8)$$

$$\frac{\dot{m}_s}{\pi} = \left[2b \int_{\eta_0}^{1} (F_1 F_2 \bar{u}\bar{\rho} + F_1 \bar{\rho} u_i + F_2 \bar{u} \rho_i + u_i \rho_i)(b\eta\, d\eta + r_i\, d\eta) + \rho_s u_s (r_w^2 - r_s^2) \right]_{j+1} \quad (9)$$

WHERE: $r = \eta b + r_i$ $\quad u = F_2 \bar{u} + u_i$ $\quad \rho = F_1 \bar{\rho} + \rho_i$

$b = r_o + r_i$ $\quad \bar{u} = u_o - u_i$ $\quad \bar{\rho} = \rho_o - \rho_i$

$r\,dr = b^2 \eta\, d\eta + b r_i\, d\eta$ $\quad \rho u = F_1 F_2 \bar{u}\bar{\rho} + F_1 \bar{\rho} u_i + F_2 \bar{u} \rho_i + u_i \rho_i$

Momentum Equation

$$\rho u^2 = F_1 F_2^2 \bar{u}^2 \bar{\rho} + 2 F_1 F_2 \bar{\rho} \bar{u} u_i + F_2^2 \bar{u}^2 \rho_i + 2 F_2 \bar{u} u_i \rho_i + F_1 \bar{\rho} u_i^2 + u_i^2 \rho_i$$

$$\left[\rho_p u_c^2 r_i^2 + 2b \int_0^{\eta_0} (\rho u^2)(b\eta\, d\eta + r_i\, d\eta) \right]_{j=n-1} - F_3\, 2 r_{Dj}\, dx \quad (10)$$

$$= \left[2b \int_{\eta_0}^{1} (\rho u^2)(b\eta\, d\eta + r_i\, d\eta) + \rho_s u_s^2 (r_w^2 - r_o^2) \right]_{j=n} +$$

$$\frac{\rho_{j+1} - \rho_j}{2} \left[(r_w^2 - r_D^2)_j + (r_w^2 - r_D^2)_{j+1} \right] \quad (11)$$

The functions F_1, F_2, F_3 and the friction coefficient C_f are taken from the literature like Schlichting and others. The flow parameters at section x_j are used in the left side of the equations, and should be known, then the right side of the equations contain the four unknowns $(r_i, \eta_0, r_o,$ and $\rho)_{j+1}$ which can be

computed from equations 3 through 6. Because the pressure is nearly constant in region I, it can be assumed that the density ρ_s and the centerline density $\rho_c = \tau_\rho$ remain constant.

Small variations in the pressure will be accounted for by changes in velocity through the use of the incompressible Bernouilli equation:

$$u_{s_{j+1}} = \sqrt{u_{s_j}^2 - \frac{2}{\rho_s}(\rho_{j+1} - \rho_j)} \qquad (12)$$

and

$$u_{c_{j+1}} = \sqrt{u_{c_j}^2 - \frac{2}{\rho_\rho}(\rho_{j+1} - \rho_j)} \qquad (13)$$

Before one can further integrate these equations one has to chose suitable functions for the velocity profile $\frac{u-u_i}{u_o-u_i} = F_2(\eta)$, the density profile $\frac{\rho-\rho_i}{\rho_o-\rho_i} = F_1(\eta)$
The dividing streamline shear stress $\tau_o = F_3(F_1, F_2, F_2', F_2'')$

The wall shear stress $\tau_w =$

$$c_f \tfrac{1}{2}\rho_w u_w^2 = F_{3(Re_{dw})}\, \tfrac{1}{2}\rho_w u_w^2$$

Another problem is the starting value of the dividing streamline shear stress τ_o. The theoretical case has zero boundary layer thickness for the flow inside and outside the nozzle. When the two flows meet at x = 0, which is the nozzle lip, then the velocity gradient is infinite and also the shear stress. Obviously this is not a realistic starting value for $\tau_{o(x=0)}$

One method to by-pass this problem, which is caused by ignoring the initial boundary layer, is to assume τ_o constant for the initial length of the mixing zone. This assumption is not bad because with an initial boundary layer present the shear stress starts with the value zero, then grows in a region of laminar flow which eventually becomes turbulent within a length less than one nozzle diameter.

Here it is assumed that τ_o remains constant over a length of mixing zone which corresponds to a growth of mixing zone width from 0 to 0.1 x r_{nozzle}.

The magnitude of $\tilde{\zeta}_0$ over this range will be evaluated at the middle of the mixing zone where η = 1/2. For conputation steps downstream of this mixing zone width the correct value of η_0 will be used, which is the dividing streamline.

The velocity profile chosen could be the error function

$$\frac{u-u_i}{u_0-u_i} = \tfrac{1}{2}(1+\operatorname{erf}\eta) \quad (14)$$ as used by Korst and which is

an exact solution for two dimensional mixing zones see Schlichting's book on Boundary Layer Theory eq(23.30). Another suitable form is the relation:

$$\frac{u-u_i}{u_0-u_i} = (1-\eta^{3/2})^2 \quad (15)$$

also derived in this text as eq(23.37). It has been shown by Peters in AEDC-TR-65-209 and by others that very good results are obtained using a cosine velocity and density profile or

$$\frac{u-u_i}{u_0-u_i} = \tfrac{1}{2}(1-\cos\pi\eta) = F_2(\eta) \quad \text{where} \quad \eta = \frac{r-r_i}{r_0-r_i} \quad (16)$$

and

$$\frac{\rho-\rho_i}{\rho_0-\rho_i} = \tfrac{1}{2}(1-\cos\pi\eta) = F_1(\eta) \quad (17)$$

This means that the profile is a cosine function which has the advantage of producing a finite width of the mixing zone with the first derivative equal to zero at the edges of the mixing zone and also simplifies the integration of the four previous equations.

Derivation:

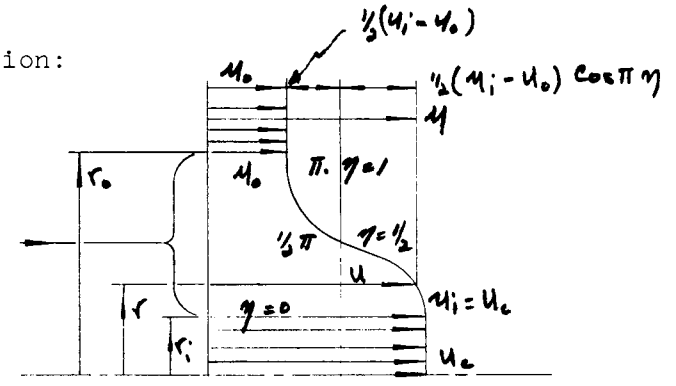

Mixing Zone

$$u = u_0 + \tfrac{1}{2}(u_i - u_0) + \tfrac{1}{2}(u_i - u_0)\cos\pi\eta$$

$$u - u_i = (u_0 - u_i) - \tfrac{1}{2}(u_0 - u_i) - \tfrac{1}{2}(u_0 - u_i)\cos\pi\eta$$

$$u - u_i = (u_0 - u_i)\tfrac{1}{2}(1 - \cos\pi\eta)$$

$$F_3(\eta) = \frac{u - u_i}{u_0 - u_i} = \tfrac{1}{2}(1 - \cos\pi\eta)$$

For the shear stress on the dividing streamline one can use Prandtl's model for turbulent flow, see Schlichting, eq. 23.3.

$$\tau = \rho l^2 \left|\frac{\partial u}{\partial r}\right| \frac{\partial u}{\partial r}$$

where l is Prandtl's mixing length. An extension of this shear stress model is: eq. 23.4.

$$\tau = \rho l^2 \frac{\partial u}{\partial r} \sqrt{\left(\frac{\partial u}{\partial r}\right)^2 + l\left(\frac{\partial^2 u}{\partial r^2}\right)^2}$$

or

$$\tau = \rho c (r_0 - r_1)(u_c - u_e)\frac{\partial u}{\partial y} \qquad (18)$$

where c is an empirical constant. Peters has used successfully the model

$$\tau = \rho c_1 (r_0 - r_1)\left(c_2(u_c - u_e) + u\right)\frac{\partial u}{\partial r} \qquad (19)$$

Region II is like region I except that $r_i = 0$ and the centerline velocity and density are now variables and must also satisfy the energy equation (5). Then one has 5 equations with as 5 unknowns

$$(\eta_D, r_0, u_c, \rho_c, \rho)_{J+1}.$$

Region III and IV are different as the pressure rise there is significant and the variable r_0 has now been replaced by the unknown η_{wall}. One could also carry on with an imaginary value for r_0 to describe the profile but r_0 will be located outside the duct.

The simultaneous solution of the four unknowns from the two continuity equations 8 and 9 and the two momentum equations 10 and 11 is greatly simplified if one assumes a simple form for the velocity and density profile in the mixing zone.

It has been shown by others that for turbulent mixing one needs to use a semi-empirical mixing length and then the choice of velocity profile does not greatly alter the likelyhood for a good match between experimental and theoretical results. Here we choose both the velocity and density profile function

$$F_1 = F_2 = \tfrac{1}{2}(1 - \cos(\pi\eta))$$

where $\eta = 0$ represents the inside of the mixing zone and $\eta = 1.0$ represents the outside of the mixing zone. The resulting required integrals are listed in table 1 , 2 , and 3 where the indefinite form is indicated by a prime and this integral evaluated at the dividing streamline or limit $\eta = \eta_0$ is shown without prime.

These integrals when evaluated over the inner part of the mixing zone carry I as second letter and for the outer part of the mixing zone it carries an 0 as second letter. The integral in continuity equation 8 can then be written as

$$2b^2\int_0^{\eta_0}\left[\bar{u}\bar{\rho}F^2\eta + (\bar{\rho}u_1 + \bar{u}\rho_1)F\eta + u_1\rho_1\eta\right]d\eta + 2br_1\int_0^{\eta_1}\left[\bar{u}\bar{\rho}F^2 + (\bar{\rho}u_1 + \bar{u}\rho_1)F + u_1\rho_1\right]d\eta = 2b^2GI + 2br_1HI$$

where GI and HI are only functions of the unknown η_0 variable

$$GI = \bar{u}\bar{\rho}\,EI + (\bar{\rho}u_1 + \bar{u}\rho_1)DI + \frac{u_1\rho_1}{2}\eta_0^2$$

and

$$HI = \bar{u}\bar{\rho}\,BI + (\bar{\rho}u_1 + \bar{u}\rho_1)AI + u_1\rho_1\eta_0$$

TABLE I

INTEGRAL	LIMIT	
	$\eta = 1.0$	$\eta = 0$
$\int d\eta = \eta$	1.0	0
$\int \eta\, d\eta = \frac{1}{2}\eta^2$	$1/2$	0
$\int (\cos \pi\eta)\, d\eta = \frac{1}{\pi} \sin \pi\eta$	0	0
$\int (\cos \pi\eta)^2 d\eta = \frac{\eta}{2} + \frac{1}{4\pi} \sin 2\pi\eta$	$1/2$	0
$\int (\cos \pi\eta)^3 d\eta = \frac{1}{\pi} \sin \pi\eta - \frac{1}{3\pi} (\sin \pi\eta)^3$	0	0
$\int \eta (\cos \pi\eta)\, d\eta = \frac{1}{\pi^2} \cos \pi\eta + \frac{\eta}{\pi} \sin \pi\eta$	$-\frac{1}{\pi^2}$	$+\frac{1}{\pi^2}$
$\int \eta (\cos \pi\eta)^2 d\eta = \frac{\eta^2}{4} + \frac{\eta}{4\pi} \sin 2\pi\eta + \frac{1}{8\pi^2} \cos 2\pi\eta$	$\frac{1}{4} + \frac{1}{8\pi^2}$	$\frac{1}{8\pi^2}$
$\int \eta (\cos \pi\eta)^3 d\eta = \frac{\eta}{12\pi} \sin 3\pi\eta + \frac{1}{36\pi^2} \cos 3\pi\eta$		
$+ \frac{3\eta}{4\pi} \sin \pi\eta + \frac{3}{4\pi^2} \cos \pi\eta$	$-\frac{7}{9\pi^2}$	$+\frac{7}{9\pi^2}$

$$F = \tfrac{1}{2}\left[1 - \cos \pi\eta\right]$$

$$F^2 = \frac{1}{4} - \frac{1}{2} \cos \pi\eta + \frac{1}{4} (\cos \pi\eta)^2$$

$$F^3 = \frac{1}{8} - \frac{3}{8} \cos \pi\eta + \frac{3}{8} (\cos \pi\eta)^2 - \frac{1}{8} (\cos \pi\eta)^3$$

TABLE 2

INTEGRAL
$\int F d\eta = AF' = 1/2\,\eta - 1/2\pi \sin \pi\eta$
$\int_0^{\eta_0} F d\eta = AF = AI \quad ; \int_{\eta_0}^{1} F d\eta = 1/2 - AF = AO$
$\int F^2 d\eta = BF' = 3/8\,\eta - 1/2\pi \sin \pi\eta + 1/16 \sin 2\pi\eta$
$\int_0^{\eta_0} F^2 d\eta = BF = BI \quad ; \int_{\eta_0}^{1} F^2 d\eta = 3/8 - BF = BO$
$\int F^3 d\eta = CF' = \frac{5\eta}{16} - \frac{1}{2\pi} \sin \pi\eta + \frac{3}{32\pi} \sin 2\pi\eta + \frac{1}{24\pi} (\sin \pi\eta)^3$
$\int_0^{\eta_0} F^3 d\eta = CF = CI \quad ; \int_{\eta_0}^{1} F^3 d\eta = 5/16 - CF = CO$
$\int F\eta\, d\eta = DF' = \frac{\eta^2}{4} - \frac{1}{2\pi^2} \cos \pi\eta - \frac{\eta}{2\pi} \sin \pi\eta$
$\int_0^{\eta_0} F\eta\, d\eta = DF + \frac{1}{2\pi^2} = DI \quad ; \int_{\eta_0}^{1} F\eta\, d\eta = 1/4 + 1/2\pi^2 - DF = DO$

TABLE 3

INTEGRAL
$\int F^2\eta\,d\eta = EF' = \frac{3\eta^2}{16} - \frac{1}{2\pi^2}\cos\pi\eta - \frac{\eta}{2\pi}\sin\pi\eta$ $+\frac{\eta}{16\pi}\sin 2\pi\eta + \frac{1}{32\pi^2}\cos 2\pi\eta$
$\int_0^{\eta_D} F^2\eta\,d\eta = EF + \frac{15}{32\pi^2} = EI$; $\int_{\eta_D}^{1} F^2\eta\,d\eta = \frac{3}{16} + \frac{17}{32\pi^2} - EF = EO$
$\int F^3\eta\,d\eta = FF' = \frac{5\eta^2}{32} - 9/32\pi^2\cos\pi\eta - 9\eta/32\pi^2\sin\pi\eta$ $+\frac{3\eta}{32\pi}\sin 2\pi\eta + \frac{3}{64\pi^2}\cos 2\pi\eta - \frac{\eta}{96\pi}\sin 3\pi\eta -$ $1/288\pi^2\cos 3\pi\eta$
$\int_0^{\eta_D} F^3\eta\,d\eta = FF + \frac{15}{64\pi^2} + \frac{1}{288\pi^2} = FI$
$\int_{\eta_D}^{1} F^3\eta\,d\eta = 5/32 + 21/64\pi^2 + 1/288\pi^2 - FF = FO$

and continuity equation 8 simplifies then to

$$\frac{\dot{m}_p}{\pi} = \left[\rho_i u_i r_i^2 + 2b^2 GI + 2b r_i HI\right]_{j=n} \qquad (20)$$

$$\text{or } b = \frac{-r_i HI + \sqrt{r_i^2 HI^2 + 2GI\left(\frac{\dot{m}_p}{\pi} - \rho_i u_i r_i^2\right)}}{2GI} \qquad (21A)$$

where $b = r_o - r_i$, the width of the mixing zone.
Similarly continuity equation 9 simplifies to

$$\frac{\dot{m}_s}{\pi} = \left[\rho_o u_o (r_w^2 - (b+r_i)^2 + 2b^2 GO + 2b r_i HO\right]_{j=n} \qquad (21B)$$

where $GO = \bar{u}\bar{\rho} EO + (\bar{\rho} u_i + \bar{u}\rho_i) DO + \frac{u_i \rho_i}{2} n_p^2$

and $HO = \bar{u}\bar{\rho} BO + (\bar{\rho} u_i + \bar{u}\rho_i) AO + u_i \rho_i (1 - n_p)$

Rather than using an iterative solution for the inner and outer radius r_i and r_o, it is easier to work the tangent of the mixing zone spreading angle β. This is called the similarity parameter σ_i and σ_o so that

$$r_{i(j=m)} = r_{i(j=m-1)} - (\sigma_i \Delta x)_{j=n}$$

and

$$r_{o(j=m)} = r_{o(j=m-1)} + (\sigma_o \Delta x)_{j=n}$$

$$j=m \quad = (r_o - r_i)_{j=m-1} + \Delta x(\sigma_o - \sigma_i)_{j=n}$$

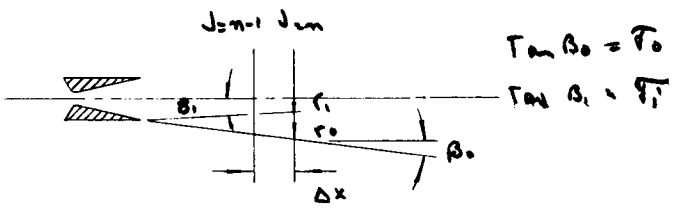

These parameters vary little from station j = n-1 to j = n and $(\Delta X)_{j=n}$ is chosen and is not an unknown variable.

The momentum equations 10 and 11 can be more easily handled in a numerical calculation if the control volume is changed from j=n-1 and j=n to a large control volume extending all the way to the nozzle exit plane. This will replace the expression for the known momentum at station j=n-1 by the constant value momentum at the nozzle exit plus a summation of all the shear stresses and pressure stresses experienced upstream of j=n-1

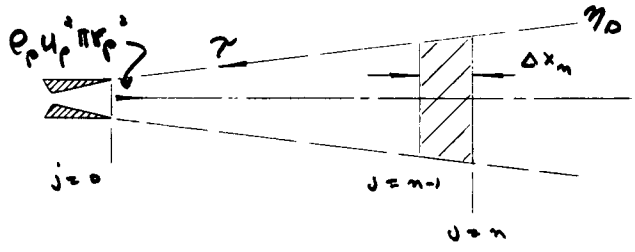

$$\left(\rho_p \pi r_{D}^2\right)_{j=0} + \left(\rho_p u_p^2 \pi r_D^2\right)_{j=0} - \sum_{j=1}^{n} (\Delta x)_j (\tau_2 \pi r_D)_{j-1} + \sum_{j=1}^{n} \frac{\rho_j + \rho_{j-1}}{2} \left(r_{D_j}^2 - r_{D_{j-1}}^2\right)\pi$$

$$= \left[\rho_i u_i^2 r_i^2 \pi + 2b\pi \int_0^{\eta_0} (\rho u^2)(b\eta\, d\eta + r_i\, d_N)\right]_{j=n} + \left(\rho \pi r_D^2\right)_{j=n}$$

Combining terms and solving for the unknown pressure $\rho_{j=n}$

$$r_{D_j} = (\eta_D b + r_i)_j \qquad \text{and } r_{D_{j=0}} = r_N$$

$$\rho_{j=n} = \frac{2}{r_{D_m}^2 + r_{D_{m+1}}^2}\left[(\rho_p + \rho_p u_p^2) r_N^2 - \sum_{j=1}^{n} (\Delta x)_j (\tau_2 (\eta_0 b + r_i)_{j+1} + \right.$$

$$\sum_{j=1}^{n-1} \frac{\rho_j + \rho_{j-1}}{2} \left(r_{D_j}^2 - r_{D_{j-1}}^2\right) + \frac{\rho_{m-1}}{2} \left(r_{D_m}^2 - r_{D_{m-1}}^2\right) - \left[\rho_i u_i^2 r_i^2 + 2b^2 VI + \right.$$

$$\left. 2br_i WI\right]_{j=n} \qquad (23A)$$

$$VI = \int_0^{\eta_0} (\rho u^2)\, \eta\, d\eta$$

$$WI = \int_0^{\eta_0} \rho u^2\, d\eta$$

similarly equation 11 becomes with $(r_w)_{j=0} = r_s$

$$P_s \pi (r_s^2 - r_N^2) + \rho_s u_s^2 \pi (r_s^2 - r_N^2) + \sum_{j=1}^{m} (\Delta x)_j (2\pi r_D)_{j-1} +$$

$$\sum_{j=1}^{m} \frac{P_j + P_{j-1}}{2} \pi \left[(r_w^2 - r_D^2)_j - (r_w^2 - r_D^2)_{j-1} \right]$$

again solving for unknown pressure $P_{j=n}$ gives

where

$$P_{j=n} = \frac{2}{(r_w^2 - r_D^2)_n + (r_w^2 - r_D^2)_{n-1}} \left[(P_s + \rho_s u_s^2)(r_s^2 - r_N^2) \right.$$

$$+ \sum_{j=1}^{m} (\Delta x)_j (2\pi r_D)_{j-1} + \sum_{j=1}^{n-1} \frac{P_j + P_{j-1}}{2} \left((r_w^2 - r_D^2)_j - (r_w^2 - r_D^2)_{j-1} \right)$$

$$+ \frac{P_{n-1}}{2} \left((r_w^2 - r_D^2)_n - (r_w^2 - r_D^2)_{n-1} \right) - \left(\rho_0 u_0^2 (r_w^2 - (b + r_i)^2 + 2b^2 VO \right.$$

$$\left. \left. + 2br_i WO \right)_{j=n} - \sum_{j=1}^{m} (\Delta x)_j (c_f + \tfrac{1}{2} \rho_0 u_0^2 2\pi r_w)_{j-1} \right] \qquad (23B)$$

where

$$VO = \int_{\eta_0}^{1} (\rho u^2) \eta \, d\eta$$

$$WO = \int_{\eta_0}^{1} (\rho u^2) \, d\eta$$

Equation 22 is used to replace the variable r_D by b and other variables. Equations 21 A & B and 23 A & B give both the continuity and momentum equations as a junction of the four unknown variables b, r_i, η_o, and $P_{j=n}$. However, these four equations can be reduced to two equations with only two unknowns, η_o and r_i by replacing b everywhere with the expression shown in equation 21A and by eliminating $P_{j=n}$ by equating equations 23A and 23B.

The computation procedure is to assume a value for η_o and then itterate r_i so as to satisfy the continuity, which is the combination of equations 21A and B. Another value for r_i is then computed by satisfying momentum which is the combination of equations 23A & B. If the two values for r_i from continuity and momentum are equal, then the correct η_o was assumed. The initial estimate of $\eta_{o_{j=n}} = \eta_{o_{j=n-1}}$ and from there small increment, in η_o are used till the difference in r_i reached a satisfactory minimum.

The dividing line shear stress τ_o and the area on which it acts in the region between j=n-1 and j=n is taken from the known velocity gradient and radius r_D at cross-section j=n-1.

The emperical expression used for the turbulent shear stress is the modified Prandtl's mixing length which was given before in eq. 18 and can be written as:

$$\tau_D = \rho c b^2 \left(\frac{u_o - u_i}{b} \right) \left(\frac{\partial u}{\partial r} \right)_{\eta_o}$$

where cb^2 is ℓ^2 which equals Prandtl's mixing length and $c < 1.0$ and is determined from experiments. $\frac{u_o - u_i}{b}$ is the average velocity gradient in the mixing zone and

$$\left(\partial u / \partial r \right)_{\eta_D} = \pi/2 \, (u_1 - u_o) \sin \pi \eta_D \frac{\partial u}{\partial r} = \left(\frac{u_o - u_i}{b} \right) \frac{\pi}{2} \sin \pi \eta_o$$

$$\text{or} \quad \tau_D = \rho c (u_o - u_i)^2 \frac{\pi}{2b} \sin \pi \eta_o \qquad (24)$$

The shear stress along the walls is a function of the local Reynolds number based on the duct diameter. For Reynolds numbers below 2000 we use the laminar form $C_f = 64/Rey$

For Reynolds numbers from 2000 to 100,000 we use Blasius relation

$$C_f = \frac{0.316}{(Rey)^{1/4}}$$

At the nozzle exit the mixing zone width b=0 and the resulting shear stress according to equation 24 will be infinite. This is because we ignored the initial internal and external boundary layer on the nozzle. To compensate for this the starting width of the mixing zone b will be assumed 0.05 r_n where r_n is the nozzle exit radius. This value will be used to compute the initial and maximum shear stress τ_o.

The energy equation is not required in Region I where the centerline velocity is part of the inviscid core. However, in Region II the centerline velocity u_c and density ρ_c must be computed each time so as to satisfy the overall energy equation. To eliminate itterations we use the known values of ρ_c and r_o at station j=n-1 in order to compute the required centerline velocity and density from the energy equation at station j=n.

Ejector Model Testing

The flow inside the ejector can be computed if one uses the proper inlet conditions, the three conservation equations in integral form, and the equation of state, where applicable. In addition, one needs a realistic model of the velocity and density profile in the mixing zone and a realistic value for the turbulent shear stress on the dividing streamline. The model used for the turbulent shear stress at the dividing streamline requires at least one experimentally-determined coefficient. The magnitude of this coefficient determines the growth rate of the mixing zone and the behavior of the ejector in general. However, this coefficient is only a function of the fluids, their temperature and velocity differences and is independent of the size of the ejector. Consequently, this method of ejector design is very useful for predicting the behavior of large size ejectors from the experimental results of a model test.

Model Description and Performance:

The vacuum facility at West Virginia University can handle only a non-condensable gas flow rate of 240 lb/day, and corrosive vapors such as steam cannot be utilized. However, a small ejector with a 2.71" inlet diameter, operating on argon or nitrogen can be operated continuously with 4.9 mm Hg exit pressure. By electrically heating the nozzle gas one can produce a nozzle exit velocity equal to that of the steam ejector. Using Quasi-one dimensional equations a computer program was written for a perfect gas ejector, operating on helium, nitrogen, argon, etc. This is shown as Program 1. * From the program it appears that using the proper nozzle total temperature, one can closely simulate all the pressures and velocities as they occur in the steam ejector. Based on the results of this program a two feet long model ejector was constructed. Static pressure taps were located at one inch axial spacing and spiralling around the perifery. The ejector was too small to permit the installation of a pitot traverse without seriously distorting the flow. The ejector was mounted in the access door of a 2 feet diameter hypersonic arc tunnel. The vacuum in the tunnel is provided by a 1500 cfm Stookes booster pump. The ejector nozzle is connected to a water cooled settling chamber in which a 78 KW Plasma Generator discharged heated argon or nitrogen.

Helium could not be used in the Plasma Generator because of its high ionization potential. The nozzle

*Figure 3.

was machined out of a 3/8" diameter and 6" long steel rod and can be moved axially in and out of the ejector inlet. The nozzle was uncooled and the gas temperature is limited by the melting temperature of the nozzle material. The nozzle mass flow rate is measured prior to the heating process with a rotary flow meter. The nozzle total pressure was measured by a 6" vacuum gage. The secondary flow was admitted through many small holes around the perifery of the ejector upstream of the nozzle.

All the static pressures were measured with an Alphatron gage, which was calibrated with a Stokes McLoad gage. The pressure measuring instruments were connected to a manifold and each pressure tap was opened in turn when taking a reading. Some typical static pressure distributions are shown in Fig. 4. This graph shows that with electrically heating the nozzle flow, the ejector did not work at all. The pressure drop experienced was only due to the ventury effect in the varying area duct. However, if the electric heating is turned off then the ejector operates under the required pressure levels at a mass flow ratio of 1 to 1. This behavior agrees with the prediction of program 1, using cold low velocity nozzle flow.

Several phenomena were observed during the tests:

a) Some pressure taps had to be sealed off because of excessive leakage around the valve stems.

b) The ejector did not behave as expected with the electrically heated nozzle flow, this is due partially to the adverse effect that heat transfer and density gradients in the mixing zone has on the entrainment process, also the heat transfer from the nozzle supply pipe to the secondary flow reduces the performance. The conclusion is that steam cannot be satisfactorily simulated by a gas like argon. The use of helium was not successful due to the adverse density gradient in the mixing zone and the unsuitable nozzle size.

c) The diffuser behaved slightly better than is predicted by the emperical formula, but the assumption of constant pressure mixing in the converging section of the mixing duct was not materialized. For this particular model ejector a better approximation would have been by assuming $p_{average} = (p_o + p_1)1/2$.

A schematic drawing and photo of the Model Ejector test block are shown as Fig. 2 and 5.

VFEA EJECTOR
MIXING ANALYSIS
FIG. 1

451-332 O - 71 - 4

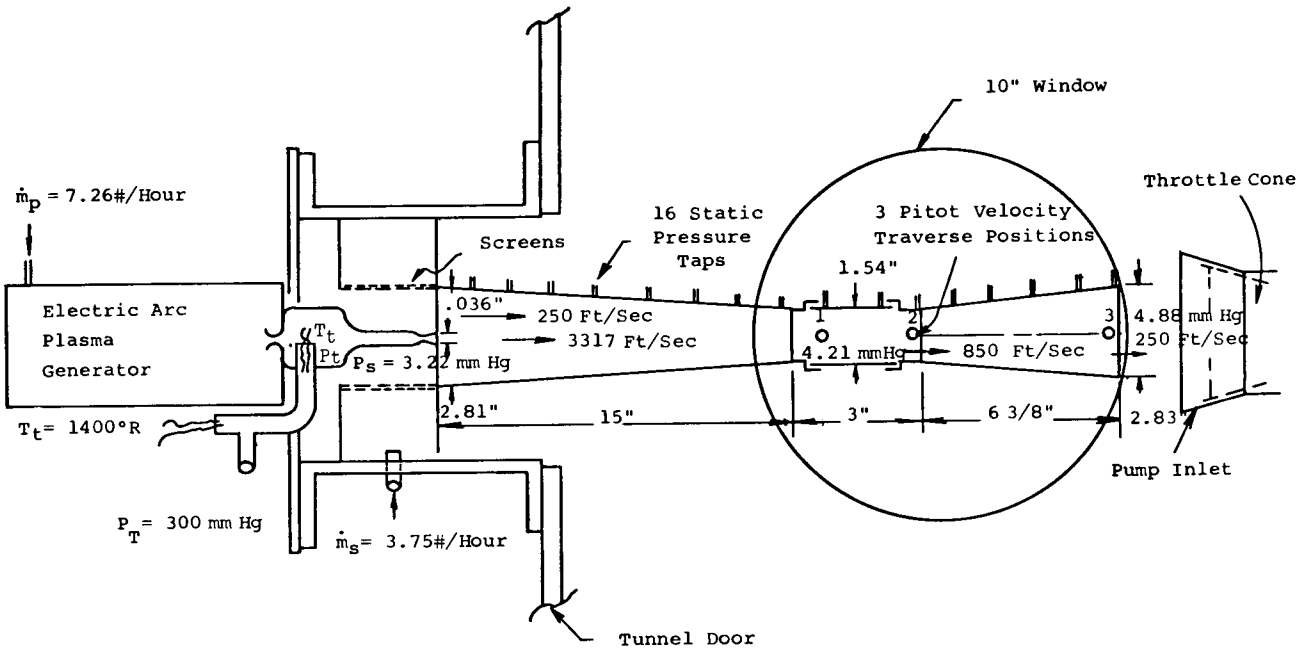

Fig. 2
Schematic Drawing
University of West Virginia
Ejector Model Test Block

PROGRAM 1 - TEST MODEL PERFORMANCE

```
 1 REM      "EJECTOR FLOW SOLUTION (TWO COMPONENT GAS FLOW)
 5 REM in the variable name, the first letter defines the flow property, the second defines the
     suffix
10 REM suffix '3' denotes the primary flow quantity
15 REM suffix '4' denotes the secondary flow quantity
20 REM suffix '1' denotes the throat exit flow quantity
25 REM suffix 'm' denotes the mixed flow quantity
30 REM suffix 'e' denotes the diffuser exit flow quantity
40 REM p = pressure in mm mercury
45 REM b = mach no.
50 REM t = temperature in rankine
55 REM r = gas constant
60 REM g = ratio of specific heats
65 REM w = molecular weight
70 REM s = speed of sound
75 REM m = mass flow rate in lb/hr.
80 REM a = area
85 REM v = flow velocity
90 REM c = constant# pressure specific heat
101 INPUT V1,M3,M4,W3,W4,G3,G4
105 LET P3=3.222*2.785
108 LET P4=P3
110 REM       po defines the primary flow total pressure
115 LET PO=8.9*2.785
120 LET B3=SQR(((PO/P3)**((G3-1)/G3)-1)*2/(G3-1))
125 LET T4=530
127 REM     to defines the primary flow total temperature
130 LET TO=530
135 LET T3=TO/(1+(G3-1)*B3**2/2)
140 LET R=1546.32*32.2
145 LET R3=R/W3
147 LET R4=R/W4
150 LET S3=SQR(G3*R3*T3)
155 LET V3=B3*S3
157 REM     d3 is primary flow density
160 LET D3=P3/(R3*T3)
163 REM     ee is a conversion factor for lb/hr to slugs/seconds
165 LET EE=3600*32.2
170 LET Q=M3/EE
175 LET A3=O/(D3*V3)
177 REM     dp is nozzle exit diameter
180 LET DP=12*SQR(4*A3/3.1416)
183 REM       d4 defines secondary flow density
185 LET D4=P4/(R4*T4)
190 LET N=M4/EE
193 LET V4=250
195 LET A=A3+N/(D4*V4)
197 REM       ds defines secondary duct diameter
200 LET DS=12*SQR(4*A/3.1416)
202 LET C3=R3*G3/(G3-1)
203 LET C4=R4*G4/(G4-1)
205 LET CM=(M3*C3+M4*C4)/(M3+M4)
210 LET T1=(C3*M3*TO+C4*M4*T4)/((M3+M4)*CM)
215 LET M=N+Q
220 LET WM=(M3*W3+M4*W4)/(M3+M4)
225 LET RM=R/WM
230 LET GM=CM/(CM-RM)
235 LET X1=M*RM*T1/V1-M*V1*(GM-1)/(2*GM)
240 LET P=.01
245 LET K=2
255 LET A1=(X1+M*V1-N*V4-Q*V3+4*P*K*M*V1)/P3
257 REM     d1 defines throat diameter
260 LET D1=12*SQR(4*A1/3.1416)
265 LET VE=250
267 REM     de defines diffuser exit diameter
270 LET DE=D1*SQR(V1/VE)
275 LET ZM=2.5*3.1416/180
280 LET ZD=6*3.1416/180
285 LET LD=.5*(DE/D1-1)*COS(ZD)/SIN(ZD)
290 LET LM=.5*(DS/D1-1)*COS(ZM)/SIN(ZM)
295 LET P1=X1/(A1*2.785)
300 LET S1=SQR(GM*RM*T1-(GM-1)*V1**2/2)
305 LET B1=V1/S1
307 LET Y=GM/(GM-1)
310 LET PT=P1*(1+(GM-1)*B1**2/2)**Y
315 LET ET=.846
317 REM       cp defines diffuser pressure recovery factor
320 LET CP=ET*(1-VE/V1)
325 LET PE=CP*M*V1/(2*A1*2.785)+P1
330 PRINT USING 335, PT,P1,CP,DP,DS,D1,DE,LD,LM
331 PRINT USING 336, B3,S3,V3,B1,S1,T1
332 PRINT USING 337, PE
335 IMAGE

pt =-.----,  p1 = -.----,  cp = .----, dp = ----.--, ds = ----.--, d1 = ----.--
336 IMAGE
b3=-.---, s3 =----.--, v3 = ----.--, b1 = -.----, s1 = ----.--, t1 = ----.-
337 IMAGE
pe = --.----
340 GO TO 101
```

EJECTOR MODEL
COMPUTER PROGRAM
FIG. 3

FIGURE 4

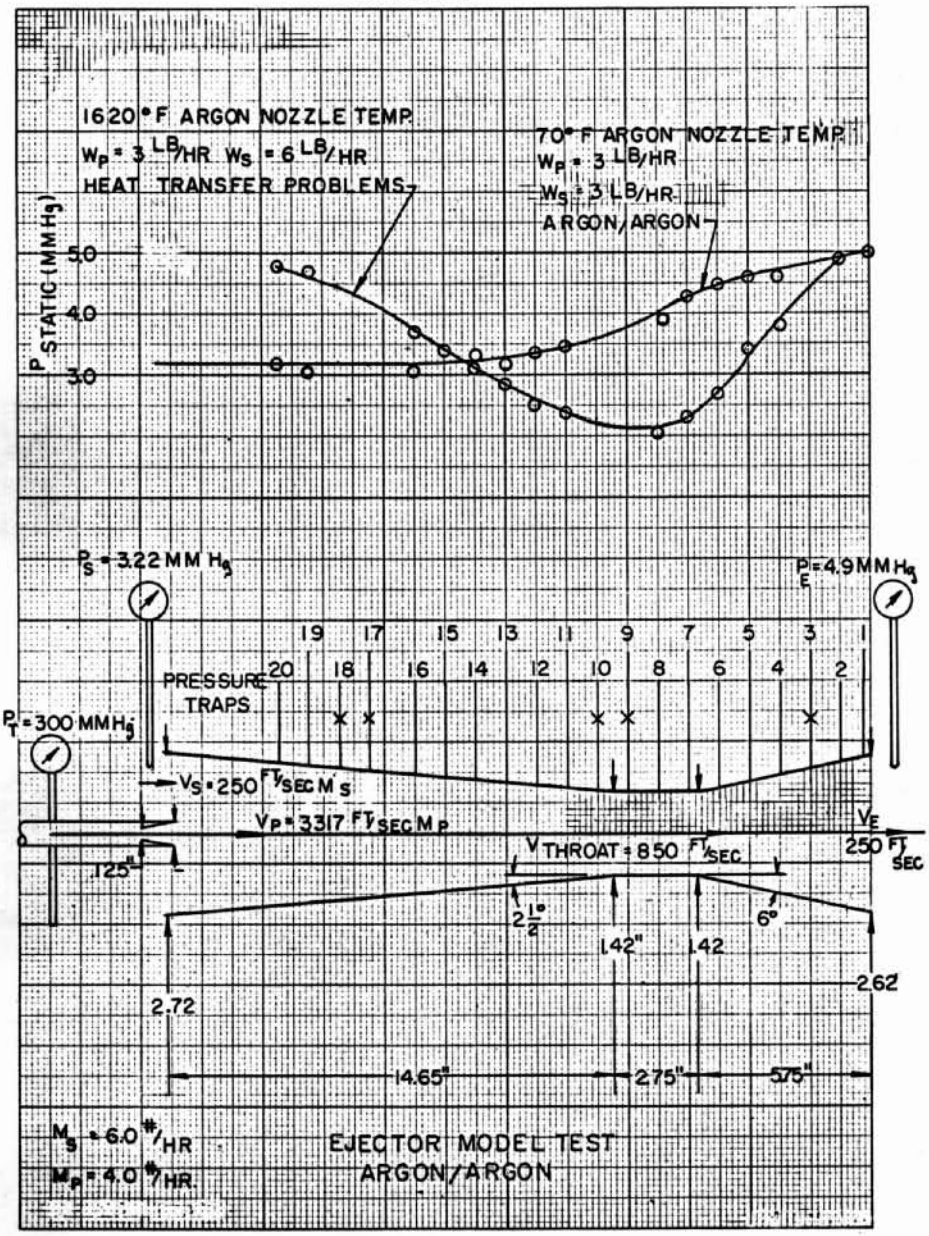

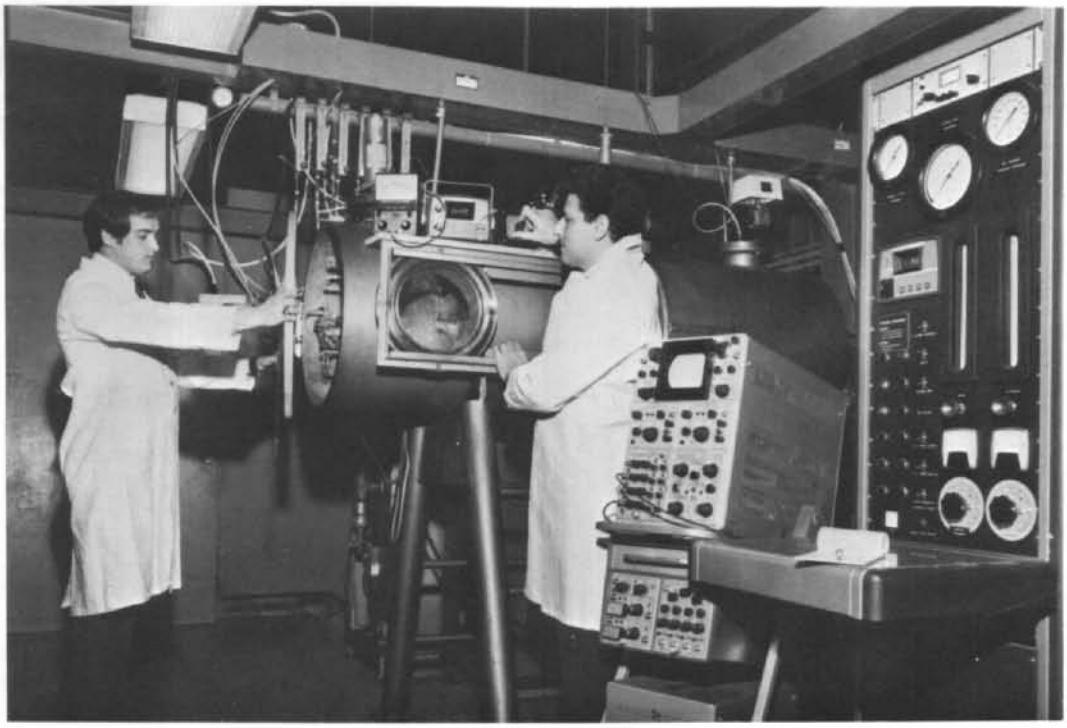

78 kw ARC TUNNEL

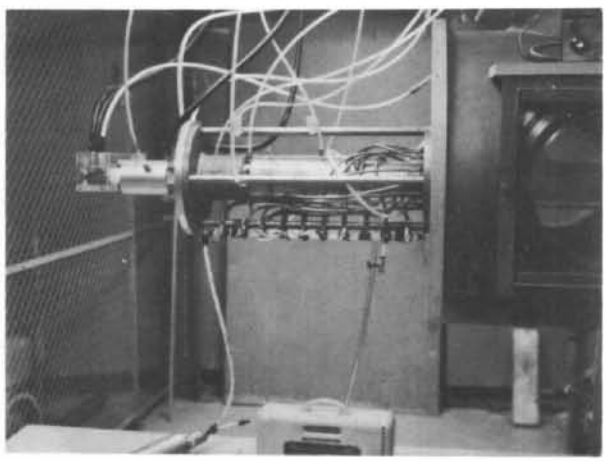

EJECTOR INSTALLED IN TUNNEL

FIGURE IV-5 EJECTOR MODEL TEST FACILITIES
University of West Virginia

V. EJECTOR BENCH SCALE TESTING

An equivalent 6,000 gpd bench size test ejector was designed, constructed and tested at Colt's Power Systems Division laboratories in Beloit, Wisconsin. An evaporator and condenser formed the nucleus of a closed cycle loop for testing the ejector. The test loop enabled testing the ejector at process conditions, using the same media (water vapor) as in the VFEA process. The loop was designed such that the primary steam pressure and temperature could be varied as well as the suction and discharge pressure of the secondary vapor flow.

Experimental testing was conducted with the primary purpose to obtain minimum mass ratio. Testing was also conducted to determine the operating characteristics of the ejector at varying process conditions.

Results and Conclusions

1. Mass Ratio vs. Pressure Rise Across the Ejector

   The ejector mass ratio* increased as the ejector outlet pressure was increased. This is as expected because as the secondary steam is raised to a higher pressure, more primary steam is needed. The conclusion is that the ejector mass ratio increased with increase in the pressure rise for the secondary steam, i.e., the condenser pressure minus the evaporator pressure.

   This relationship is well established in fig. 1. The corelation is quite impressive due to the fact that the data plotted included a wide range of variables as shown below:

Evaporator pressure	3.02 to 3.35 mm Hg abs.
Condenser pressure	4.85 to 5.0 mm Hg abs.
Primary steam flow rate	83.2 to 92.5 lb./hr.

2. Nozzle Efficiency

   The isentropic efficiency of the nozzle is defined as:

   $$\text{Nozzle efficiency} = \frac{\text{Velocity at the nozzle outlet}}{\text{Max. velocity at the outlet of isentropic nozzle}}$$

$$*\text{Mass ratio} = \frac{\text{Mass flow rate of primary steam}}{\text{Mass flow rate of secondary steam}}$$

The nozzle efficiency was found to be of the order of 96%. For a convergent divergent nozzle of large pressure ratio (300 to 3.35 mm Hg abs.) this is a very good efficiency.

3. Diffuser Efficiency

Diffuser efficiency is defined as follows:

$$\text{Diffuser efficiency} = \frac{\text{Total press. at diffuser outlet}}{\text{Total press. at diffuser inlet}}$$

The diffuser efficiency varied from 84% to 98.5%. Diffuser efficiency was greatly affected by the velocity profile at the inlet of the diffuser. The more uniform the velocity profile, the higher the diffuser efficiency. For runs with a uniform velocity profile, the average efficiency was 95%. This trend is well established in technical literature*. Therefore, if care is taken in designing the mixing cone, a diffuser efficiency of 95% is obtainable.

4. Effect of Primary Steam Pressure

The effect of primary steam pressure on the mass ratio of the ejector is shown in figure 2. Fig. 2 is based on data from test series #3. The optimized performance runs were based on test series #4 and #5 and hence the plotted data is not interchangeable without corrections. Fig. 2 shows that the minimum mass ratio was obtained for a primary steam pressure of about 300 mm Hg abs. This trend was expected, since the nozzle was designed for 300 mm Hg abs. At other primary steam pressures the nozzle was at off design conditions and operated under or over-expanded, with losses in efficiency. It may also be pointed out that the curves in fig. 2 are rather flat near the point of minimum mass ratio, thereby indicating that small fluctuations in the primary steam pressure ($\pm$ 10 mm Hg abs.) will have very little effect on the mass ratio, which is very desirable from process control point of view.

5. Primary Steam Temperature

Primary steam is the motive force behind the ejector. The energy content of the steam is determined almost entirely by its temperature (not the pressure). Therefore, if the steam is superheated to a higher temperature, lesser

*Schlichting, Boundary Layer Theory, 6th Ed., McGraw Hill, P. 590-592.

amount of primary steam will be needed to move a given amount of secondary steam, i.e., with increase in the temperature of the primary steam the mass ratio will decrease. This trend is shown in fig. 3. It may be pointed out that the nozzle was designed for 250°F steam, and therefore, it is conceivable that if the nozzle was designed for 265°F, a still lower mass ratio would have resulted. A lower mass ratio will have a direct effect on the size of the absorber, concentrator and the absorbant heat exchanger and, therefore, will be a factor of plant cost.

6. Ejector Operation - Stability:

The operation of the test ejector over the range requirement of the process was extremely stable. The test ejector did not operate in a stall region or did backflow exist due to flow separation.

Ejector Operation - Start-up:

No special start up procedures were necessary during startup. As soon as the evaporator pressure gets below the primary steam pressure, the ejector can be started. The ejector continues to draw the evaporator pressure down to the operating level.

Ejector Operation - Droplet Carryover:

The test evaporator was designed without a droplet carryover separator. Because the test loop operated with a 15% NaCl solution a carryover of high salt concentration was sucked into the test ejector. Most of the salt carryover was deposited on the diffuser wall, from which it was washed off periodically. There was no appreciable degeneration of performance due to carryover during bench scale testing.

Ejector Operation - Noise:

The test ejector operates without any appreciable noise.

Ejector Operation - Freeze Up:

During bench scale testing there were no instances of ejector freeze up. At start up the nozzle is cold and a portion of the primary steam condenses and forms an icicle. This icicle then disappears as the nozzle warms up.

Data Reduction

The data was recorded after the ejector had reached stable operation. The ejector loop was considered to have stabilized when all pressures, temperatures and flow rates reached a steady state.

The following pages show a typical raw and processed data sheets. The data for pitot traverse #1 and #2 are not shown. Pitot traverse #1 is a single reading taken at the exit of the nozzle to determine the velocity of the steam at the nozzle exit. This data was used to compute nozzle efficiency. Pitot traverse #2 was undertaken a few times in the early stages of the ejector testing. This traverse was done in the mixing jet growth region to develop some insight into the pehnomena of viscous drag. Pitot traverse #3 is made in the ejector throat at the entrance to the diffuser. This is used to determine the flow rate through the ejector (primary plus the secondary steam) and to plot the velocity profile at the entrance to the diffuser.

Static pressure traverse is done along the length of the ejector to plot the static pressure (at the wall) along the ejector.

Pitot Tube:

If the flow is supersonic, a locally normal shock would occur at tip of the pitot tube and the pitot tube will read the stagnation pressure after the normal shock, p_{oy}. If the static pressure before the shock is p_x, then the following equation* can be used to compute the mach number before the shock, M_x.

$$p_{oy}/p_x = \left(\frac{k+1}{2} M_x^2\right)^{k/(k-1)} \Big/ \left(\frac{2k}{k+1} M_x^2 - \frac{k-1}{k+1}\right)^{1/(k-1)}$$

Using a value of k=1.324 for steam, the above equation reduces to

$$p_{oy}/p_x = (1.162\ M_x^2)^{4.086} \Big/ (1.139\ M_x^2 - .1394)^{3.086}$$

The above equation is plotted in figure 6.

If the flow is subsonic, then the pitot tube reads the stagnation pressure, p_o, and if the static pressure is p , then the free stream mach number, M, can be computed using the following equation:

*Holman, Experimental Methods for Engineers, eqn. (7-52)

EJECTOR TEST DATA (Sample)

Test No. 6-2 Date 8/31/71

All pressures in mmHg Abs.

Static Press. Trav.

Evaporator		3.31
Mixing Cone	1	-
	2	-
	3	3.23
	4	3.24
	5	3.24
	6	3.36
	7	3.55
Throat	8	3.63
	9	3.90
Diffuser	10	4.23
	11	4.74
	12	4.88
	13	4.90
	14	4.90
Condenser		4.90

Pitot Traverses

#1 P_{oy} / P_x = /

#2

Location	P_o

#3 Ejector Throat

Location	$P_o - p$
1	
2	
3	
4	
C	2.64
5	1.97
6	1.36
7	1.06
8	0.96

Steam pressure into the nozzle	=	300	mmHg Abs.
Steam temperature	=	265.5	^oF
Pressure in desuperheater	=	-	psig
Δp orifice	=	-	in. H_2O

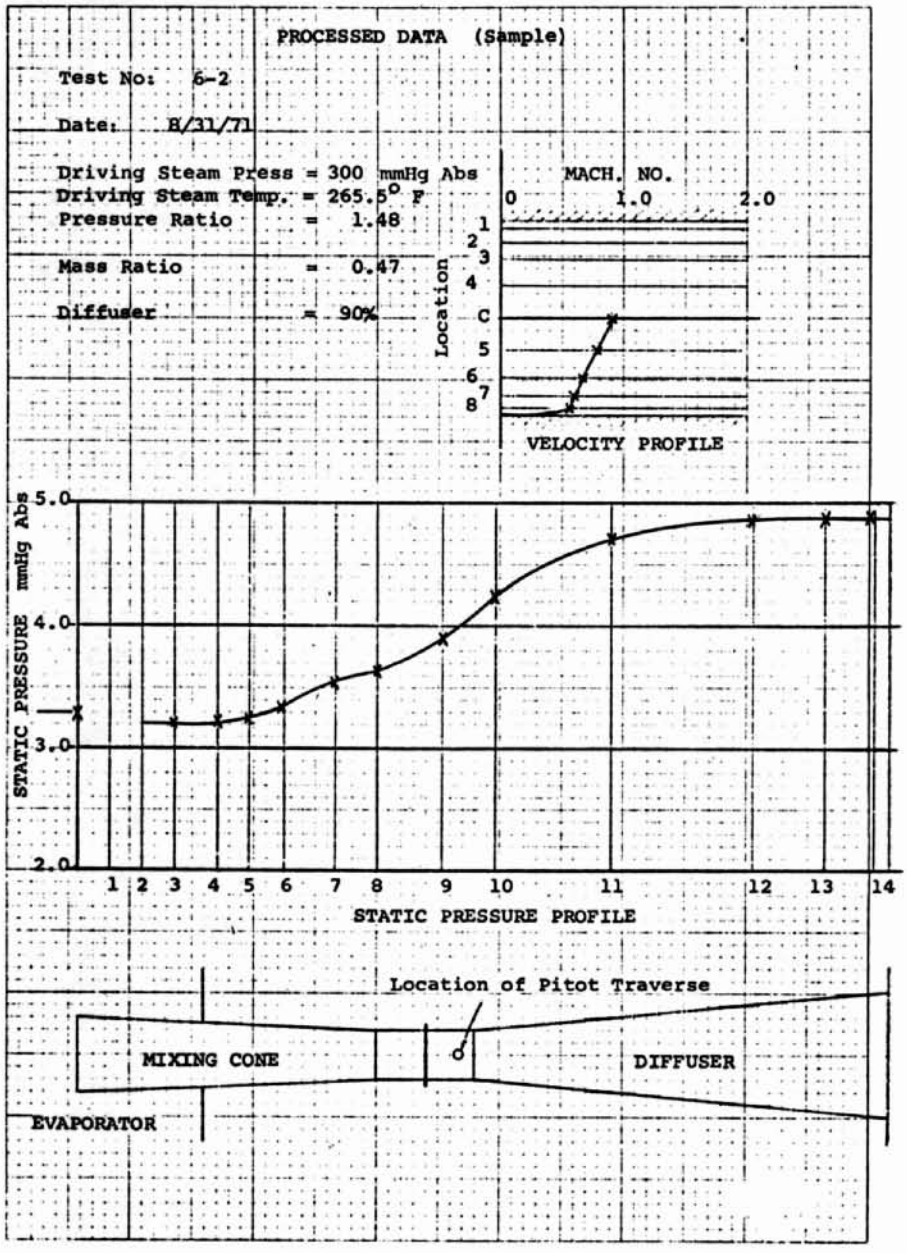
PROCESSED DATA (Sample)
Test No: 6-2
Date: 8/31/71
Driving Steam Press = 300 mmHg Abs
Driving Steam Temp. = 265.5° F
Pressure Ratio = 1.48
Mass Ratio = 0.47
Diffuser = 90%
MACH. NO.
0
1.0
2.0
Location
1
2
3
4
C
5
6
7
8
VELOCITY PROFILE
STATIC PRESSURE mmHg Abs
5.0
4.0
3.0
2.0
1 2 3 4 5 6 7 8 9 10 11 12 13 14
STATIC PRESSURE PROFILE
Location of Pitot Traverse
MIXING CONE
DIFFUSER
EVAPORATOR

$$p_o/p = (1 + \frac{k-1}{2} M^2)^{k/(k-1)}$$

for k = 1.324 we get

$$p_o/p = (1 + .162\ M^2)^{4.0864}$$

The above equation is also plotted in figure 6.

For subsonic flows

$$p_o - p = p\ (p_o/p - 1)$$

$(p_o - p)$ is plotted against M for various values of p, in Figure 7.

Ejector Flow Rate:

Data collected includes $(p_o - p)$ traverse at the ejector throat and the static temperature at the throat. From the pitot traverse readings the mach number profile is drawn and average mach number, M, computed.

Velocity of sound, c, is given by

$$c = 60.47\sqrt{T} \text{ ft/sec}$$

The above equation is plotted in Fig. 8.

So the average velocity of steam at the throat
$= 60.47\ M\sqrt{T}$

Density of steam at throat $= \frac{p}{RT}$

So the mass flow rate of the steam at the throat

$$m_{ej} = \frac{\pi}{4} D^2\ 60.47\ M\sqrt{T}\ \frac{p}{RT}$$

Where D = 7.75"

$$R = 1545.3/18 \text{ ft } lb_f/lb_m\ ^\circ R$$

Converting all quantities in convenient units, we get

$$\dot{m}_{ej} = 2312\ Mp/\sqrt{T} \quad lb_m/hr$$

Where p is in mm Hg Abs.

T is in °R

Mass Flow Rate Through Nozzle:

Mass flow rate through a chocked nozzle is given by

$$m_{noz} = C_d\, A^* \sqrt{\frac{k}{R}\,\frac{2}{k+1}^{(k+1)/(k-1)}\,\frac{p_o}{T_o}}$$

Where C_d is the discharge coefficient, assumed = .98

A^* is the area of cross section at throat.

For nozzle #1, throat diameter = .61"

p_o is the stagnation pressure at the inlet to the nozzle. If the inlet velocity is low, the static pressure stagnation pressure.

T is the stagnation pressure at the nozzle inlet. If the inlet velocity is low, the static temperature stagnation temperature.

k = 1.324 for steam

R = 1545.3/18 lb_f ft/lb_m °R

Substituting the values of A^*, k and R and converting the equation into convenient units, we get

$$\dot{m}_{noz} = 8.2\, p_o/\sqrt{T_o}$$

The above equation is plotted in Fig. 9.

Mass Ratio:

$$\text{Mass ratio} = \frac{\text{Primary steam flow rate}}{\text{Secondary steam flow rate}}$$

$$= \dot{m}_{noz}/(\dot{m}_{ej}-\dot{m}_{noz})$$

Diffuser Efficiency:

$$\text{Diffuser eff.} = \frac{\text{Total pressure at the diffuser outlet}}{\text{Total pressure at the diffuser inlet}}$$

Total pressure at diffuser outlet = Condenser pressure.

Total pressure at the diffuser inlet can be computed from the pitot traverse #3, which gives mean (p_o-p) and the static pressure profile, which gives p

So total pressure at the diffuser inlet

$$= (p_o-p)/_{\text{traverse } \#3} + \text{Static press.}$$

Thus the diffuser efficiency can be calculated.

Test Facilities

A test ejector was designed to be compatible with a plant size of 6000 gpd. The ejector was tested in a fashion, which vigorously duplicated the actual operating conditions. The actual operating conditions of an ejector are listed below with an explanation of how these were simulated in the bench scale test loop:

1. Primary Steam: The ejector is driven by primary steam at 300 mm Hg and 250°F. (design condition) generated in the sodium hydroxide concentrator. In the test loop, this steam was generated in a special desuperheater provided with temperature and vacuum regulators. The equipment was so designed and controlled that the primary steam can be supplied at any desired pressure and temperature, in the neighborhood of the design point. Once the controllers were set to the desired values, the desuperheater operated automatically.

2. Secondary Steam: The ejector removes secondary steam saturated at 3.35 mm Hg Abs. (design point) from the freezer. In the test loop a brine evaporator was used to provide the secondary steam for the ejector. For ease in the test loop set up and operation, the brine in the evaporator was not allowed to freeze. This was accomplished by using a high concentration of brine (15% NaCl solution). The secondary steam provided by the brine evaporator simulated the actual secondary steam pressure exactly and the temperature within about 2°F. It was estimated that this difference of about 2°F. in the secondary steam (between actual and simulated) had negligible effect on the ejector operation. The secondary steam pressure was controllable and once set, maintained itself automatically.

3. Compressed Steam: The ejector discharges compressed steam at 4.9 mm Hg abs. into the melter. In the test loop a spray condenser was used to maintain a desired pressure at the ejector outlet. The spray condenser absorbed the condensibles on the spray, and the non-condensibles were removed by the air removal loop using blowers, condensers and a vacuum pump. The pressure in the condenser could be varied and automatically maintained constant at any desired value.

The piping schematic and the controls are shown in fig. 4.

Controls

1. Primary steam controls: When the desuperheater tank was half filled with water, it was brought to boiling by bubbling shop steam into it. The steam generated in the desuperheater was almost saturated steam regardless of shop steam quality. This steam was then throttled to the desired pressure by a vacuum regulator. The temperature after throttling depended upon the pressure of the saturated steam in the desuperheater. A temperature controller was used to monitor the steam temperature after throttling to control the steam pressure in the desuperheater. With proper settings on the vacuum and temperature regulators, the primary steam could be supplied at any combination of pressures and temperatures.

2. Brine supply temperature control: The brine tank was maintained at a constant temperature of about 23°F. The refrigerator had an evaporator pressure regulator (back pressure regulator) which was used to set the back pressure of Freon at about 50 psia, saturation temperature about 12°F. (15% brine freezing temperature, 12.5°F). The temperature in the brine tank was controlled by a thermostat which could be set at any value in between 20 and 55°F.

3. Condenser pressure control: The condenser was maintained at a steady pressure of 4.9 mm Hg abs. A pressure transmitter was installed to transmit the condenser pressure to a multi-trol which in turn controlled a valve to regulate brine flow rate into the condenser.

4. Evaporator pressure control: The vapor pressure of the brine in the evaporator is governed by the concentration of the brine (kept constant at 15%) and the temperature of the brine. The

temperature of the brine in the evaporator was manipulated by injecting either the cold brine (to lower the evaporator pressure) or the hot brine (to increase the evaporator pressure). The cold brine flow was automatically controlled by a temperature regulator, see fig. 4.

The ejector bench scale test loop operated extremely well. All the controls functioned properly. Thermally, the loop was very stable. Once the test conditions were set, the loop operated the whole day without manipulations. This was a great asset for data collection, which often took 30 to 60 minutes.

Instrumentation

The test loop was amply instrumented for the measurements of pressure, temperature, flow rates, velocity profiles and pressure profiles. See fig. 5.

1. Flow rate measurements: The flow rates of brine in various loops were calibrated for a sp. gr. of 1.115 (15% NaCl solution at 32°F). No density correction was needed as the brine concentration was kept very close to 15.0% (+ .05%) and temperature was in the range of 24-32°F. This results in a density change of less than 0.5%. Thus, the brine flow rates were read off directly.

   Steam flowing out of the desuperheater was measured by an orifice-meter. Temperature and pressure at the inlet of the orifice were measured and used to compute the density. The pressure drop across the orifice was measured in inches of water by a differential pressure gage and from this data the flow rate of steam was computed.

   The flow rate of the vapor at the inlet of the diffuser was measured by a pitot tube tranverse. The static pressure read off a tap on the duct diameter and total pressure traverse was made across the horizontal and vertical diameter of the duct (Dia. = 7.75"). A 16 point traverse was used, with pitot tube being placed 1.37, 2.37, 3.06 and 3.62 inches away from the center.

2. Temperature measurements: All temperatures were sensed by copper-construction thermocouples and recorded on a 24 point recorder.

3. Pressure Measurements: Pressure above atmospheric occurred in the steam lines and brine lines and these were measured by Bourdon pressure gages.

Pressure below atmospheric but above about 25 torr were measured on Vertical Absolute Manometers. Pressures below 25 torr were measured on Inclined Manometers. The low pressure ends of these manometers were maintained at 10 microns or less so the readings were in absolute pressure. These inclined manometers, ranges 0-25, 0-12, 0-7 torr, were mounted on a board and so set up that they could be used either for the measurement of an absolute pressure or a differential pressure (pitot traverse).

4. Brine Concentration: Brine concentration was measured by titration, and maintained at 15%.

All instruments functioned well. The data collected was very reliable and repeatable.

451-332 O - 71 - 5

TABLE 1 SUMMARY OF PROCESSED DATA

TEST #	$P_{evap.}$ mm Hg. Abs.	$P_{cond.}$ mm Hg Abs.	PRESS RATIO	MASS RATIO	P_{nozzle} mm Hg Abs.	DIFFUSER EFF.	REMARKS
3-5	3.07	4.90	1.60	1.03	330		
3-6	3.21	4.90	1.53	.86	330		
3-7	2.99	4.8	1.60	.88	300		
3-8	3.1	4.9	1.58	.98	270		
3-10	3.26	4.9	1.50	.68	300		
3-11	3.07	4.90	1.60	.84	301		
3-12	3.25	4.90	1.51	.85	310		
3-13	3.16	4.90	1.55	.82	250		
3-14	3.24	4.90	1.51	.82	251		
3-15	3.15	4.90	1.56	1.0	272		
3-16	3.25	4.9	1.51	.755	271		
3-17	3.15	4.9	1.56	.89	251		
4-1	3.1	4.9	1.58	.74	298		
4-2	3.19	4.9	1.53	.67	296		
4-3	3.11	4.93	1.58	.73	300		
4-4	3.23	4.85	1.50	.65	300		
4-5	3.3	4.97	1.50	.62	300		
4-6	3.07	4.97	1.62	.76	330	97	
4-7	3.27	4.93	1.51	.70	332	98	
4-8	3.07	4.90	1.60	.99	270	98.5	
4-9	3.20	5.0		.77	302		Effect
4-10	3.21	4.85		.61	302		of back
4-11	3.23	4.97		.79	302		pressure
5-1	3.18	4.9	1.54	.685	302	95.5	
5-2	3.02	4.9	1.62	.79	310	95.6	
5-6	3.20	4.9	1.53	.67	300	95.6%	
5-7	3.35	4.9	1.46	.52	300	93.6%	
5-8	3.26	4.9	1.50	.57	300		
6-1	3.08	4.9	1.59	.65	300	95.0%	Temp=265°F
6-2	3.31	4.9	1.48	.47	300	89.4%	Temp=265°F
6-3	3.26	4.9	1.50	.64	300	95.3	Temp=235°F

FIG. 1 MASS RATIO VS. PRESSURE RISE ACROSS THE EJECTOR

TEST SERIES 4 & 5

Variable	Range
Evaporator press	3.02 - 3.35 mm Hg Abs.
Condenser press	4.85 - 5.0 mm Hg Abs.
Primary steam flow	83.2 - 92.5 lb./hr.

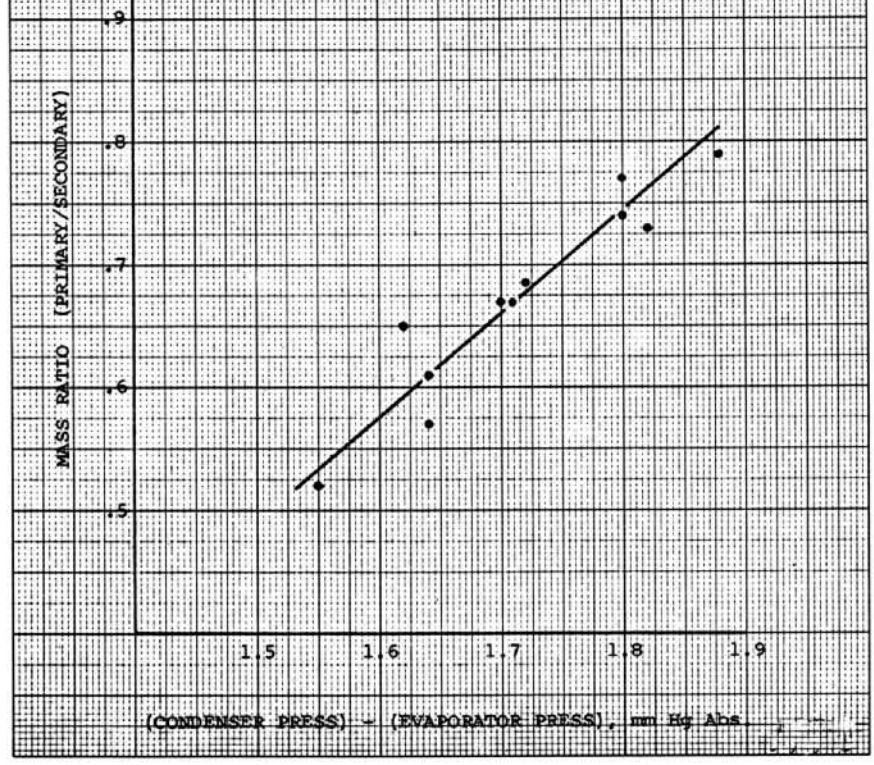

FIG. 2 EFFECT OF PRIMARY STEAM PRESS. ON MASS RATIO

TEST SERIES #3
(INTERPOLATED)

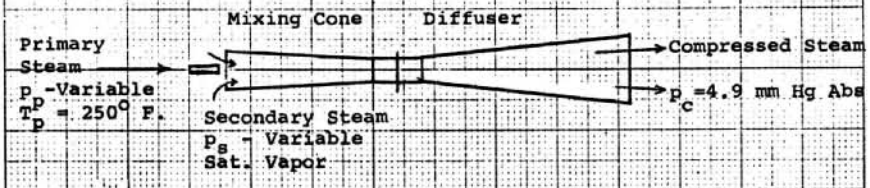

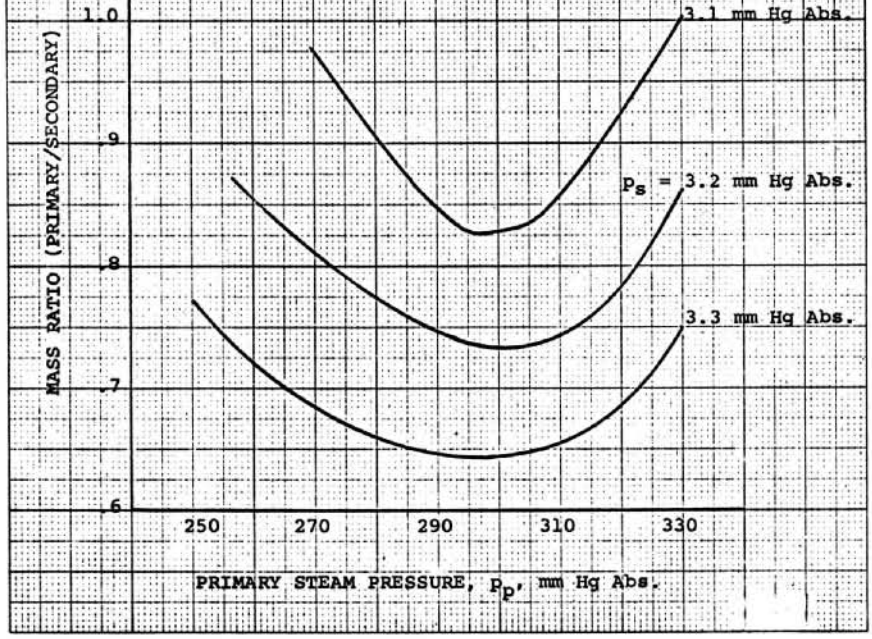

FIG. 3 EFFECT OF PRIMARY STEAM TEMPERATURE

TEST SERIES #5,6
(INTERPOLATED)

OPERATING CONDITIONS:

Evaporator press.	3.3 mm Hg Abs.
Condenser press.	4.9 mm Hg Abs.
Primary steam press.	300.0 mm Hg Abs.

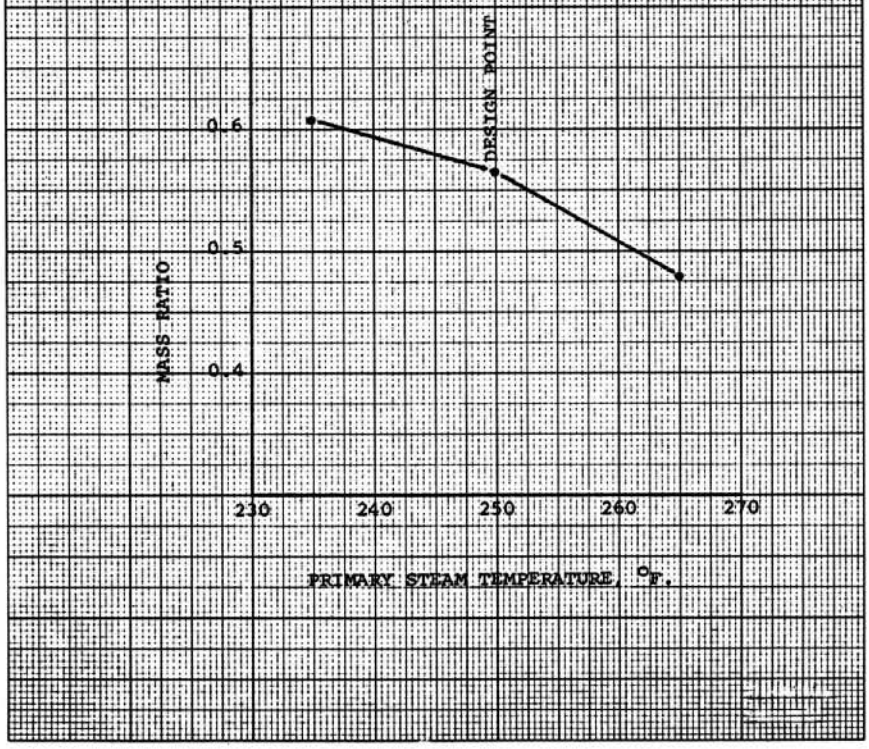

FIG. 4 PIPING SCHEMATIC & CONTROLS FOR EJECTOR BENCH SCALE TEST COOP.

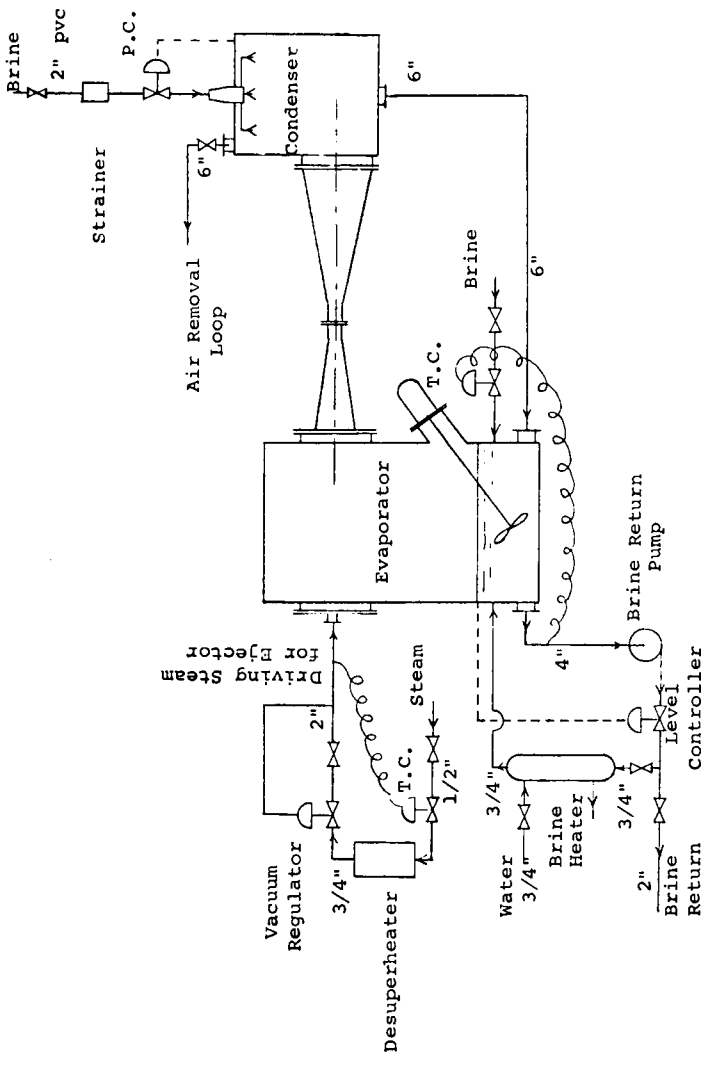

FIG. 5 INSTRUMENTATION

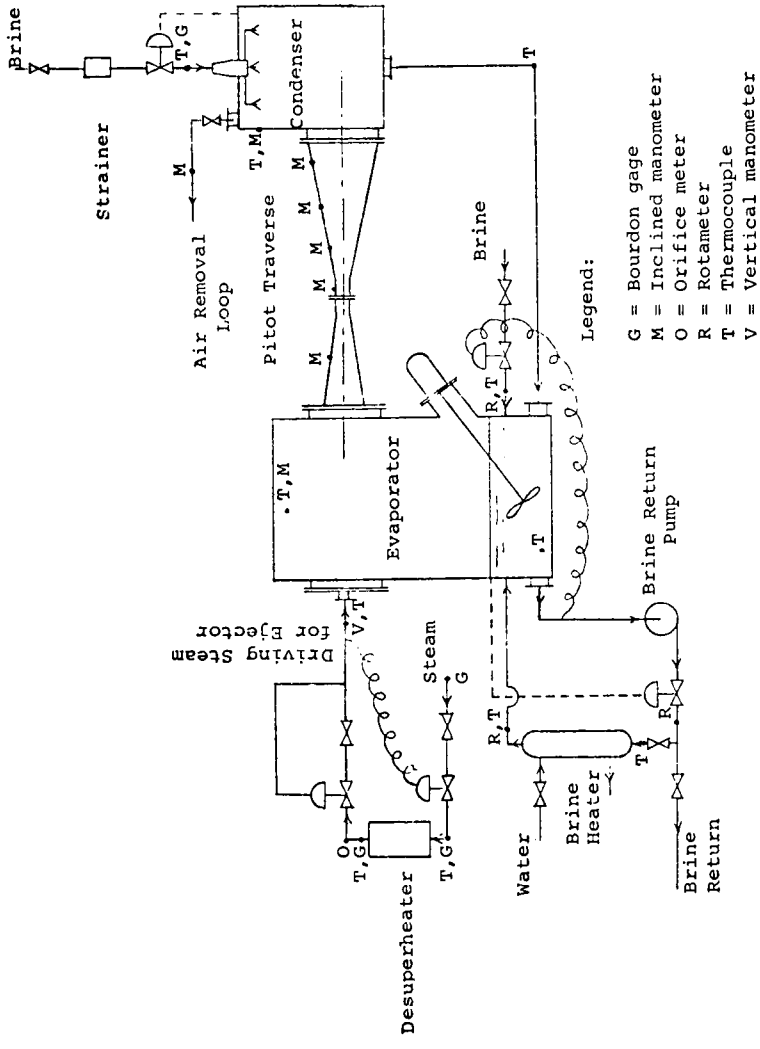

FIG. 6

PITOT TUBE
FOR
SUPERSONIC AND SUBSONIC FLOWS

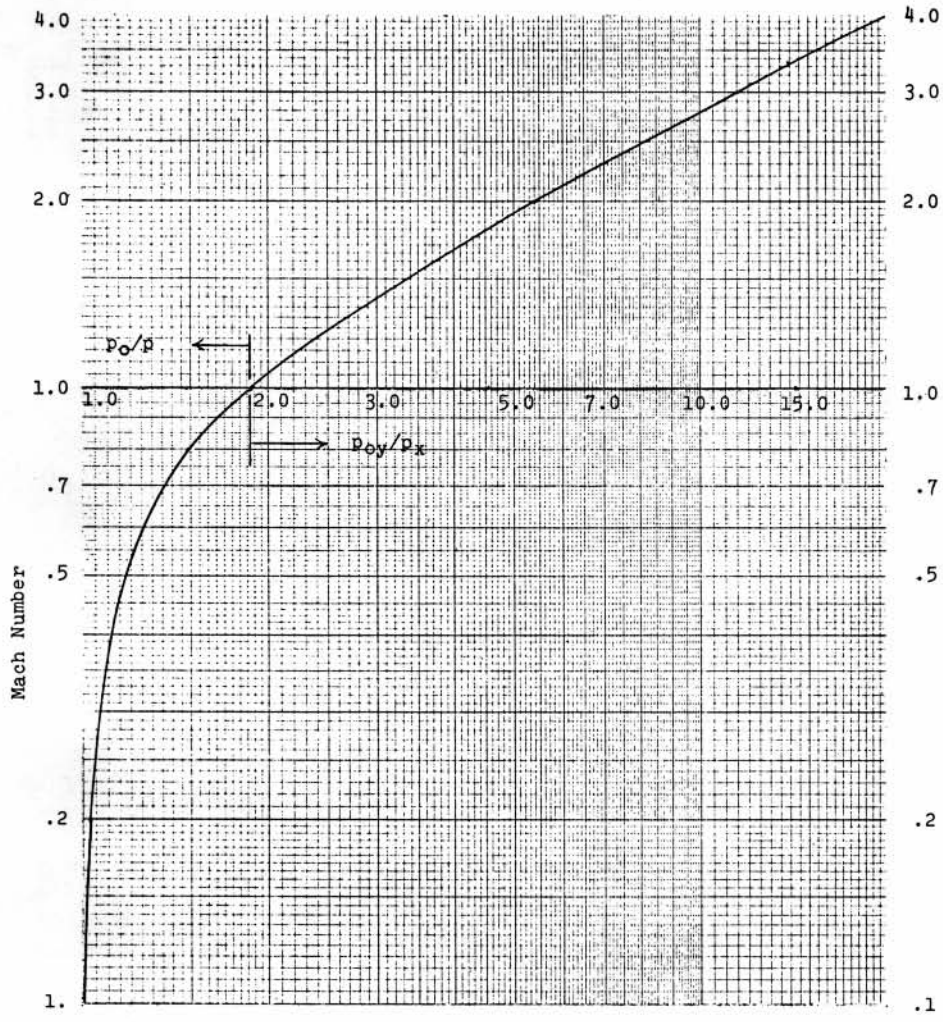

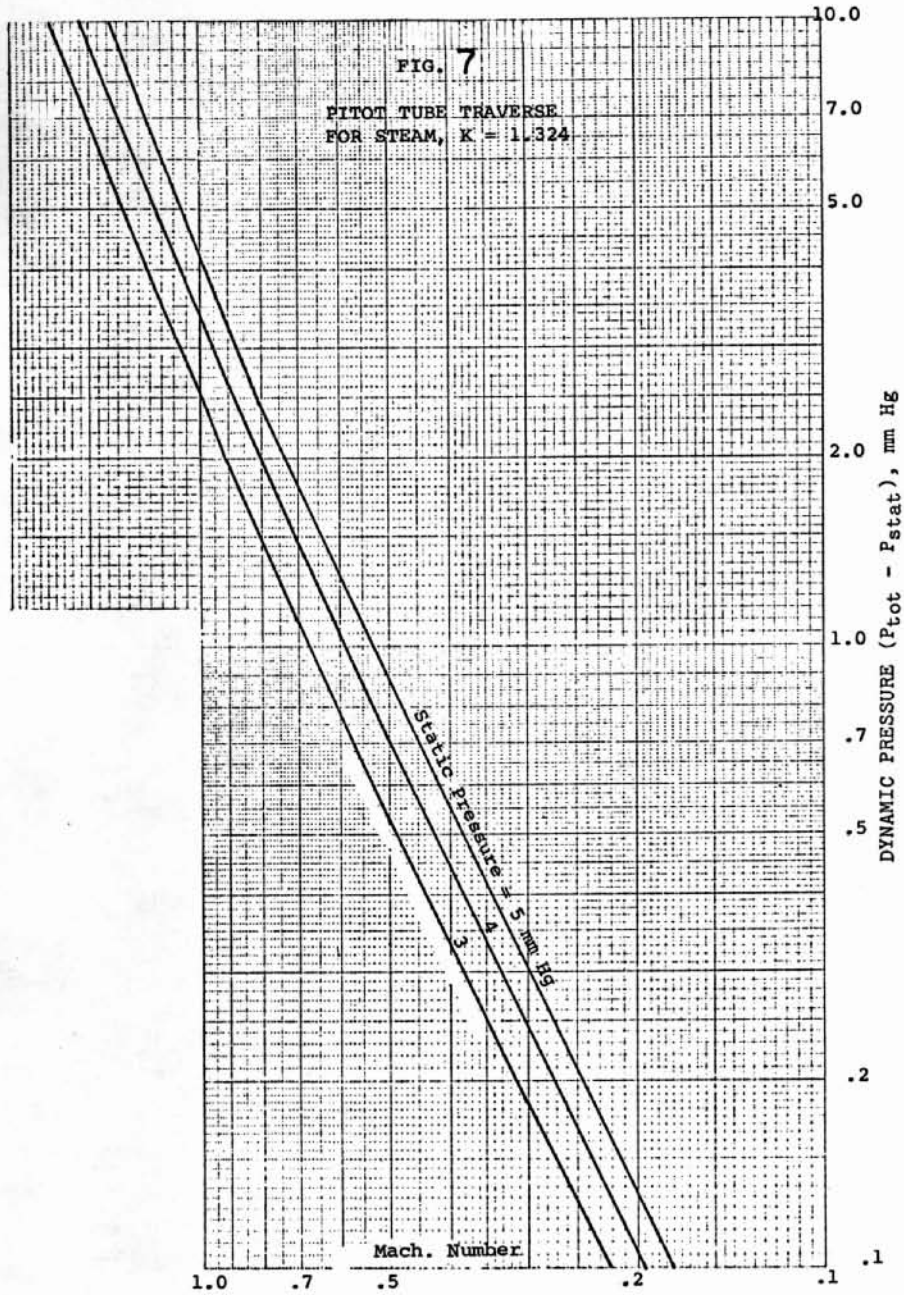
FIG. 7
PITOT TUBE TRAVERSE
FOR STEAM, K = 1.324
10.0
7.0
5.0
2.0
1.0
.7
.5
.2
.1
DYNAMIC PRESSURE ($P_{tot} - P_{stat}$), mm Hg
Static Pressure = 5 mm Hg
4
3
Mach. Number
1.0
.7
.5
.2
.1

FIG. 8

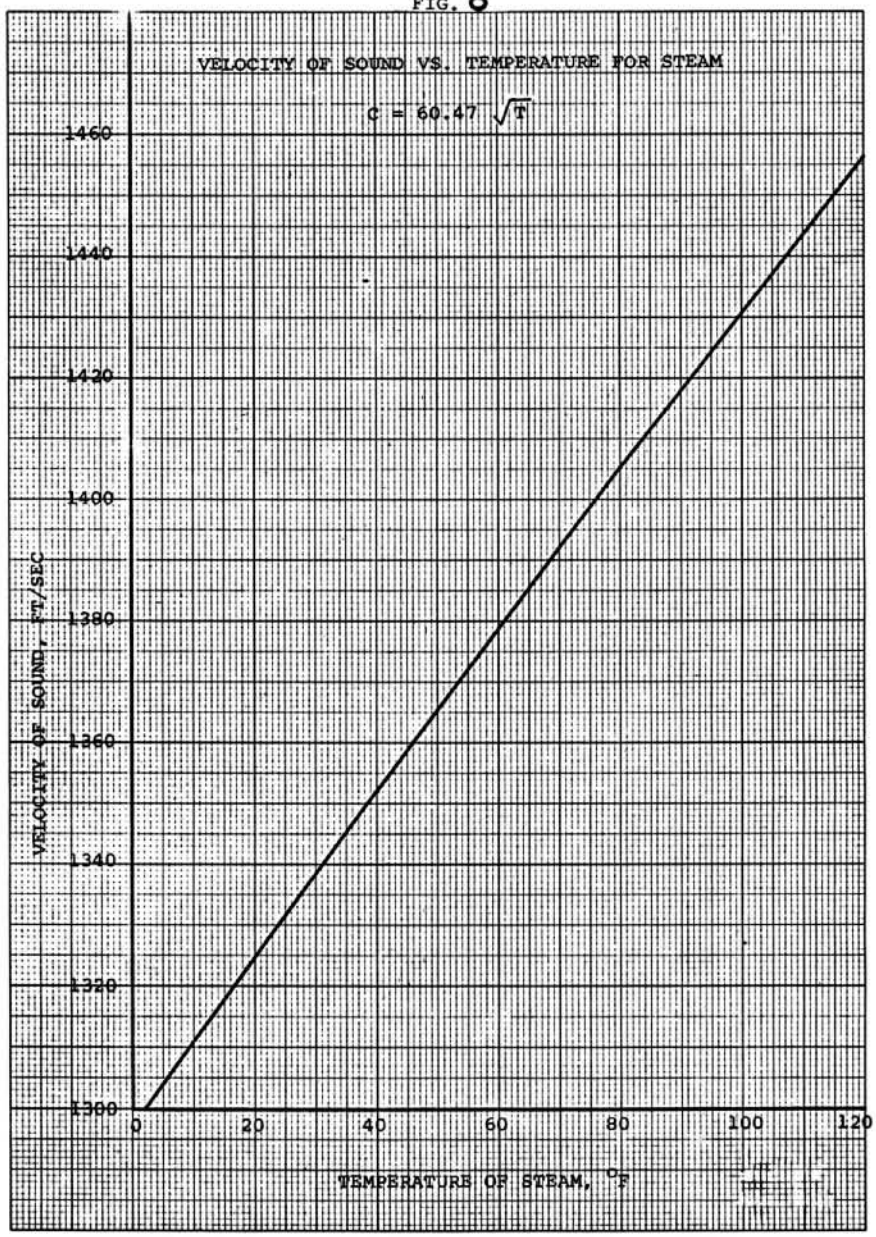
VELOCITY OF SOUND VS. TEMPERATURE FOR STEAM
$C = 60.47 \sqrt{T}$
VELOCITY OF SOUND, FT/SEC
1460
1440
1420
1400
1380
1360
1340
1320
1300
0
20
40
60
80
100
120
TEMPERATURE OF STEAM, °F

FIG. 9

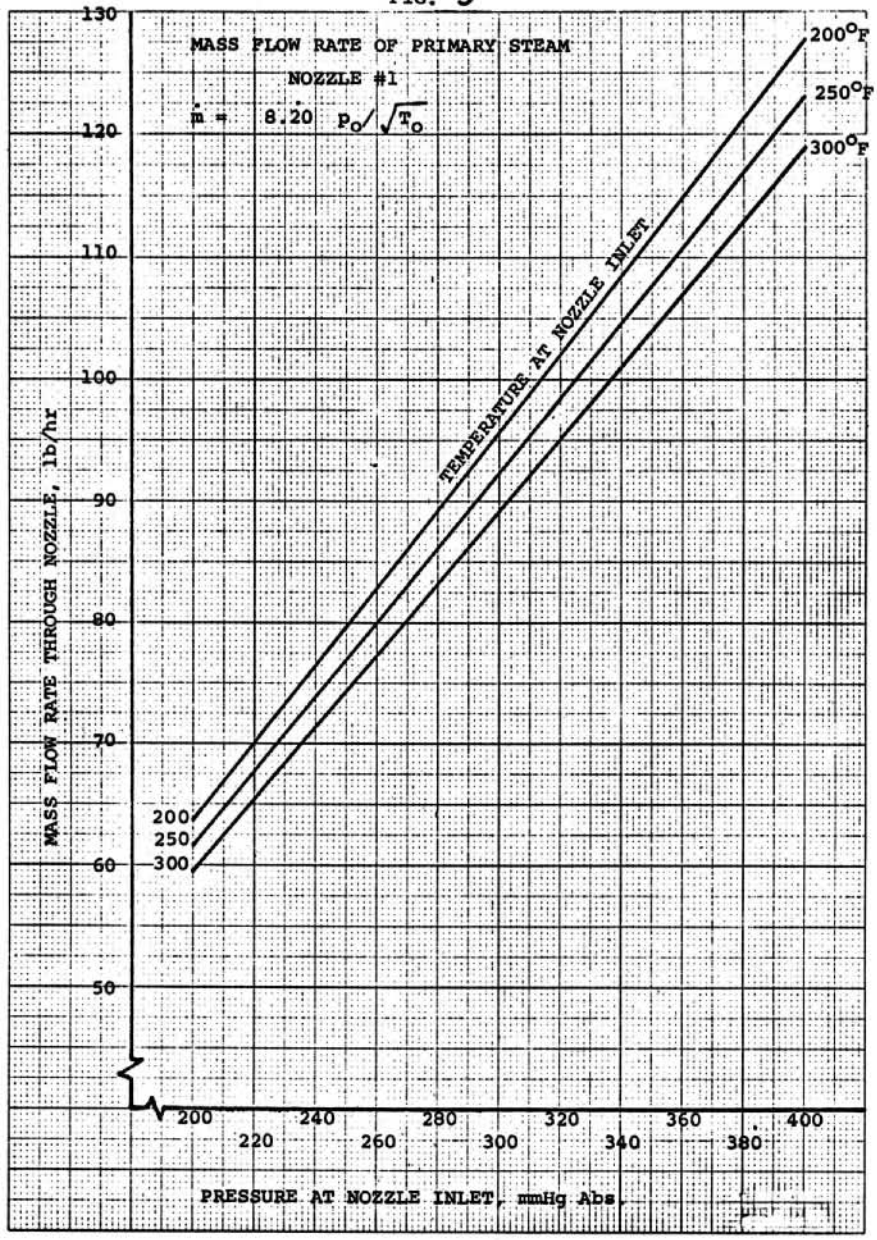
MASS FLOW RATE OF PRIMARY STEAM
NOZZLE #1
$\dot{m} = 8.20\ p_o/\sqrt{T_o}$
MASS FLOW RATE THROUGH NOZZLE, lb/hr
130
120
110
100
90
80
70
60
50
200
250
300
TEMPERATURE AT NOZZLE INLET
200°F
250°F
300°F
200
220
240
260
280
300
320
340
360
380
400
PRESSURE AT NOZZLE INLET, mmHg Abs

NOTES

1. NOTED DIA'S MUST BE CONCENTRIC WITH .609 DIA. WITHIN .003 TIR
2. 250/ ALL OVER EXCEPT AS NOTED.

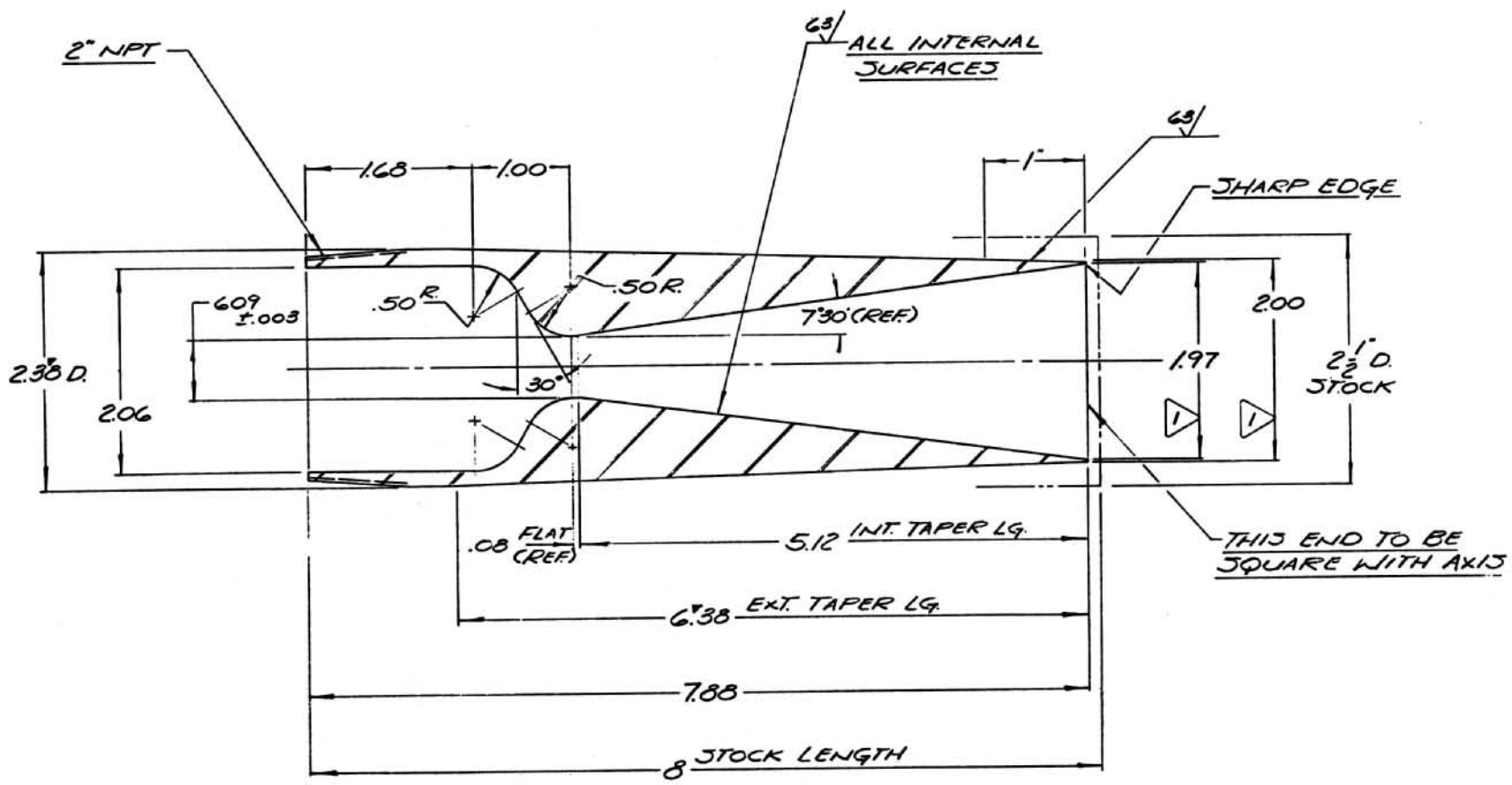

TEST EJECTOR
NOZZLE
FIG. 10

451-332 O - 71 (Face p. 71) No. 2

NOTES

1. NOTED SURFACES MUST BE SQUARE WITH CONE AXIS.
2. NOTED WELDS MUST BE CONTINUOUS & VACUUM TIGHT.
3. ALL INTERNAL WELD SEAMS TO BE GROUND. ALL INTERNAL SURFACES TO BE FREE OF BURRS. TRANSITION BETWEEN CONE & CYLINDER MUST BE SMOOTH & GRADUAL.

PAINT NOTES

PRIME ALL OVER ACCORDING TO ENG'R'G INST. 9305-FM.

FINISH COAT INSIDE SURFACE WITH "PLASITE" EPOXY POLYMID #7533H (WHITE) ACCORDING ENG'R'G INST. 9300-FM.

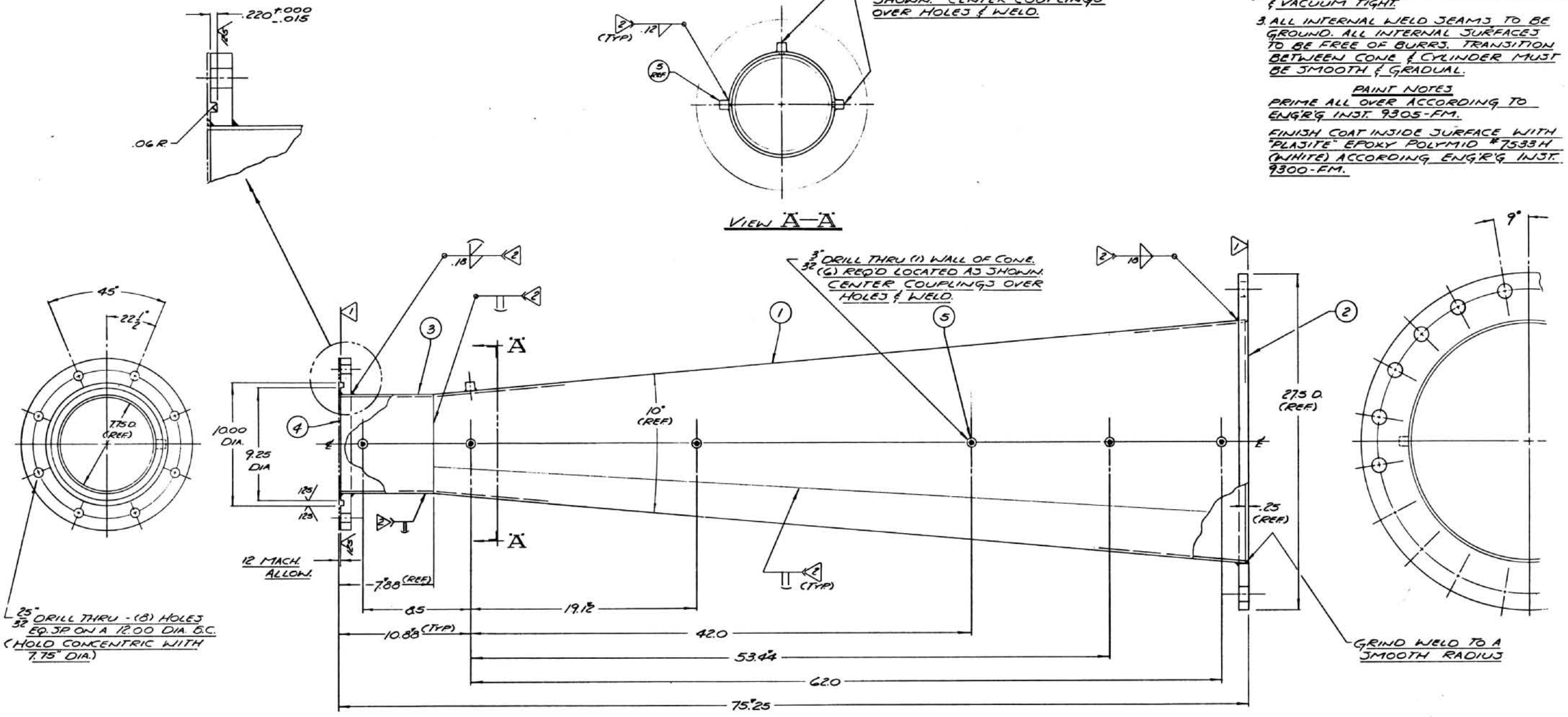

TEST EJECTOR
DIFFUSER
FIG. 11

70

451-332 O - 71 (Face p. 71) No. 3

FIGURE V-12 EJECTOR BENCH TEST FACILITIES
Steam Desuperheater, Steam Piping and Controls

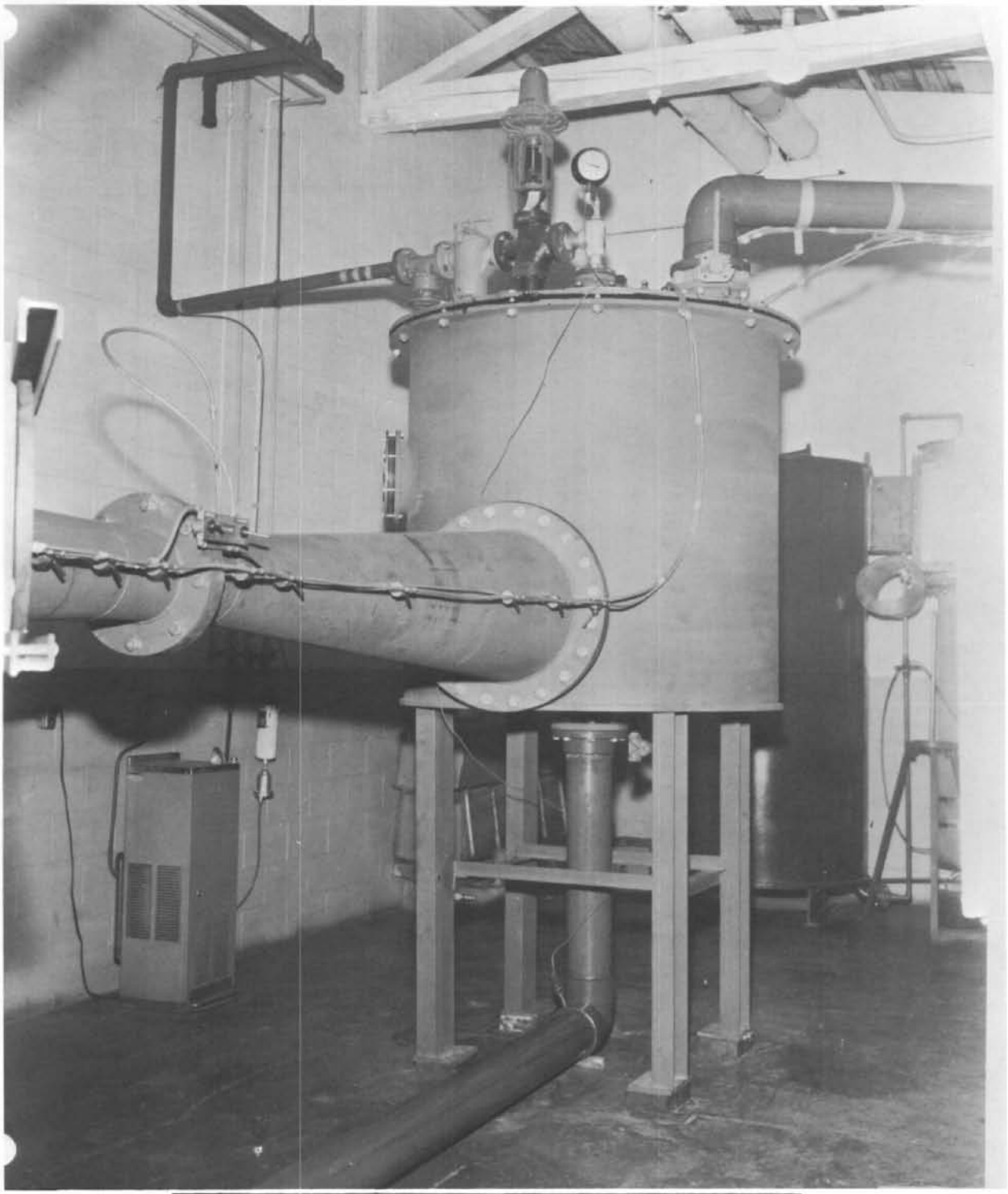

FIGURE V-13 EJECTOR BENCH TEST FACILITIES
Test Ejector and Spray Condenser

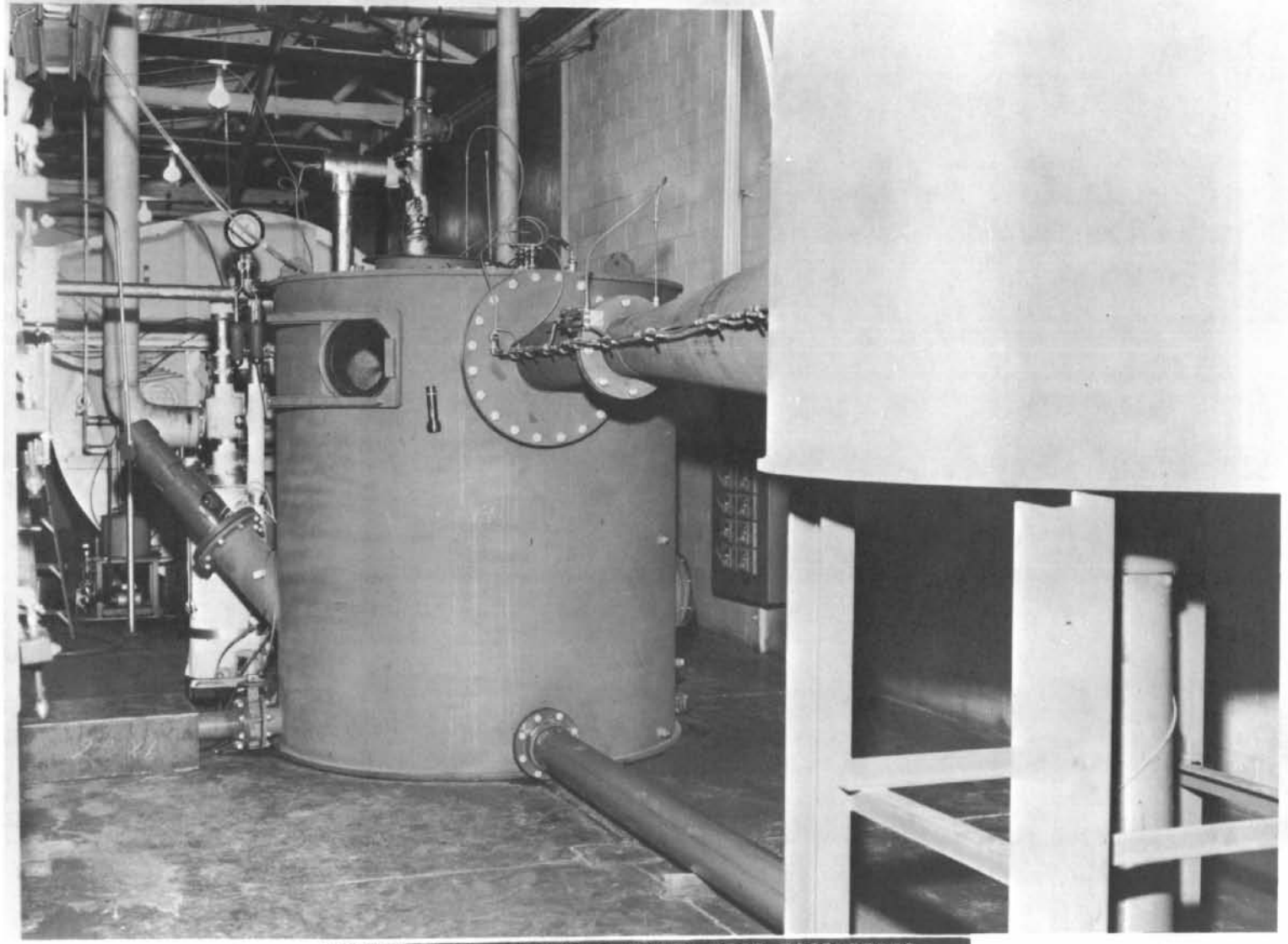

FIGURE V-14 EJECTOR BENCH TEST FACILITIES
Test Ejector and Evaporator

VI. ABSORBER BENCH SCALE TEST

Experimental test work was conducted to determine the performance of various absorber configurations for achieving optimum heat and mass transfer with minimum surface area. Various tube bundle core designs were tested, of various configurations, tube spacing arrangements and tube sizes. Analytical and experimental work was conducted to determine the parameters effecting the mass and heat transfer coefficient at various temperatures and NaOH concentration.

A 6000 gpd open and closed cycle bench scale test loop was erected at Colt's Power Systems Division Laboratory in Beloit, Wisconsin. The hydraulic and mechanical operation of the test loop was excellent, with continuous six hours per day operation, during eight months of testing.

Results and Conclusions

1. Heat Transfer Coefficients

   The heat transfer coefficient was found to be dependent on the viscosity by a relationship of the form;

$$h_{ca} \propto \mu_m^{-.75}$$

   one should note that the viscosity is a function of the NaOH concentration and temperature.

   The potential for heat transfer is based on the log mean temperature difference between the NaOH solution and the cooling water.

   The heat transfer coefficient obtained during bench scale testing is plotted in Fig. 1.

2. Mass Transfer Coefficients

   Mass transfer coefficients for water vapor into NaOH solution of up to 6#/hr.-Ft.^{2}-mmHg have been obtained during bench scale testing. The mass transfer coefficient was found to be dependent on the viscosity by a relationship of the form;

$$u_{am} \propto u_m^{-3.85}$$

As in the case of the heat transfer coefficient, the rate at which the NaOH solution is sprayed over the tubes and the rate of absorption of water vapor have no direct effect on the mass transfer coefficient, u_{am}

The driving potential for mass transfer is based on the log mean difference between the pressure of water vapor in the absorber and the vapor pressure of the sodium hydroxide solution.

The mass transfer coefficient obtained during bench scale testing is plotted in Fig. 2.

3. NaOH Carry Over

During the entire period of testing checks were made periodically to determine if there was any carryover of NaOH solution from the concentrator. The steam boiled off in the concentrator was condensed and the condensate tested by phenolphthalein indicator for the presence of any sodium hydroxide in it. The tests were negative, therefore, it was concluded that no carryover of the NaOH occurred with the steam in the concentrator.

4. Vapor Pressure of NaOH Solution

The vapor pressure of NaOH solution is a very important property, as this is used to determine the driving potential for mass transfer. Vapor pressure is a function of the concentration and the temperature of the NaOH solution. Vapor pressure data is available in literature, but the two sources of information * available did not agree with each other. Therefore, vapor pressure data was developed in the laboratory and is shown plotted in Fig. 3.

The data generated in the laboratory agrees with the data shown in the Caustic Soda Handbook in the entire range of interest and with Perry's Handbook data within the range of 40-42% concentration. At concentrations higher than 42% the lab data differed progressively with Perry's data.

*1. Perry, Chemical Engineers Handbook, 3rd Ed., p. 173.
2. Caustic Soda Handbook, published by Diamond Chemical.

All but one of the solutions used to measure the vapor pressure were made from NaOH flakes (these same flakes were used to prepare NaOH solution for the absorber loop). In order to determine if the NaOH solution which had been in the loop for several months had different vapor pressure properties than the freshly made solutions, one of the samples tested for the vapor pressure was taken from the loop. It was found that this solution had the same vapor pressure properties as the freshly prepared solutions.

Throughout this report the vapor pressure data has been taken from Fig. 3.

5. Nozzle Spray Angle and Pressure Drop

Nozzles used in the absorber were square pattern nozzle, standard and wide angle, purchased from the Spraying Systems. It is important to know the pressure drop across the nozzle and the spray angle for various flow rates and for various nozzles, as these were found to be different from the published data (which was supposedly for water). In general, the spray cone angle was much narrower and the pressure drops much greater than published. Also it was observed that the spray was much wider in spread and much more atomized when the absorber was at atmospheric pressure than when the absorber was at operating pressures. The spray nozzle characteristics are tabulated on the following page.

It is recommended that wide angle nozzles be used as these have wider spray angles. Material could be steel, PVC or stainless steel.

6. Optimum Recirculation Rate

Recirculation rate did not appear to have any direct effect on either the heat or the mass transfer rates. Therefore, it is sufficient to recirculate only as much of the NaOH solution as is necessary to keep all the tubes wet. It was observed that a recirculation (spray) rate of 5 gpm/ft.^{2} of the top cross sectional area of tube bundle was adequate.

451-332 O - 71 - 6

SPRAY NOZZLE CHARACTERISTICS (at absorber operating pressure)

Nozzle Size & Model #	Flow Rate GPM	Spray Cone Angle, °	Differential Press. PSI	Remarks
1/2 HH 35 W SQ Steel (Wide Angle)	2.0 3.0 4.0	50 55 57	19 28 31	Poor spray pattern for flow less than 2 gpm
3/8 HH 15 SQ PVC	2.0	45	35	
1/2 HH 29 SQ PVC	3.3 6.0	45 47	26 35	Poor spray for less than 3 gpm
3/4 HH 50 SQ PVC	4.3 5.3	45 47	14 29.5	Poor spray for less than 4 gpm

7. Tube Bundle Design

Horizontal spacing of tubes is very important for proper dripping of NaOH solution. If this spacing is too small the NaOH solution does not drip over the tubes vertically below, rather it sticks to the tubes diagonally below. This results in dry patches on the tubes. On the basis of experience gained from the tube bundles tested it is recommended that the horizontal spacing between the tubes be no less than 1/2".

Vertical spacing between the tubes is not critical. Therefore, it can be determined on the basis of the mechanical strength of the end plates and the arrangement of headers, etc.

If the tube bundle is very wide and the vapor has to go through a number of column of tubes to reach the inner columns of the tube bundle then the vertical clearance should be designed to provide adequate free passage to vapor into the tube bundle. In general, this requirement is not critical.

8. Selection of Material

A guide for material selection is presented below. No attempt is made to include all the material that could be used, rather, this guide includes only those materials that have been tried and found to be adequate. Also, whenever possible, cheaper material is specified if it can be used.

GUIDE FOR MATERIAL SELECTION

Component	Cold NaOH Soln. 140°F Conc 50%	Hot NaOH Soln. 140°F Conc 50%
a. Piping	Steel (prefer), PVC	Stainless Steel
b. Pumps	All parts C.I. or steel	All wetted parts stainless steel or molded epoxy
c. Vessels	C.I. or steel with coal tar epoxy	Stainless steel
d. Heat Exch.	Stainless Steel	Stainless Steel
e. Absorber: Vessel	C.I. or steel with coal tar epoxy	-

GUIDE FOR MATERIAL SELECTION (Continued)

Component	Cold NaOH Soln. 140°F Conc 50%	Hot NaOH Soln. 140°F Conc 50%
Tubes	Carbon steel	-
End plates & headers	Steel	-
Nozzles	Steel	-
Bolts & Nuts, etc.	Steel	-
f. Concentrator Vessel	-	Stainless Steel
Tubes	-	70-30 Cu-Ni
End plates & headers	-	Stainless Steel
Bolts & Nuts, etc.	-	Stainless Steel
g. Gaskets, seals, packings, etc.	Nylon-Type 6, Neoprene	Nylon-Type 6, up to 300°F. Teflon up to at least 300°F. Penton, below 250°F. Molded or extruded chloroprene (Neoprene) up to 240°F. Molded or extruded Butyl (Isobutylene-isoprene), up to 300°F. Butadiene-Acrylonitrite (Nitrite), up to 250°F
h. For sealing threaded joints	Teflon tape Locktite Glyptol paint (for vacuum lines).	Teflon tape Locktite

Discussion

1. Heat Transfer

Driving Potential:
The hot NaOH solution is sprayed over the tube bundle and then it trickles down. The cooling water enters at the bottom row of the tube bundle and after a number of passes leaves the tube bundle at the top row. As such it is nearly a counter flow heat exchanger and overall potential for heat transfer shall be log mean temperature difference, defined as

$$LMTD = \frac{(T_{10} - T_3) - (T_6 - T_2)}{\ln((T_{10} - T_3)/(T_6 - T_2))}$$

This LMTD is then corrected for the fact that the flow is not truly counter current and the correction factor * was found to be about .95, so

$$\Delta T_a = .95 \frac{(T_{10} - T_3) - (T_6 - T_2)}{\ln((T_{10} - T_3)/(T_6 - T_2))}$$

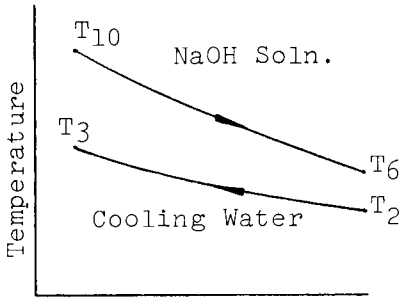

Overall Heat Transfer Coefficient:
It is defined as follows -

$$H_{aw} = U_a A_a \Delta T_a$$

where H_{aw} is the total heat transfer in the absorber

computed as $H_{aw} = Q_{wa} (T_3 - T_2)$

where Q_{wa} is the cooling water flow rate

$(T_3 - T_2)$ is the temperature rise of the

cooling water

A_a is the total tube bundle surface area for heat transfer

*Krieth, Principles of Heat Transfer, 2nd Ed., International Textbook Co., Fig. 11-12

Mechanism of Heat Transfer:
As the water vapor is absorbed on the exposed surface of the NaOH solution film over the tubes, the latent heat of vaporization is released on that surface. This heat then flows through the film of the solution by conduction and by diffusion. The thermal diffusion is controlled mainly by viscosity while the conduction is controlled by the thermal conductivity of the solution and the thickness of the film. Thickness of the falling film of NaOH solution is controlled by the viscosity of the solution. The convection of heat from the solution to the cooling tube is also controlled by viscosity via Reynolds Number.

Tests were run without absorbing any vapor in the absorber. The NaOH recirculation rate, Q_{sr}, was maintained at 13 gpm.

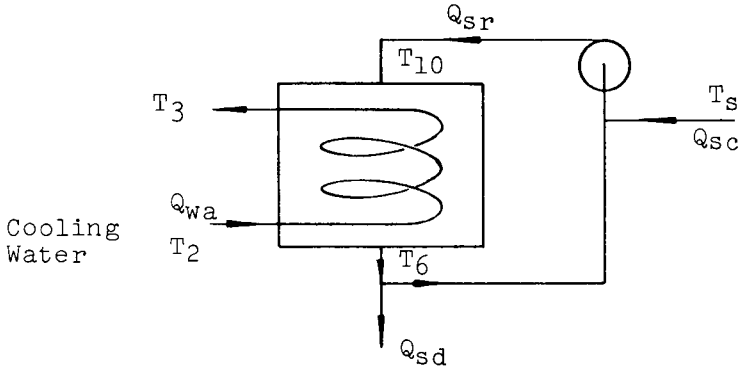

and the concentration of the solution in the whole loop was at about 49% (no absorption or regineration). The heat load on the absorber was raised by changing T_8 and Q_{sc} and thereby T_{10}. Also Q_{wa} was changed by setting different values for T_6.

All the tests were done on tube bundle #2.

Overall heat transfer coefficient, U_a, was computed on the basis of tube surface area using the mean tube diameter, i.e., (I.D. + O.D.)/2. The conductive resistance in the tube metal was neglected. Heat transfer coefficient on the water side, h_{aw}, was then computed and from these the heat transfer coefficient on the NaOH side, h_{as}, was computed using the equation

$$1/U_a = 1/h_{aw} + 1/h_{as}$$

The summary of the data collected and the results of computation are tabulated in Table 1.

Experimental data is plotted in Fig. 1. It shows that the heat transfer coefficient is a function of the mean viscosity, μ_m of the NaOH solution and can be expressed as

$$h_m \propto \mu_m^{-.75}$$

Apart from the viscosity various other physical properties also have an influence on the heat transfer rate, e.g., density, chemical conductivity, etc. but within the operating ranges of the temperature and concentration in the absorber these properties do not change very much, while the viscosity changes considerably.

2. Mass Transfer

Driving Potential:
The driving potential for the mass transfer is the difference between the vapor pressure of the NaOH solution and the pressure of the water vapor in the absorber. The water vapor pressure in the absorber is essentially constant everywhere because the velocities are very low. The vapor pressure of the NaOH solution is a function of the concentration of the solution and its temperature.

As the NaOH solution flows over the tubes it absorbs some water vapor and thus its concentration decreases. The temperature of the NaOH solution also changes as it flows down the tubes, as a result of cooling from the cooling tubes and heating due to the absorption of the water vapor. Due to the changes in the concentration and the temperature of the NaOH solution the vapor pressure of the NaOH solution also changes as it flows down the tubes. It can easily be shown by qualitative discussion that the change in the vapor pressure of the NaOH solution is unidirectional (i.e., either increases or decreases, but not both) and continuous from the inlet to the outlet of the absorber as follows:

The data has shown that the change in the concentration across the absorber is small, about 1%, and therefore the vapor pressure is almost entirely controlled by the temperature of the

solution. The temperature of the solution tends to increase due to the absorption of the water vapor (vapor releases its latent heat) and tends to decrease due to the cooling from the cooling coils. The heating and the cooling rates tend to self adjust; if the temperature of the solution is high the cooling rate increases because of larger temperature potential and the absorption rate (and hence the heating rate) decreases because of lower potential for mass transfer. The converse is true too. In the absorber the solution enters at high temperature (about 80-100°F) and leaves at lower temperature (about 70-80°F). It is inconveivable that the temperature of the solution would increase beyond the entering temperature. The temperature of the solution would be decreasing continuously as it flows over the tubes.

The above point is established with only one purpose, that is, to establish a criteria for overall potential for mass transfer. Even though the actual vapor pressure of the solution is not known throughout its flow in the absorber, it can be assumed that the vapor pressure changes continuously from the inlet to the outlet. Under these conditions the overall potential for mass transfer will be taken as the log mean vapor pressure differential, defined as

$$\Delta P_a = \frac{(P_{va} - P_{sd}) - (P_{va} - P_{sr})}{\ln((P_{va} - P_{sd})/P_{va} - P_{sr}))}$$

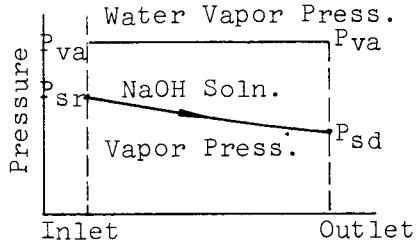

Mass Transfer Coefficient:
Striking the analogy between the heat and mass transfer, the overall mass transfer coefficient in the absorber, U_{am}, is defined as follows:

$$\dot{m}_v = U_{am} A_a \Delta P_a$$

where $\dot{m}_v$ is the mass of the vapor absorbed in the absorber A_a is the total surface area (of the tube bundle) available for heat and mass transfer.

Mechanism of Mass Transfer:
As NaOH solution flows over the tubes it absorbs water vapor on its exposed surface. As water vapor is absorbed the NaOH solution at the surface becomes diluted and heated, and these increase the vapor pressure of the solution, thereby reducing the potential for further mass

transfer. In order that the water be absorbed continuously the water molecules must diffuse into the layer of NaOH solution to raise the concentration on the surface. This diffusion is controlled by the viscosity of the solution. In addition to the diffusion of mass the heat must also be carried away from the surface towards the cooling tube.

A number of tests were run for absorber performance. The data and the results are summarized in the Table 2.

Test #2 through #11 were made on tube bundle #1 and the rest of the tests were made on the tube bundle #2. In plotting the relationship between the mass transfer coefficient and the mean viscosity only tests on tube bundle #2 were used.

Various tests were conducted on tube bundle #2 by varying the NaOH recirculation rate, absorber temperature and rate of absorption. Considering all these variations it is remarkable that the mass transfer coefficient corelated so well with the mean viscosity.

Mean viscosity was computed on the basis of mean NaOH temperature, i.e., $(T_6 + T_{10})/2$, and the mean NaOH concentration, i.e., $(C_r + C_d)/2$, across the absorber. Viscosity curves were obtained from Caustic Soda Handbook, published by the Diamond Chemical Co.

The data for each run included, either the determination of the concentration of the NaOH solution samples by titration and direct measurement of temperatures in the loop, or, the direct measurement of the vapor pressures and temperatures of the NaOH samples from the loop. In each case the vapor pressure curve was used to find the vapor pressure of the NaOH solution at the inlet and the outlet of the absorber.

The mass of the vapor absorbed in the absorber was computed from the mass of the vapor boiled off in the concentrator at steady state operation. Mass of the vapor boiled off in the concentrator was measured by timed weighing of the condensate of the steam used to heat the concentrator. Condensate was collected in a can of known volume. Another method available for finding the mass of the vapor boiled off in the concentrator was to measure the condensate of the vapor

boiled off. The condensate was collected in a gaging tank under vacuum. The vacuum pump removed a portion of this vapor (before condensation) along with the non-condensibles from the condenser. The amount of vapor removed by the vacuum pump was not constant, nor known, as this depended upon the operating temperature of the vacuum pump and the condenser. This, along with the fact that the gaging tank level was hard to measure accurately, made this method unreliable.

The mass transfer experimental data is plotted in Fig. 2, it shows the coefficient is a function of the NaOH mean viscosity, μ_m, and can be expressed as

$$K_{om} \propto \mu_m^{-3.85}$$

Absorber Test Facilities

The absorber/concentrator test facilities were located at Colt's Power Systems Division Laboratories. The test loop and absorber/concentrator components were designed to simulate actual VFEA process conditions and component requirements. The heat transfer surface areas were based on an equivalent 6000 gpd pilot plant requirements.

The test loop was designed to operate either on open or closed loop so that modification could be made without interrupting the test schedule. The operation of the loop, hydraulically, mechanically, and thermally was excellent. The test loop operated 6 hours per day continuously during 8 months of testing.

Fig. 4 shows the absorber/concentrator schematic along with the process controls and instrumentation.

Operation of the Loop:

Generator contains water which flashes off to produce vapor which is absorbed in the absorber. In order to prevent the water from freezing (due to evaporative cooling) the circulating water coils maintain a temperature of 35-40°F in the generator. This results in a pressure of about 6 mm Hg abs. in the generator. This vapor is led into absorber through a 10" pipe (to keep velocity low) and a butterfly valve, photo Figure 5.This valve throttles the vapor down to the pressure desired in the absorber (about 3.3 mm Hg abs.). The absorber is thus filled with the vapor to be absorbed by the NaOH solution.

The absorber contains a tube bundle through which cold water is circulated to cool the NaOH solution which flows over the coils, photo Fig. 6. Concentrated NaOH solution enters the absorber at the top and is sprayed uniformly over the cooling boils by three nozzles. As the solution flows over the tubes it absorbs water vapor and is kept cool by the coils. Dilute solution is collected at the bottom.

A small amount of dilute NaOH solution (2-3 gpm) is pumped by the dilute pump into the concentrator through a heater. The heater raises the temperature of the solution almost up to its boiling temperature in the concentrator. In the concentrator, photo Fig. 7, more heat (by shop steam) is added and sufficient amount of water boiled off to concentrate the solution. This concentrated solution is pumped by a concentrate pump into a cooler where the solution is cooled down to about 80-110°F. This cooled concentrated solution is then mixed with the dilute solution from the bottom of the absorber and pumped by the

recirculation pump into the absorber. This completes the cycle for NaOH solution.

The steam boiled off in the concentrator is condensed in a condenser and the condensate collected in a tank, under vacuum.

A bypass line is installed which permits the operation of the absorber or the concentrator alone, if so desired. Most of the testing was done on a closed NaOH solution loop, and thus the bypass line was not used. A drain, for NaOH solution, is provided in the bypass line, to drain off excess NaOH solution or to empty the system. Drain is on the discharge side of the dilute and the concentrate pump and thus the drainage occurs under pressure.

A NaOH make-up tank is provided on the suction side of the dilute pump to fill the system (or make-up) with the NaOH solution.

Non-condensibles are removed from the Absorber, the Concentrator and the generator (only during the start up) by the vacuum pumps as shown.

Controls:

The temperature in the absorber, the generator, the heater and the cooler were controlled by self contained automatic temperature regulators. The level in the absorber was controlled by a pneumatic level controller. The level in the concentrator was not directly controlled, as the amount of NaOH solution in the loop was fixed and the level was controlled in the absorber. A high and low level alarm was used in the concentrator to warn the operator should a malfunction occur. The butterfly valve in the 10" line was manually controlled to maintain a desired vapor pressure into the absorber. Once the loop reached a steady state this butterfly valve needed no manipulation.

Amount of steam used to heat the concentrator was also manually set. This controlled the amount of steam boiled off in the concentrator and under steady state operations this was equal to the amount of water vapor absorbed in the absorber. As the rate of absorption was one of the variables that was prescribed for a test the steam valve was set for each run. Once set there was no need to adjust it during a test.

Instrumentation:

Figure 4 shows the location of instruments. All the temperatures were sensed by Cu-Constanton thermocouples and recorded on a 24 point strip chart recorder, range 0-300°F. All the pressures (donated by M or Figure 4) were measured by inclined manometers reading absolute pressures (low pressure end of the manometers was maintained at a pressure of less than 10 microns).

The pressure in the concentrator was measured by a Vertical U-tube Absolute Pressure Mercury manometer.

Flow rates of NaOH solution were measured by stainless steel rotameters using a magnetic drive for reading the float positions. Water flow rates were measured by Fullview rotameters. The steam flow rates were measured by collecting the condensate in a can of known volume and measuring the time needed to fill the can.

The rate of absorption in the absorber is equal to the rate at which the steam is being boiled off in the concentrator (at steady state) and this is approximately equal to the rate at which the heating steam is being used in the concentrator. This is true because the NaOH solution enters the concentrator at just about saturation temperature and the steam used for heating has only a slight superheat. Therefore, the rate of absorption in the absorber was measured by weighing the heating steam condensate in the concentrator. Rate of steam boiled off in the concentrator could also have been measured by gaging the condensate from the condenser. This was found to be unreliable and not repeatable because of the difficulty in measuring the level in the tank accurately (tank being of large diameter and sitting on the floor) and also because the vacuum pump was removing some steam with non-condensibles and this amount varied with the pressure and the temperature in the condenser.

Concentration of the NaOH solution was measured by drawing a sample from the loop and titrating it against standard HCl solution (about 1.0 N). From the measured concentration and the temperature the vapor pressure of the NaOH solution may be found, if desired using Figure 3. Conversely, the vapor pressure and the temperature of the sample may be measured directly, using the apparatus shown in photo Fig. 9 and from this data the concentration may be found or the vapor pressure found at a different temperature, using Figure 3.

TABLE 1 HEAT TRANSFER IN ABSORBER

Tube bundle #2
NaOH recirculation rate = 13 gpm
NaOH concentration 49%

#	T_2	T_3	T_6	T_{10}	h_{as}	ΔT_a	ψ_m	Q_{sc}	T_8	Q_w
1	53	75	75	80			50	2.2	90	2
2	53	69	70	77				2.2	90	3
3	53	60	66	70.5	164	11.2	70	2.2	90	10
4	53	56.5	63	69	146	10.7	80	2.2	90.5	21
5	53.5	73	75	82				2.2	100	3.3
6	53.5	57	62	71	160	10.5	80	2.2	100	22.3
7	54	61	68	81	197.5	16.2	53	3.45	108	19.6
8	54	68.5	72	84	243	16.0	50	3.3	108	7.9
9	54	70	74	85	217	16.6	47	3.45	107.5	6.5
10	54.5	78	82	98.5	252	22.8	38	3.75	125	6.5

TABLE 2 SUMMARY ABSORBER TEST DATA

Test No.	T_{10}	C_r	P_a	U_{am}	ΔT_a	h_{as}	Q_{cc}	Q_{sr}	η_m	Remarks
1-2	79	49.8	1.2	1.53	16.9	245	.13	6.8		
1-3	81	49.8	1.0	1.64	17.2	157	.12	6.4		
1-4	75	49.2	1.3	1.3	13.0	222	.12	7.0		Initial tests
1-5	86	50.2	.7	2.4	22.7	65	.12	7.0		Absorber Tube Bundle #1
1-6	81.5	50.2	1.1	1.6	17.6	129	.12	6.0		Poor Spray Pattern
1-7	81.5	51.5	1.4	1.25	17.1	152	.12	6.8		
1-8	91.0	52.2	.6	2.3	27.5	81	.1	6.4		
1-9	81	47.2	.6	2.95	15.5	176	.12	6.0		
1-11	84	48.9	.6	2.7	18.9	162	.12	5.8		
2-1	81	48.5	.8	2.6	15.1	354	.12	10.0	43	
2-2	79	48.7	.9	3.0	19.0	242	.16	12.0	47	
2-3	84	--	--	--	21.2	162	--	10.0	--	
	87.5	49.3	.4	5.1	24.25	146	.12	10.0	39.7	
	83	49.0	.5	5.2	21.7	192	.15	10.0	42.5	
2-4	82	47.1	.8	2.1	17.5	324	.1	13.0	40.5	
	81.5	48.5	.9	3.0	17.0	243	.16	13.0	46	
2-5	84	50.3	1.2	2.1	20.0	229	.15	13.0	50	
2-6	84	47.8	.325	6.0	23.7	132.5	.12	6.0	38.2	
	85	48.2	.345	5.6	24.2	117	.12	6.0	37.7	
2-7	81	47.8	.32	6.0	21.5	184	.12	18.0	39	
2-8	77.5	50.1	1.34	1.5	19.5	155	.12	16.0	54	
2-9	78	50.0	1.52	1.3	17.0	144.5	.12	13.0	60.5	Poor spray pattern
2-10	84	49.5	.55	3.5	23.0	143	.12	10.0	44	
	85	48.0	.33	5.8	22.75	155	.12	10.0	37.2	

ABSORBER CONCENTRATOR TEST
SUMMARY OF RAW DATA

Table 3

TEST NO.		2-1	2-2	2-3	2-4	2-5	2-6	2-7	2-8	2-9	2-10
ABSORBER											
Water Flow Rate gpm	Q_{wa}	10.8	16.7	15.5	14.5	13.9	22.5	18.0	25.5	22.5	13.5
Water Temperature in, °F	T_2	57.0	58.0	54.5	55.0	53.5	55.0	54.0	54.0	54.0	54.0
Water Temperature out, °F	T_3	70.0	68.0	65.0	65.0	65.0	61.0	63.0	59.5	59.0	64.5
Recirculation pump flow rate, gpm	Q_{sr}	10.0	12.0	10.0	13.0	13.0	6.0	18.0	16.0	13.0	10.0
Dilute pump flow rate, gpm	Q_{sd}	1.5	2.5	2.0	2.4	3.0	2.8	2.5	2.85	2.8	2.8
NaOH Temperature in, °F	T_{10}	81.0	79.0	83.0	81.5	84.0	85.0	81.0	77.5	78.0	85.0
NaOH Temperature out, °F	T_6	77.0	75.0	80.0	72.5	74.0	73.5	79.0	75.0	69.0	79.0
Absorber(vapor)pressure mmHg	P_{va}	3.22	3.22	3.36	3.2	3.2	3.2	3.2	3.2	3.2	3.24
Absorber(vapor) temp., °F	T_4	82.5	86.0	90.5	87.0	87.0	89.0	86.0	83.5	86.0	88.0
NaOH concentration in, %	C_r	48.52	49.3	49.7	48.8	50.9	49.7	48.6	50.7	51.0	48.7
NaOH concentration out, %	C_d	48.25	47.9	48.0	48.0	50.8	49.3	47.3	50.5	50.2	48.5
NaOH vapor press.(at inlet) mmHg	P_{sr}	2.62	2.32	2.12	2.64	2.26	2.32	2.18	2.18	1.84	2.54
NaOH vapor press. (at outlet), mmHg	P_{sd}	2.24	2.54	2.10	2.64	2.18	2.06	2.47	1.90	2.2	2.38
GENERATOR											
Water drainage flow rate,gpm	Q_{wd}										
Water temp. out, °F	T_5	55.0	47.0	50.5	49.0	46.0	47.0	46.5	47.5	47.0	46.5
Generator (water) temp,°F	T_1	40.0	33.0	34.0	38.5	36.5	35.0	34.0	38.5	38.0	34.0
Generator (press.) mmHg	P_g	6.0	6.0		5.0	5.0	5.0	4.5	5.0	5.0	5.0
Vapor line (10" dia.) press., mmHg	P_{vp}										
CONCENTRATOR											
Steam press. in, psig	P_c	14.3	10.6	3.0	6.8	5.5	5.9	5.4	4.9	6.2	3.0
Steam temp. in, °F	T_{19}	233.0	225.0	228.0	222.0	220.0	232.0	239.0	220.0	227.5	227.0
Condensate (H.P.steam) flow rate, gpm	Q_{cc}	.122	.163	.146	.155	.15	.118	.116	.12	.117	.116
NaOH temp. out, °F	T_{14}	219.0	207.5	211.0	200.0	200.0	206.0	205.0	200.0	203.0	198.0
NaOH temp. at the bottom °F	T_{16}	214.0	206.0	207.0	199.0	198.0	204.0	203.0	200.0	202.0	195.0
NaOH flow rate out, gpm	Q_{sc}										
NaOH concentration out, %	C_c	49.71	50.0								
NaOH concentration at the bottom, %	C_b										
Pressure in the conc.,mmHg	P_{vc}	136	112	105.0	94.0	83.0	97.0	84.0	85.0	87.0	84.0
Vacuum in the condenser, in. Hg		25"									
Vacuum in the tank, in. Hg		24"									
Condensate (L.P. steam) flow rate, gpm	Q_v	.093	.111	.102	.094	.08		.086	.087	.086	.082
Vap.Press. of conc. NaOH/temp,mmHg/°F			2.61								

451-332 O - 71 - 7

ABSORBER CONCENTRATOR TEST
SUMMARY OF RAW DATA

Table 4

TEST NO.		1-1	1-2	1-3	1-4	1-5	1-6	1-7	1-8	1-9	1-10	1-11
ABSORBER												
Water Flow Rate gpm	Q_{wa}		10.5	11.5	13.2	15.1	10.0	12.25	21.0	11.0		10.5
Water Temp. in, °F	T_2		52.5	56.0	56.5	56.0	56.5	56.5	56.0	56.0		55.0
Water Temp. out, °F	T_3		66.0	66.0	65.0	61.5	66.5	65.8	62.0	66.0		67.0
Recirculation pump flow rate, gpm	Q_{sr}		6.75	6.4	7.0	7.0	6.0	6.8	6.4	6.0		5.8
Dilute pump flow rate, gpm	Q_{sd}		1.62	1.8	1.1	3.1	1.1	1.95	2.3	1.1		1.3
NaOH Temperature in, °F	T_{10}		79.0	81.0	75.0	86.0	81.5	81.5	91.0	81.0		84.0
NaOH Temperature out, °F	T_6		74.0	75.5	73.0	77.0	77.0	75.0	82.0	72.0		76.0
Absorber (vapor)press. mmHg	P_{va}		3.14	3.19	3.16	3.18	3.27	3.19	3.23	3.2		3.22
Absorber (vapor)temp., °F	T_4		85.0	86.0	82.5	89.0	89.0	86.3	91.0	78.0		86.0
NaOH Concentration in, %	C_r			49.55	49.2	50.23	50.20	51.45	52.2	47.21		48.90
NaOH Concentration out, %	C_d		49.48	49.12	48.69	49.86	49.30	51.13	51.88	46.9		48.67
NaOH vapor press. (at inlet) mmHg	P_{sr}											
NaOH vapor press. (at outlet), mmHg	P_{sd}											
GENERATOR												
Water drainage flow rate, gpm	Q_{wd}		13.5							8.18		6.92
Water temp. out, °F	T_5		59.0	59.5	58.0	60.0	60.5	60.2	53.0	52.0		48.0
Generator (water) temp. °F	T_1		50.0	51.25	50.0	51.5	53.0	53.0	46.0	49.0		33.5
Generator (press.) mmHg	P_g		9.0	9.2	7.0	9.0	9.5	10.0	8.0	8.0		5.0
Vapor line (10" dia.) press., mmHg	P_{vp}		3.08	3.13	3.16	3.14	3.26			3.2		3.2
CONCENTRATOR												
Steam press. in, psig	P_c		3.0					3.0		2.5		4.2
Steam temp. in, °F	T_{19}		238.0	243.0	218.0	251.5	223.0	242.0	225.0	221.0		234.0
Condensate (H.P. steam) flow rate, gpm	Q_{cc}		.1281	.12	.1198	.1198	.12	.1198	.096	.1198		.1198
NaOH temp. out, °F	T_{14}		210.0	218.5	206.0	202.0	204.5	205.8	198.0	206.0		212.0
NaOH temp. at the bottom °F	T_{16}		207.5	216.7	204.0	200.0	203.0	205.5	196.0	201.0		208.0
NaOH flow rate out, gpm	Q_{sc}		2.1	1.8	1.5	2.8	1.4	1.71	2.5			
NaOH concentration out, %	C_c		50.54	50.66	51.26	50.64	51.83	52.46	52.86	49.14		51.02
NaOH concentration at the bottom, %	C_b								52.82			
Pressure in the conc., mmHg	P_{vc}		112.0	145.0	88.0	88.0	84.0	94.0	72.0	108.0		117.0
Vacuum in the condenser, in. Hg			27"	26"	28"	30"	30"	29"	29"	26"		26"
Vacuum in the tank, in. Hg			26"	25"	27"	28"	29"	28"	28"	26"		26"
Condensate (L.P. steam) flow rate, gpm	Q_v		.1174	.1198	.0874	.1198	.085	.1165	.071	.1958		.07
Vap. press. of conc. NaOH/temp. mmHg/°F												

Fig. 1 Effect of NaOH viscosity on heat transfer coefficient

(Heat transfer with no mass transfer)

Concentration ≃ 49%

Recirculation rate = 13 gpm

Tube Bundle #2

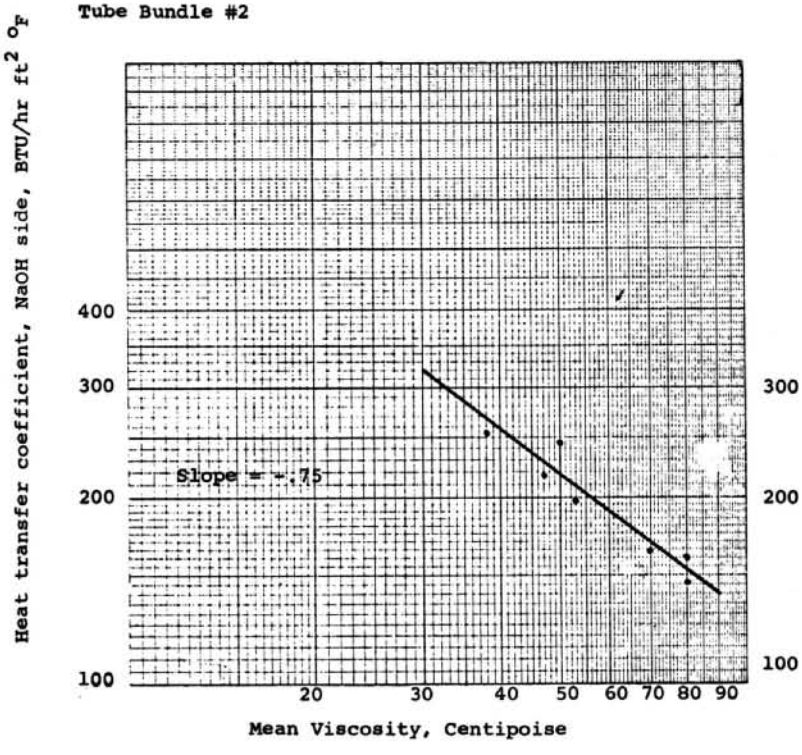

(Computed at mean NaOH soln. temp.)

Fig. 2. Effect of NaOH viscosity on mass transfer coefficient

Tube Bundle #2

(Recirculation rates 6 - 18 gpm)

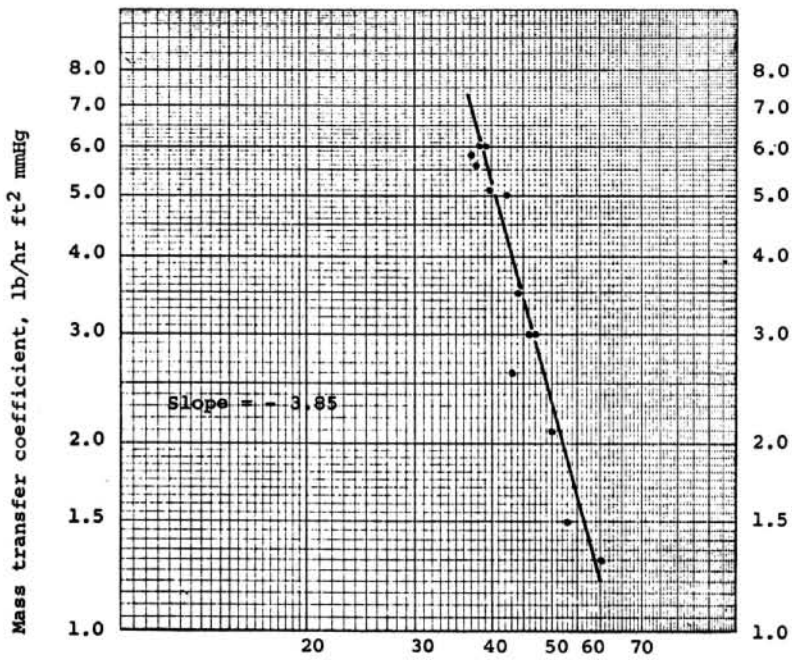

(Computed at mean NaOH soln. temp.)

ABSORBER RESULTS

NaOH Solution Vapor Pressure Data

Fig. 3. (Based on data obtained in the Lab)

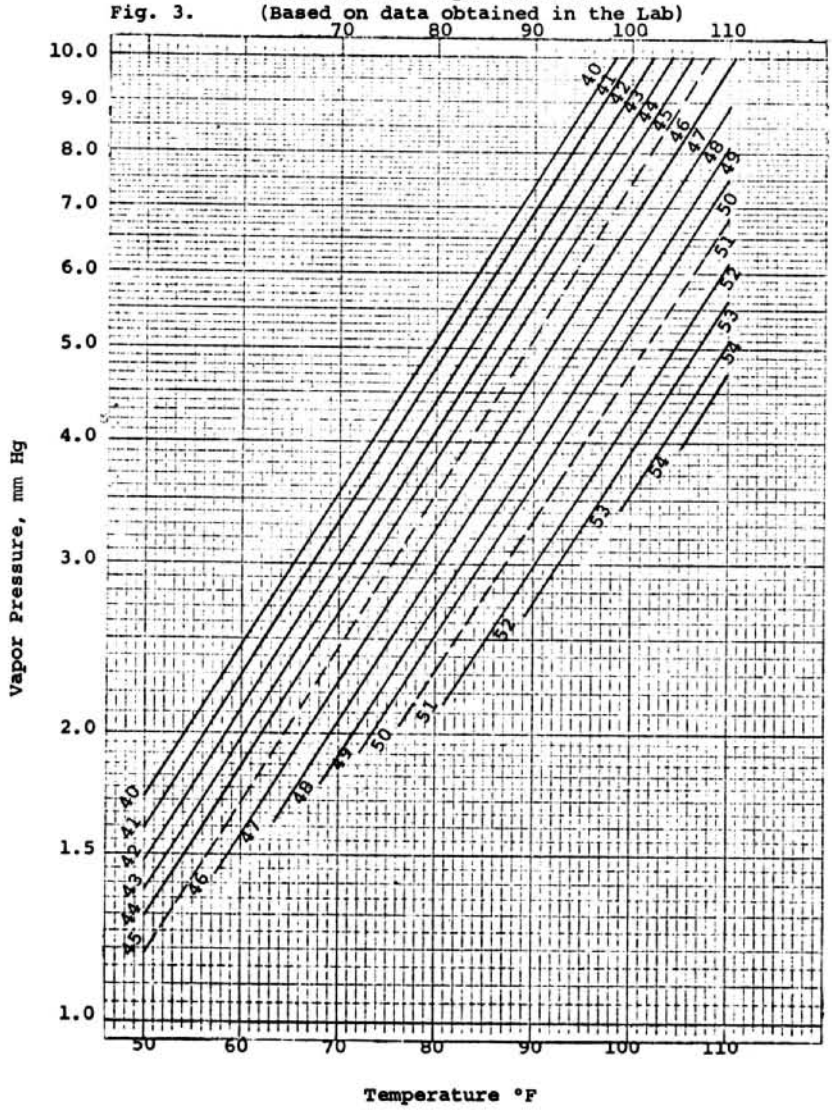

FIG. 4

ABSORBER CONCENTRATOR LOOP

PIPING, INSTRUMENTATION & CONTROLS

INSTRUMENTATION SYMBOLS

B - BOURDON PRESSURE / VACUUM GAGE
C - SAMPLE OUTLET FOR CONCENTRATION MEASUREMENT
G - FLOW RATE MEASURED BY GAGING TANK
M - CONNECT TO INCLINED MANOMETER
R - ROTAMETER
T - THERMOCOUPLE
V - CONNECT TO VERTICAL MANOMETER

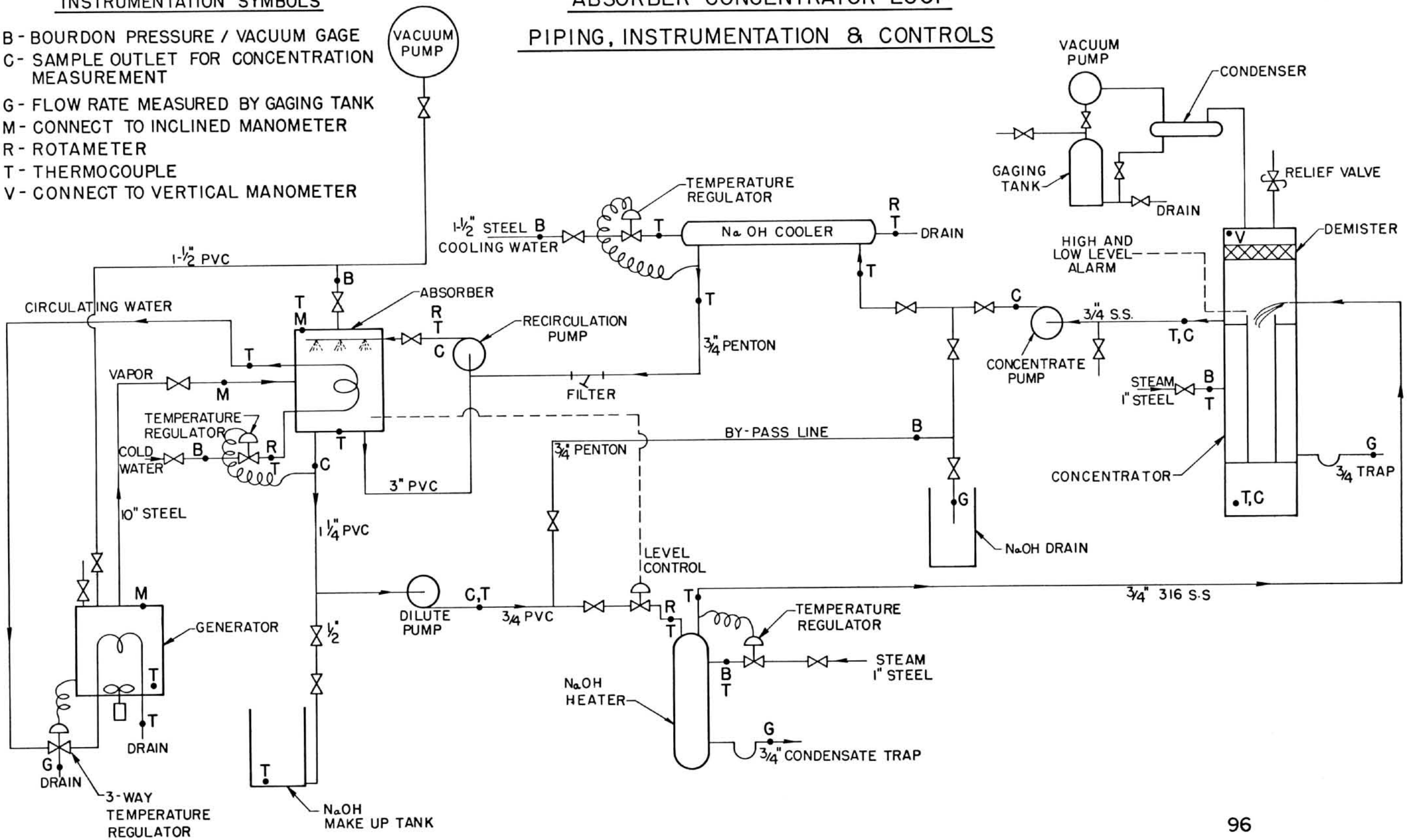

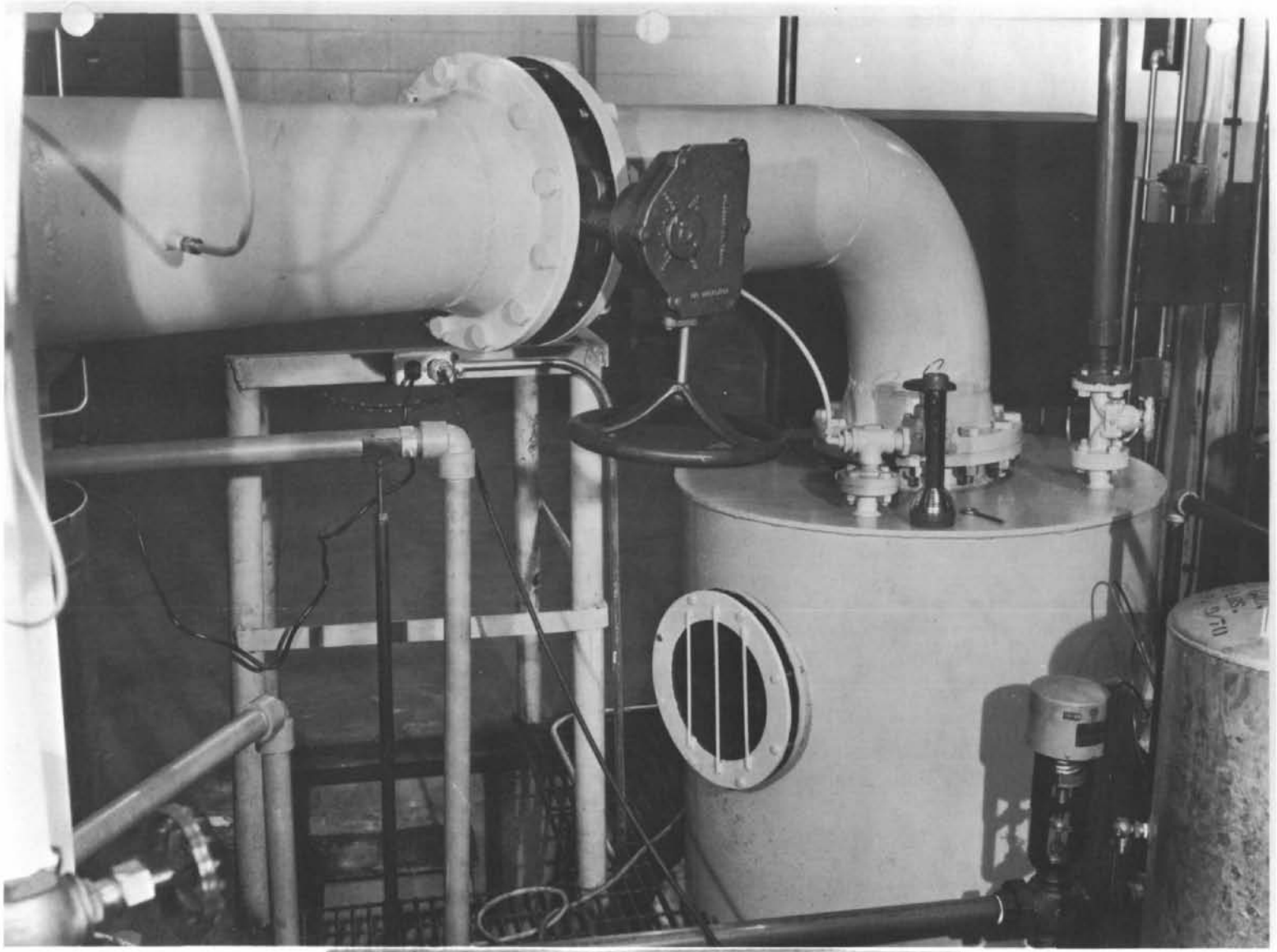

FIGURE VI-5 ABSORBER BENCH TEST FACILITIES
Vapor Generator and Connecting Vapor Line to Absorber.

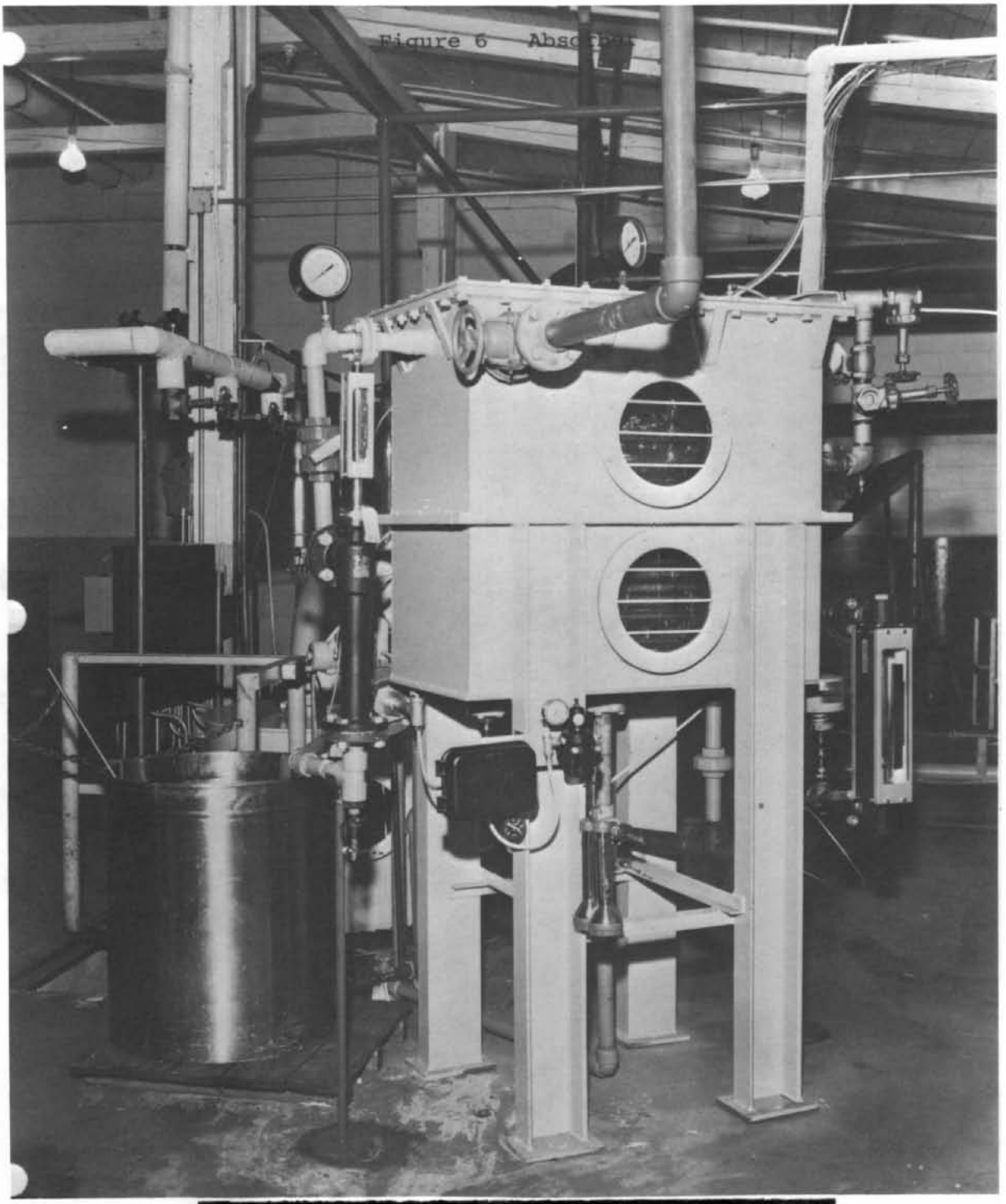

FIGURE VI-6 ABSORBER BENCH TEST FACILITIES
Absorber and NaOH Make Up Tank

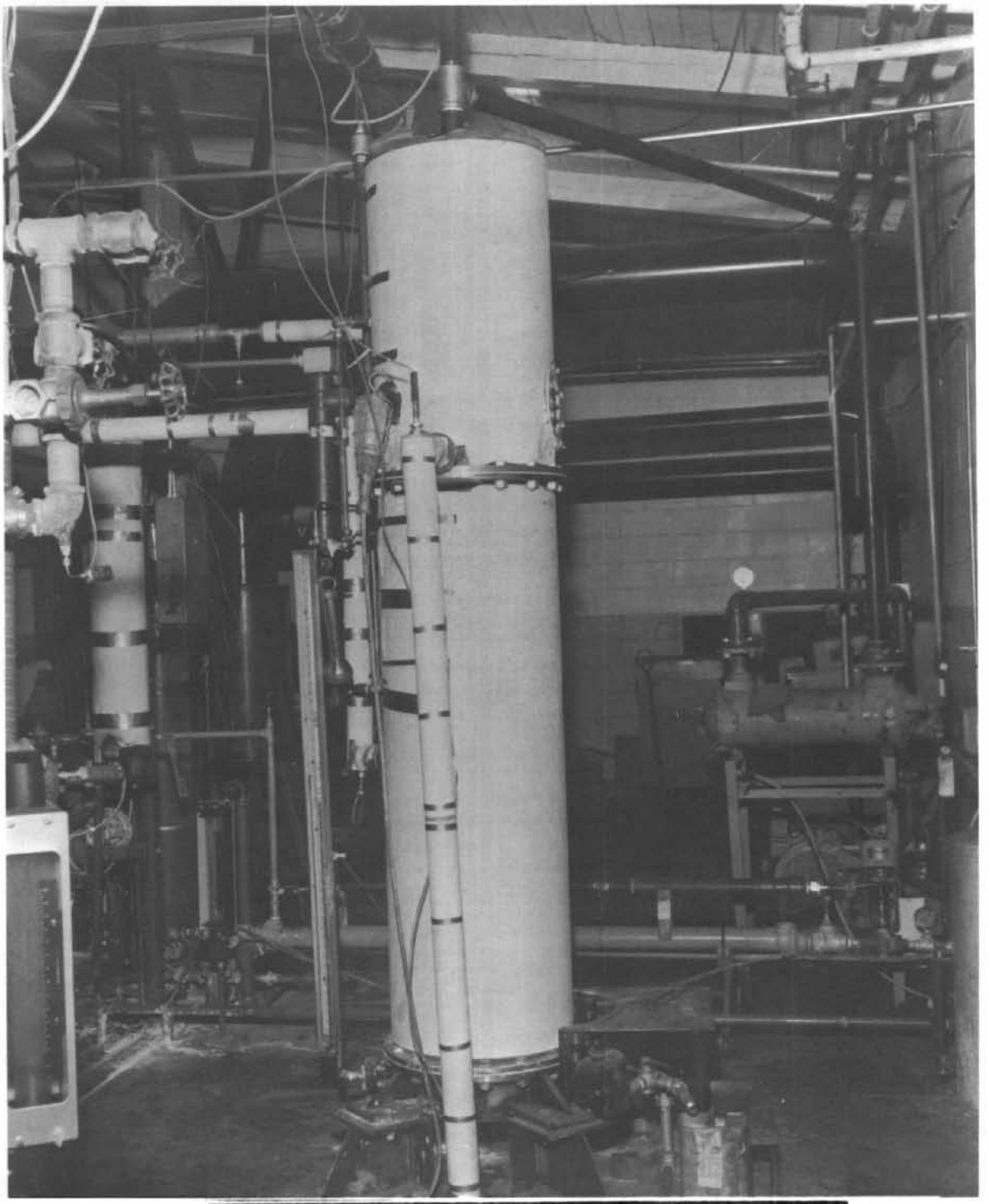

FIGURE VI-7 ABSORBER BENCH TEST FACILITIES
Vertical Concentrator

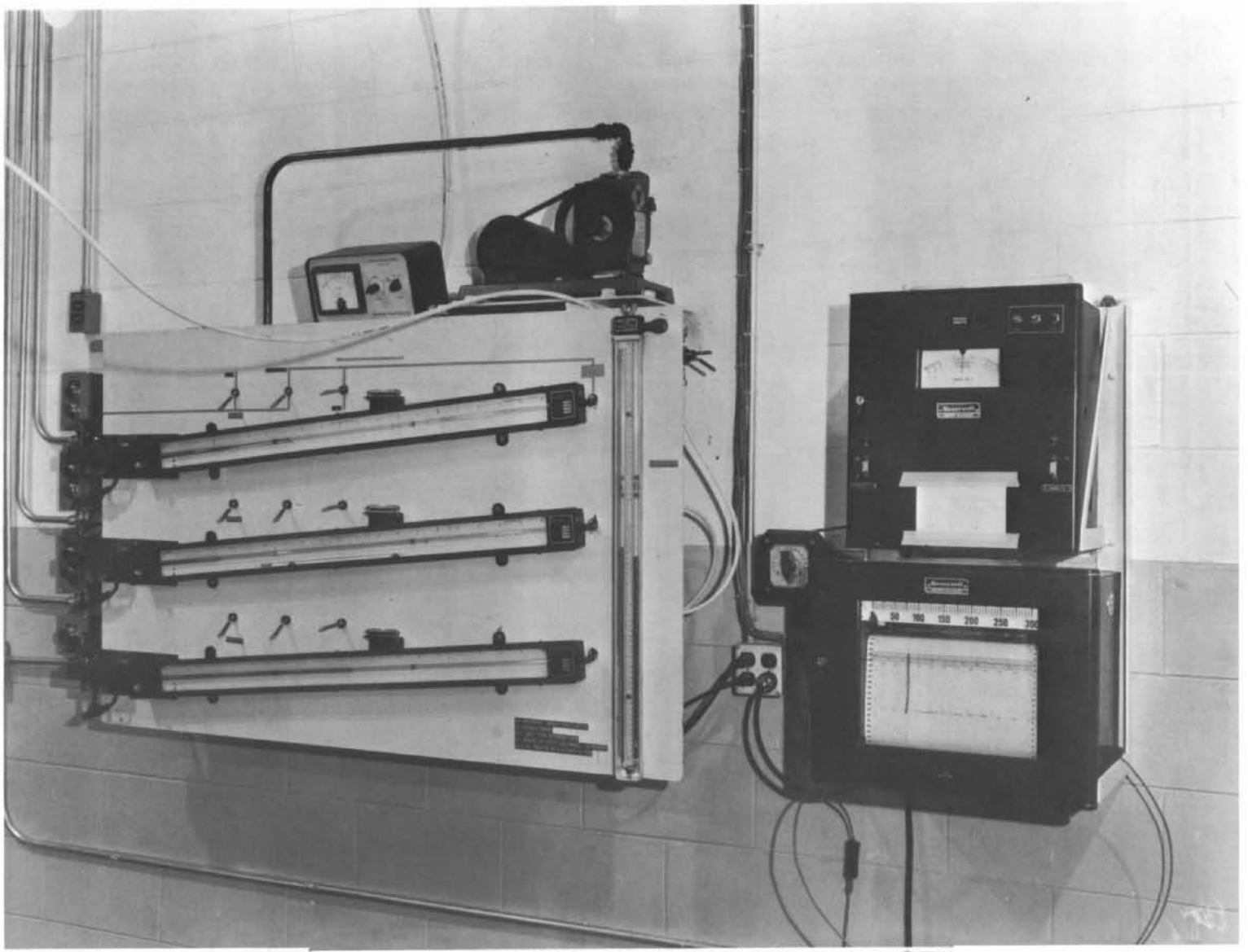

FIGURE VI-8 ABSORBER BENCH TEST FACILITIES
Manometer Panel and Temperature Recorders

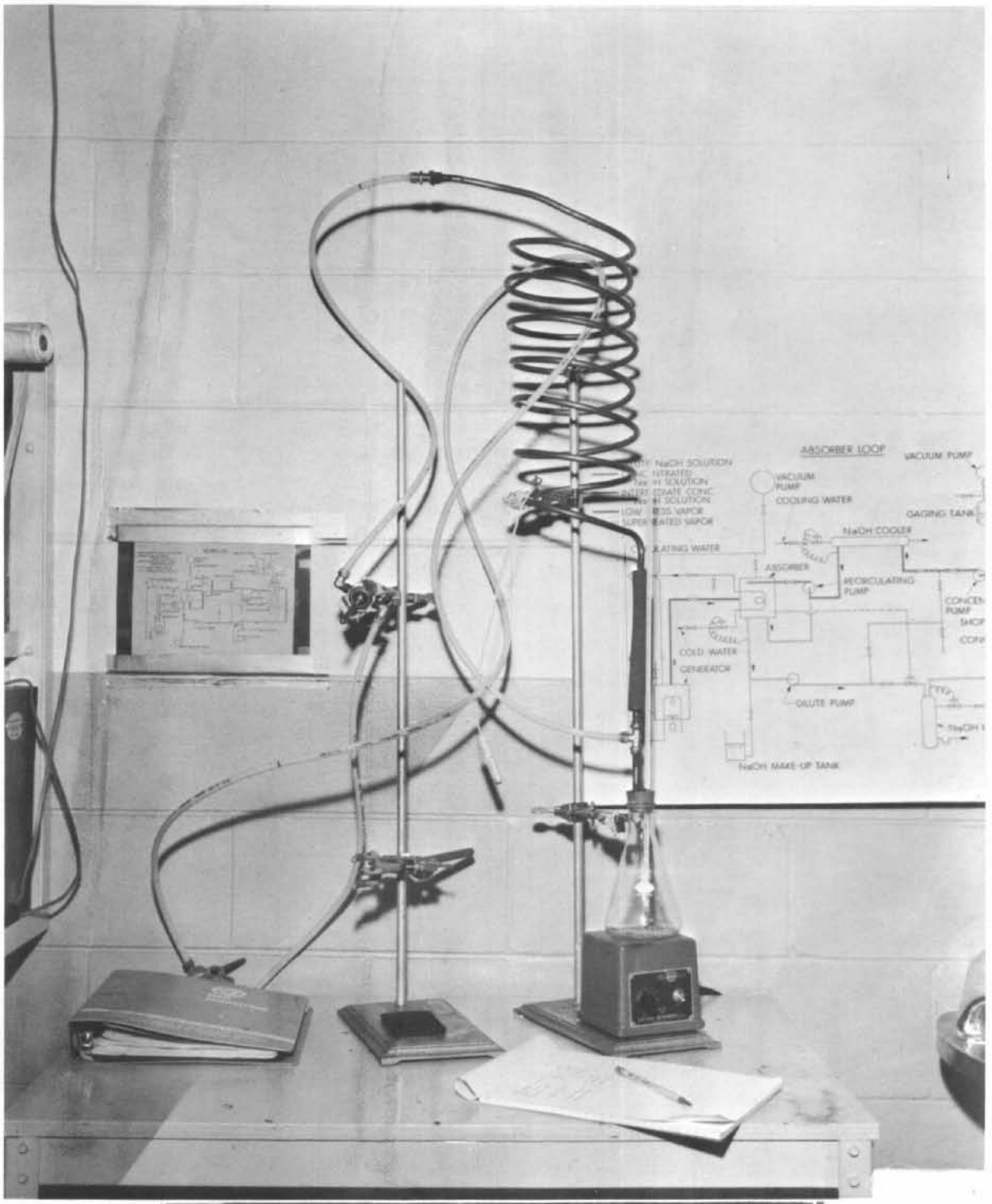

FIGURE VI-9 ABSORBER BENCH TEST FACILITIES
Apparatus for Direct Measurement of the NaOH Vapor Pressure

LIST OF SYMBOLS USED

SYMBOLS	EXPLANATION	UNITS
A_a	Heat and mass transfer area in absorber	ft^2
C_b	Conc. of NaOH soln. at the bottom of concentrator	%
C_c	Conc. of NaOH soln. at the discharge of concentrate pump	%
C_d	Conc. of NaOH soln. at the discharge of dilute pump	%
C_r	Conc. of NaOH soln. at the discharge of recirc. pump	%
h_{as}	Heat transfer coeff. on NaOH side in absorber	btu/hr.-ft^2-°F
h_{aw}	Heat transfer coeff. on water side in absorber	btu/hr.-ft^2-°F
H_{aw}	Total heat transfer in absorber, based on water	btu/hr.
$\dot{m}_v$	Mass of vapor absorbed in the absorber	lbs./hr.
P_c	Press. of heating steam into the concentrator	psig
P_g	Press. in the generator	mm Hg abs.
P_{sd}	Vapor Press. of NaOH soln. at absorber outlet	mm Hg abs.
P_{sr}	Vapor press. of NaOH soln. at absorber inlet	mm Hg abs.
P_{va}	Pressure in the absorber	mm Hg abs.
P_{vc}	Pressure in the concentrator	mm Hg abs.
P_{vp}	Pressure in the 10" vapor duct after butterfly valve	mm Hg abs.
ΔP_a	Log mean vapor pressure difference in absorber	mm Hg abs.
Q_{cc}	Heating steam (condensate) flow rate to concentrator	gpm

LIST OF SYMBOLS USED

SYMBOLS	EXPLANATION	UNITS
Q_{sc}	NaOH flow rate through concentrate pump	gpm
Q_{sd}	NaOH flow rate through dilute pump	gpm
Q_{sr}	NaOH flow rate through recirculation pump	gpm
Q_{wa}	Cooling water flow rate through absorber	gpm
Q_{wd}	Water drainage flow rate between absorber and generator	gpm
Q_v	Absorption rate = steam boil off rate (measured as condensate)	gpm
T_1	Generator water temperature	°F
T_2	Circulating water entering the absorber	°F
T_3	Circulating water out of absorber	°F
T_4	Temperature of absorber (measured near air removal)	°F
T_5	Circulating water out of generator	°F
T_6	NaOH temperature out of absorber	°F
T_7	Cooling water temp. entering the cooler	°F
T_8	NaOH temperature out of the cooler	°F
T_9	Cooling water temp. out of the cooler	°F
T_{10}	NaOH temperature entering the absorber	°F
T_{12}	NaOH temperature entering the heater	°F
T_{13}	NaOH temperature out of the heater	°F
T_{14}	NaOH temperature out of the concentrator	°F

LIST OF SYMBOLS USED

SYMBOLS	EXPLANATION	UNITS
T_{15}	NaOH temperature entering the cooler	°F
T_{16}	NaOH temperature at the bottom of concentrator	°F
T_{17}	Steam temperature entering the heater	°F
T_{19}	Steam temperature entering the concentrator	°F
ΔT_a	LMTD in absorber	°F
U_a	Overall heat transfer coeff. in absorber	btu/hr.-ft^2-°F
U_{am}	Overall mass transfer coeff. in absorber	lb./hr.-ft^2-mmHg
μ_m	Viscosity of NaOH soln. in absorber, computed at concentration $(C_r + C_d)/2$ and temp. $(T_{10} + T_6)/2$	centipoise

VII. STUDY OF POTENTIAL ABSORBENTS

Absorbents for water vapor

Extensive investigations have been carried out over many years in a search for an absorbent for water vapor that would make it possible to air cool a water absorption ("lithium bromide") air conditioning system. Sixty or more materials have been considered, some thirty of which have been listed in publications. Others have been listed only in proprietary in-house reports. A number of absorbents have been developed which have substantially lower vapor pressures than lithium bromide. These materials have not been perfect absorbents, some being corrosive, others unstable at high temperatures, etc.

In Figure 1 and Table 1 are given data on two of the better absorbent combinations, compared to lithium bromide and sodium hydroxide. These two are not proposed as possible absorbents for the VFEA system but are intended only as indications of the vapor pressure reductions and absorption temperatures that have been reached. As indicated in table 1, the vapor pressure lines of figure 1 and the equilibrium temperatures at 3 mm pressure are for solution concentrations having crystallization temperatures in the neighborhood of 80°F. For binary salt solutions there may be two saturation temperatures depending on the direction from which saturation is approached.

Discussions with suppliers indicate that the cost of the LiBr-LiSCN will be equivalent to that of LiBr. While LiBr is listed in market publications at $1.70/lb. in ton lots, we understand that it is being bought at under a dollar a pound, and that the LiSCN would also be in that range. While these are not high cost chemicals, their costs are nevertheless some ten times the cost of sodium hydroxide.

The lithium bromide-lithium chloride-zinc bromide solution was studied many years ago. This solution is reputed to be very corrosive, requiring ceramic or organic lined vessels. The importance of such absorbents when used in water cooled systems is that higher UΔt products may result and/or that warmer cooling water may be utilized.

The following list indicates some of the published materials which have been considered or investigated as absorbents for water.

Lithium Acetate
Potassium acetate-Potassium formate
Trimethyl phosphate
Triethyl phosphate
Ethylene Glycol
Propylene Glycol
Glycerol
Triethylene Glycol
Dimethoxitetraethylene glycol
Diethylene triamine
Dipropylene triamine
Triethylene tetramine
Tetraethylene pentamine
Sec-butyl amine
Triethanol amine
Hydroxyethyl ethylene diamine
Lithium chloride
Lithium iodide
Zinc bromide
Zinc iodide
Calcium nitrate-calcium chloride
Zinc chloride-potassium chloride-lithium chloride
Zinc chloride-calcium chloride
Phosphoric acid
Sulfuric acid
Lithium bromide-lithium iodide
Lithium bromide-ethylene glycol
Lithium bromide-lithium iodide-ethylene glycol
Lithium bromide-cesium bromide

Sodium hydroxide has among the best vapor pressure and crystallization characteristics, and should form a good basis for improved combination of absorbents.

The materials in the above and other lists may be divided into classifications, such as: Organic, inorganic; liquid, solid; single component, binary or ternary mixture, etc. So as not to neglect anything, solid absorbents, such as, silica gel, molecular sieves, etc., should also be mentioned.

The organic materials have generally had the disadvantage that some decomposition may occur at boiler temperatures. Decomposition rates which may be insignificant in other fields can be excessive in a sealed air conditioner intended to operate for fifteen or twenty years, often unattended.

In a municipal water plant of far larger size, less

stringent specifications may be acceptable. As long as the decomposition products are not harmful, either to the product water or to the equipment, low decomposition rates may not be objectionable. If necessary, means of removing the decomposition products may be included and fresh absorbent can be added to the system periodically. Hence, organic materials can conceivably play a larger part in VFEA systems than they have in air conditioning concepts. As an example, the addition of ethylene glycol to lithium bromide solutions reduces the vapor pressure substantially. The only data available shows a reduction of vapor pressure from 7mm. to 4mm. by the addition of 18% ethylene glycol to the lithium bromide solution. However, the measurements of the vapor pressure of the lithium bromide solution made in that series of tests, do not match the accepted data from the literature. So, until better data are found this can only be an indication of a possibility.

Unfortunately many of the organic materials will have perceptible vapor pressures at generator temperatures and would therefore be carried over into the product water. This may be the major limitation to their use in the VFEA system.

Inorganic materials are usually less subject to decomposition than organics, but are more likely to be corrosive. However, within limits, the same approach may be taken. In air conditioners, corrosion is a problem, not so much due to the thinning or perforation of the metal, but because of the effect of the hydrogen gas in the vacuum system. Since in the VFEA system the vapor from the generator goes to the ejector and the melter, instead of recirculating in the system, greater formation of hydrogen can be tolerated. Corrosiveness may therefore be less of an objection than in air conditioners.

Liquid materials should have an advantage over solids in that they should present no crystallization problems. However, they are more likely to have perceptible vapor pressures at generator temperatures. In addition, the only inorganic liquids in the list are sulfuric acid and phosphoric acid.

Thus we are led toward the solid inorganic materials as providing a broader group of likely absorbent materials. Data on the individual materials is

generally available in sufficient quantity for a quick judgement of their suitability. Few are individually better than lithium bromide or equal to sodium hydroxide.

Mixtures of absorbents take on special importance because it is not uncommon for a binary or ternary mixture to have better properties than any of the individual components. There may also be valuable flexibility in the relative proportions of the components. The mixtures high in thiocyanate have the lowest vapor pressures. But the viscosity table shows that the solutions high in Bromide have the lowest viscosities. Since, at the lower vapor pressures the rates of absorption and heat transfer may be reduced by viscosity, a compromise between the best vapor pressures and viscosities may give the best results.

Mixtures may therefore provide the best opportunities to tailor the absorbent to the system requirements. However, multiple salts are generally more corrosive than the individual components, so compromises may be required here also.

Additives

The additives that have come into use in lithium bromide systems to enhance the overall performance are generally alcohols of the seven and eight carbon chain variety. 2 ethyl hexanol is commonly used. There are other materials as well.

The term, additive, refers to materials used in low concentrations, of the order of 200-400 parts per million. They do not affect the vapor pressure or the viscosity of the lithium bromide solution. The surface tension is presumably affected, but the effect differs from that of the usual surfactants; the latter do not improve performance as the heptyl and octyl alcohols do. The additives enhance the kinetics or rate of absorption rather than the potential for absorption.

A paper published by Burnett & Himmelblau is a good review of the effect of this type of surface active agent on the rate of absorption of a gas or vapor onto a static liquid surface. It attributes the acceleration in absorption to longitudinal variations in the surface tension which produces visible turbulence on the surface, the Marangoni effect. A good bibliography is given.

The Himmelblau paper gives data on the effects of alcohol, amine and amide additives on the rate of absorption of ammonia into water.

The procedure used to test the effect of additive materials was to expose a shallow dish containing the absorbent solution plus additive in a chamber of water vapor. The rate of pressure drop in the chamber was then timed. Some materials accelerated the rate of pressure drop while others reduced it. Materials such as eleven and twelve carbon chain alcohols, ethylene glycol and others, slowed the rate of absorption. Six, seven and eight carbon alcohols accelerated absorption while those in between had little effect. The best material accelerated the rate of pressure drop several fold. When the materials which showed up best in this test were added to a lithium bromide unit devoid of additive, they improved the refrigerating capacity of the unit by 20-25%. Some tests showed as much as 30% gain. It is also stated that units with marginal absorbers are improved the most, while those with ample or excess absorber surface may show little effect.

The additives seem to affect the rate of absorption by bringing about localized eddies or turbulence on thick films. Thin films are apparently not affected. The effects on static surfaces may be relatively greater than on moving films.

In the water-lithium bromide system the molecular structure of the alcohol seems to be important. Normal octyl alcohol is not very good while its isomer, 2 ethyl hexanol, is one of the best materials. The hydroxyl group should apparently be on a side chain or on the second or third carbon atom.

The hexyl, heptyl and octyl alcohols all have appreciable vapor pressures at generator temperatures, and boil off in the generator. In the VFEA system they would be carried off in the product water. The cost of continual replacement probably would not be excessive; 2 ethyl, hexyl alcohol is listed at 11¢/lb.

Discussion

As a result of the above information a number of tempting directions can be seen as means of reducing absorber size and cost.

451-332 O - 71 - 8

Beginning with the additives; since additives are more effective on thick films than thin, there should be a good probability that they can improve absorption in the viscous sodium hydroxide solutions more than they do in lithium bromide. This possibility should extend to other absorbents well suited to the VFEA process, if we assume that there will be a tendency to high viscosity in all absorbents for use at 3mmHg vapor pressure.

Further, the Himmelblau paper, which showed that amines and amides performed as well as alcohols, indicates that other polar compounds, properly chosen, may be equally good. This leads to the consideration that the sodium salts of medium carbon chain organic acids may perform well. Such salts should not only be far less objectionable in water but the amounts from vaporization should be insignificant if vaporization occurs at all.

We may also question whether the 25% improvement is a limit on the absorber itself or on the unit as a whole. If the absorber has been the limiting factor in overall unit performance, improving it will improve unit performance up to the point that another component takes over as the limit on the overall system. The static tests indicate more than 25% gain. It is possible that additives may cause more than a 25% reduction in an absorber per se. While the manufacturers may supply some information in this regard a trial on the absorber test apparatus will give a more direct and quantitative answer.

All in all however, there are good reasons to expect that additives can be used in the VFEA water plant and to assume that they may reduce the size of the absorber substantially.

The next subject is that of the absorbents themselves. It appears that low vapor pressures can be obtained in a variety of ways. Combinations of absorbents can result in much lower vapor pressures than those of any of the components. It may also be possible to improve viscosities in some cases. However, it is likely that other characteristics such as corrosiveness, decomposition, health hazards, may become decisive factors. Considering the requirements of a water plant, sodium hydroxide has advantages over lithium compounds both in vapor pressures and in health factors. It may be desireable to modify it with compatible materials to provide still lower vapor pressures. Sodium and potassium hydroxides, carbonates, phosphates, nitrates and silicates may be

good candidates for a low cost combination and likely to be acceptable from corrosion, decomposition and health standpoints. If it became necessary to investigate the halides, the calcium, magnesium and zinc combinations may be promising on all counts. It is also possible that developments in the organic chemistry field can be helpful.

This all leaves the opinion that if improvements over sodium hydroxide are necessary there are good opportunities to achieve results similar to those in figure 1, but with materials better suited to a water plant.

TABLE 1

Properties of Potential Absorbents

Solution	Viscosity Range	Equilibrium Temperature at 3mm Hg	Solution Concentration
LiBr	3-6 cps	96°F	62% LiBr
NaOH	25-40 cps	119°F	54.5% NaOH
LiBr-LiSCN	10-20 cps	128°F	Sat. at 86°F
LiBr-LiCl-$ZnBr_2$	--	156°F	Sat. at 77°F

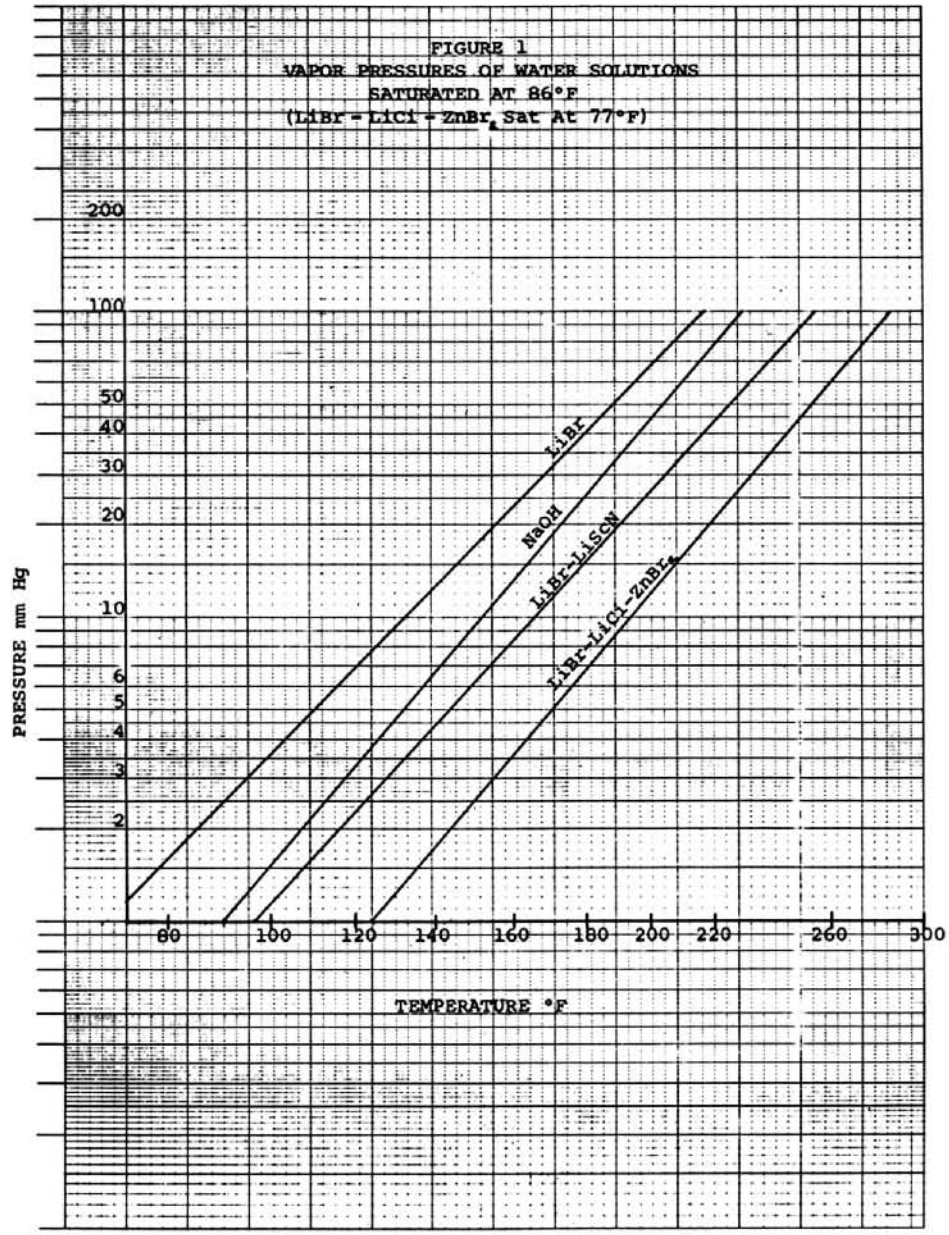
FIGURE 1
VAPOR PRESSURES OF WATER SOLUTIONS
SATURATED AT 86°F
(LiBr - LiCl - ZnBr2 Sat At 77°F)
PRESSURE mm Hg
200
100
50
40
30
20
10
6
5
4
3
2
LiBr
NaOH
LiBr-LiSCN
LiBr-LiCl-ZnBr2
80
100
120
140
160
180
200
220
260
300
TEMPERATURE °F

VIII PRELIMINARY PILOT PLANT DESIGN

Preliminary design drawings of a 60,000 gpd, VFEA pilot plant are included in this section. The design is based on the following concepts:

1. All vessels and systems will be erected and subassembled on skids in our Beloit Works. This will keep field erection requirements to a minimum and will allow the checkout of systems in our factory and thus reduce plant start up problems to a minimum.

2. Plant will be designed such that individual component modification can be made with minimum downtime.

3. Conceptual design of the ejector and absorber will be similar to the successful bench scale unit.

4. The plant is designed such that the following objectives can be achieved during pilot plant testing:

   General objective of the VFEA pilot plant is to develop the process such that it is a commercially feasible process and future desalting plants can be constructed to produce product water at less cost than present desalting plants.

   Specific Objectives:

   1. Evaluate the VFEA operational problems which may be encountered.

   2. Conduct an extended run at system design capacity for an overall system evaluation.

   3. Evaluate and test these individual components

      a. Ejector

      b. Absorber

      c. Concentrator

      d. Condenser

      e. Single vessel counterwasher/melter

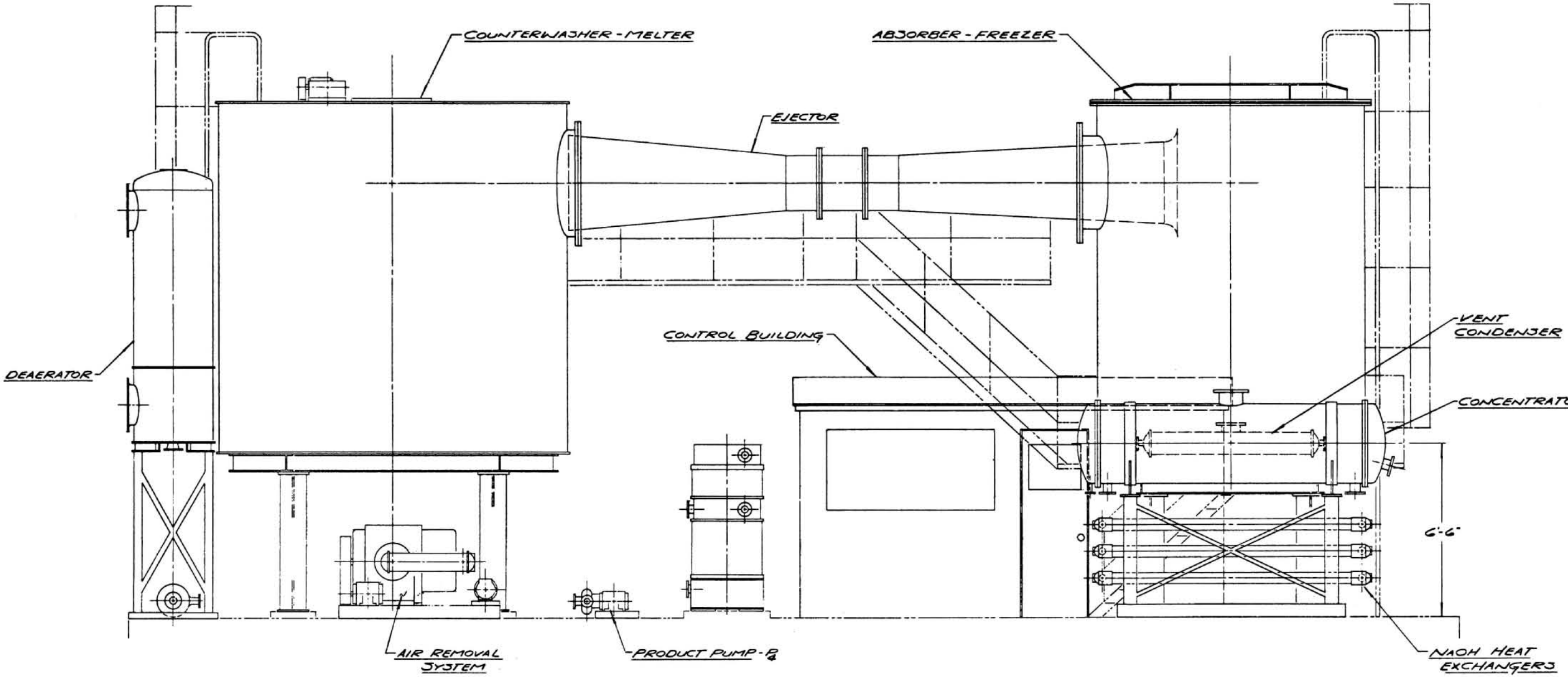

VFEA
PILOT PLANT DESIGN
REAR ELEVATION VIEW

FIG. 1

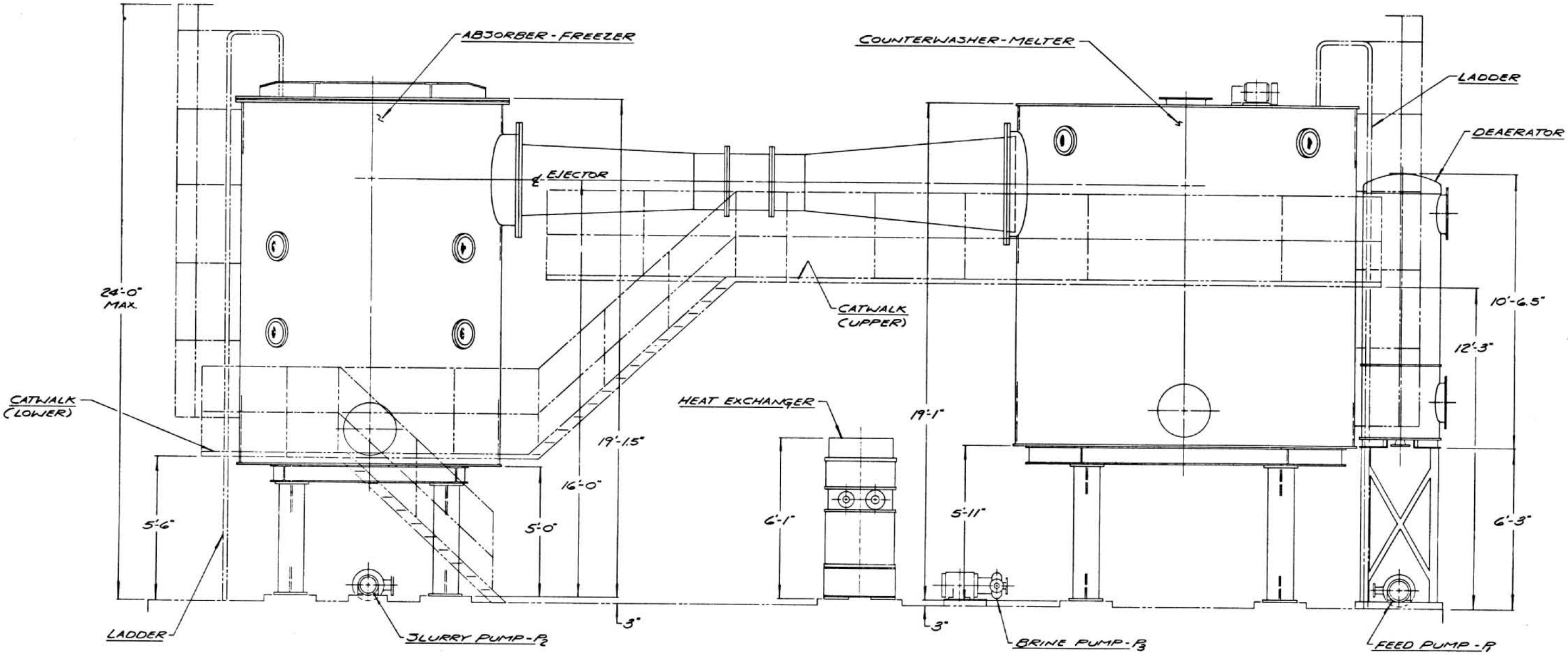

VFEA
PILOT PLANT DESIGN
FRONT ELEVATION VIEW

FIG. 2

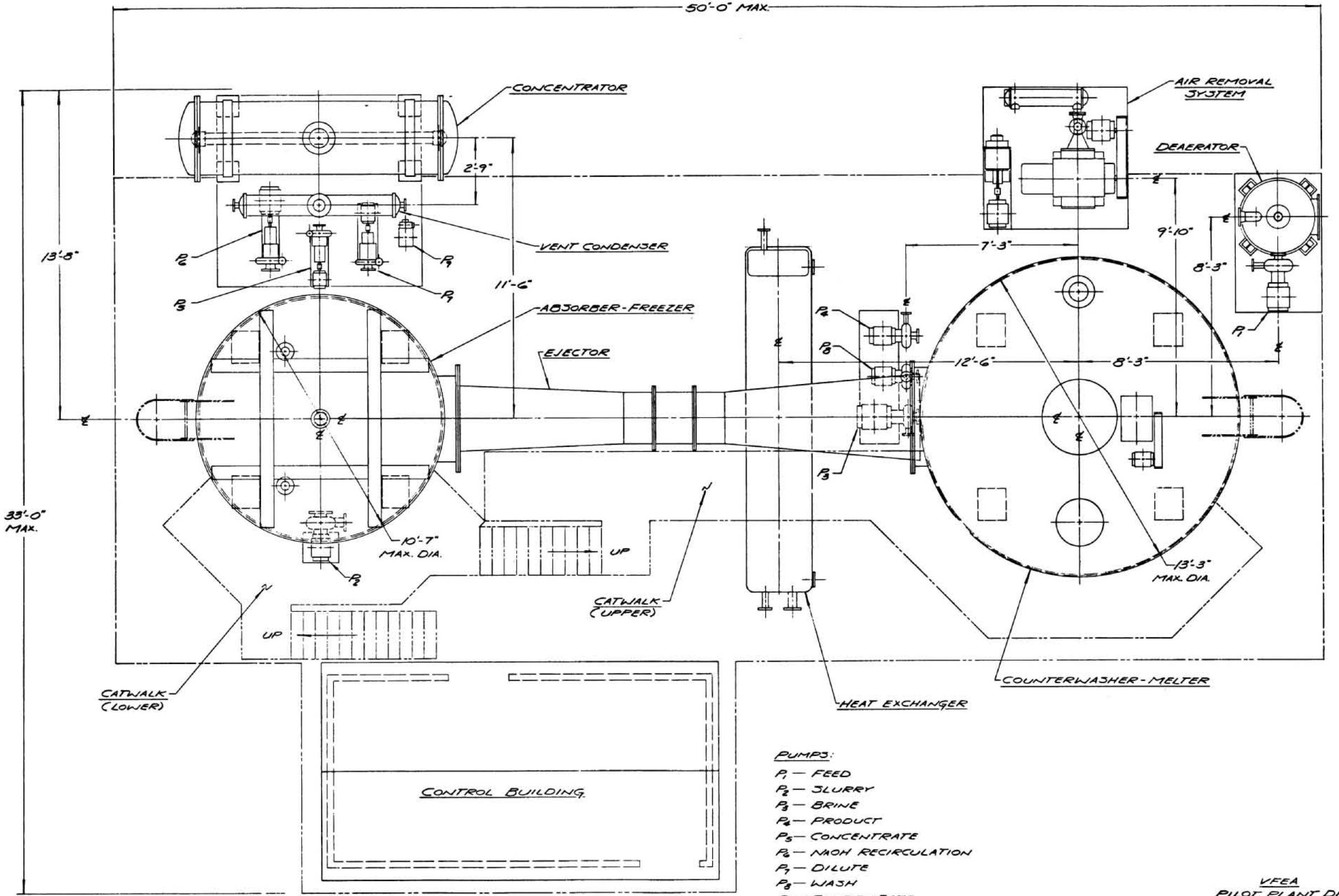

PUMPS:

- P_1 — FEED
- P_2 — SLURRY
- P_3 — BRINE
- P_4 — PRODUCT
- P_5 — CONCENTRATE
- P_6 — NAOH RECIRCULATION
- P_7 — DILUTE
- P_8 — WASH
- P_9 — CONDENSATE

VFEA
PILOT PLANT DESIGN
PILOT PLANT PLAN VIEW

FIG. 3

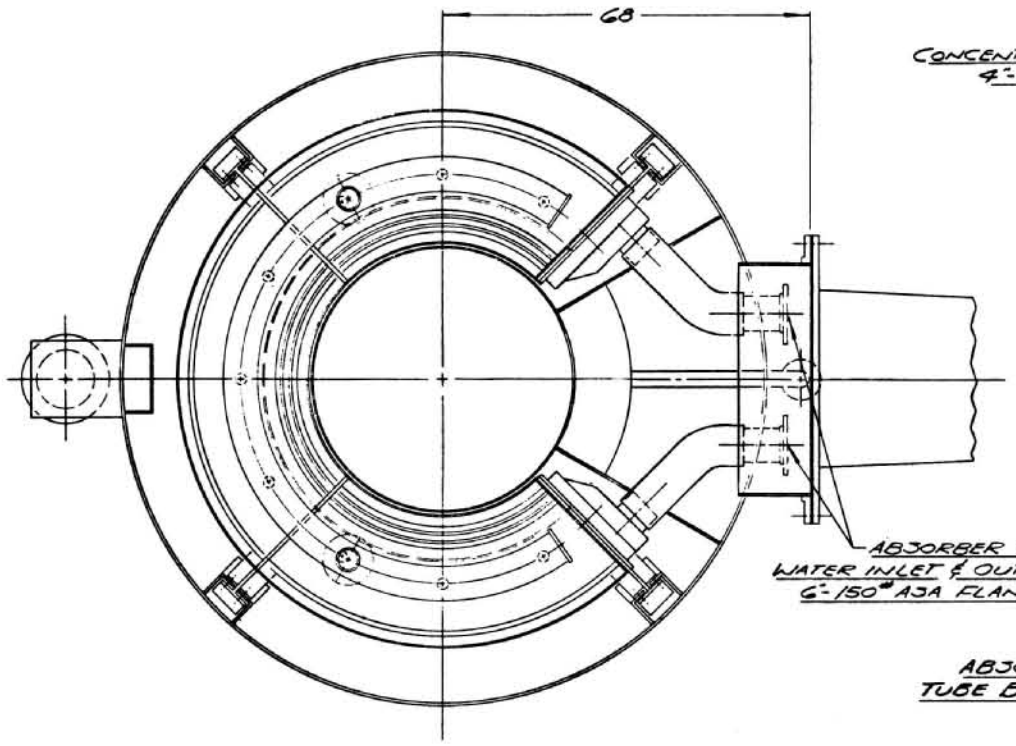

SECTION 'A'—'A'

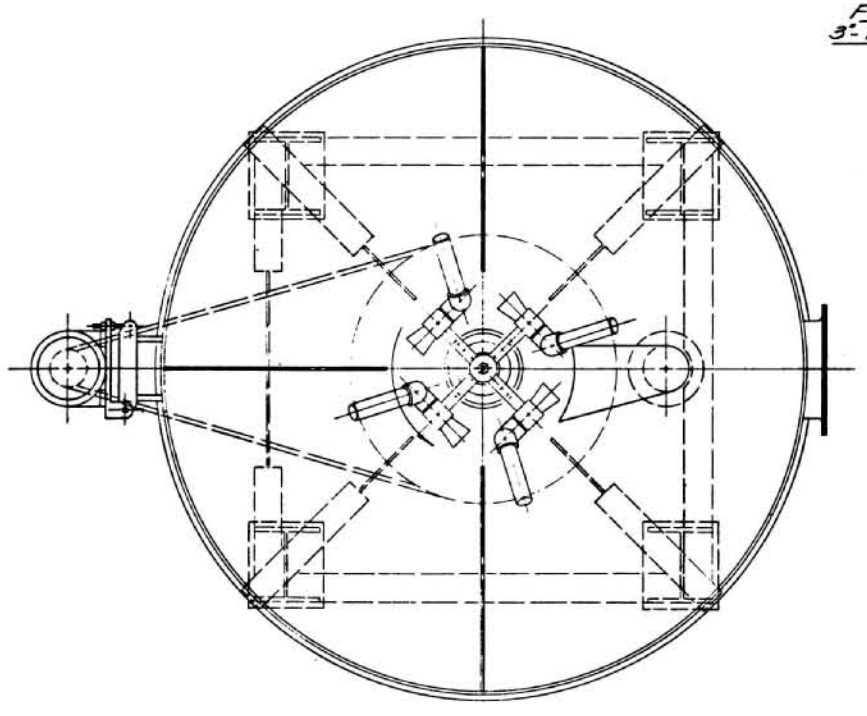

SECTION 'B'—'B'

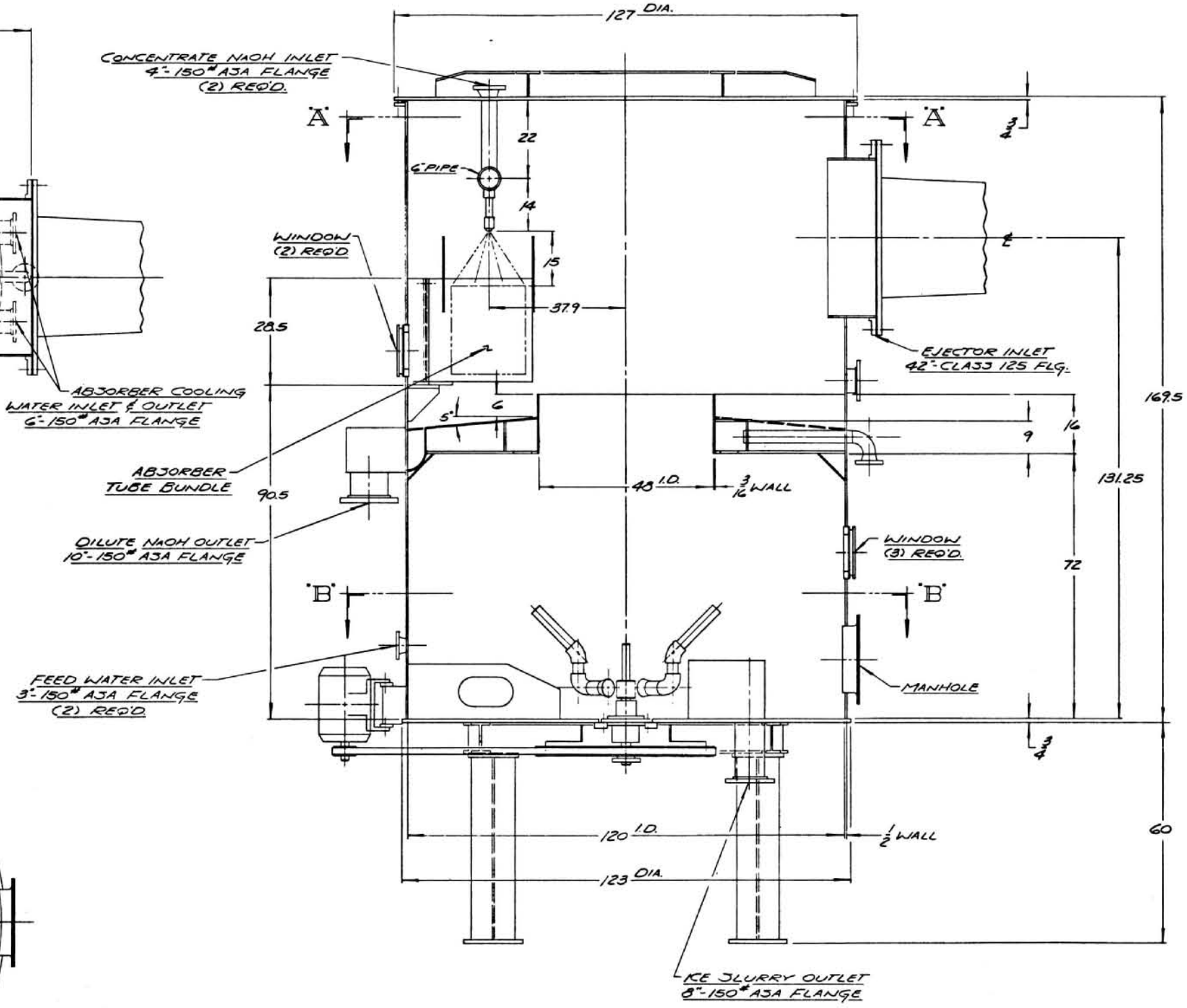

VFEA
PILOT PLANT DESIGN
ABSORBER-FREEZER

FIG. 4

451-332 O - 71 (Face p. 114) No. 8

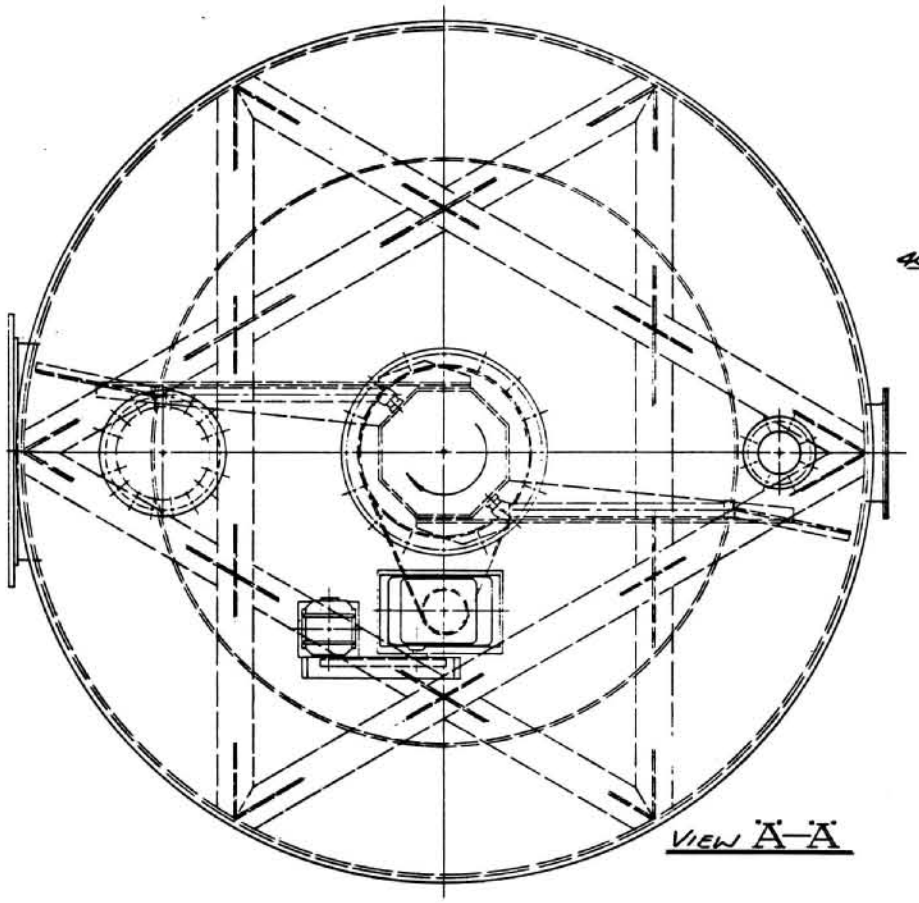

VIEW A–A

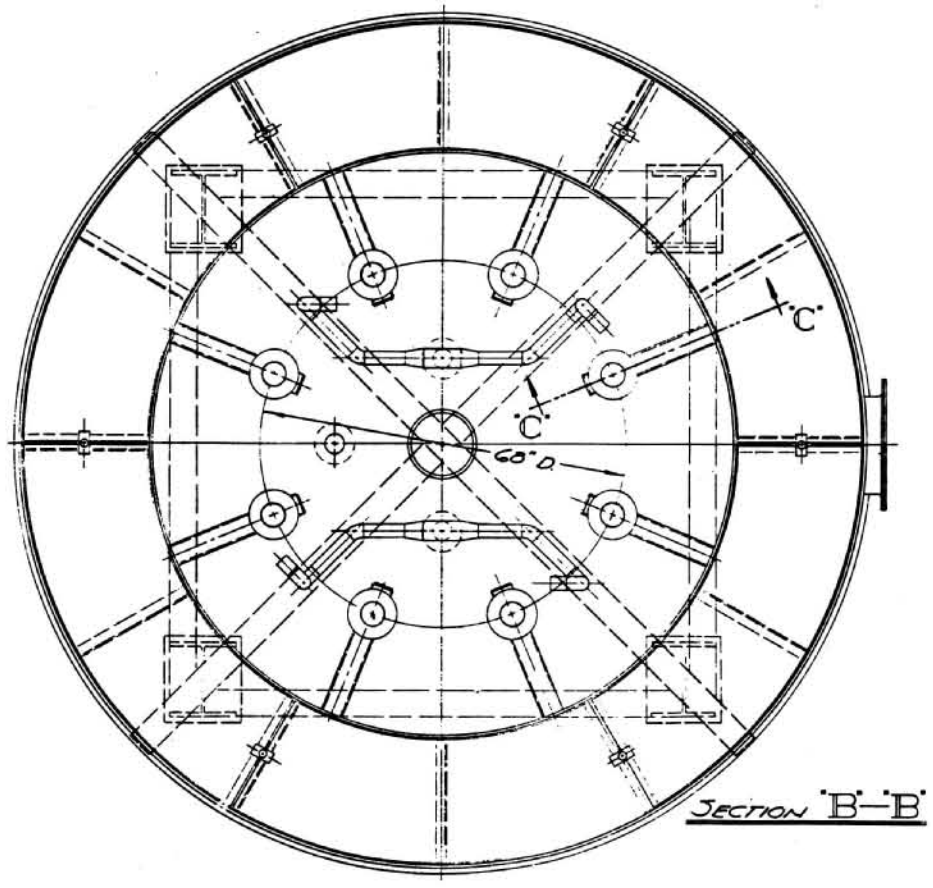

SECTION 'B'–'B'

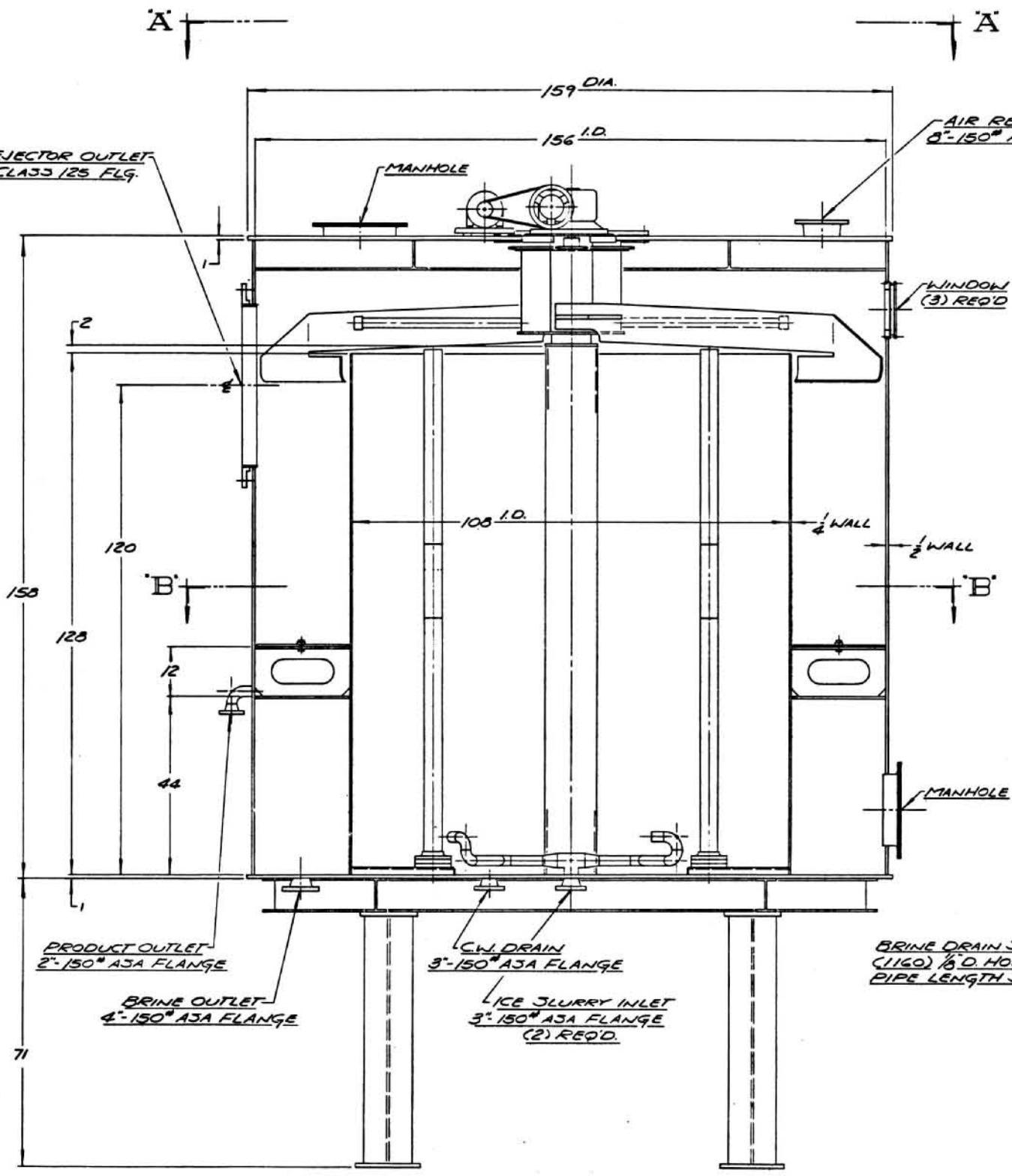

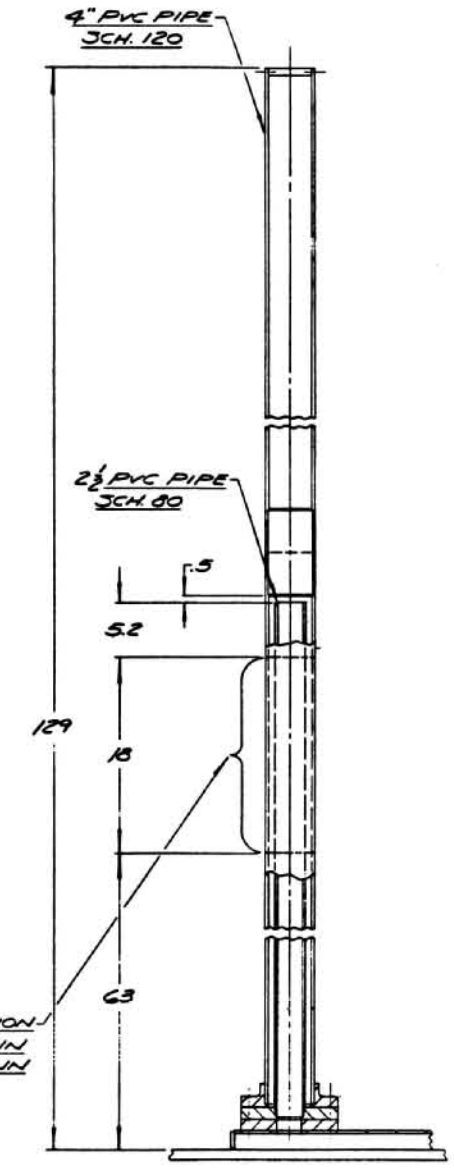

SECTION 'C'–'C'

VFEA
PILOT PLANT DESIGN
COUNTERWASHER - MELTER

FIG. 5

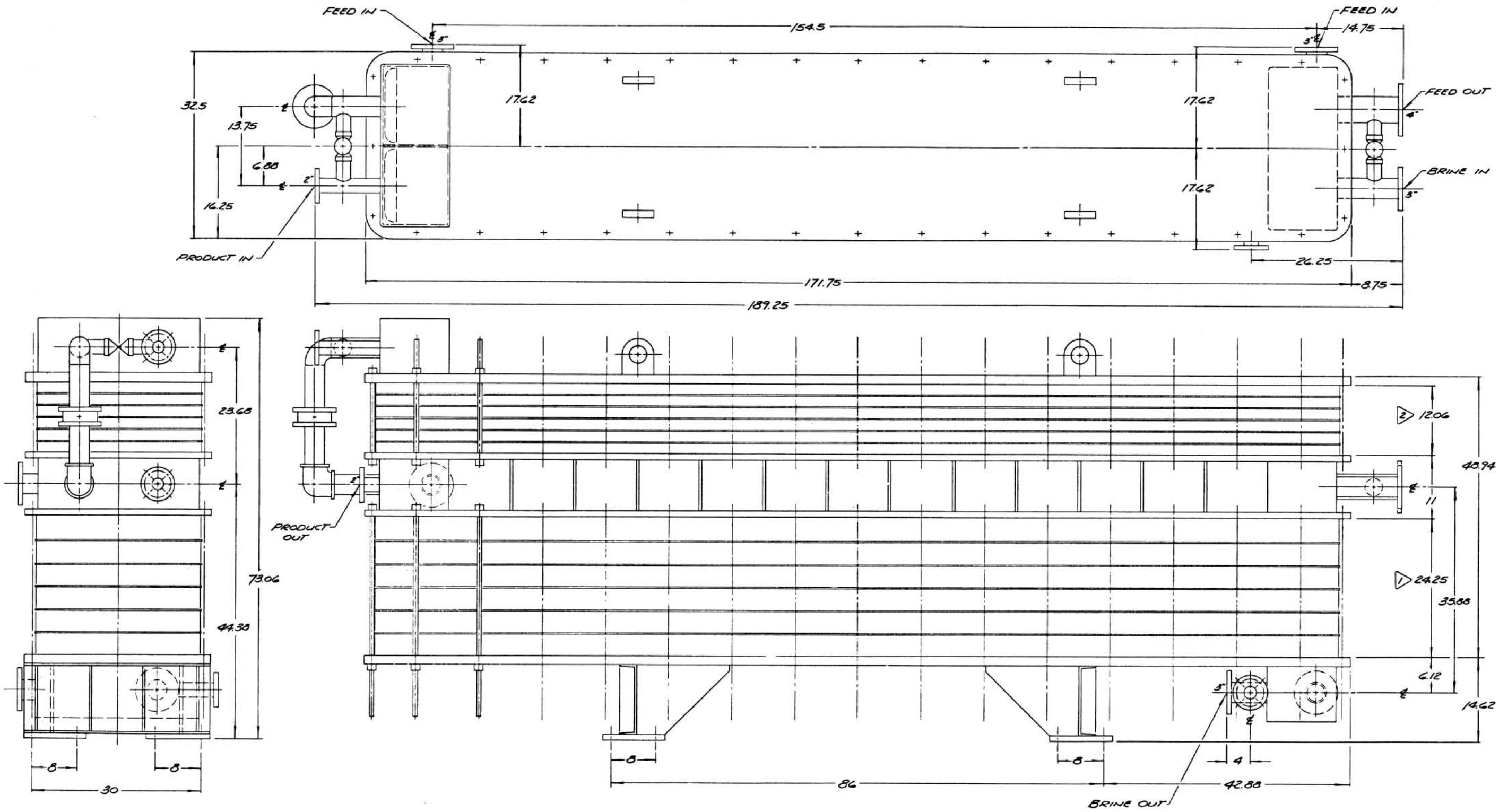

(1) BRINE — 9 PASS 5 SECTIONS
10 PASS 1 SECTION
TOTAL No. SHEETS = 115

(2) PRODUCT — 4 PASS 6 SECTIONS
TOTAL No. SHEETS = 54

VFEA
PILOT PLANT DESIGN
HEAT EXCHANGER

FIG. 6

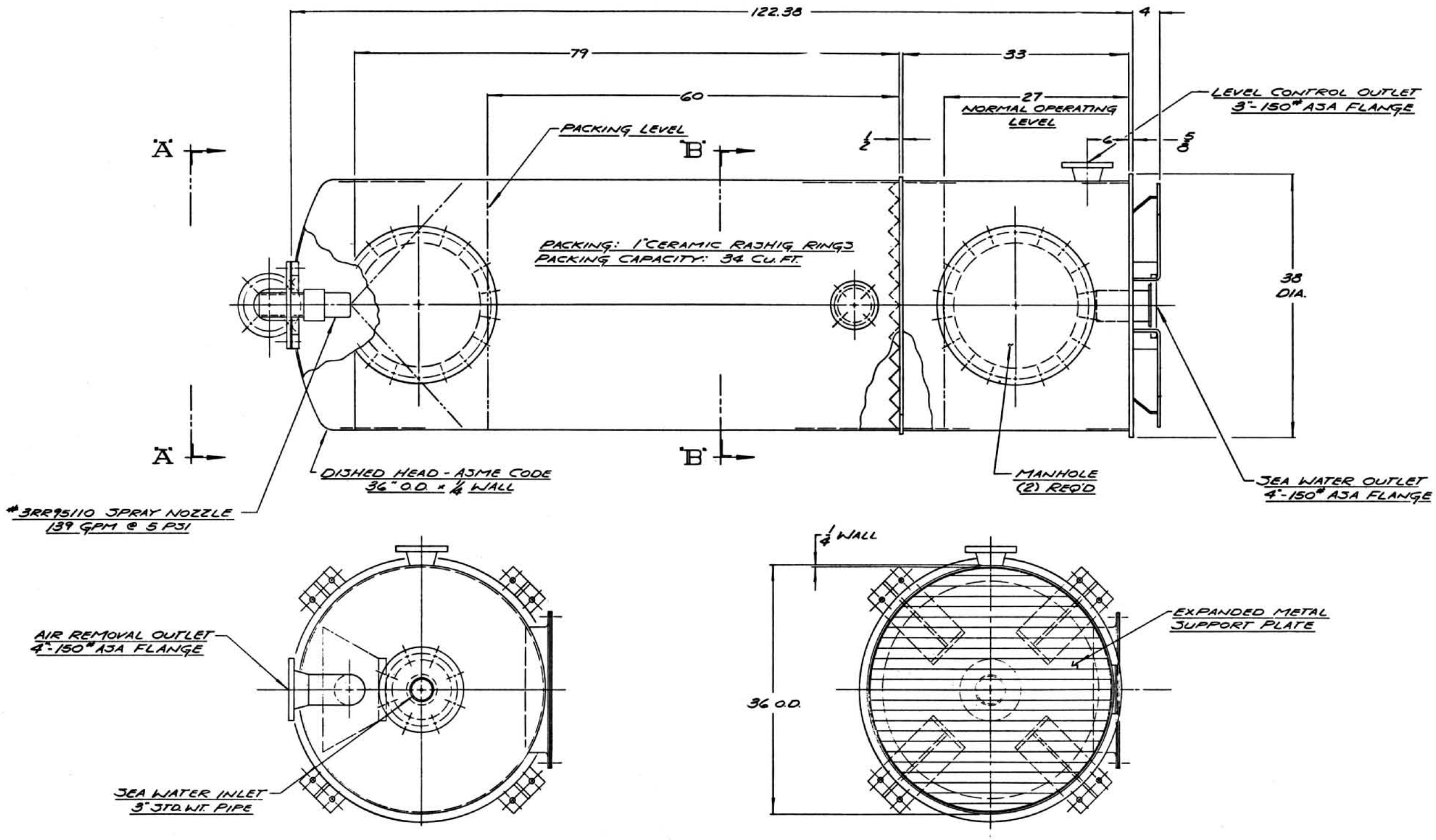

VIEW A—A

SECTION B-B

VFEA
PILOT PLANT DESIGN
DEAERATOR

FIG. 7

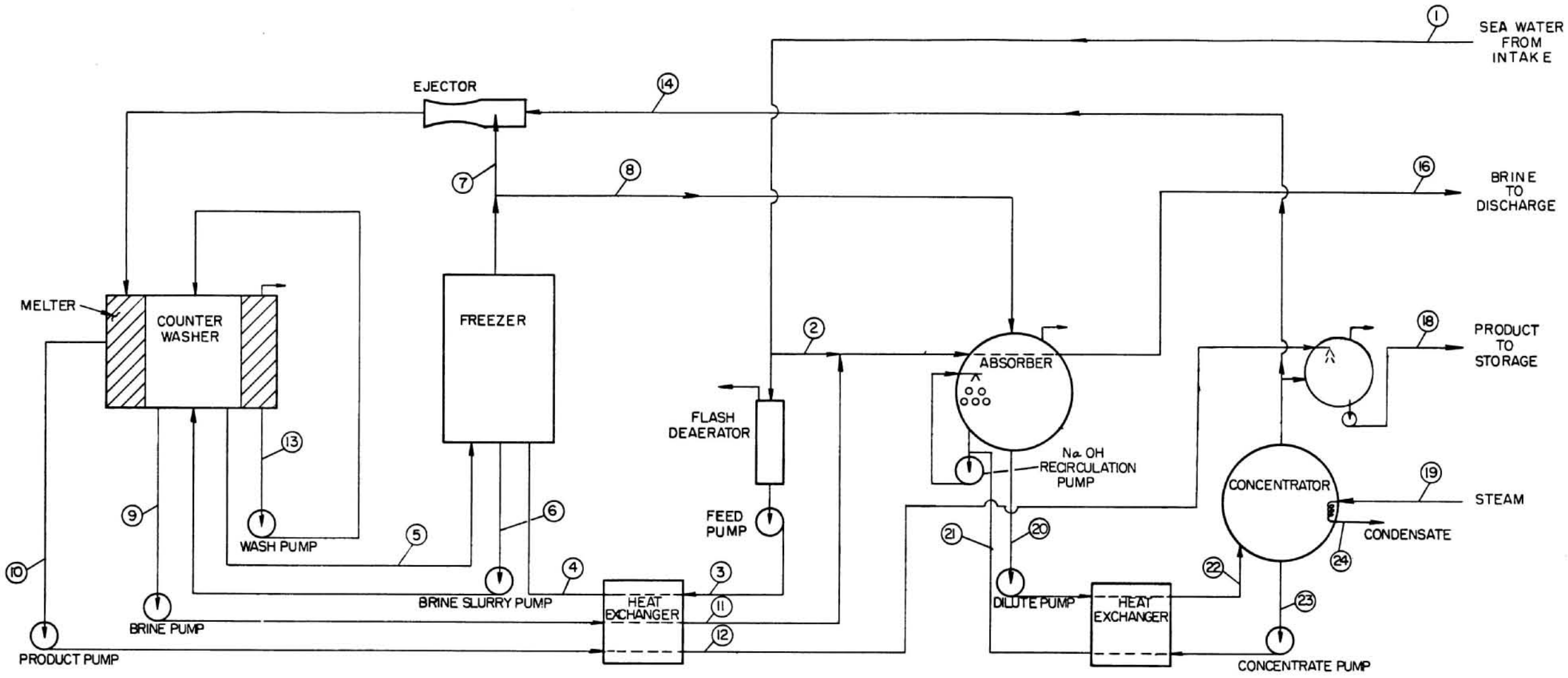

	① SEA WATER	② SEA WATER	③ SEA WATER FEED	④ SEA WATER FEED	⑤ BRINE RECIRCULATION	⑥ BRINE SLURRY	⑦ VAPOR	⑧ VAPOR	⑨ BRINE	⑩ PRODUCT	⑪ BRINE	⑫ PRODUCT	⑬ PRODUCT WASH	⑭ STEAM	⑯ BRINE	⑱ PRODUCT	⑲ STEAM (30 PSIG)	⑳ DILUTE Na OH	㉑ CONCENTRATED Na OH	㉒ DILUTE Na OH	㉓ CONCENTRATED Na OH	㉔ CONDENSATE
G.P.M.	383	244.1	138.9	138.3	112.2	244.8			96.6		97	40.8	16.7			41.66						
TEMP	80	80	80	32	27.15	27			27.15	33.2	78.1	76.5	33.2	250	90	98.5	275	87	97	230		275
CONCENTRATION	3.5	3.5	3.5	3.5	4.95	I = 15%			4.95		4.95				3.92			50	53.5	50	53.5	
FLOW # I MIN - LIQUID	3263	2080	1183.3	1183.3	971.6	1790.6			836.3	339.9	836.3	339.9	138.8		2916	347		333	355	355	333	
- VAPOR							26.45	21.85						15.35								
- SOLID						316											34.5					34.5
SP. GR	1.023	1.023	1.023	1.027	1.039				1.039		1.035				1.026							
Cp	.954	.954	.954	.952	.936				.936		.938				.955							
VISCOSITY																						
H BTU I# - LIQUID	247.3	247.3	247.3	201.95	198.1	198			198.1	201.2			201.2					363.4	335.1	454.6	490.9	444
- VAPOR							1272.2	1272.2						1371			1382					
- SOLID						54.1																

MASS & ENERGY DIAGRAM

FIG. 8

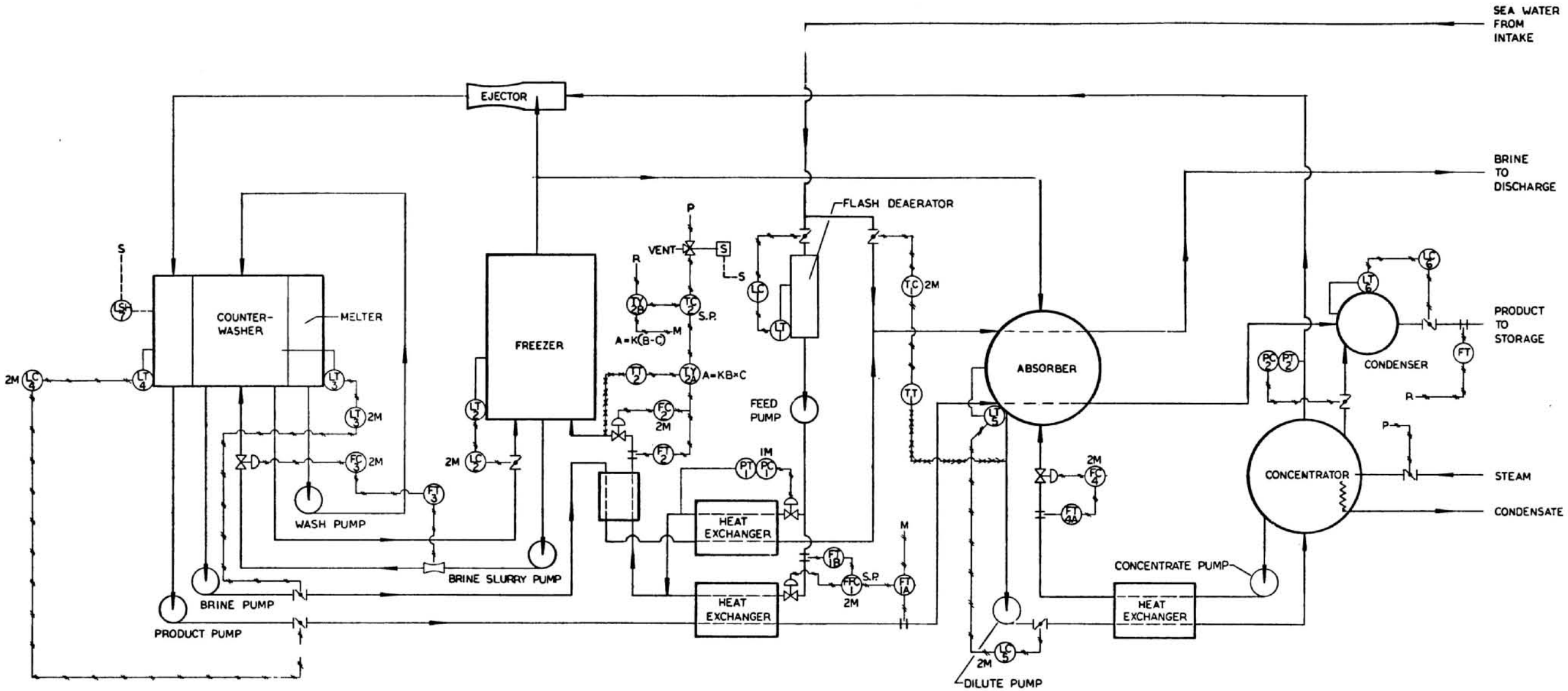

VFEA
CONTROLS SCHEMATIC
FIG. 9

IX. VFEA LARGE PLANT DESIGN CONCEPT

The following page contains a design concept for large VFEA desalting plants. Although the component designs are similar to their respective pilot plant component design, the horizontal single vessel concept enables the VFEA process to be projected to plants of increased size.

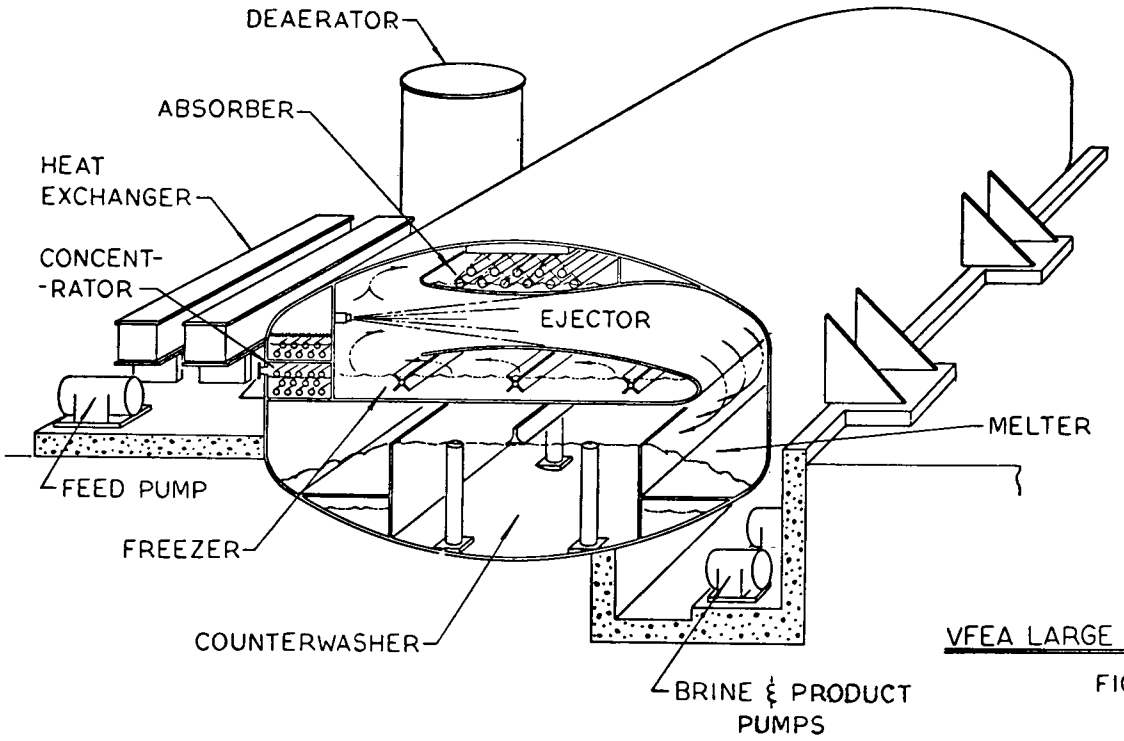

VFEA LARGE PLANT CONCEPT

FIG. 1

X. PROCESS MATHEMATICAL STUDY

By Dr's. Mixon and Orcutt
Research Triangle Institute

SECTION 1. CONCLUSIONS

A detailed mathematical analysis of the VFEA process has been completed, including both steady state and dynamic analysis of each individual process component.

A program for design optimization by digital computer has been developed that searches over possible design parameters to find the design corresponding to minimum cost of water. Results of computations using the program indicate that the cost of water

a) decreases with increasing conversion from 20 percent to 50 percent conversion,

b) increases, but only very slightly, with increasing freezer pressure from 3.1 to 3.25 mm Hg,

c) decreases with increasing feed temperature to the freezer from 31^{o} to 33^{o}F with an optimum somewhere above 33^{o}F,

d) increases significantly with increased ejector efficiency, and

e) decreases with increasing plant capacity.

The optimal cost of water produced by the VFEA process has been estimated at 30.46 cents per k gal at the 1 mgd level, exclusive of labor costs. This cost is not strongly sensitive to changes in operating conditions. Details of the optimal design are included in Section 2.7.

A simulation by analog computer of the dynamics of the integrated process has indicated that the process is well behaved and should be amenable to relatively simple control techniques. No inherent instabilities were discovered.

Finally, the utilization of ejectors to reduce the refrigeration capacity required in the absorption system is clearly highly advantageous. We believe that the VFEA process represents a significant advance in freeze desalting technology and strongly support construction and demonstration of an integrated process by Colt Industries.

SECTION 2. DESIGN OPTIMIZATION BY DIGITAL COMPUTER

In this section we give a discussion of the results and conclusions of the digital design optimization. The effects upon the optimal design of variations in several of the operating conditions are presented first. There follows a detailed print-out of the computed optimal process design including process specifications, equipment specifications, and process economics (SECTION 2.7).

The detailed bases for economic evaluation are discussed in a later section. We note here, however, that the present figures do not include labor, brine disposal, water treatment, and land costs. These items should not affect the optimization appreciably. They should be more or less constant and, with the exception of labor, relatively small contributions.

Finally, we give a discussion in general terms of the strategy followed in performing the optimization calculations.

The detailed print-outs of all cases studied are being transmitted to Colt under separate cover. The results of Section 2. 7 are representative as to format and contents.

2.1 THE EFFECT OF CONVERSION

It was planned to study the effect of conversion over the range from 20 percent to 50 percent at at constant value of the freezer pressure of 3.264 mm Hg. We discovered in doing this that at the higher levels of conversion a lower freezer pressure is required in order to generate sufficient driving force for freezer operation. The effect on optimal design of conversion over the range from 20 to 40 percent was investigated at the higher pressure (3.264 mm Hg), and the effect of conversion from 40 to 50 percent was studied at a lower pressure of 3.075 mm Hg. The results are summarized in Table 2.1.

It can be seen that the water cost decreases with increasing conversion over the range investigated. This decrease is due predominantly to the fact that a smaller main heat exchanger is required for the higher conversions.

FIGURE 2.1

THE EFFECT OF CONVERSION

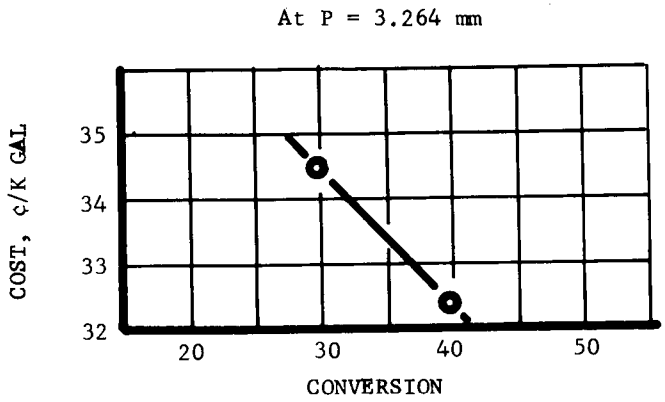

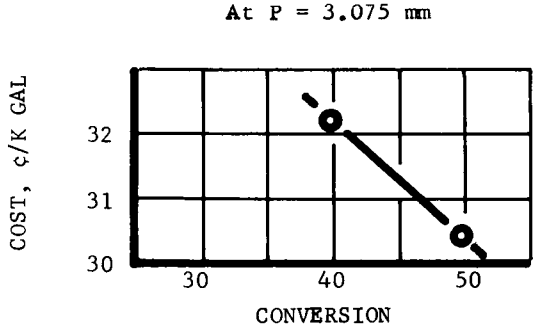

TABLE 2.1

THE EFFECT OF CONVERSION

At P = 3.264 mm			
Run No.	Brine Concentration	Conversion	$\frac{\text{Cost}}{\text{K Gal}}$
7	.0436	20%	42.48
8	.0498	30%	34.49
9	.05800	40%	32.38
6	.05833	40%	32.34

At P = 3.075 mm			
Run No.	Brine Concentration	Conversion	$\frac{\text{Cost}}{\text{K Gal}}$
11	.05800	40%	32.19
10	.0695	50%	30.46

2.2 THE EFFECT OF PRESSURE

The effect of pressure on the optimal design is a relatively small one as indicated by the results of Table 2.2. The lower cost at the lower pressure results primarily from the fact that a smaller freezer is required at the higher driving force.

2.3 THE EFFECT OF FEED TEMPERATURE INTO THE FREEZER

Over the range of values of feed temperature into the freezer that was investigated, the water cost decreased as the freezer feed temperature increased as illustrated by the results of Table 2.3. The decrease in cost is due primarily to a smaller main heat exchanger.

As the feed temperature increases, there is an accompanying increase in the amount of vapor which must be handled in the absorber loop. Consequently, the cost of absorber equipment increases as the main heat exchanger cost decreases. The optimal balance occurs at a freezer feed temperature that is apparently slightly in excess of $33^{o}F$.

2.4 THE EFFECT OF EJECTOR PRIMARY TO SECONDARY RATIO

As is indicated in Table 2.4, the cost increases slightly as the ejector becomes less efficient. This cost increase is the direct result of the fact that slightly more of the freezer vapor must be diverted through the absorber loop to the ejector primary. The absorber loop must be correspondingly larger to handle the increased vapor load.

FIGURE 2.2

THE EFFECT OF PRESSURE

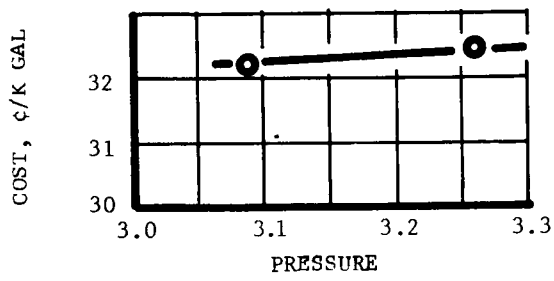

FIGURE 2.3

THE EFFECT OF FEED TEMPERATURE INTO THE FREEZER

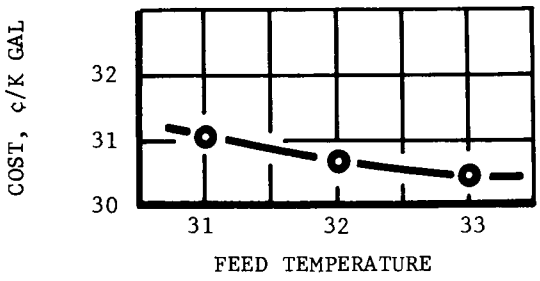

FIGURE 2.4

THE EFFECT OF EJECTOR PRIMARY TO SECONDARY RATIO

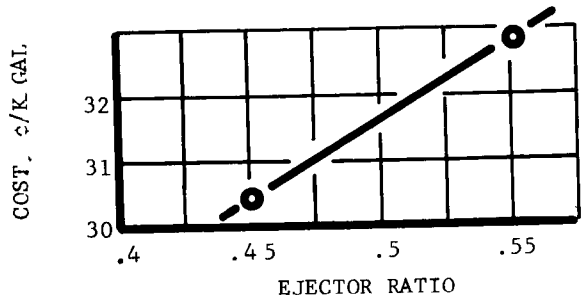

451-332 O - 71 - 9

TABLE 2.2

THE EFFECT OF PRESSURE

Run No.	Pressure	Conversion	$\frac{\text{Cost}}{\text{K Gal}}$
11	3.075	40%	32.19
9	3.264	40%	32.38

TABLE 2.3

THE EFFECT OF FEED TEMPERATURE INTO THE FREEZER

Run No.	Conversion	Feed Temperature	$\frac{\text{Cost}}{\text{K Gal}}$
12	50%	31	31.04
13	50%	32	30.70
10	50%	33	30.46

TABLE 2.4

THE EFFECT OF EJECTOR PRIMARY TO SECONDARY RATIO

Run No.	Ejector Ratio	$\frac{\text{Cost}}{\text{K Gal}}$
10	.45	30.46
15	.55	32.82

2.5 THE EFFECT OF ABSORBER TEMPERATURE

We do not have available a table of data to indicate specifically the effect of absorber temperature on the water cost. This is because the optimization procedure automatically searches over values for the absorber temperature and picks that particular value which leads to the minimum cost of the entire absorber loop. From the results of detailed print-outs of the individual steps taken by the computer in doing the search, it has been obeerved that over the range of absorber temperatures from $68^{o}F$ to $72^{o}F$, the effect on the total absorber loop operating cost is less than 2/3 percent.

TABLE 2.5
THE EFFECT OF PLANT SIZE

Run No.	Plant Size	$\frac{\text{Cost}}{\text{K Gal}}$
10	1 MGD	30.46
17	5 MGD	29.88

FIGURE 2.5
THE EFFECT OF PLANT SIZE

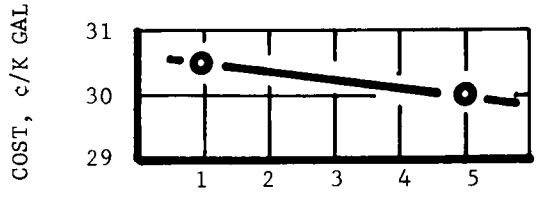

SECTION 2.6 THE EFFECT OF PLANT SIZE

Over the range from 1 to 5 GMD, the economics are not strongly affected by plant size. As expected, the cost per k gal is smaller in the larger plant, but the reduction is only about a half cent per k gal, or about 1.5 percent.

In still larger plants, it is reasonable to expect continued reduction in the cost of water.

SECTION 2.7 OPTIMAL VFEA PLANT DESIGN FOR 1.00 MGD PLANT

RUN NO. 10

ECONOMICS

WATER PL.0.100E 01 MGD
CAPACITY FACTOR: 330 DAYS
INTEREST RATE: 5% PLANT LIFE: 25 YRS OUTPUT: 330000. KGAL/YR

	CAPITAL COSTS IN $1000	ANNUAL COSTS IN $1000	WATER COST C/KGAL	%
CAPITAL COST CENTERS				
1. DESALTING EQUIPMENT	269.61	19.13	5.80	19.0
RECURRING COST CENTERS				
2. TAXES AND INSURANCE		5.34	1.62	5.3
TOTAL ANNUAL FIXED COSTS		24.47	7.41	24.3
OPERATION AND MAINTENANCE COST CENTERS				
3. MAINTENANCE LABOR		1.33	0.40	1.3
4. GENERAL AND ADMINISTRATIVE		0.46	0.14	0.5
5. SUPPLIES AND MAINTENANCE MATERIALS		1.33	0.40	1.3
6. STEAM		62.48	18.93	62.2
7. ELECTRIC POWER		10.43	3.16	10.4
8. OTHER (PAYROLL EXTRAS)		0.0020	0.0006	0.0020
TOTAL OPERATION AND MAINTENANCE COSTS		76.03	23.04	75.7
TOTAL FIXED PLUS O AND M COSTS		100.50	30.46	100.0

ABSORBER

VAPOR RATE	0.18503E 05	LB/HR
TEMPERATURE	0.66200E 02	DEGREES F
PRESSURE	0.30750E 01	MM HG
CAUSTIC CONCENTRATION	0.44000E 00	WT FRACTION
EQUILIBRIUM CONCENTRATION	0.40901E 00	WT FRACTION
MASS TRANSFER COEFFICIENT	0.22142E 02	LB/HR-FT(SQUARE)-DILUTION
AREA REQUIRED	0.48534E 04	SQUARE FEET
FEET OF 3/4-INCH TUBING,	0.17649E 05	FEET
ABSORBER CAPITAL COST	0.13625E 05	DOLLARS

LOW TEMPERATURE HEAT EXCHANGER

ABSORBER TEMPERATURE	0.66200E 02	DEGREES F
INTERMEDIATE TEMPERATURE	0.14813E 03	DEGREES F
DILUTE CAUSTIC RATE	0.18133E 06	LB/HR
CONCENTRATED CAUSTIC RATE	0.16282E 06	LB/HR
ABSORBER FEED TEMPERATURE	0.74853E 02	DEGREES F
LOW CONCENTRATOR FEED TEMPERATURE	0.13200E 03	DEGREES F
HEAT DUTY	0.99387E 07	BTU/HR
NUMBER OF PARALLEL FLOW CHANNELS	16.	
SERIES PLATES PER PASS	3.	
PLATES REQUIRED	90.	
END PLATES REQUIRED	9.	
PRESSURE DROP	0.18641E 02	LB/SQUARE INCH
TOTAL COST	0.15360E 05	DOLLARS

LOW TEMPERATURE CONCENTRATOR

VAPOR RATE	0.25365E 04	LB/HR
DILUTE CAUSTIC RATE	0.18133E 06	LB/HR

DILUTE CAUSTIC TEMPERATURE	0.13200E 03	DEGREES F
CONCENTRATED CAUSTIC RATE	0.17879E 06	LB/HR
CONCENTRATED CAUSTIC TEMPERATURE	0.12932E 03	DEGREES F
HEAT DUTY	0.32301E 07	BTU/HR
STEAM TEMPERATURE FROM HIGH CONCENTRATOR	0.24880E 03	DEGREES F
AREA OF TUBING REQUIRED	0.75938E 02	SQUARE FEET
FEET OF 1 1/4 INCH TUBING	0.17457E 03	FEET
CAPITAL COST OF CONCENTRATOR	0.68116E 03	DOLLARS

HIGH TEMPERATURE HEAT EXCHANGER

LOW CONCENTRATOR TEMP	0.12932E 03	DEGREES F
HIGH CONCENTRATOR TEMP	0.24880E 03	DEGREES F
DILUTE CAUSTIC RATE	0.17879E 06	LB/HR
CONCENTRATED CAUSTIC RATE	0.16282E 06	LB/HR
LOW CONCENTRATOR FEED TEMPERATURE	0.14813E 03	DEGREES F
HIGH CONCENTRATOR FEED TEMPERATURE	0.22100E 03	DEGREES F
HEAT DUTY	0.13654E 08	BTU/HR
NUMBER OF PARALLEL FLOW CHANNELS	16.	
SERIES PLATES PER PASS	2.	
PLATES REQUIRED	60.	
END PLATES REQUIRED	6.	
PRESSURE DROP REQUIRED	0.12427E 02	PSI
CAPITAL COST	10240.00	DOLLARS

HIGH TEMPERATURE CONCENTRATOR

VAPOR RATE	0.15966E 05	LB/HR
DILUTE CAUSTIC RATE	0.17879E 06	LB/HR
DILUTE CAUSTIC TEMPERATURE	0.22100E 03	DEGREES F
CONCENTRATED CAUSTIC RATE	0.16282E 06	LB/HR
CONCENTRATED CAUSTIC TEMPERATURE	0.24880E 03	DEGREES F
HEAT DUTY	0.26294E 08	BTU/HR
STEAM TEMPERATURE	0.30000E 03	DEGREES F

AREA OF TUBING	0.14426E 04	SQUARE FT
FEET OF 1 1/4 INCH TUBING	0.33164E 04	FEET
CAPITAL COST OF CONCENTRATOR	12940.40	DOLLARS

PUMPS IN ABSORBER LOOP

ABSORBER PUMP		
PRESSURE DROP	0.18641E 02	PSI
CAPACITY	0.18133E 06	LB/HR
HORSEPOWER	0.65333E 01	HP
COST	731.97	DOLLARS
LOW CONCENTRATOR PUMP		
PRESSURE DROP	0.12427E 02	PSI
CAPACITY	0.17879E 06	LB/HR
HORSEPOWER	0.51791E 01	HP
COST	617.37	DOLLARS
HIGH CONCENTRATOR PUMP		
PRESSURE DROP	0.31068E 02	PSI
CAPACITY	0.16282E 06	LB/HR
HORSEPOWER	0.81668E 01	HP
COST	862.05	DOLLARS

CONDENSER		
VAPOR RATE	0.25365E 04	LB/HR
DIAMETER	0.82386E 01	FT
CAPITAL COST OF CONDENSER	1558.82	DOLLARS

FREEZER-WASHER OUTPUT

FREEZER PRESSURE	3.075	MM HG
DELTA P	0.20184E 00	MM HG
DELTA T	0.11921E 01	DEGREES F
PRODUCT:VOLUME RATIO	0.13401E 03	LB/HR-CUBIC FEET
MEAN HOLDING TIME	0.10373E 00	HOURS
POOL VOLUME	0.25900E 04	CUBIC FEET
POOL MASS	0.16524E 06	LBS
POPULATION SIZE	0.16460E 09	NO.
MEAN CRYSTAL SIZE	0.25475E 00	MM
2ND. MOMENT	0.40822E 01	MM-SQUARED
3RD. MOMENT	0.19000E 03	MM-CUBED
FREEZER VESSEL DIAMETER	0.30107E 02	FEET
FREEZER POOL DEPTH	0.36400E 01	FEET
FREEZER VESSEL COST	14455.24	$
AGITATOR POWER	0.71154E 02	HP
AGITATOR COST	3201.91	$
ICE RISE RATE	0.64459E 03	LB/HR-FT SQUARE
WASHER VESSEL AREA	0.49427E 03	SQUARE FEET
DIAMETER	0.25093E 02	FEET
HEIGHT	0.10000E 02	FEET
COST	10724.31	$
SLURRY PUMP POWER	0.47327E 02	HP
COST	2178.24	$
WASH WATER RATE	0.13883E 06	LB/HR
PUMP POWER	0.30934E 01	HP
COST	423.15	$
TOTAL POWER FREEZER-WASHER	0.12157E 03	HP
COST	15.24	$/DAY
TOTAL F.W. EQUIP. COST	39658.04	$

AMORTIZED F.W. EQUIP. COST	19.63	$/DAY
TOTAL FREEZER-WASHER OP. COST	34.87	$/DAY

MELTER OUTPUT (INCLUDES EJECTOR, MAIN HEAT EXCHANGERS

MELTER PRESSURE	5.740	MM HG
MELTER DELTA T	0.46089E 01	DEGREES F.
MELTER LIQUID	0.34455E 06	LB/HR
MELTER AREA	0.30526E 03	SQUARE FEET
DIAMETER	0.19720E 02	FEET
HEIGHT	0.60000E 01	FEET
PRODUCED PUMP POWER	0.27644E 02	HP
BRINE PUMP POWER	0.37870E 02	HP
FEED PUMP POWER	0.45133E 02	HP
PRODUCT PUMP COST	1757.18	$
BRINE PUMP COST	1979.92	$
FEED PUMP COST	2132.80	$
TOTAL HEAT EXCHANGER + PUMP COST	7513.46	$/DAY
TOTAL HEAT EXCHANGER + PUMP POWER COST	13.86	$/DAY
HEAT EXCHANGER COST	23184.00	$
HEAT EXCHANGER OPERATING COST	28.25	$/DAY
MELTER VESSEL COST	6390.74	$
EJECTOR CAPITAL COST	23797.25	$
MELTER/EJECTOR/HEAT EXCHANGER CAP. COST	79039.50	$
AMORTIZED COST	39.12	$/DAY
TOTAL OP. COST	52.99	$/DAY
EJECTOR NOZZLE AREA	0.27727E 00	SQUARE FEET
NOZZLE COST	3210.00	$

EJECTOR

MASS RATE OF SECONDARY	0.28243E 05	LB/HR
MASS RATE OF PRIMARY	0.12709E 05	LB/HR
PRESSURE AT NOZZLE EXHAUST	0.30031E 01	MM HG
NOZZLE EXHAUST VELOCITY	0.31868E 04	FT/SEC
EXHAUST PRESSURE	0.57400E 01	MM HG
EXHAUST VELOCITY	0.25000E 03	FT/SEC
THROAT PRESSURE	0.28243E 01	MM HG
THROAT VELOCITY	0.14318E 04	FT/SEC
THROAT AREA	0.20254E 03	SQUARE FT
NOZZLE AREA	0.27727E 00	SQUARE FT
CAPITAL COST OF EJECTOR	23797.25	DOLLARS

MISCELLANEOUS

BRINE RECYCLE/FEED RATIO	0.13622E 01	
FREEZER VAPOR/FEED RATIO	0.67340E-01	
FREEZER BRINE COMPOSITION	0.70632E-01	WT. FRACTION
CONVERSION	0.50000E 00	
FREEZER VAPOR TEMP.	0.23462E 02	DEGREES F
FREEZER VAPOR RATE	0.46745E 05	LB/HR
SLURRY RATE	0.15930E 07	LB/HR
RECYCLE RATE	0.94561E 06	LB/HR

MAIN HEAT EXCHANGER

FEED INLET TEMPERATURE	0.70000E 02	DEGREES F
FEED OUTLET TEMPERATURE	0.33000E 02	DEGREES F
BRINE TEMP. FROM WASHER	0.24772E 02	DEGREES F
PRODUCT TEMP. FROM WASHER	0.36609E 02	DEGREES F
FEED RATE	0.69417E 06	LB/HR
BRINE RATE	0.34708E 06	LB/HR
PRODUCT RATE	0.34708E 06	LB/HR
HEAT LOAD	0.25684E 08	BTU/HR
PARALLEL FLOW CHANNELS	69	
SERIES PLATES PER PASS	2	
PLATES REQUIRED	276	
END PLATES REQUIRED	5	
CAPITAL COST	23184.00	$

COST BREAKDOWN

(NOTE: *INDIVIDUAL COSTS NOT CORRECTED FOR CURRENT COST INDEX.
TOTAL AND AMORTIZED CAP. COSTS ARE CORRECTED FOR CURRENT COST INDEX.)

FREEZER/WASHER

FREEZER VESSEL COST *	14455.24	$
AGITATOR COST *	3201.91	$
SLURRY PUMP COST *	2178.24	$
WASHER VESSEL COST *	10724.31	$
WASH WATER PUMP COST *	423.15	$
TOTAL F/W EQUIPMENT COST	39658.04	$
AMORTIZED COST	19.63	$/DAY
POWER COST	15.24	$/DAY
OPERATING COST	34.87	$/DAY

MELTER/EJECTOR/MAIN HEAT EXCHANGERS

MELTER VESSEL COST *	6390.74	$
EJECTOR COST *	23797.25	$
NOZZLE COST *	3210.00	$
PRODUCT PUMP COST *	1757.18	$
BRINE PUMP COST *	1979.92	$
FEED PUMP COST *	2132.80	$
TOTAL PUMP COST	7513.46	$
MAIN HEAT EXCHANGER COST *	23184.00	$
TOTAL CAP. COST MELT/EJ/HTEX	79039.50	$
TOTAL AMORTIZED COST OF MELT/EJ/HTEX	39.12	$/DAY
TOTAL POWER COST	13.86	$/DAY
TOTAL MELT/EJ/HTEX OPERATING COST	52.99	$/DAY

ABSORBER/REGENERATOR COSTS

ABSORBER CAP. COST *	13624.96	$
REG. CAP COST *	7683.96	$
CONDENSER VESSEL COST *	1558.82	$
HT EXC. COST (H) *	10240.00	$
HT EXC. COST (L) *	15360.00	$
TOT. HT. EX. COST *	25600.00	$
A1 PUMP COST *	731.97	$
R1 PUMP COST *	617.37	$
R2 PUMP COST *	862.05	$
TOT. REG/ABS/COND CAP. COST	51298.32	$
AM. CAP. COST	25.39	$/DAY
TOTAL POWER COST	2.49	$/DAY
TOTAL STEAM COST	189.32	$/DAY
TOTAL ABSORBER OPERATING COST	217.21	$/DAY

END

451-332 O - 71 - 10

SECTION 2.8 OPTIMIZATION STRATEGY

In this section we wish to outline in non-mathematical terms the general strategy followed by the computer in calculating and optimum process design. The detailed formulations for the various process components, together with the assumptions involved in their derivations, are discussed in a following section. It is our purpose here to delineate the ideas involved in the optimization.

In the first step, certain variables termed global variables are read into the computer and assumed to be maintained constant through a particular calculation. Their effect is then studied by varying the input to the computer from run to run. These variables are the following:

The design product rate
The reject brine concentration
The inlet sea water concentration
The product concentration
The freezer pressure
The slurry ice concentration
The net wash fraction ice loss

With these variables preset, it is possible, by taking heat and mass balances around the freezer, to compute the conversion, the vapor rate from the freezer, the freezer recycle ratio, and the salt concentration in the freezer slurry. These results constitute starting points for further calculations.

The next step is the optimal design of the absorber loop. The net vapor from the freezer is comprised of two parts: a) that whose latent heat is necessary to balance the latent heat of freezing, and b) that whose latent heat is to balance the heat leakage into the process, the sensible heat load resulting from heat exchanger inefficiency, and that which enters the process by other means. To maintain the process in thermal equilibrium, only the vapor of part a) should be returned to the melter. The vapor in part b) represents excess above that which is required to melt the ice and, consequently, is to be removed in the absorber

section. Thus, the total vapor required by the absorber section is that required to drive the ejector plus that generated by the process inefficiencies. If the primary to secondary ratio in the ejector is specified and the vapor requirement due to process inefficiencies can be estimated, then mass balance calculations in the absorber loop will fix the flows in that section of the process.

Considering that portion of the vapor to be rejected in the absorber loop, a certain fraction (ALP) is to be vaporized in the No. 1 concentrator. The balance (1 - ALP) must be vaporized in the No. 2 concentrator along with the vapor required to drive the ejector. A heat balance around the No. 1, or low temperature, concentrator determines this split.

In order to do the heat balance on the No. 1 concentrator, which was just discussed, it is necessary to know the temperature into and out of this vessel. These temperatures are determined as follows: The concentrator temperature is taken to be that which is in equilibrium at the concentrator composition and the condenser pressure, which is assumed known (a global variable). If two additional temperatures are assumed, these are sufficient to calculate from heat balances the inlet and exit temperatures of all streams in both of the absorber loop heat exchangers. Thus, the number of transfer units required by each exchanger can be determined. The computer is programmed to design by trial and error the minimum cost heat exchangers to produce the required number of transfer units. This is done by searching over the possible designs to select the one particular design that minimizes the total cost of operation.

Having ascertained the best heat exchangers for assumed values of the temperatures in the absorber-concentrator loop, the next step in the optimization procedure is to search over the permissible values for these temperatures, ascertaining those which produce the minimum cost for the entire absorber loop. This cost is comprised of the heat exchanger cost, the pumping cost, and the amortized capital cost of the vessels involved.

This portion of the optimization is contained in a subroutine designated "AOPCOS."

The next optimization is that of the melter-ejector combination. The computer is programmed to search over a reasonable range of values for the melter pressure to ascertain that pressure which results in the

most economical balance between the melter and the ejector. A large melter pressure results in a large driving force for melting and, thus, a smaller melter. However, a larger ejector is required to produce this higher pressure. The portion of the program which does the optimization of the melter-ejector also contains the optimization of the main heat exchanger as a subroutine. The main heat exchanger is optimized in the same manner as the absorber loop heat exchangers, as described previously.

In this study no optimization has been done on the freezer-counter washer combination. The indicated balance would normally be between the freezer size and the washer size via a search over the ice particle size produced in the freezer. A larger freezer produces a larger particle size which leads to a smaller washer. Operating experience has shown, however, that the particle size produced in the freezer vessel is in the neighborhood of 0.2 mm and is relatively insensitive to freezer operating conditions. Therefore, the optimization calculations have been omitted for the freezer-counter washer part of the process.

SECTION 3. DYNAMIC STUDIES BY ANALOG COMPUTER

The analog computer simulation of the dynamics of the integrated VFEA process has been mechanized, debugged, and subjected to critical review by representatives of the Research Triangle Institute, Colt Industries, Electronic Associates, Inc., and the Office of Saline Water. This review was accomplished during a working session at the EAI Computation Center located at West Long Branch, New Jersey, on September 29 and 30, 1971.

The simulation appears to be a good one in that it now represents the process dynamics in a way consistent with our understanding of the behavior. The multichannel recorder tracings delineating the dynamic response of the process were turned over to representatives of Colt Industries at the termination of the working session. Analog computer circuitry and wiring diagrams were forwarded to Colt under separate cover a few days later.

It is anticipated that the analog simulation will be useful in interpreting and evaluating the performance of the integrated, bench-scale unit to be assembled and tested at Beloit. Subsequently, a revised version of the analog simulation based on operating experience obtained with the bench-scale unit should be of value in the design and evaluation of control systems for full-scale operating plants.

VFEA PROCESS

ANALOG COMPUTER PROGRAM

NOMENCLATURE

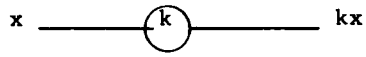

Multiplication By A Constant

Inversion

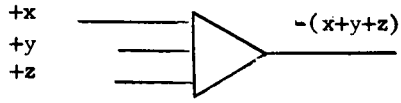

Summation

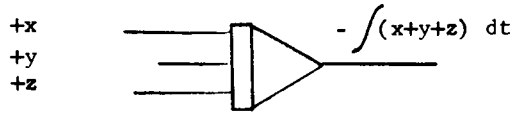

Integration

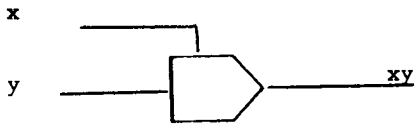

Multiplication of Variables

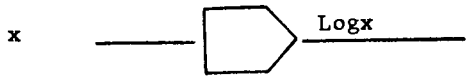

Function Generation

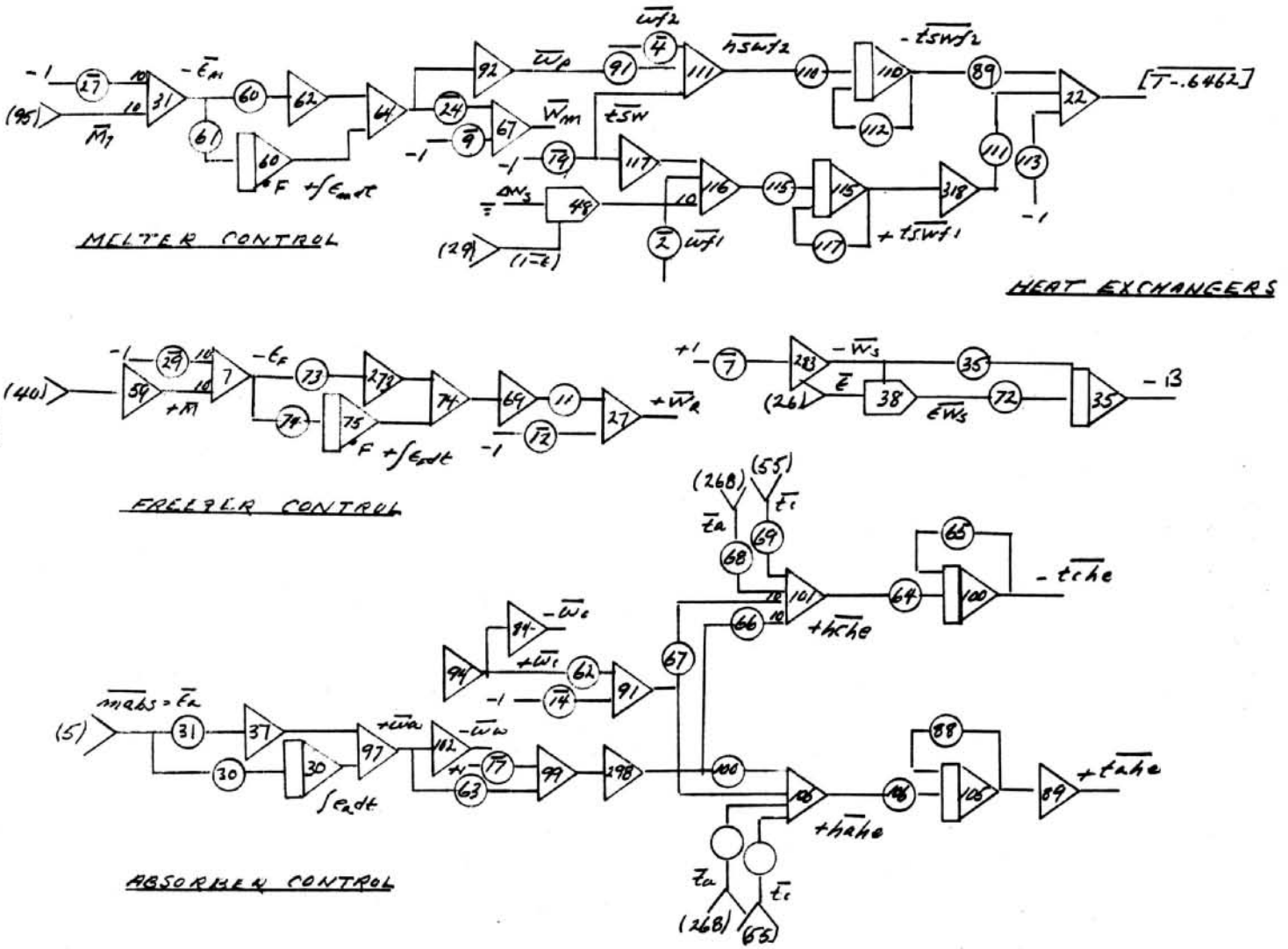
MELTER CONTROL
HEAT EXCHANGERS
FREEZER CONTROL
ABSORBER CONTROL

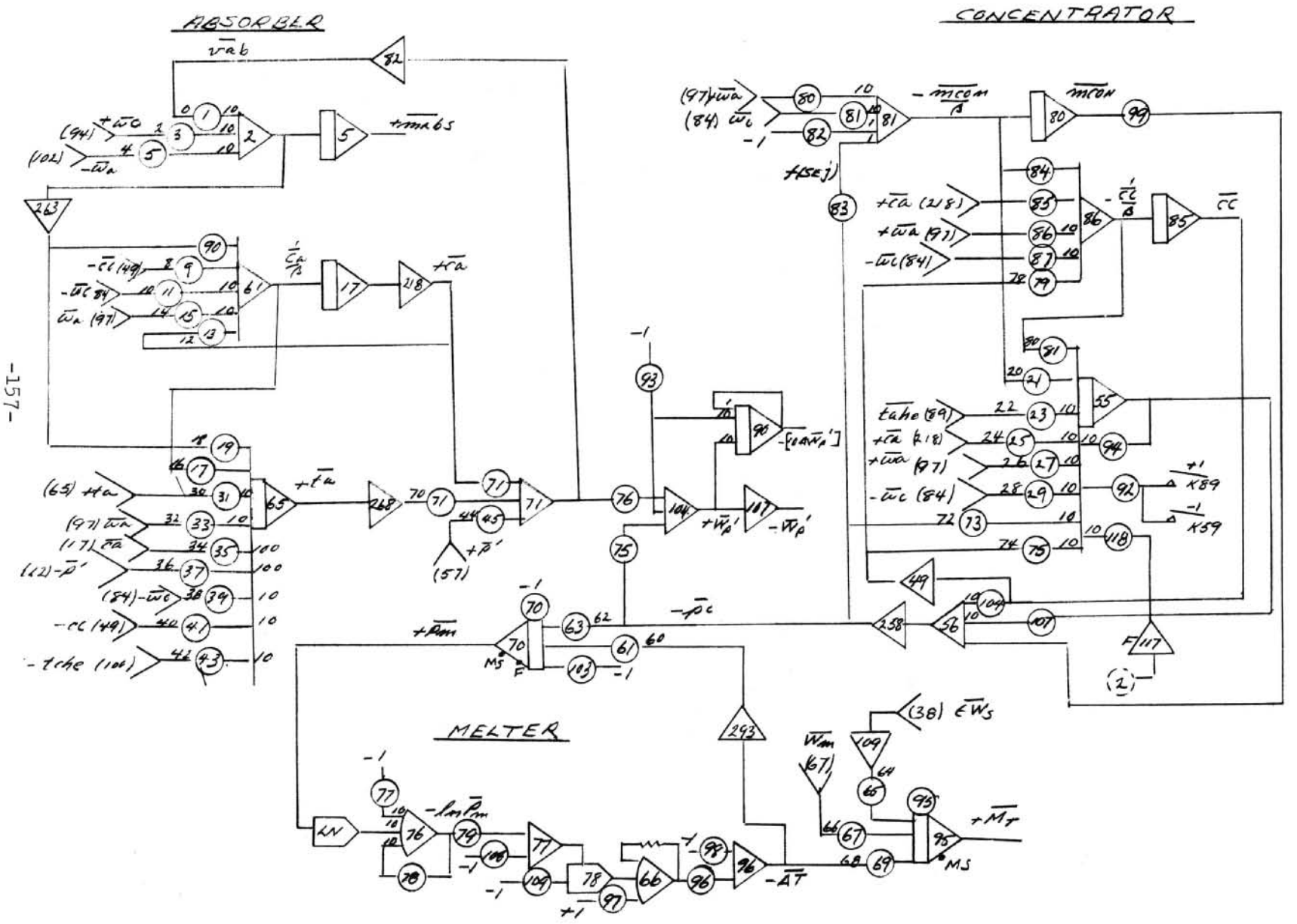
ABSORBER
CONCENTRATOR
MELTER
LN
MS
F

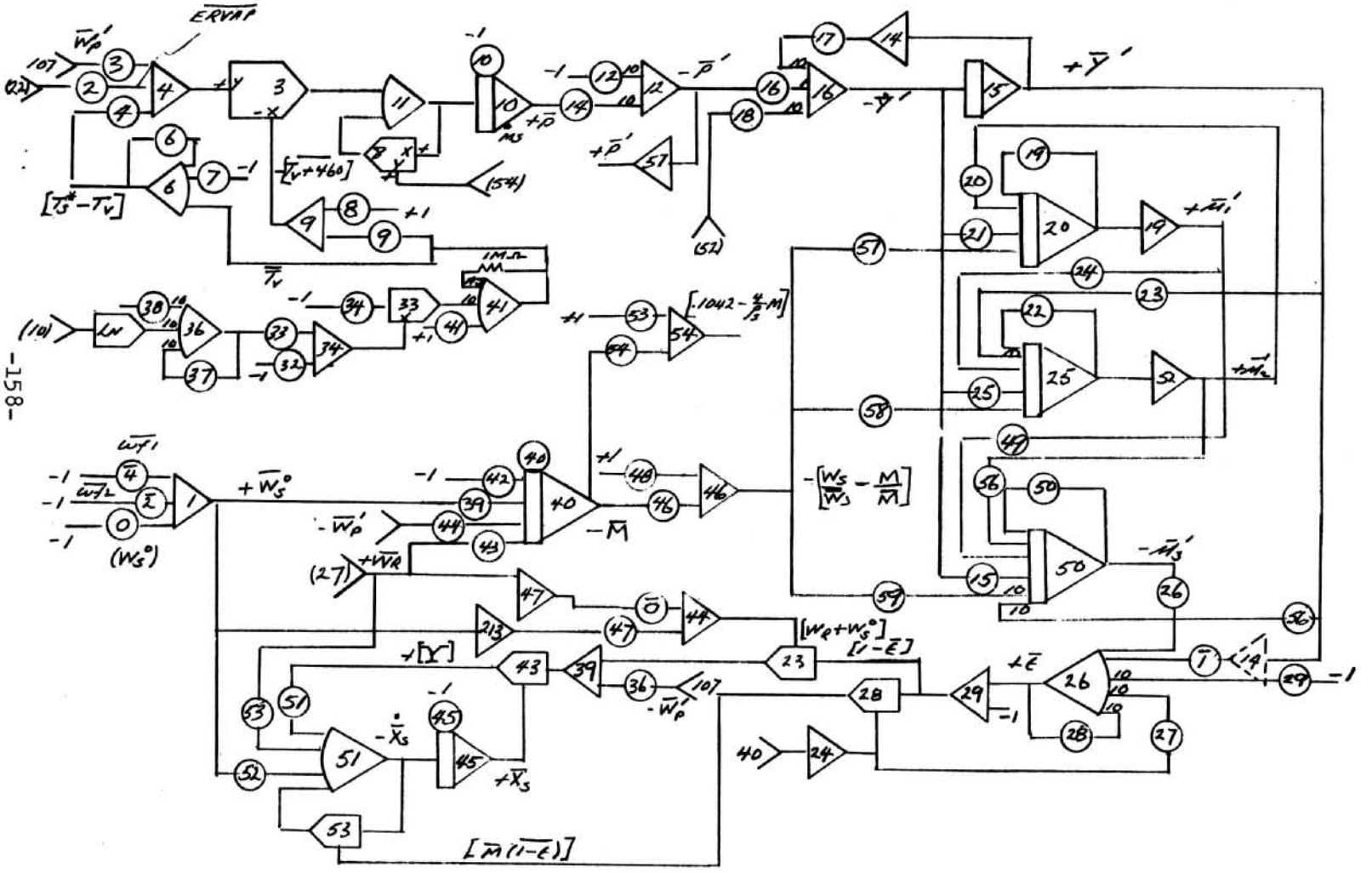
ERVAP
$\bar{W}_p'$
$+\bar{y}'$
$-\bar{p}'$
$+\bar{p}'$
$-\bar{y}'$
$[\bar{T}_s^* - \bar{T}_v]$
$[\bar{T}_v + 460]$
$\bar{T}_v$
$+\bar{m}_1'$
$+\bar{m}_2$
$-\bar{m}_3'$
$[.1042 - \frac{\bar{x}}{\bar{s}}\bar{m}]$
$-[\frac{W_s}{W_3} - \frac{M}{M}]$
$\bar{W}_{f1}$
$\bar{W}_{f2}$
(W_s°)
$+\bar{W}_s^\circ$
$-\bar{W}_p'$
$-\bar{M}$
$+\bar{W}_R$
$+[\bar{x}]$
$-\dot{\bar{x}}_s$
$+\bar{x}_s$
$[\bar{m}(1-\bar{e})]$
$[W_R + W_s^\circ]$
$[1-\bar{e}]$
$\pm\bar{e}$
$-\bar{W}_p'$
(101)
(102)
(107)
(27)
(52)
(54)
-158-
FREEZER

VFEA Process Control Study

Analog Computer Simulation Print Outs

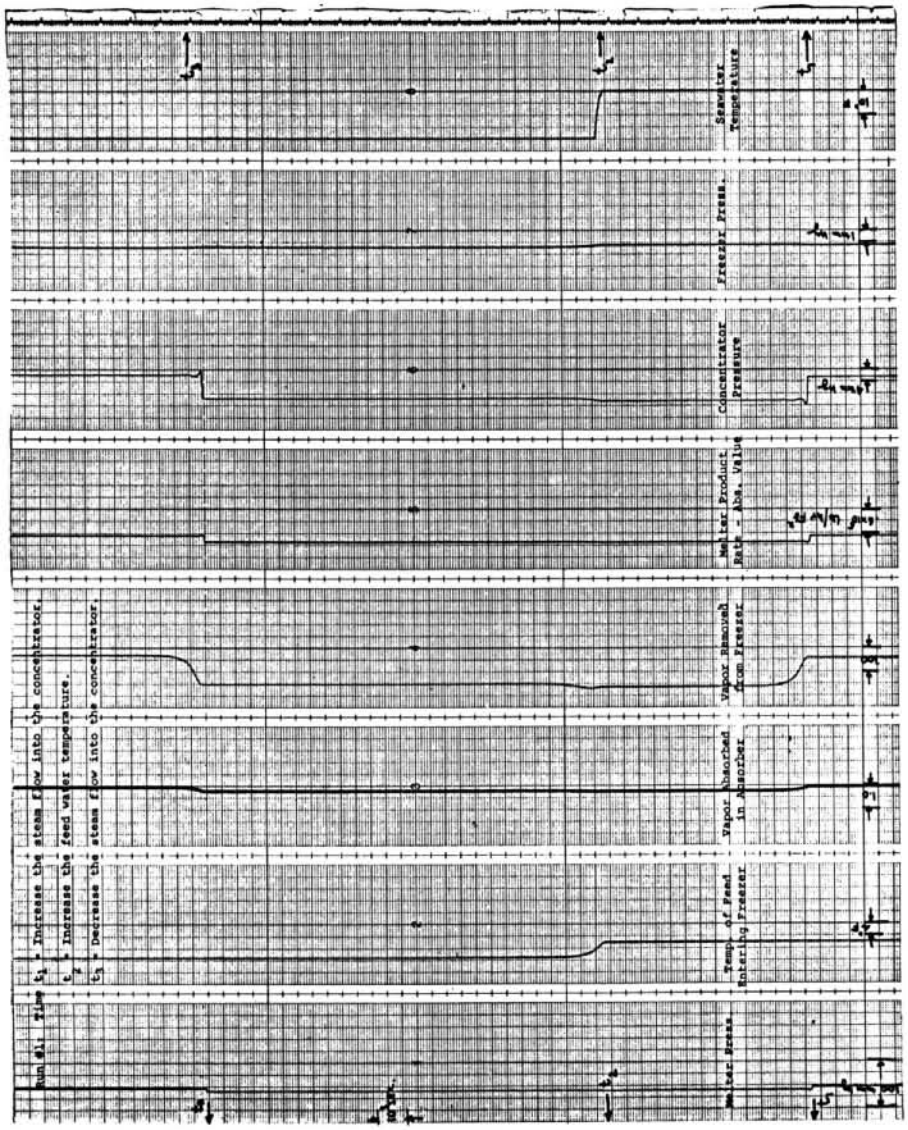

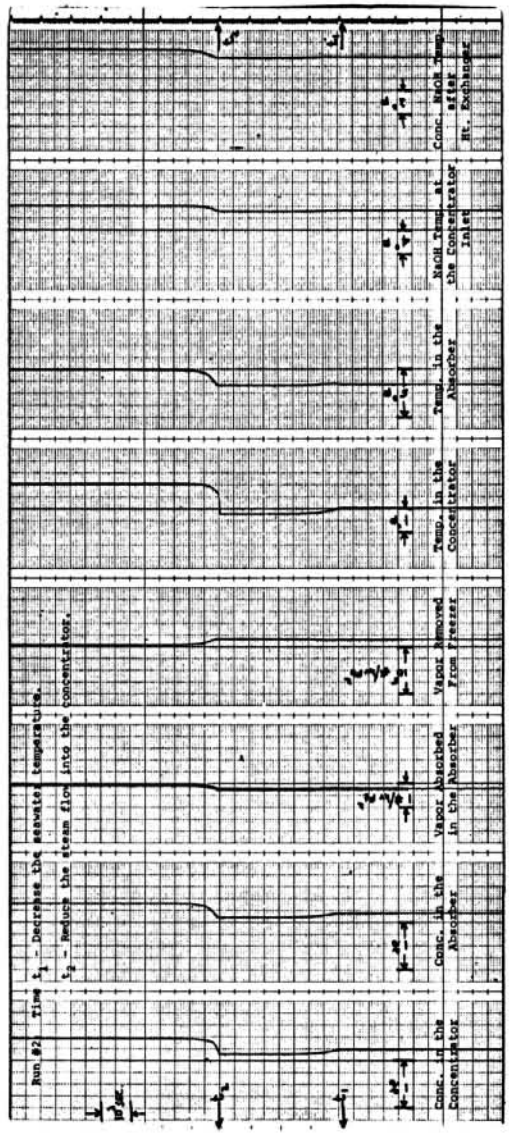
Run #2
Time t_1 - Decrease the seawater temperature.
t_2 - Reduce the steam flow into the concentrator.
Conc. in the Concentrator
Conc. in the Absorber
Vapor Absorbed in the Absorber
Vapor Removed From Freezer
Temp. in the Concentrator
Temp. in the Absorber
KnOH Temp. at the Concentrator inlet
KnOH Temp. Conc. after Ht. Exchanger

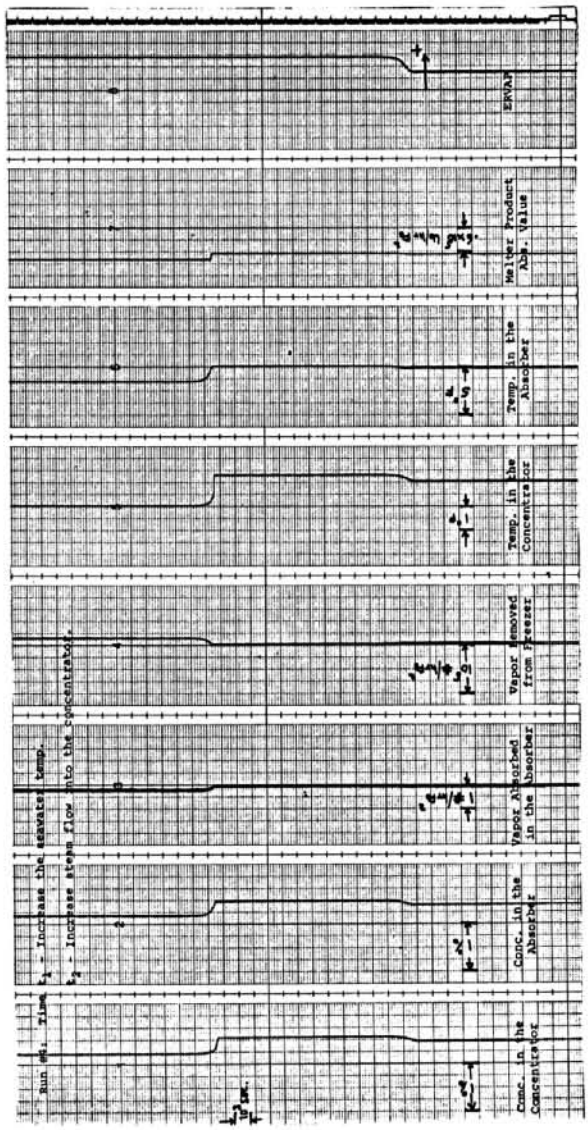
Run ofs. Time
t_1 - Increase the seawater temp.
t_2 - Increase steam flow into the Concentrator
Conc. in the Concentrator
Conc. in the Absorber
Vapor Absorbed in the Absorber
Vapor Removed from Freezer
Temp. in the Concentrator
Temp. in the Absorber
Water Product Abs. Value
ENVAP

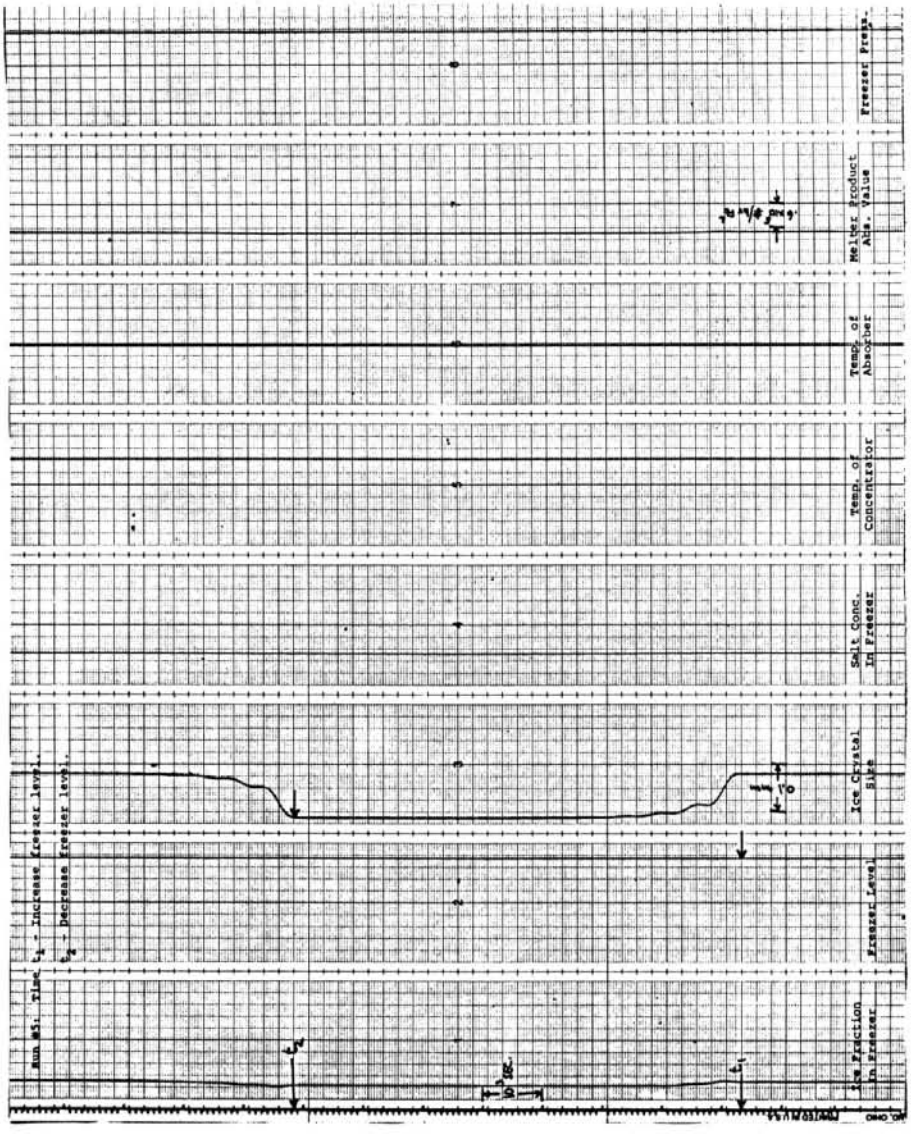
Run No.: Time: t_1 - Increase Freezer level.
t_2 - Decrease Freezer level.
Ice Fraction In Freezer
Freezer Level
Ice Crystal Size
Salt Conc. In Freezer
Temp. of Concentrator
Temp. of Absorber
Meltec Product Alka. Value
Freezer Temp.

Ice Friction In Freezer
Run ph: rise
Freezer Level
Ice Crystal Size
Salt Conc. In Freezer
Temp. of Concentrator
Temp. of Absorber
Meiter Product Abs. Value
Freezer Press.
t1
t2
30 sec.

SECTION 4. STEADY STATE MODELS OF THE PROCESS COMPONENTS

4.1 THE STEADY STATE ABSORBER

4.1.1 ASSUMPTIONS

In developing equations for absorber behavior, the following assumptions have been made:

1. The gas pressure is constant throughout the absorber.
2. The liquid interfacial temperature is equal to the bulk liquid temperature. This assumption will be defended in a later section of the report and shown to involve only a small error.
3. Sensible heat transfer to the vapor can be neglected for several reasons; first, rates are slow because the film coefficient is small; second, quantities of heat involved are small because of the low vapor heat capacity; and third, the absorption is liquid film controlled--only the gas pressure (not its temperature) enters into the absorption rate expressions.
4. The recirculation rate to the absorber spray nozzles is sufficiently high that the absorbing liquid can be considered as perfectly mixed.

4.1.2 ABSORBER EQUATIONS

With the above assumptions the absorber equations and calculation procedure are the following:

$$CA = .44 \qquad \text{E 4.1.1}$$

$$XA = \frac{1 - CA}{CA} \qquad \text{E 4.1.2}$$

E 4.1.1 states the operating concentration of the absorber to be 0.44 wt fraction NaOH; E 4.1.2 converts to a dilution. Find TA to maximize the expression

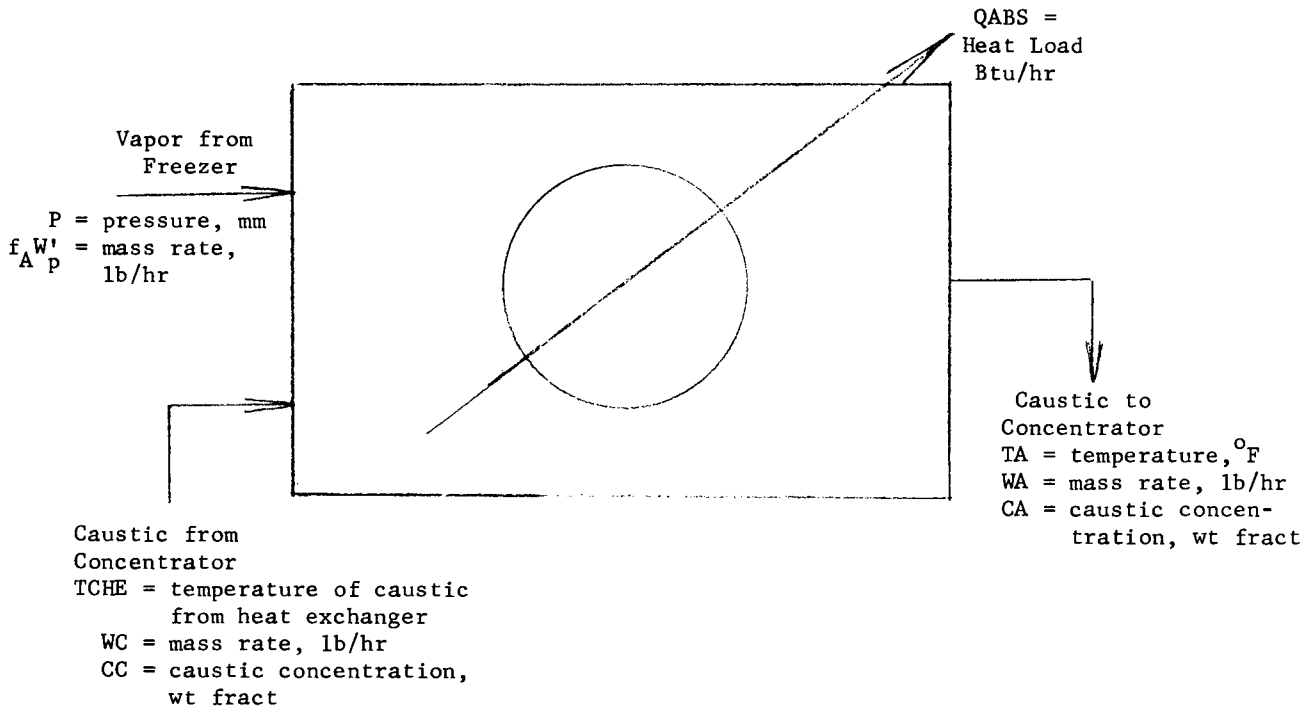

Figure F 4.1

ABSORBER SCHEMATIC

451-332 O - 71 - 11

$$RABS = (MTC)[XEQ(TA,P) - XA] \qquad E\ 4.1.3$$

i.e., find the temperature to maximize the absorption rate per unit area, where the mass transfer coefficient and equilibrium concentration are found from E 6.1.9 and E 6.1.10, and the equilibrium dilution is

$$XEQ(TA,P) = \frac{1 - CEQ}{CEQ} \qquad E\ 4.1.4$$

TA should be around 70 to 80 to remain within the limits of the experimental data.

The absorber area is then

$$ABSA = \frac{f_A W'_p}{(MTC)[XEQ(TA,P) - XA]} \qquad E\ 4.1.5$$

The estimated cost is

$$ABSC = ABCOA \cdot ABSA \qquad E\ 4.1.6$$

The heat to be removed from the absorber is given by

$$QABS = WC \cdot H(T4,CC) + f_A W'_p\ HVAP(T) - WA \cdot H(TA,CA) \qquad E\ 4.1.7$$

4.1.3 DRIVING FORCES IN THE ABSORBER

Consider the local conditions within an absorber in which aqueous NaOH is absorbing saturated water vapor. As vapor condenses, it liberates as sensible heat at the vapor-liquid interface its latent heat of

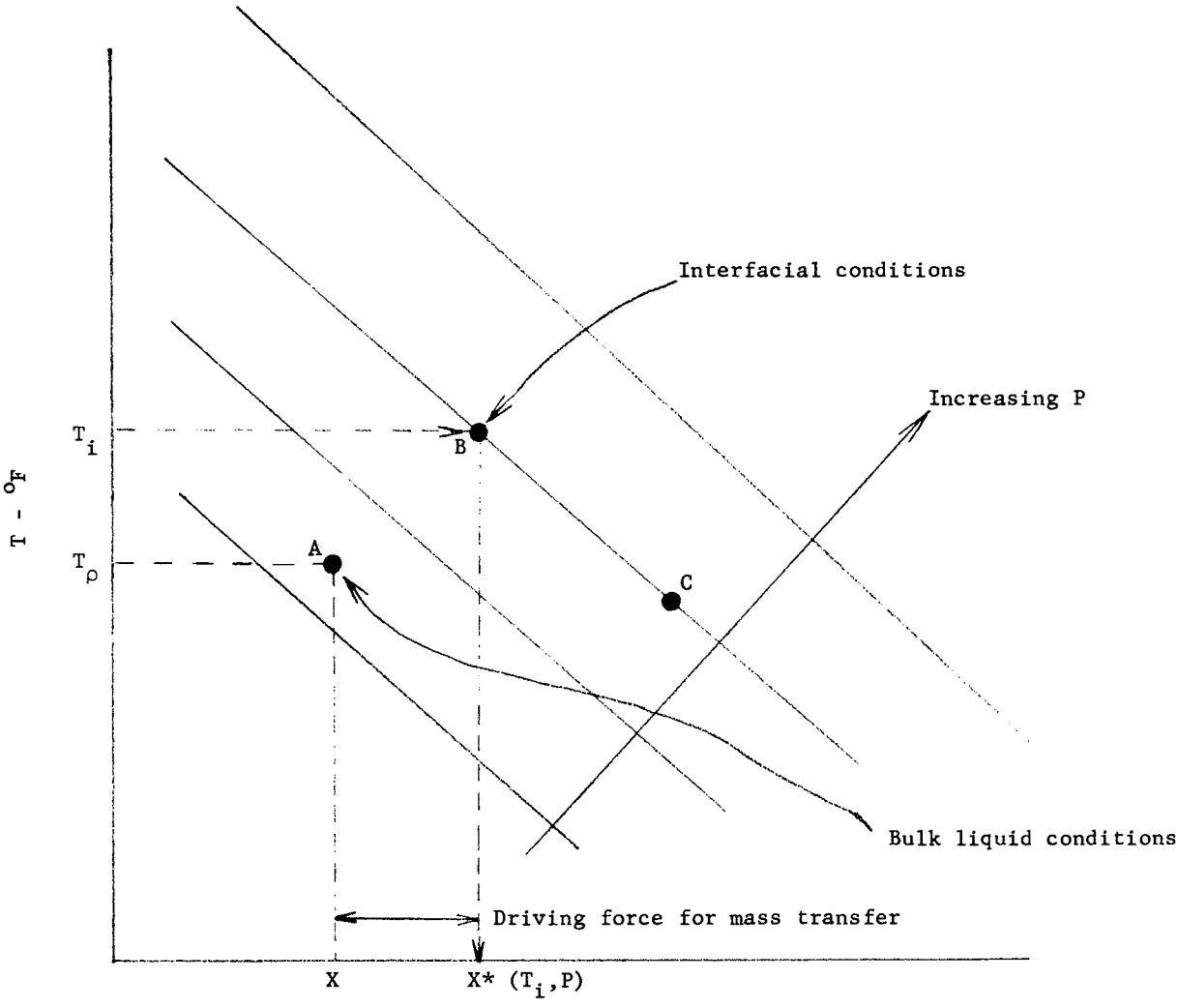

A represents liquid conditions at some point in the absorber.

B represents interface conditions, hotter and more dilute.

C represents vapor conditions, some pressure but much cooler.

Figure F 4.2

HYPOTHETICAL LOCAL CONDITIONS IN AN ABSORBER

vaporization which must be removed from the interface by conduction or convention mechanisms.

The necessity for the existence of a driving force for the removal of this heat then causes the interfacial temperature to differ from the bulk liquid temperature. The magnitude of this temperature difference is important, since it directly influences the rate of absorption, as explained in the following paragraph.

Assuming proper functioning of the deaerator, the vapor entering the absorber is virtually air-free. If there are no non-condensibles present, then there is no vapor phase resistance to mass transfer, and one can assume that the interface is in partial equilibrium with the vapor. By partial equilibrium is meant that the interfacial temperature may differ from the vapor temperature; but whatever the interfacial temperature happens to be, the interfacial composition will be that which is in equilibrium with the vapor at this interfacial temperature and at the absorber pressure. Designating this interfacial composition, expressed as a dilution, by $X^*(T_i,P)$, the driving force for absorber mass transfer can be taken as $X^*(T_i,P) - X$, where X refers to the bulk liquid dilution. (X has dimensions of lbm H_2O/lbm NaOH.) These remarks are illustrated schematically in Figure 1, in which conditions in the absorber are illustrated on an equilibrium diagram.

It should be clear that the interfacial temperature needs to be elevated in order to calculate the mass transfer driving force. In the following paragraphs it is shown that with only small errors the interfacial temperature can be taken equal to the bulk liquid temperature.

Begin with a heat balance at the interface:

$$Q(\text{liquid to interface}) + Q(\text{latent, released at interface})$$

$$= Q(\text{interface to vapor}). \qquad \text{E 4.1.8}$$

Inserting standard expressions for the Q's, and taking the latent heat at 1000 Btu/lbm and the mass transfer rate to be

$$N = k_l \Delta C \ , \qquad \text{E 4.1.9}$$

there results

$$h_l(T_l - T_i) + 1000\ k_l \Delta C = h_v(T_i - T_v) \ . \qquad \text{E 4.1.10}$$

Expressing h_v in terms of h_l by

$$h_v = \epsilon h_l \ , \qquad \text{E 4.1.11}$$

then

$$\frac{h_l}{\rho C_p k_l} \rho\, C_p [(T_l - T_i) - \epsilon(T_i - T_v)] = -\ 1000 \Delta C \ . \qquad \text{E 4.1.12}$$

From the usual j-factor analogies,

$$\frac{h_l}{\rho C_p k_l} = \left(\frac{\alpha}{D}\right)^{2/3} \qquad \text{E 4.1.13}$$

where α and D are diffusivities for heat and mass, respectively. Inserting typical values and simultaneously converting concentrations to weight percentages, there results

$$0.363 \Delta W = (T_l - T_i) - \epsilon(T_i - T_v) \qquad \text{E 4.1.14}$$

where ΔW is the concentration driving force converted to weight percent.

The value of ϵ, the ratio of the vapor to liquid h-values, can be estimated as follows. For coexistent flow of two phases, liquid and vapor, the shear stresses at the phase boundary must balance. This implies that

$$f(\tfrac{1}{2}\rho v^2)_{liq} = f(\tfrac{1}{2}\rho v^2)_{vapor} \qquad \text{E 4.1.15}$$

Since the friction factors are not widely different, equality of shear stresses is provided, in the main, by velocity differences relative to the interface velocity. Inserting typical density values into the above equation, one gets, for the ratio of linear velocities

$$V_{vap}/V_{liq} \approx 550. \qquad \text{E 4.1.16}$$

Since the friction factors in the two phases are about equal, so also are the j-factors for heat transfer, defined as

$$j_h = \frac{h}{\rho C_p V_f} (Pr)^{2/3} \qquad \text{E 4.1.17}$$

Taking the ratio, vapor to liquid, and inserting typical physical property data along with the velocity ratio estimated above, one finds that

$$\epsilon = \frac{h_v}{h_l} \approx .003 \qquad \text{E 4.1.18}$$

If this value of ϵ is inserted into E 4.1.14 above,

$$0.363\Delta W = (T_l - T_i) - .003(T_i - T_v) \qquad \text{E 4.1.19}$$

with $\Delta W = 5\%$

$T_l = 70^{\circ}F$

$T_v = 30^{\circ}F$

the resulting T_i is approximately $68^{\circ}F$.

Under these conditions, which are roughly typical, the error that results from taking the interfacial temperature equal to the bulk liquid temperature is on the order of 3 percent. This is certainly sufficiently accurate for our purposes and has been adopted in absorber theory.

4.1.4 ABSORBER NOTATION

ABSA = absorber area required
ABSC = absorber capital cost
ABCOA = absorber cost per unit area
CA = absorber concentration, wt fraction NaOH
CEQ = equilibrium concentration in absorber, wt fraction NaOH
$f_A W'_p$ = absorber vapor flow, lb/hr
MTC = mass transfer coefficient, $lbm/hr\text{-}ft^2$
P = absorber pressure
QABS = absorber heat load, Btu/hr
RABS = rate of absorption per unit area
TA = absorber temperature, $^{\circ}F$
WA = caustic rate from absorber, lb/hr
WC = caustic rate from concentrator, lb/hr
XA = absorber dilution, lb H_2O/NaOH
XEQ = absorber equilibrium dilution

4.2 THE STEADY STATE ABSORBER LOOP HEAT EXCHANGERS

In this section we shall outline some general results applicable to both the absorber heat exchangers and the main heat exchanger. Subsequently we then adapt the general results to the specific application, the absorber exchangers in this section and the main exchangers in Section 4.6.

4.2.1 BALANCED HEAT EXCHANGERS, GENERAL RESULTS

The differential equations representing the behavior of a balanced, two-fluid heat exchanger with (n/2) parallel channels each for both the hot and the cold fluid are

$$\begin{vmatrix} dT_1/d\xi \\ dT_2/d\xi \\ dT_3/d\xi \\ \cdot \\ \cdot \\ \cdot \\ dT_{n-1}/d\xi \\ dT_n/d\xi \end{vmatrix} = \begin{vmatrix} -1 & 1 & & & & & & \\ -1 & 2 & -1 & & & & & \\ & 1 & -2 & & 1 & & & \\ & & \cdot & & & & & \\ & & & \cdot & & & & \\ & & & & \cdot & & & \\ & & & 1 & & -2 & 1 & \\ & & & & & -1 & 1 & \end{vmatrix} \begin{vmatrix} T_1 \\ T_2 \\ T_3 \\ \cdot \\ \cdot \\ \cdot \\ T_{n-1} \\ T_n \end{vmatrix} \qquad \text{E 4.2.1}$$

where

$$\xi = \frac{U A x}{m C_p} \qquad \text{E 4.2.2}$$

with A = the area per unit length (or width) of a single sheet

m = the mass rate of one fluid in a single channel.

This system is difficult to solve for arbitrary values of n; hence, we give solutions for n = 2, n = 4, and n = ∞ and conclude that in most

situations of practical interest, the result for n = ∞ is a sufficiently accurate approximation to the actual performance.

A. Two Fluid--Single Channel. For n = 2 the equations are

$$\begin{vmatrix} \frac{dT_1}{d\xi} \\ \\ \frac{dT_2}{d\xi} \end{vmatrix} = \begin{vmatrix} -1 & 1 \\ \\ -1 & 1 \end{vmatrix} \begin{vmatrix} T_1 \\ \\ T_2 \end{vmatrix} \qquad \text{E 4.2.3}$$

$$\frac{\text{Approach}}{\text{Spread}} = \frac{1}{1 + \text{NTU}} \qquad \text{E 4.2.4}$$

where the spread is the difference in entering temperatures, i.e., the inlet hot fluid temperature minus the inlet cold fluid temperature, and

$$\text{NTU} = \frac{U\ AL}{\dot{m}\ Cp} \qquad \text{E 4.2.5}$$

with (AL) being the area of a single sheet.

B. Two Fluid--Double Channel. For n = 4 the equations are

$$\begin{vmatrix} \frac{dT_1}{d\xi} \\ \\ \frac{dT_2}{d\xi} \\ \\ \frac{dT_3}{d\xi} \\ \\ \frac{dT_4}{d\xi} \end{vmatrix} = \begin{vmatrix} -1 & 1 & & \\ \\ -1 & 2 & -1 & \\ \\ & 1 & -2 & 1 \\ \\ & & -1 & 1 \end{vmatrix} \begin{vmatrix} T_1 \\ \\ T_2 \\ \\ T_3 \\ \\ T_4 \end{vmatrix} \qquad \text{E 4.2.6}$$

with the solution as follows:

$$\begin{Bmatrix} T_1 \\ T_2 \\ T_3 \\ T_4 \end{Bmatrix} = \begin{vmatrix} 1 & & & 0 \\ & 1 & & \\ & & 1 & \\ 0 & & & 1 \end{vmatrix} + \frac{\eta}{\sqrt{2}} \begin{vmatrix} -1 & 1 & & 0 \\ -1 & 2 & -1 & \\ & 1 & -2 & 1 \\ 0 & & -1 & 1 \end{vmatrix}$$

$$+ \left(\frac{-1 + \cosh \eta}{2}\right) \begin{vmatrix} 0 & 1 & -1 & 0 \\ -1 & 2 & 0 & -1 \\ -1 & 0 & 2 & -1 \\ 0 & -1 & 1 & 0 \end{vmatrix} \qquad \text{E 4.2.7}$$

$$+ \left(\frac{-\eta + \sinh \eta}{2^{3/2}}\right) \begin{vmatrix} -1 & 1 & 1 & -1 \\ -1 & 3 & -1 & -1 \\ 1 & 1 & -3 & 1 \\ 1 & -1 & -1 & 1 \end{vmatrix} \begin{matrix} T_{h\text{-}in} \\ T_{C1\text{-}out} \\ T_{h\text{-}in} \\ T_{C2\text{-}out} \end{matrix}$$

where $\eta = \sqrt{2}\ \xi$ E 4.2.8

$$T_{C1\text{-}out} = \frac{A_1 B_{22} - A_2 B_{12}}{B_{11} B_{22} - B_{12} B_{21}} \qquad \text{E 4.2.9}$$

$$T_{C2\text{-}out} = \frac{A_2 B_{11} - A_1 B_{21}}{B_{11} B_{22} - B_{12} B_{21}} \qquad \text{E 4.2.10}$$

for

$$A_1 = T_{C\text{-}in} + (2\ NTU + H_1 + 2H_2)\ T_{h\text{-}in} \qquad \text{E 4.2.11}$$

$$A_2 + T_{C\text{-}in} + (NTU - H_1)\ T_{h\text{-}in} \qquad \text{E 4.2.12}$$

$$\begin{vmatrix} B_{11} & B_{21} \\ B_{21} & B_{22} \end{vmatrix} = \begin{vmatrix} (1 + 2\ NTU + 2H_1 + 3H_2) & -(H_1 + H_2) \\ -(H_1 + H_2) & (1 + NTU + H_2) \end{vmatrix} \qquad \text{E 4.2.13}$$

where $H_1 = \left(\frac{-1 + \cosh \sqrt{2}\ NTU}{2}\right)$ E 4.2.14

$$H_2 = \left(\frac{-\eta + \sinh \sqrt{2}\ NTU}{2^{3/2}}\right) \qquad \text{E 4.2.15}$$

Utilizing these results, it can be shown after some rather tedious algebra that the performance of the two-pass heat exchanger can be represented by

$$\frac{\text{Approach}}{\text{Spread}} = \frac{1}{2}\left(\frac{2 + 3\ NTU + 4H_1 + 6H_2}{B_{11}B_{22} - B_{12}B_{21}}\right) \qquad \text{E 4.2.16}$$

where the individual terms are as defined above.

C. Two Fluid--Infinite Number of Channels. For n = ∞ the equations are

$$\begin{vmatrix} \frac{dT_1}{d\xi} \\ \\ \frac{dT_2}{d\xi} \end{vmatrix} = \begin{vmatrix} -2 & 2 \\ \\ -2 & 2 \end{vmatrix} \begin{vmatrix} T_1 \\ \\ T_2 \end{vmatrix} \qquad \text{E 4.2.17}$$

As in the single-channel case, these equations are easily integrated, the temperature profiles are linear, and the results can be simplified to

$$\frac{\text{Approach}}{\text{Spread}} = \frac{1}{1 + 2\ \text{NTU}} \cdot \qquad \text{E 4.2.18}$$

At this point we can conclude that it is entirely proper to represent the end effect as a correction to the overall heat transfer coefficient, as is the usual Colt practice. This type of correction shows up in our results as a correction to the number of transfer units which is equivalent to a correction in the heat transfer coefficient.

Relative to the datum of an infinite number of passes, the correction to be applied for the single-pass case should be 50 percent; that for the double-pass case and probably all remaining cases is somewhat more complicated.

D. Three fluid--Large Number of Passes.

In the Colt three-fluid configuration, the process stream arrangement is a repetition of the module

P, S, B, S, B, S

where P, S, and B represent product, sea water, and brine streams,

respectively. The behavior of the six streams that comprise the module can be simplified to equations describing only four streams as follows: Of the three S streams, only two types need be distinguished--an S that sees P and B, say S_1, and an S that sees two B's, say S_2. Furthermore, the B's are all identical--each sees an S_1 and an S_2.

With this simplification, the modular arrangement then becomes

$$P,\ S_1,\ B,\ S_2,\ B,\ S_1$$

involving the four independent variables P, B, S_1, and S_2.

The differential equations describing the system are

$$\begin{vmatrix} \frac{dP}{d\xi} \\ \frac{dS_1}{d\xi} \\ \frac{dB}{d\xi} \\ \frac{dS_2}{d\xi} \end{vmatrix} = \begin{vmatrix} -2 & +2 & & & P \\ -1 & +2 & -1 & & S_1 \\ & 1 & -2 & 1 & B \\ & & -2 & +2 & S_2 \end{vmatrix} \qquad \text{E 4.2.19}$$

The solution to this system with appropriate boundary conditions is the following:

Let

$$H_1 = \left(\frac{-1 + \cosh \sqrt{3}\ \xi}{3}\right) \qquad \text{E 4.2.20}$$

$$H = \left(\frac{-\sqrt{3}\ \xi + \sinh \sqrt{3}\ \xi}{\sqrt{3}\ 3}\right) \qquad \text{E 4.2.21}$$

Then

$$\begin{matrix} P \\ S_1 \\ B \\ B_2 \end{matrix} = \left\{ \begin{vmatrix} 1 & & & \\ & 1 & & 0 \\ & & 1 & \\ 0 & & & 1 \end{vmatrix} + \xi \begin{vmatrix} -2 & 2 & & \\ -1 & 2 & -1 & \\ & 1 & -2 & 1 \\ & & -2 & 2 \end{vmatrix} \right.$$

$$+ H_1 \begin{vmatrix} 2 & 0 & -2 & 0 \\ 0 & 1 & 0 & -1 \\ -1 & 0 & 1 & 0 \\ 0 & -2 & 0 & 2 \end{vmatrix} + H_2 \begin{vmatrix} -4 & 2 & 4 & -2 \\ -1 & 2 & 1 & -2 \\ 2 & -1 & -2 & 1 \\ 2 & -4 & -2 & 4 \end{vmatrix} \left. \begin{matrix} P_{in} \\ S_{1\text{-out}} \\ B_{in} \\ S_{2\text{-out}} \end{matrix} \right\}$$

E 4.2.22

where

$$S_{1\text{-out}} = \frac{A_1 B_{22} - A_2 B_{12}}{B_{11} B_{22} - B_{12} B_{21}} \qquad \text{E 4.2.23}$$

$$S_{2\text{-out}} = \frac{A_2 B_{11} - A_1 B_{21}}{B_{11} B_{22} - B_{12} B_{21}} \qquad \text{E 4.2.24}$$

with

$$A_1 = S_{in} + (P_{in} + B_{in})\ NTU + H_2(P_{in} - B_{in}) \qquad \text{E 4.2.25}$$

$$A_2 = S_{in} + (2\ B_{in})\ NTU + 2H_2(B_{in} - P_{in}) \qquad \text{E 4.2.26}$$

and

$$\begin{vmatrix} B_{11} & B_{12} \\ B_{21} & B_{22} \end{vmatrix} = \begin{vmatrix} (1 + 2\ NTU + H_1 + 2H_2) & -(H_1 + 2H_2) \\ -2(H_1 + 2H_2) & (1 + 2\ NTU + 2H_1 + 4H_2) \end{vmatrix} \qquad \text{E 4.2.27}$$

As in the case of the two-fluid, double-channel exchanger, the entire solution is moderately unwieldy. However, if one defines the "Approach" and the "Spread" intuitively in terms of the average inlet and outlet temperatures, i.e.,

$$\text{Approach} = \frac{2\ S_{1\text{-out}} + S_{2\text{-out}} - (P_{in} + 2\ B_{in})}{3} \qquad \text{E 4.2.28}$$

$$\text{Spread} = \frac{3\ S_{in} - (P_{in} + 2\ B_{in})}{3} \qquad \text{E 4.2.29}$$

then a bit of fairly tedious algebra produces the gratifying result

$$\frac{\text{Approach}}{\text{Spread}} = \frac{1}{1 + 2\ NTU} \qquad \text{E 4.2.30}$$

This result leads to the conclusion that a 3-fluid heat exchanger behaves identically to a 2-fluid exchanger in terms of the total approach and spread provided that inlet and outlet streams are arithmetically averaged. The conclusion, furthermore, is that Colt's method for sizing and costing a 3-fluid heat exchanger is not approximate in a theoretical sense but is rigorously accurate.

Thus, this type of simplification has been used in simulation and optimization studies.

NOTE: In the preceeding material NTU has been based on the area of a single sheet and the mass flow in a single channel. In terms of the total area and the total mass flow of a single stream,

$$NTU = \frac{U\ A_T}{\dot{M}\ Cp} \qquad \text{E 4.2.31}$$

where A_T is now the total area in the exchanger and M is the total mass rate of a single stream.

This formulation is consistent with the results of section 4.2.1 A and 4.2.1 C, as is evident from the following: The formulations are exactly equivalent for the single channel case, and for the infinite channel case, $A_T = 2nA$, $\dot{M} = 2n\dot{m}$. Thus,

$$NTU(overall) = 2 \times NTU(single\ channel)\ . \qquad \text{E 4.2.32}$$

Thus, if one considers NTU to be everywhere calculated from total area and total mass flow, then NTU is uniformly given by

$$NTU = \frac{U\ A_T}{\dot{M}\ Cp} \qquad \text{E 4.2.33}$$

and (APP/SPR) is uniformly given by

$$\frac{APP}{SPR} = \frac{1}{1 + NTU}\ . \qquad \text{E 4.2.34}$$

4.2.2 UNBALANCED HEAT EXCHANGERS, GENERAL RESULTS

The system of differential equations for steady operation of an unbalanced heat exchanger is

$$\frac{d}{d(\frac{x}{L})} H = - NTU(H - C) \qquad E\ 4.2.35$$

$$\frac{d}{d(\frac{x}{L})} C = m\ NTU(H - C) \qquad E\ 4.2.36$$

with boundary conditions

$$H(0) = H_{IN} \qquad E\ 4.2.37$$

$$C(1) = C_{IN} \qquad E\ 4.2.38$$

where NTU = the number of transfer units based on the hot fluid flow rate
m = the ratio of WCp for the cold fluid to that for the hot fluid.

The solution to this system is the following:

$$f(NTU,m) = \exp\left[(\frac{1 - m}{m})NTU\right] - 1 \qquad E\ 4.2.39$$

and

$$\frac{APP(HOT)}{SPR} = \left[\frac{1}{1 + \frac{f}{1 - m}}\right] = \frac{H_{IN} - C_{OUT}}{H_{IN} - C_{IN}} \qquad E\ 4.2.40$$

$$\frac{APP(COLD)}{APP(HOT)} = \left[1 + \frac{f}{1 - m} - \frac{mf}{1 - m}\right] = \frac{H_{OUT} - C_{IN}}{H_{IN} - C_{OUT}} \qquad E\ 4.2.41$$

451-332 O - 71 - 12

This result can also be expressed in matrix-vector form as follows:

$$\begin{matrix} H_{OUT} \\ C_{OUT} \end{matrix} = \frac{1}{1 + f - m} \begin{bmatrix} (1 + f)(1 - m) & mf \\ f & 1 - m \end{bmatrix} \begin{matrix} H_{IN} \\ C_{IN} \end{matrix} \qquad \text{E 4.2.41a}$$

It is convenient and instructive to develop a linearized perturbation form for this solution. This is done by expanding the above matrix-vector equation about a balanced state in terms of perturbation values for the number of transfer units in the hot stream and the cold stream.

After the required algebra, the result, in terms of perturbation values, is

$$\begin{matrix} \tilde{H}_{OUT} \\ \tilde{C}_{OUT} \end{matrix} = \begin{bmatrix} \frac{1}{1 + N} & -(1 + \frac{N}{2}) & \frac{N}{2} \\ & -\frac{N}{2} & (1 + \frac{N}{2}) \end{bmatrix} \begin{matrix} \Delta f \\ \Delta g \end{matrix} \qquad \text{E 4.2.42}$$

where N = the number of transfer units for a balanced exchanger

Δf, Δg = the product of the approach for a balanced exchanger by the perturbation in the number of transfer units for the hot and cold fluids, respectively.

4.2.3 DESIGN EQUATIONS FOR THE ABSORBER HEAT EXCHANGERS

Figure F 4.2.1 shows the flow schematic and designates the stream notation for the heat exchanger design calculations. With notational changes to adapt the general results of the preceeding sections to the high temperature and low temperature absorber exchangers, the working equations become the following:

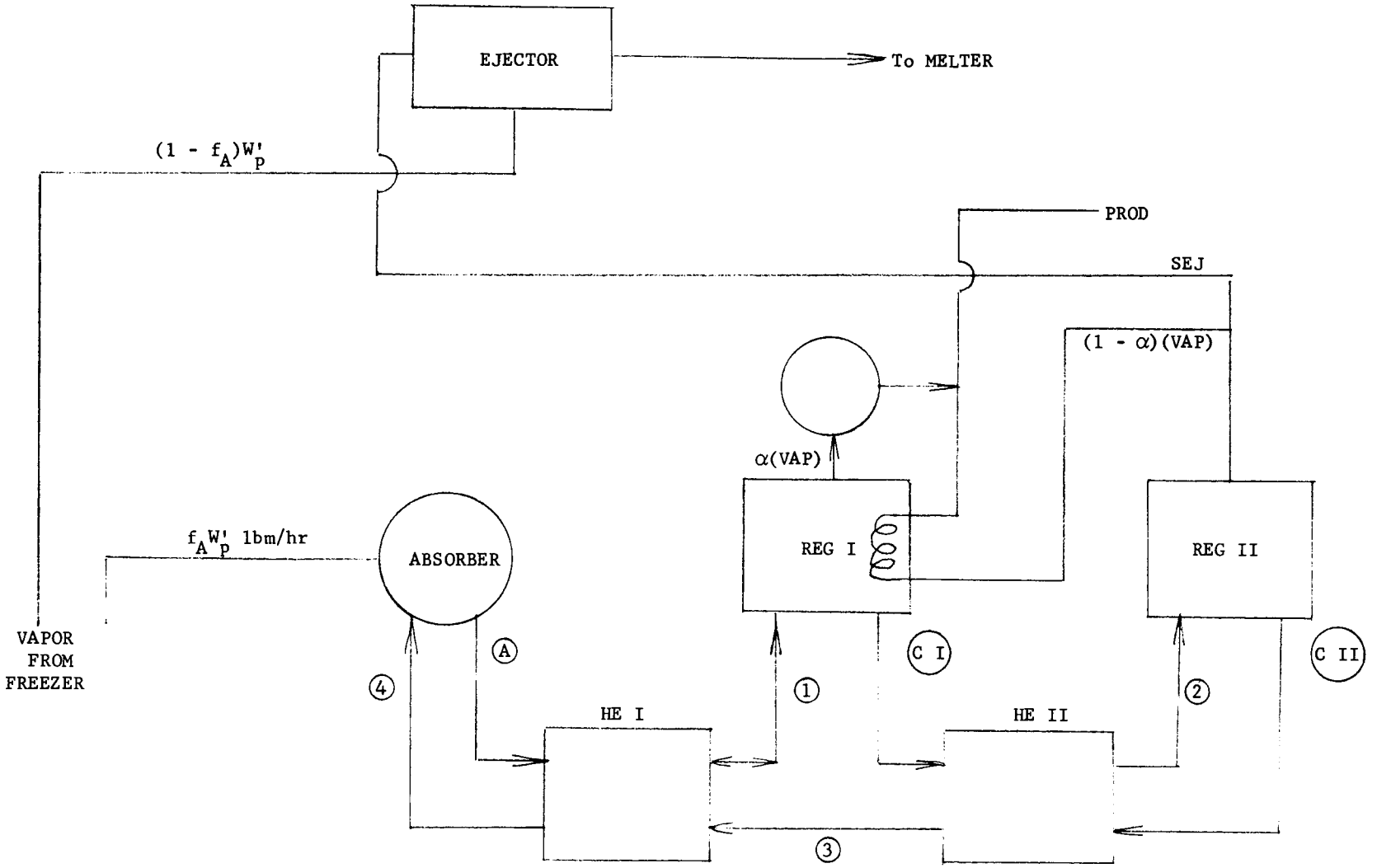

Figure 4.3

ABSORBER LOOP FLOW SCHEMATIC

$$WA = W1 = WC(1 + XA) \qquad \text{E 4.2.43}$$

$$WC1 = W2 = WC(1 + XCI) \qquad \text{E 4.2.44}$$

$$WCII = W3 = W4 = WC(1 + XCII) \qquad \text{E 4.2.45}$$

$$ML = \frac{WA}{W4} \qquad \text{E 4.2.46}$$

$$MH = \frac{W2}{WCII} \qquad \text{E 4.2.47}$$

$$AOSH = \frac{TCII - T2}{TCII - TCI} \qquad \text{E 4.2.48}$$

$$FH = [\frac{1}{AOSH} - 1]MH[- 1 + \frac{1}{MH}] \qquad \text{E 4.2.49}$$

$$NTUH = \ln[1 + FH]/(- 1 + \frac{1}{MH}) \qquad \text{E 4.2.50}$$

$$AOAH = 1 - \frac{FH}{(- 1 + \frac{1}{MH})} + \frac{FH}{MH(- 1 + \frac{1}{MH})} \qquad \text{E 4.2.51}$$

$$T3 = AOAH(TCII - T2) + TCI \qquad \text{E 4.2.52}$$

$$AOSL = \frac{T3 - T1}{T3 - TA} \qquad \text{E 4.2.53}$$

$$FL = [\frac{1}{AOSL} - 1]ML(-1 + \frac{1}{ML}) \qquad \text{E 4.2.54}$$

$$NTUL = \ln[1 + FL]/(-1 + \frac{1}{ML}) \qquad \text{E 4.2.55}$$

$$AOAL = 1 - \frac{FL}{(-1 + \frac{1}{ML})} + \frac{FL}{ML(-1 + \frac{1}{ML})} \qquad \text{E 4.2.56}$$

$$T4 = (T3 - T1)AOAL + TA \qquad \text{E 4.2.57}$$

Since the areas are doubly effective, replace NTUH and NTUL by (NTUH/2) and (NTUL/2), respectively.

Heat Exchanger Design

$$\dot{M} = W4 \qquad \text{E 4.2.58}$$

Pick integral values for $\{\frac{PH}{PL}\}$ such that

$$2000 \leq M/\{\frac{PH}{PL}\} \leq 10{,}000 \ . \qquad \text{E 4.2.59}$$

Calculate

$$UOMH = \frac{UH(\frac{\dot{M}}{PH})}{(\frac{\dot{M}}{PH})} \qquad \text{E 4.2.60}$$

$$UOML = \frac{UL(\frac{\dot{M}}{PL})}{(\frac{\dot{M}}{PL})} \qquad \text{E 4.2.61}$$

where the heat transfer coefficients, corrected for viscosity are

$$UH(X) = \frac{97.0 + .053\ X}{1 + R[97.0 + .053\ X]} \qquad \text{E 4.2.62}$$

$$UL(X) = \frac{58.6 + .0322\ X}{1 + R[58.6 + .0322\ X]} \qquad \text{E 4.2.63}$$

$$R = \begin{Bmatrix} .0001 \\ .0003 \\ .0005 \end{Bmatrix}$$

for the high and low temperature exchangers, respectively.

$$SH = \frac{NTUH}{30}\ \frac{1}{UOMH} \qquad \text{E 4.2.64}$$

$$SL = \frac{NTUL}{30}\ \frac{1}{UOML} \qquad \text{E 4.2.65}$$

Select smallest integer $\geq \frac{SH}{SL} = \{\frac{\overline{SH}}{\overline{SL}}\}$.

Select smallest integer $\geq \frac{\{\frac{PH}{PL}\}}{15} = \frac{BH}{BL}$.

Heat exchanger cost

$$\{\begin{matrix} H \\ L \end{matrix}\} = CPEP(\frac{\overline{SH}}{\overline{SL}})(\frac{BH}{BL} + 1) + CPS(\frac{\overline{SH}}{\overline{SL}})(2\ \frac{PH}{PL} - \frac{BH}{BL}) \qquad \text{E 4.2.66}$$

$$\text{Total Cost} = \text{Cost H} + \text{Cost L} \qquad \text{E 4.2.67}$$

Total pressure drop; high, is

$$\text{TPDH} = (6 \times 10^{-8})\left(\frac{\dot{M}}{PH}\right)^2 \overline{SH} \qquad \text{E 4.2.68}$$

(constrained to be ≤ 35)

$$\text{TPDL} = (6 \times 10^{-8})\left(\frac{\dot{M}}{PL}\right)^2 \overline{SH} \qquad \text{E 4.2.69}$$

(constrained to be ≤ 35)

BHP per pump is

$$\frac{\dot{M}}{\rho}\left\{\frac{\text{TPDH}}{\text{TPDL}}\right\}\frac{144}{60(33{,}000)} \qquad \text{E 4.2.70}$$

for $\rho = 94.0$

$$\begin{aligned}\text{Total Cost} = {} & \text{Absorber} \\ & + \text{Heat Exchangers} \\ & + \text{Regenerators} \\ & + \text{Pumps}\end{aligned} \qquad \text{E 4.2.71}$$

Search over T1 and T2 to minimize.

The rationale for the heat exchanger optimization is as follows: For assumed values of the inlet and outlet temperatures and flow rates, one can then calculate the number of transfer units required. The total flow to the exchanger must be divided into an integral number of parallel

paths so that the flow through each path does not exceed, say, 10,000 lbm/hr. Having chosen an integral number of parallel paths, then one must select an integral number of series paths so as to provide sufficient area for the required number of transfer units.

Having determined tentative values for the required numbers of parallel and series paths, a constraint is introduced that for every fifteen parallel paths (or remaining fraction thereof), one must install an end or bracer plate for structural stability. From this constraint, the number of end plates and interior sheets can be determined and the capital cost based on the unit cost per plate or sheet.

In the optimization the cost factors used must be the amortized cost factors that reflect the relative contributions of the various process components to the total operating cost. One must thus include factors for debt service, operating costs, and power costs as well as the capital equipment costs.

4.2.4 HEAT EXCHANGER NOTATION

AOA = approach cold end/approach hot end
AOS = approach over spread, hot end of exchanger
B = number of heat exchanger sections
CPEP = cost per end plate
CPS = cost per sheet
F = function of NTU
-H = the high temperature exchanger
-L = the low temperature exchanger
NTU = number of transfer units, (UA)/MCp(HOT)
P = number of parallel passes required in heat exchanger
R = resistance factor in heat transfer coefficient
ρ = Mass density
S = number of series passes
$\overline{S}$ = rounded to integral
TPD = total pressure drop
U = overall heat transfer coefficient
UOM = U over mass rate
W = mass rate at designated point

NOTE: A change during report preparation has been to deduct the costs of the heat exchanger end plates. Colt has advised that there is included in the plate cost an allowance for end plates.

4.3 THE STEADY STATE CONCENTRATORS OR REGENERATORS

In the digital design optimization a two-stage concentrator is designed as is indicated in the flow schematic F 4.2.1.

4.3.1 DESIGN EQUATIONS

The design equations are the following:

Preliminary calculations:

$$CA = .44 \qquad \text{E } 4.3.1$$

$$CCII = .49 \qquad \text{E } 4.3.2$$

$$XA = \frac{1 - CA}{CA} \qquad \text{E } 4.3.3$$

$$XCII = \frac{1 - CCII}{CCII} \qquad \text{E } 4.3.4$$

$$WC = \frac{f_A W'_p}{(XA - XCII)} \qquad \text{E } 4.3.5$$

$$REJ = 0.45 \qquad \text{E } 4.3.6$$

$$SEJ = REJ(1 - f_A)W'_p \qquad \text{E } 4.3.7$$

$$VAP = f_A W'_p - SEJ \qquad \text{E } 4.3.8$$

The following set of equations is to be solved for ALP. Set PPRI = 300.
Enthalpy balance, low temperature regenerator:

$$WC(1 + XA)h(T1,XA) + (1 - ALP)(VAP)DHVAP(PPRI) = (1 + XCI)h(TC1,XCI)WC + ALP(VAP)HVAP(TC1) \qquad \text{E 4.3.9}$$

Mass Balance

$$XCI = XA - \frac{ALP(VAP)}{WC} \qquad \text{E 4.3.10}$$

T1 is a search variable, to be varied later for optimization.

<u>Thermodynamic Functions for Above Equations</u> from Section 6.
Enthalpy of Caustic Solutions

$$h(T,X) = -222.3 + .833\ T + \frac{570}{1 + X} \qquad \text{E 6.1.9}$$

Enthalpy of Water Vapor

$$HVAP(T) = 1060.06 + .452\ T \qquad \text{E 6.1.7}$$

Enthalpy of Vaporization

$$DHVAP(P) = 1054.5 - .2091\ P \qquad \text{E 6.1.8}$$

Also, Equilibrium Relationship

$$TC1 = \frac{-10838}{[\ln PC - 25.3848 + \frac{8.96}{1 + XC1}]} - 460 \qquad \text{E 6.1.10}$$

Possible Procedure

1. Pick a condenser pressure

$$PC = 20$$

2. Assume ALP

$$0 < ALP < 1$$

3. Compute XCI, mass balance

4. Compute TCI, equilibrium relationship

5. Compute h(TCI,XCI)
   HVAP(TCI)
   DHVAP(PPRI)

6. Solve enthalpy balance for ALP, and adjust ALP for convergence.

Heat loads, temperatures, etc.

$$STRI = (1 - ALP)(VAP) \qquad \text{E 4.3.11}$$

$$QRI = (STRI)DHVAP(PPRI) \qquad \text{E 4.3.12}$$

$$TCII = \frac{-10838}{\ln PPRI - 25.3848 + \frac{8.96}{1 + XCII}} - 460 \qquad \text{E 4.3.13}$$

Choose T2, later to be varied for optimization.

$$QR2 = WC(1 + XCII)h(TCII,XCII) + [(1 - ALP)(VAP) + SEJ]hVAP(TCII) \qquad \text{E 4.3.14}$$

$$- (1 + XCI)h(T2,XCI)WC$$

$$AII = \frac{QR2}{356(TST - TCII)} ; \quad TST = 250 \qquad \text{E 4.3.15}$$

$$AI = \frac{QRI}{356(TCII - TCI)} \qquad \text{E 4.3.16}$$

$$\text{Capital Cost of Regenerator} = RCPA(AI + AII) \qquad \text{E 4.3.17}$$

$$\text{Primary Steam to Process} = \frac{QR2}{945} \qquad \text{E 4.3.18}$$

4.3.2 CONCENTRATOR NOTATION

AI = area of regenerator I

AII = area of regenerator II

ALP = fraction of VAP produced in regenerator I

CA = absorber concentration, wt fraction NaOH

CCII = ditto for concentrator II

DH VAP(P) = enthalpy of vaporization

h(T,X) = enthalpy of NaOH solutions

hVAP(T) = enthalpy of vapor

PC = condenser pressure, mm Hg

PPRI = primary pressure, i.e., that to ejector, mm Hg

QRI = heat load, concentrator I, Btu/hr

QR2 = heat load, concentrator II, Btu/hr

RCPA = regenerator cost per area

REJ = primary to secondary ratio for ejector

SEJ = primary stream flow to ejector

STRI = steam to concentrator I, lb/hr

T1 = feed temperature to concentrator I

T2 = feed temperature to concentrator II

T3 = temperature between heat exchangers

T4 = feed temperature to absorber

TCI = temperature in concentrator I

TCII = temperature in concentrator II

TST = temperature of steam to regenerator II

VAP = vapor produced in concentrators that does not go to the ejectors

WC = mass rate dry caustic, lbm/hr

XA = dilution, lb H_2O/lb NaOH in absorber

XCI = dilution in concentrator I

XCII = dilution in concentrator II

4.4 THE STEADY STATE EJECTOR

The equations to be used for ejector design in the digital optimization program are taken from the Loth model and are the following.

4.4.1 STEADY STATE EQUATIONS

Assume that rates (lbm/sec), temperatures (^{o}F), and pressures are given for the primary and secondary streams into the ejector. The calculation then proceeds in the following sequence:

Primary nozzle area required, calculated via isentropic expansion from regenerator conditions to sonic velocity in the nozzle throat.

$$A_p(\text{sq ft}) = \frac{m_p \sqrt{Tp + 460}}{0.06234\ P_p} \qquad \text{E 4.4.1}$$

Density of secondary, computed from the ideal gas law at secondary conditions.

$$\rho_s = 0.03245 \frac{P_s}{T_s + 460} \qquad \text{E 4.4.2}$$

Pressure at nozzle exhaust, computed assuming a pressure decrease corresponding to a secondary acceleration to 250 ft/sec.

$$P_o = P_s - 348.47\ \rho_s \qquad \text{E 4.4.3}$$

Entropy of primary stream, Btu/lbm.

$$h_p = 1052.14 + 0.452(Tp + 460) \qquad \text{E 4.4.4}$$

$$Sp = \frac{1}{2.212}[\ln(h_p - 1052.14) - 0.2429\ P_p - 0.2035] \qquad \text{E 4.4.5}$$

Enthalpy of primary after expansion, assuming isentropic expansion.

$$\ln(h'_p - 1052.14) = 2.212\ Sp + 0.2429\ \ln P_o + 0.2035 \qquad \text{E 4.4.6}$$

Enthalpy change and nozzle exhaust velocity, assuming complete conversion of enthalpy to kinetic energy.

$$\triangle h = h'_p - h_p \qquad \text{E 4.4.7}$$

$$V_p = 217(\triangle h)^{1/2} \qquad \text{E 4.4.8}$$

Enthalpy of secondary stream.

$$h_s = 1052.14 + .452(T_s + 460) \qquad \text{E 4.4.9}$$

Choose exhaust pressure, P_e, and velocity, V_e, and solve the following simultaneously for P_1, V_1, and A_1.

a) Momentum

$$m_p V_p + m_s V_s = 1.04(m_p + m_s)V_1 + 89.68\ A_1(P_1 - P_o) \qquad \text{E 4.4.10}$$

b) Energy

$$778\left(\frac{m_s}{m_s + m_p} h_s + \frac{m_p}{m_s + m_p} h_p\right) = 12.067 \frac{P_1 A_1 V_1}{m_s + m_p} + .01553 V_1^2 \quad \text{E 4.4.11}$$

c) Diffuser recovery

$$.846\left(1 - \frac{V_e}{V_1}\right) = 179.35 \frac{P_e - P_1}{\rho_s V_1^2} \quad \text{E 4.4.12}$$

It is assumed that the ejector cost can be expressed in terms of the primary area, A_p, and the throat area, A_1.

4.4.2 THE EJECTOR AREA

Mixing Section

The ejector surface area is calculated from the following geometric relationships.

$$LM = 7.8\ D \quad \text{E 4.4.13}$$

$$\text{Large R} = \text{Small R} + LM \text{ TAN } 2.5^\circ \quad \text{E 4.4.14}$$

$$\text{Small R} = \frac{D}{2} \quad \text{E 4.4.15}$$

A. $\text{Area} = \pi(\text{Large R} + \text{Small R})\sqrt{(LM)^2 + (\text{Large R} - \text{Small R})^2}$ E 4.4.16

Diffuser Section

$$LD = 4D \quad \text{E 4.4.17}$$

451-332 O - 71 - 13

$$\text{Large R} = \text{Small R} + \text{LD TAN } 5^{\circ} \qquad \text{E 4.4.18}$$

$$\text{Small R} = \frac{D}{2} \qquad \text{E 4.4.19}$$

$$\text{B. Area} = \pi(\text{Large R} + \text{Small R})\sqrt{(\text{LD})^2 + (\text{Large R} - \text{Small R})^2} \qquad \text{E 4.4.20}$$

Throat

$$\text{C. Area} = 2\pi D^2 \qquad \text{E 4.4.21}$$

$$\text{Total Ejector Area} = A + B + C \qquad \text{E 4.4.22}$$

The ejector cost is based on this total area.

4.4.3 EJECTOR NOTATION

A_1 = throat area required, ft^2
Ap = primary nozzle area, ft^2
h_p = enthalpy of primary stream, Btu/lbm
h'_p = enthalpy of primary stream after expansion, Btu/lbm
h_s = enthalpy of secondary stream, Btu/lbm
m_p = mass rate of the primary stream, lb/hr
P_1 = pressure in throat of ejector, mm Hg
P_e = ejector exhaust pressure, mm Hg
P_o = pressure at nozzle exhaust, mm Hg
P_s = pressure of secondary stream, mm Hg
ρ_s = density of secondary stream, lbm/ft^3
Sp = entropy of primary stream Btu/lbm, ^{o}R
Tp = temperature of primary stream, ^{o}F

T_s = temperature of secondary stream, ^oF

V_1 = velocity in throat of ejector, ft/sec

V_e = ejector exhaust velocity, ft/sec

V_p = nozzle exhaust velocity, ft/sec

NOTE: A late modification to the ejector design equations, introduced after preparation of the report at Colt's suggestion, was to design for a

$$\text{Diffuser Efficiency} = \frac{\text{Static Pressure at Exit}}{\text{Total Pressure at Throat}} = 96\%$$

$$\text{Mixer Efficiency} = \frac{P_{\text{throat}} - P_o}{P_{\substack{\text{throat} \\ \text{inviscid}}} - P_o} = 95\%$$

$$\text{Nozzle Efficiency} = \left(\frac{V_{\text{actual}}}{V_{\text{isentropic}}}\right)^2 = 90\%$$

The net effect of these changes is to replace the 1.04 by 1.00 in E 4.4.10 and to replace E 4.4.12 by

$$P_e = .90[.05\ P_o + .95\ P_1 + \tfrac{1}{2}\ \rho_s V_1^2] \ .$$

4.5 THE STEADY STATE FREEZER

4.5.1 STEADY STATE HEAT AND MATERIAL BALANCES

When the process is operating at steady state, heat and material balances must be satisfied, and certain dependent variables can be calculated provided that other independent quantities are known or assumed. From the design-optimization point of view, a convenient set of quantities for which values can be assigned is

W_v = product rate, gal/day, or W_p, lbs/hr
X_p = product salinity, TDS
X_B = reject brine salinity, TDS
X_s^o = sea water feed salinity, TDS
ϵ = weight fraction ice in slurry
f_c = net fraction wash water loss (Colt definition)
T_s^o = sea water inlet temperature, ^oF
P = freezer pressure, mm Hg

From Colt's process calculations it is noted that the wash water is defined on the basis of the total product formed in the freezer. That is,

$$W'_p + W_I = \frac{W_p}{1 - f_c} \qquad \text{E 4.5.1}$$

where W'_p = product vapor from freezer, lbs/hr
W_I = ice from freezer, lbs/hr

The effect of the net wash loss on the salt concentration of the freezer brine can be found by appropriate balances around freezer and washer. If the recycle brine has the same salt concentration as the reject brine, X_B, then salt and ice balances around the freezer together

with the definition of the net wash loss, the freezer brine concentration can be expressed as

$$X_s = \frac{1}{R_x}\left(\frac{\epsilon}{1-\epsilon}\right)\frac{(X_s^o + R\,X_B)}{\left(\frac{1}{1-f_c} - \frac{R'_p}{R_x}\right)} \quad . \qquad \text{E 4.5.2}$$

where $R_x = W_p/W_s^o$ = ratio of product to feed

$R'_p = W'_p/W_s^o$ = ratio of vapor to feed

$$R_x = \left(\frac{X_B - X_s^o}{X_B - X_p}\right)$$

A further result of these calculations is an expression for the vapor/feed ratio, R'_p, which is

$$R'_p = \frac{1}{1-\epsilon}\left[\frac{R_x}{1-f_c} - \epsilon(1+R)\right] \qquad \text{E 4.5.3}$$

An enthalpy balance around the freezer at steady state can be made to include the effect of wash loss on the freezer brine concentration. This enthalpy balance can be solved for the recycle ratio, R, if the enthalpies are known as functions of temperature and composition. The result is

$$R = \frac{\left[\left(\frac{R_x}{1-f_c}\right) - \epsilon\right]\left(\frac{\triangle_g + \epsilon}{1-\epsilon}\right) - (\triangle_o + \epsilon)}{\left[\triangle_R + \epsilon + \left(\frac{\epsilon}{1-\epsilon}\right)(\triangle_g + \epsilon)\right]} \qquad \text{E 4.5.4}$$

where $\triangle_g = (h_g - h_\ell)/(h_\ell - h_s)$

$\triangle_o = (h_\ell^o - h_\ell)/(h_\ell - h_s)$

$\triangle_R = (h_\ell^R - h_\ell)/(h_\ell - h_s)$

and h_g = enthalpy of water vapor at freezer temperature, T_s, Btu/lb

h_ℓ = enthalpy of brine leaving freezer at temperature, T_s, and salt concentration, X_s, Btu/lb

h_s = enthalpy of ice at T_s, Btu/lb

h_ℓ^R = enthalpy of recycle brine at concentration X_B and the appropriate temperature from the washer, Btu/lb

h_ℓ^o = enthalpy of feed sea water at entrance temperature and salt concentration, Btu/lb

The brine enthalpies have been expressed in terms of empirical equations which were fitted to the h-T-X-charts in the OSW Saline Water Conversion Data Book (Chart 12.30).

The empirical formulas for enthalpies are as follows:

Vapor enthalpy:

$$h_g = 1052 + 0.452(T + 460), \text{ Btu/lb} . \qquad \text{E 4.5.5}$$

Brine enthalpy:

For $32 < T \leq 90\ ^oF$ and $0 \leq X \leq 0.08$, wt fract TDS

$$h_\ell = 200 + (T - 32) + (76.5 - 1.10\ T)X, \text{ Btu/lb} \qquad \text{E 4.5.6}$$

For $32 - 104\ X < T \leq 32$ and $0 \leq X \leq 0.08$

$$h_\ell = 200 - 1.395(32 - T) + 52.0\ X, \text{ Btu/lb} \qquad \text{E 4.5.7}$$

For brine at temperatures below the equilibrium freezing point at the given salt concentration, $0 \leq X \leq 0.08$,

$$h = h_s + (250 + \frac{13,500}{32 - T})X, \text{ Btu/lb} \qquad \text{E 4.5.8}$$

where h_s = ice enthalpy

$$= h_o \exp[-b(32 - T)] \qquad \text{E 4.5.9}$$

and $h_o = 59.4$, $b = 0.01121$ $\Big\}$ $0 \leq T \leq 30$

$h_o = 200$, $b = 0.619$ $\Big\}$ $30 \leq T \leq 32$

The equations for R, R'_p, and X_s satisfy both heat and mass balance requirements for the freezer. Observations of freezer operation have shown that the exit brine is normally at the equilibrium temperature of the triple point at the exit brine composition, which is given quite closely as

$$T_S^* = 32 - 104\ X_s\ . \qquad \text{E 4.4.10}$$

On OSW Chart 12.30, the brine enthalpy along the equilibrium curve is given in terms of X alone as

$$h_\ell = 200 - 62.5\ X, \text{ Btu/lb.} \qquad \text{E 4.5.11}$$

Therefore, equation E 4.5.11 will be used to compute exit brine enthalpies in the usual steady operating cases.

The vapor pressure of brine at its freezing point is given by the empirical formula

$$P^* = 4.58 - 18.45\ X, \text{ mm Hg.} \qquad \text{E 4.5.12}$$

Since the pressure, P, maintained in the vapor space in the freezer must be less than P^* for vaporization to occur, the pressure driving force can be taken as

$$\triangle P = P^* - P \text{ mm Hg.} \qquad \text{E 4.5.13}$$

The temperature of water vapor in equilibrium with ice at pressure P can be approximated closely by

$$T_V = \frac{4839}{10.4969 - \log_{10} P} - 460, \ ^oF \qquad \text{E 4.5.14}$$

P given in mm Hg. The temperature driving force can then be taken as

$$\triangle T = T_S^* - T_V, \ ^oF \qquad \text{E 4.5.15}$$

where T_S^* is the triple point temperature at the freezer exit brine salt composition.

The computations required to obtain R, R_p', and X_s must be done by an iterative procedure, since they are non-linear because of the empirical enthalpy formulas. The procedure may be outlined as follows:

1) Assign values for T_s^o, X_s^o, X_B, P, ϵ, f_c, and R_x (all presumed known or available).
2) Calculate the vapor temperature, T_V, from E 4.5.14.
3) For the first trial value of X_s, select $X_{s,j} \equiv X_B$.
4) Calculate all enthalpies and values of R and R_p' from equations E 4.5.3 and E 4.5.4.
5) Calculate the improved value $X_{s,j}$ from equation E 4.5.2.
6) Using the improved value of X_s, begin again with step (4) and repeat until agreement of successive values of X_s is obtained.

The corresponding values of R and R_p' are then available as the final values at steady state, as well as the values of $\triangle P$ and $\triangle T$.

This method converges very rapidly, and usually requires only two iterations to reach agreement in X_s values of less than 0.0001.

4.5.2 STEADY STATE CRYSTAL POPULATION EQUATIONS

The steady values of the variables representing the crystal population have been derived by setting time derivatives of the dynamic population balances (Section 5.5) to zero and solving for the moments of the size distribution. These moments are needed to estimate the mean crystal size and the weight fraction ice in the freezer slurry. These are given in terms of the mean freezer holding time $\tau = M/W_s$, the freezer pressure driving force $\triangle P$, and three empirical parameters a, B_o, and γ_o, which are, respectively, the particle collision frequency, the nucleation rate, and the initial nucleus size.

The moment equations at steady state are

$$\mu_1 = \frac{\gamma_o}{2} + \frac{1}{2}\sqrt{\frac{2}{\phi B_o \tau} - \gamma_o^2} \qquad \text{E 4.5.16}$$

$$\mu_2 = \mu_1/\tau\phi B_o\gamma_o \qquad \text{E 4.5.17}$$

$$\mu_3 = \tau/\mu_2 \phi B_o \gamma_o^3 + 3 a N \mu_1 \mu_2 \qquad \text{E 4.5.18}$$

$$N = \frac{2(\mu_2 \phi B_o \tau - 1)}{\tau} \qquad \text{E 4.5.19}$$

If γ_o is small, then

$$\mu_1 \cong \sqrt{\frac{1}{2 \phi B_o \tau}} \qquad \text{E 4.5.16a}$$

$$\mu_2 = \mu_1/\tau \phi B_o \gamma_o \text{ , as before} \qquad \text{E 4.5.17a}$$

$$\mu_3 \cong 6\mu_1^3/\tau \phi B_o \gamma_o^2 \qquad \text{E 4.5.18a}$$

In these equations μ_1 = first moment = mean crystal diameter, mm
μ_2 = second moment of size distribution, mm^2
μ_3 = third moment of size distribution, mm^3
N = number of crystals in the population
$\phi = 2.78 \triangle P/\rho_s L$
L = slurry pool depth, ft
ρ_s = slurry density, lbm/ft^3

The third moment is related to the mass fraction ice in the slurry, i.e.,

$$M\epsilon = k' \rho_I N \mu_3 \qquad \text{E 4.5.20}$$

where M = mass of slurry in freezer, lbm

ϵ = weight fraction ice

ρ_I = ice density, lbm/ft^3

k' = $\pi/6$, if spherical particles

The total ice production rate can be expressed as

$$W_I = W_s \epsilon = \frac{W_s}{M} M\epsilon = \frac{1}{\tau} k' \rho_I N \mu_3 \ . \qquad \text{E 4.5.21}$$

Combining equations E 4.5.21, 16 a, and 18 a with E.4.5.18 gives the following expression for the ice production rate

$$W_I = \frac{3k'\rho_I}{a(\phi B_o)^3 \gamma_o^3 \tau^5} \ , \text{ lbs/hr.} \qquad \text{E 4.5.22}$$

This expression in turn can be combined with equation E 4.5.1 to give the product rate, W_p, as a function of the nucleation rate

$$W_p = \left[\frac{a(\phi B_o)^3 \gamma_o^3}{3k' \rho_I (1 - f_c)} \left(\frac{R_x \rho_s V}{1 + R - R'_p} \right) \right]^{1/4} \ , \text{ lbs/hr.} \qquad \text{E 4.5.23}$$

where V = freezer pool volume, ft^3.

Estimation of ϕ

In order for vaporization to occur, the pressure at any slurry depth must be less than the equilibrium vapor pressure. The depth at which vaporization ceases must therefore be given by

$$P + \rho_s \ell = P^*$$

where P = pressure in vapor space

P^* = equilibrium vapor pressure

If P and P^* are in mm Hg, and ℓ and ρ_s are in English units, ℓ is given by

$$\ell = \frac{g_c}{g_L} \times \frac{1}{\rho_s} \times \frac{14.7 \times 144}{760}(P^* - P) = \frac{2.78}{\rho_s} \Delta P, \text{ feet} .$$

If the mean depth of the slurry is L, the ℓ/L is the fraction of the slurry within which vaporization and nucleation will occur; and therefore

$$\phi = \frac{2.78\ \Delta P}{\rho_s L} = \frac{C_1 \Delta P}{\rho_s L} \qquad \text{E 4.5.24}$$

$$\leq 1$$

Substituting for ϕ in E 4.5.23 gives

$$W_p = \left[\frac{a B_o^3 \gamma_o^3}{3k' \rho_I} \left(\frac{C_1}{L \rho_s}\right)^3 (1 - f_c)^{-1} \left(\frac{R_x \rho_s V}{1 + R - R_p'}\right)^5 \right]^{1/4} \Delta P^{3/4} \qquad \text{E 4.5.25}$$

which predicts that the product rate should vary as $\Delta P^{3/4}$. Colt's data shows the product rate as a linear function of ΔP, but the range is relatively small and a significant difference in goodness of fit between a linear function of ΔP and $\Delta P^{3/4}$ would probably be very difficult to prove.

At any rate, E 4.5.22 is not inconsistent with the facts as found by Colt's freezer data.

An equation of the type

$$W_p = C_I \Delta P^{3/4} \qquad \text{E 4.5.26}$$

has been fitted to Colt's operating data of W_p vs. ΔP with the result that C_I was found to have the value 115×10^3 lb/hr (mm Hg)$^{3/4}$. From typical operating conditions and the further assumption that γ_o = 8.1 microns[1] and that the mean crystal size was 0.2 mm, the values for B_o and a could be estimated. They are as follows:

$$B_o = 3.0741 \times 10^4 \ , \quad \text{no./(mm)}^2\text{hr}$$

$$a = 3.5673 \times 10^{-6} \ , \quad \text{hrs}^{-1}$$

These values have been used to estimate freezer performance for steady state operation.

Computational Procedure

Steady state material balances require a value for ϵ which is specified. Solution of the moment equations give ϵ in terms of N and μ_3; and therefore, the population equations need to be solved subject to the agreement of the calculated ϵ with the specified value. There are four moment equations plus the relation E 4.5.20 from which to obtain five unknowns, μ_1, μ_2, μ_3, N, and τ. This solution can be effected by an iterative procedure. This is best done as follows:

[1] Final Report, OSW Contract No. 14-01-0001-960, June 1968.

1) Express E 4.5.16a in terms of the specific product rate using the definitions for τ and φ, giving

$$\left(\frac{W_p}{V}\right)_j = \frac{2C_1 B_o R_x \triangle P}{(1 + R - R'_p)L} (\mu_1)_j^2 \qquad \text{E 4.5.27}$$

where $(W_p/V)_j$ = specific product rate, lb product/ft^{3}hr
L = slurry pool depth, ft
j = trial index, $j = 1, 2, \ldots$

2) Calculate $(W_p/V)_j$ for a trial value of (μ_1).

3) Calculate

$$\tau_j = \frac{\rho_s R_x}{\left(\frac{W_p}{V}\right)_j (1 + R - R'_p)}$$

4) Calculate $(\mu_2)_j$, $(\mu_3)_j$, N_j,

$$M_j = \left(\frac{V}{W_p}\right)_j W_p \rho_s$$

and

$$G_j = k' \rho_I N_j (\mu_3)_j / M_j \ .$$

5) Compare ϵ_j with the specified value of ϵ; make an appropriate adjustment to (μ_1); and repeat until some agreement criterion

is satisfied. The final values are then used to compute the costs associated with the size of the freezer vessel V_j and the size and power requirements for the counter washer as affected by the mean crystal size, μ_1.

4.6 THE MAIN HEAT EXCHANGER

The formulation of the design equations for the steady state operation of the main heat exchanger follows the result of Section 4.2, particularly E 4.2.30

$$\frac{APP}{SPR} = \frac{1}{1 + 2\ NTU} \qquad \text{E 4.2.30}$$

With inlet and outlet temperatures assumed, one calculates the NTU required to produce this heat exchange and then proceeds according to the following design algorithm.

4.6.1 DESIGN EQUATIONS

Assuming as known the mass rate per stream, $\dot{M}$, and the NTU required (calculated from E 4.2.30 above), choose integral values for P such that

$$2000 \leq \frac{\dot{M}}{P} \leq 10{,}000 \qquad \text{E 4.6.1}$$

Calculate

$$\frac{U(\frac{\dot{M}}{P})}{\frac{\dot{M}}{P}}$$

where

$$U(X) = \frac{100 + .055\ X}{1 + .0003(100 + .055\ X)} \ . \qquad \text{E 4.6.2}$$

Calculate

$$S = \frac{NTU}{40} \frac{1}{\left[\frac{U(\dot{M}/P)}{\dot{M}/P}\right]} .$$

Select smallest integer $\geq S = \bar{S}$.

Select smallest integer $\geq \frac{P}{15} = B$.

Heat exchanger cost is

$$\$1000(\bar{S})(B + 1) + 84(\bar{S})(2P - B) .$$

Total pressure drop is

$$TPD = (6 \times 10^{-8})(M/P)^{2}\bar{S}$$

(Constrained to be ≤ 35) .

BHP per pump is

$$\frac{\dot{M}}{\rho}(TPD)\frac{144}{60(33,000)}$$

at 100% efficiency .

The final value for P is taken at that which minimizes the cost of the heat exchanger and pumps.

451-332 O - 71 - 14

4.6.2 HEAT EXCHANGER NOTATION

BHP = brake HP per pump

$\dot{M}/P$ = flow per path

P = parallel paths

$\overline{S}$ = series paths

$\overline{S}(B + 1)$ = end-plates required

$\overline{S}(2P - B)$ = plates required

TPD = total pressure drop

$U(\dot{M}/P)$ = heat transfer coefficient

NOTE: A change during report preparation has been to deduct the costs of the heat exchanger end plates. Colt has advised that there is included in the plate cost an allowance for end plates.

4.7 THE STEADY STATE MELTER

Colt's procedure has been followed in formulating the equations for estimating the size of the melter. The cross-sectional area of the ice pack required to melt (condense) a given hourly mass rate of ice (vapor) is found by dividing the required heat load by the product of an empirical heat transfer coefficient and the temperature driving force based on the melter water outlet conditions. The heat transfer coefficient was found by Colt to depend on the partial pressure of inerts in the melter vapor.

Let

P_M = total pressure on the melter, mm Hg
P_A = partial pressure of inert gases, mm Hg
ΔP_L = pressure losses throughout the melter.

The temperature driving force, ΔT, is then taken as

$$\Delta T = T_v - 32 \ , \ ^oF$$

where T_v is found as the equilibrium temperature at the pressure P_v, where

$$P_v = P_M - (P_A + \Delta P_L) \ .$$

The heat load on the melter is found as the product of the vapor rate and the difference between the inlet vapor enthalpy and the exit water enthalpy at T_v. The inlet vapor enthalpy is as that of the ejector exhaust steam. If this total heat load is Q_I, then the melter cross-sectional area is found to be

$$A_M = \frac{Q_I}{h_M \Delta T} \qquad \text{E 4.7.1}$$

where A_M = melter cross-sectional area, ft^2

h_M = effective melter heat transfer coefficient, Btu/hr ft^2 ^oF

The value for h_M at a partial pressure of inerts of 0.08 mm Hg is 30,000 Btu/hr ft^2 ^oF.

4.8 THE STEADY STATE COUNTER WASHER

Equations describing the behavior of the counter washer have been adapted from our previous work, "The Secondary Refrigerant Freezing Process: A Mathematical Study," Final Report to the United States Department of the Interior on Contract No. 14-01-0001-960, June 14, 1968. Slight modifications were necessary, since the equations as previously derived were for drained filter screens, and flooded screens constitute the configuration of present interest.

4.8.1 GENERAL RELATIONSHIPS

Consider as input variables to the washer the slurry rate, composition, and particle size. These variables are then converted to washer variables utilizing the following equations:

Slurry feed velocity

$$v_s = \frac{W_s}{\rho_s A_w} \qquad \text{E 4.8.1}$$

Free drain velocity (ft/hr for D_e in mm)

$$v_o = 385\ D_e \qquad \text{E 4.8.2}$$

(for $\epsilon_B = 0.5$)

Internal dimensionless velocities

$$V_s = \frac{v_s}{v_o} \qquad \text{E 4.8.3}$$

$$V_i^s = \frac{\alpha}{1 - \epsilon_B} V_s \qquad \text{E 4.8.4}$$

$$V_b^s = \frac{1 - \alpha}{\epsilon_B} V_s \qquad \text{E 4.8.5}$$

$$V_b^b = V_b^s + \left(\frac{1 - \epsilon_B}{\epsilon_B}\right)(V_i^s - V_i^b) \qquad \text{E 4.8.6}$$

4.8.2 DESIGN EQUATIONS

The maximum velocity that the ice can have is of necessity equal to the free drain velocity of the bed. At this point, the interstices will be filled with fluid, and washing will no longer be effective. Thus, one should normally operate at

$$V_i = \frac{v_i}{v_o} \leq 1 \qquad \text{E 4.8.7}$$

For preliminary design, the value of 0.9 has been selected. Then, by E 4.8.4

$$V_s = \frac{1 - \epsilon_B}{\alpha}(0.9) \qquad \text{E 4.8.8}$$

$$v_s = V_s v_o \qquad \text{E 4.8.9}$$

where v_o is calculated from E 4.8.2.

Then the area required is

$$A_w = \frac{W_s}{\rho_s v_s} \qquad \text{E 4.8.10}$$

The ice rise rate is

$$IRR = \frac{\epsilon W_s}{A} \qquad \text{E 4.8.11}$$

4.8.3 WASHER NOTATION

A_w = washer area

α = volume fraction ice in slurry

ϵ = mass fraction ice in slurry

ϵ_B = bed voidage

ρ_s = slurry density

v_s = slurry feed velocity

V_s = non-dimensional slurry velocity

(all capital V s are dimensionless)

V_i^s = velocity--sub ice, super steady state

V_b^s = velocity--sub brine, super steady state

V_b^b = velocity--sub brine, super in the bed

The following identities are valid:

$$\alpha = \frac{1}{1 + (\frac{1 - \epsilon}{\epsilon})\frac{\rho_I}{\rho_B}}$$

$$\rho_s = \alpha\rho_I + (1 - \alpha)\rho_B$$

$$\rho_I = 0.92 \times 62.4 = 57.4$$

$$\rho_B = 65.8$$

$$\frac{\rho_I}{\rho_B} = 0.871$$

SECTION 5. DYNAMIC MODELS OF THE PROCESS COMPONENTS

The preferred procedure in dynamic simulation is to derive the differential equations representing the transient behavior of the process and then to proceed directly to the analog mechanization and simulation. In many cases, particularly those involving the dynamics of temperature, concentration, and flow rate interactions, the equations as originally derived are highly non-linear and require excessive analog hardware for mechanization. In these cases it is convenient to develop linear approximations to the non-linear equations by expanding them about some convenient reference state.

The procedure is to replace each dependent variable by its reference value plus a perturbation and to do the indicated algebra, neglecting terms of squared and higher order in the perturbation variables. The resulting approximate equations are linear and thus especially well suited to analog computation. Typically, if the reference state is well chosen, the linearized system is entirely adequate for a dynamic simulation control system design.

In this section of the report are presented, for each process component, the non-linear differential equations as originally derived, the linearized or perturbation form of the equations, and a tabulation of the reference state about which the perturbation was developed.

The notation convention is to utilize capital letters for variables in the non-linear equations, the same capital letters for the reference value of the variable in the perturbation equation, with small letters designating the time dependent perturbation. Thus, the notation

$$MABS = MABS + mabs$$

is taken to mean that the mass content of the absorber can be taken as the reference value MABS plus the perturbation value mabs.

5.1 THE DYNAMIC ABSORBER

The absorber mass balance is

$$\frac{d}{dt}[MABS] = WC + VAB - WA \ . \qquad \text{E 5.1.1}$$

The absorber caustic balance is

$$\frac{d}{dt}[MABS \cdot CA] = WC \cdot CC - WA \cdot CA \ . \qquad \text{E 5.1.2}$$

The enthalpy balance on the absorber is

$$\frac{d}{dt}[MABS \cdot HC(TA,CA)] = - Q(ABS) + WC \cdot HC[TCHE,CC] - WA \cdot HC[TA,CA] + VAB \cdot HVAP(TA) \ . \qquad \text{E 5.1.3}$$

The vapor rate is

$$VAB = MTC[CEQ(TA,P) - CA] \qquad \text{E 5.1.4}$$

where

$$MTC = 37.7 \exp[- 8.82 + .148 \ TA] \qquad \text{E 5.1.5}$$

and the equilibrium relationship is

$$CEQ(TA,P) = \frac{-1}{8.96}[\ln P - 25.3848 + 10838\ (\frac{1}{460 + TA})]\ . \qquad E\ 5.1.6$$

5.1.1 THE LINEARIZED ABSORBER

The linearized versions of the equations of the preceeding section are the following

Mass balance

$$\frac{d}{dt}(mabs) = wc + vab(ABSA) - wa \qquad E\ 5.1.7$$

Caustic balance

$$\frac{d}{dt}[MABS \cdot ca + mabs \cdot CA] = + WC \cdot cc + wc \cdot CC - WA \cdot ca - wa \cdot CA \qquad E\ 5.1.8$$

Enthalpy balance

$$\frac{d}{dt}[MABS(.833\ ta + 570\ ca + 86.81(mabs)] = - qabs + WC[.833\ tche + 570\ cc]$$
$$+ wc(140.30) - wa(86.81) - WA[.833\ ta + 570\ ca]$$
$$+ ABSA[(3.73)(.452\ ta) + 1376.46(-\ .2046\ ta + 6.017\ p + 176\ ca)]$$

E 5.1.9

$$QABS = (UABS)(ABSA)[70 + ta - TS] = (UABS)(ABSA)[(\triangle T) + ta] \qquad E\ 5.1.10$$

$$qabs = (UABS)(ABSA)ta \qquad E\ 5.1.11$$

Absorption rate

$$VAB = 3.73 - .2046\ ta + 6.017\ p + 176\ ca \qquad \text{E 5.1.12}$$

The following relationships between the reference values of the variables must be satisfied:

$$0 = WC + 3.73(ABSA) - WA \qquad \text{E 5.1.13}$$

$$0 = WC \cdot CC - WA \cdot CA$$

$$0 = -(UABS)(ABSA)(\triangle T) + WC \cdot 140.30 - WA \cdot 86.81 + ABSA[(3.73)(1376.46] \qquad \text{E 5.1.14}$$

5.1.2 REFERENCE VALUES AND NOTATION

ABSA = $(.713 \times 10^4)$ = absorber area, ft^2

CA = (.44) = absorber concentration

MABS = (10,000 lb) = absorber mass content, lbm

P = (3.264 mm) = system pressure, mm

QABS = absorber heat load, Btu/hr

TA = (70^o) = absorber temperature, ^oF

TAHE = (220^o) = temperature of absorber effluent after heat exchange, ^oF

TC = (250^o) = concentrator temperature, ^oF

TCHE = (100^o) = temperature of concentrator effluent after heat exchange, ^oF

TS = sea water temperature, ^oF

UABS = (70) = absorber heat transfer coefficient, Btu/hr ft^2 ^oF

WA = $(.262 \times 10^6)$ = absorber mass rate, lbm/hr

WC = $(.235 \times 10^6)$ = concentrator mass rate, lbm/hr

5.2 THE DYNAMIC ABSORBER LOOP HEAT EXCHANGER

A few preliminary results are needed prior to the absorber loop heat exchanger formulation.

5.2.1 BALANCED OR UNBALANCED HEAT EXCHANGER--TRANSIENT OPERATION

The set of differential equations describing the transient behavior of an unbalanced heat exchanger can be written as

$$-\frac{\partial H}{\partial \theta} = \frac{1}{NH}\frac{\partial}{\partial(\frac{x}{L})} H + (H - C) \qquad \text{E 5.2.1}$$

$$\frac{\partial C}{\partial \theta} = \frac{1}{NH}\frac{\partial}{\partial(\frac{x}{L})} C + (H - C) \qquad \text{E 5.2.2}$$

with boundary conditions

$$H(0,\theta) = H_{IN}(\theta) \qquad \text{E 5.2.3}$$

$$C(1,\theta) = C_{IN}(\theta) \qquad \text{E 5.2.4}$$

where θ is non-dimensional time,

$$\theta = \frac{t}{\frac{A_c \rho C_p}{U A_h}} \qquad \text{E 5.2.5}$$

with A_c = the cross-sectional area

A_h = the heat transfer area per unit of length.

Thus, θ is equal to time divided by a scale factor having dimensions of time and resembling a heat path length (A_c/A_h) divided by a diffusion velocity for heat ($U/\rho Cp$).

By standard techniques, the first-order solution to this system representing the long-time approximation to the response is given by

$$\begin{matrix} \tilde{H}_{OUT} \\ \tilde{C}_{OUT} \end{matrix} = \frac{1}{2(1+N)(1+NS)} \begin{bmatrix} 2 & 2N & -2-N(1+S) & N \\ 2N & 2 & -N & 2+N(1+S) \end{bmatrix} \begin{matrix} \tilde{H}_{IN} \\ \tilde{C}_{IN} \\ \Delta f \\ \Delta g \end{matrix} \qquad \text{E 5.2.6}$$

where N is the number of transfer units for the balanced exchanger and Δf and Δg are as defined in the preceeding section.

5.2.2 GENERALIZED RESPONSE OF UNBALANCED HEAT EXCHANGER

The generalized response is developed as a perturbation about some steady response of a balanced heat exchanger as follows: Defining the perturbation variables as the deviation of the transient, unbalanced variable from the steady, balanced variable, i.e.,

$$\begin{matrix} H_{OUT} \\ C_{OUT} \end{matrix}\Bigg]_{TRANS} = \begin{matrix} H_{OUT} \\ C_{OUT} \end{matrix}\Bigg]_{STEADY} + \begin{matrix} \tilde{H}_{OUT} \\ \tilde{C}_{OUT} \end{matrix}\Bigg] \qquad \text{E 5.2.7}$$

$$\begin{matrix} H_{IN} \\ C_{IN} \end{matrix}\Bigg]_{TRANS} = \begin{matrix} H_{IN} \\ C_{IN} \end{matrix}\Bigg]_{STEADY} + \begin{matrix} \tilde{H}_{IN} \\ \tilde{C}_{IN} \end{matrix}\Bigg] \qquad \text{E 5.2.8}$$

$$\begin{bmatrix} NTU_{HOT} \\ NTU_{COLD} \end{bmatrix}_{TRANS} = \begin{bmatrix} N \\ N \end{bmatrix}_{STEADY} + \begin{bmatrix} f \\ g \end{bmatrix} \qquad \text{E 5.2.9}$$

The balanced steady response is given by

$$\begin{bmatrix} H_{OUT} \\ C_{OUT} \end{bmatrix}_{STEADY} = \frac{1}{1+N} \begin{bmatrix} 1 & N \\ N & 1 \end{bmatrix} \begin{bmatrix} H_{IN} \\ C_{IN} \end{bmatrix}_{STEADY} \qquad \text{E 5.2.10}$$

And the transient perturbation variables are given (in the S-domain) by

$$\begin{matrix} \sim \\ H_{OUT} \\ \sim \\ C_{OUT} \end{matrix} = \frac{1}{2(1+N)(1+NS)} \begin{bmatrix} 2 & 2N & -2-N(1+S) & N \\ 2N & 2 & -N & 2+N(1+S) \end{bmatrix} \begin{matrix} H_{IN} \\ C_{IN} \\ \Delta f \\ \Delta g \end{matrix} \qquad \text{E 5.2.11}$$

These results are to be applied to the heat exchanger configuration given in F 5.1.

5.2.3 THE GENERAL HEAT EXCHANGER FORMULATION

With the notational changes as indicated in F 5.1, the general formulation for the absorber heat exchanger is

$$\begin{matrix} tche \\ tahe \end{matrix} = \frac{1}{2(6)(1+5s)} \begin{bmatrix} 2 & 10 & -2-5(1+s) & 5 \\ 10 & 2 & -5 & 2+5(1+s) \end{bmatrix} \begin{matrix} tc \\ ta \\ 30\ nh \\ 30\ nc \end{matrix} \qquad \text{E 5.2.12}$$

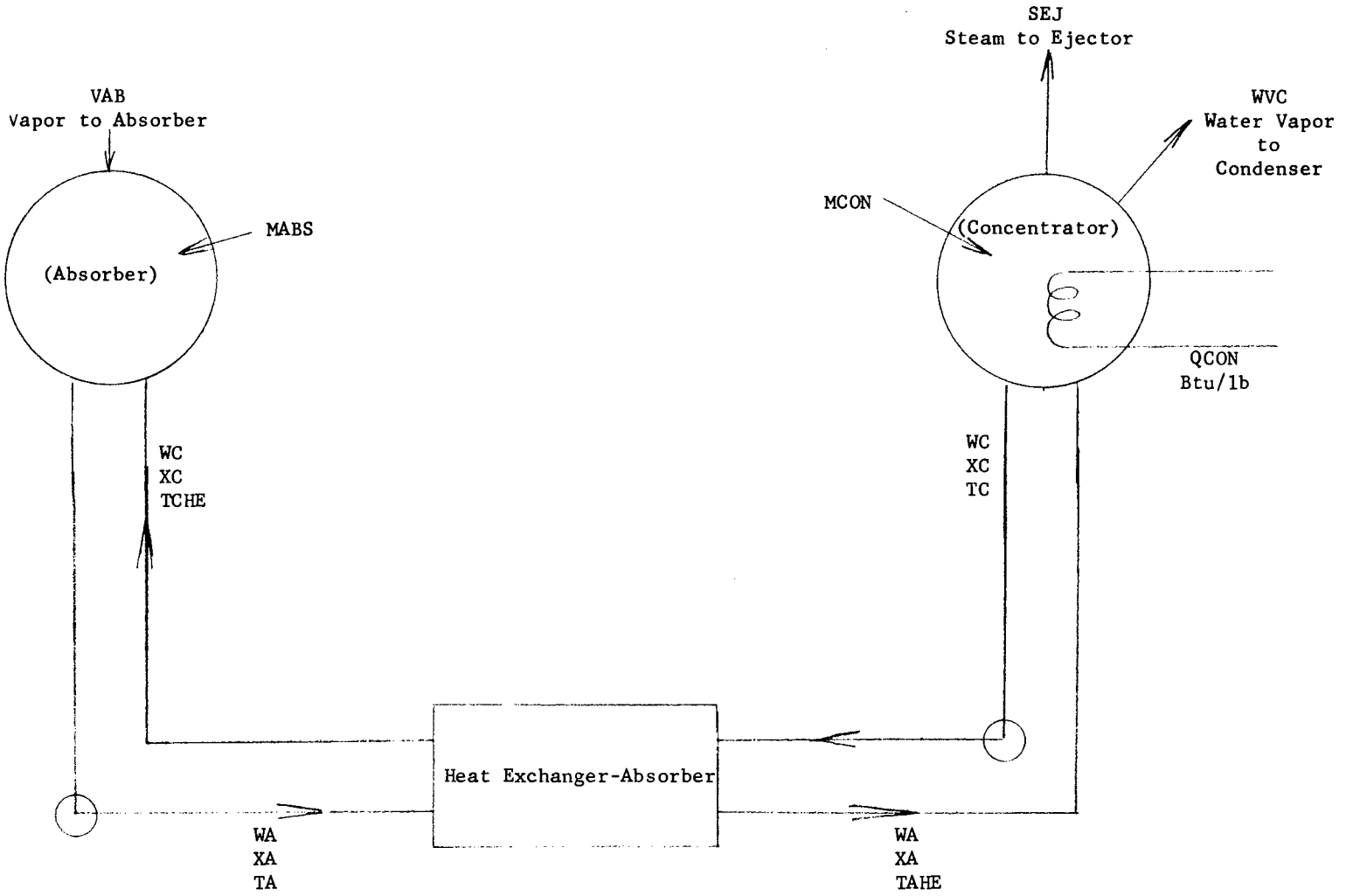
SEJ
Steam to Ejector
VAB
Vapor to Absorber
WVC
Water Vapor
to
Condenser
MCON
(Concentrator)
MABS
(Absorber)
QCON
Btu/lb
WC
XC
TCHE
WC
XC
TC
Heat Exchanger-Absorber
WA
XA
TA
WA
XA
TAHE

Figure F 5.1

where

$$nh = 5\left[\frac{WA - WC}{2WC} - \frac{wc}{WC}\right]\left[1 - \frac{wc}{WC}\right] \qquad \text{E 5.2.13}$$

$$nc = 5\left[\frac{WC - WA}{2WA} - \frac{wa}{WA}\right]\left[1 - \frac{wa}{WA}\right] \qquad \text{E 5.2.14}$$

Here s is the transform of dimensionless time, related to real time by:

$$T\ NOND = \frac{TR}{\frac{VOL}{2.5(VOL\ RATE)}} \qquad \text{E 5.2.15}$$

5.2.4 THE LINEARIZED HEAT EXCHANGER RESPONSE

In this circumstance a portion of the linearization has been done in deriving the approximate solution to the differential equations. The balance of the linearization involves only the perturbation transfer units, nh and nc. In the linear approximation they are

$$nh = 5\left[\left(\frac{WA - WC}{2WC}\right) - \left(\frac{WA + WC}{2WC}\right)\frac{wc}{WC}\right] \qquad \text{E 5.2.16}$$

$$nc = 5\left[\left(\frac{WC - WA}{2WA}\right) - \left(\frac{WC + WA}{2WA}\right)\frac{wa}{WA}\right] \qquad \text{E 5.2.17}$$

5.2.5 REFERENCE VALUES

WA, WC } see Section 5.1

TA = 70°F

TAHE = 220°F

TC = 250°F

TCHE = 100°F

VOL/2.5(VOL RATE) = 0.01 hr

5.3 THE DYNAMIC CONCENTRATOR

The overall concentrator mass balance is

$$\frac{d}{dt}[MCON] = WA - WC - SEJ - WVC \ . \qquad \text{E 5.3.1}$$

The concentrator caustic balance is

$$\frac{d}{dt}[MCON \cdot CC] = WA \cdot CA - WC \cdot CC \ . \qquad \text{E 5.3.2}$$

The enthalpy balance is

$$\frac{d}{dt}[MCON \cdot HC(TC,CC)] = QCON + WA \cdot HC[TAHE,CA] - WC \cdot HC[TC,CC] - (SEJ + WVC)[HWV(PC)] \qquad \text{E 5.3.3}$$

where the heat flow into the concentrator is

$$Q = UA(TST - TC) \qquad \text{E 5.3.4}$$

and TST is a control variable.

The thermodynamic relationships are the following:

$$HC[T,C] = -222.3 + 0.833\ T + 570\ C \qquad \text{E 6.1.9}$$

451-332 O - 71 - 15

$$HVAP[T] = 1060.06 + 0.452\ T \qquad \text{E 6.1.7}$$

$$\ln PC = 25.3848 - 10838\left(\frac{1}{460 + T}\right) - 8.96\ C \qquad \text{E 6.1.10}$$

for P in mm Hg, T in ^{o}F, and C in wt fraction.

The steam flow to the ejector is given by

$$SEJ = \frac{NOZA(0.06324)(3600)PC}{\sqrt{460 + TC}} \qquad \text{E 5.3.5}$$

where NOZA is the ejector nozzle area in square feet.

5.3.1 THE LINEARIZED CONCENTRATOR

The linearized versions of the equations of the preceeding section are the following:

Mass balance

$$\frac{d}{dt}(mcon) = wa - wc - sej - wvc \qquad \text{E 5.3.6}$$

Caustic balance

$$\frac{d}{dt}[MCON \cdot cc + mcon \cdot CC] = WA \cdot ca + wa \cdot CA - wc \cdot CC - WC \cdot cc \qquad \text{E 5.3.7}$$

Enthalpy balance

$$\frac{d}{dt}[MCON(.833\ tc + 570\ cc) + 265.25\ mcon] = -\ (UCON)(ACON)\ tc$$

$$+ WA[.833\ tahe + 570\ ca] + 211.76\ wa - WC[.833\ tc + 570\ cc]$$

$$- 265.25\ wc - [(NOZA)(153.76\ pc - 33.34\ tc) + WVC](1173.06)$$

$$- 47{,}329\ NOZA(.452\ tc)$$

E 5.3.8

The following relationships among unperturbed variables must be satisfied:

$$0 = WA - WC - SEJ \qquad \text{E 5.3.9}$$

$$0 = WA \cdot CA - WC \cdot CC \qquad \text{E 5.3.10}$$

$$0 = (UCON)(ACON)\triangle T + WA(211.76) - WC(265.25) - 2629.4\ NOZA(1173.06)$$

$$QCON = QCON + qcon = (UONC)(ACON)[\triangle T - tc] \qquad \text{E 5.3.11}$$

5.3.2 REFERENCE VALUES AND NOTATION (see also 5.1.2)

ACON = (2,650) = concentrator area, ft^2

MCON = (10,000 lb) = mass content of concentrator, lbm

NOZA = (0.5620) = nozzle area, ft^2

PC = (307.8) = concentrator pressure, mm Hg

SEJ = $(.266 \times 10^5)$ = steam to ejector primary, lbm/hr

UCON = (400) = heat transfer coefficient, Btu/hr ft^2 ^oF

5.4 THE DYNAMIC EJECTOR

It is assumed that the ejector responds instantaneously and delivers a constant primary to secondary ratio, REJ. In the analog simulation, REJ is taken to be 0.6.

5.5 THE DYNAMIC FREEZER

Since the freezer is a central component of the system, its description should be as complete as possible so that practical simplification will retain the features most important to optimization and simulation.

Unlike the secondary refrigerant process, simulation of the vacuum freezing process freezer does not need to be concerned with accounting for the effects of a second immiscible phase. This simplifies the problem considerably not only from the standpoint of eliminating several equations, but also by simplifying the crystal growth equations.

In the secondary refrigerant process, the presence of vaporizing refrigerant is believed to be responsible for local temperature gradients much larger than probably exist in the vacuum freezer. From this belief and the practical observation that the mean crystal size in the vacuum freezer is insensitive to operating changes, it will be conjectured that the mechanism for crystal growth is by agglomeration rather than by additions to the crystal lattice and depends only on particle collisions and not on a temperature driving force. Nucleation is assumed to occur at a rate proportional to the surface area of the crystals and only in that portion of the freezer at which the total pressure (vapor pressure plus hydrostatic head) is low enough to permit vaporization.

With these and the further assumption that the freezer vessel is completely mixed, ordinary non-linear differential equations may be derived for the change in time of the following dependent freezer variables:

X_s = brine salt concentration (mass fraction)
T_s = freezer temperature, ^oF
μ_1 = mean crystal size (diameter), mm
μ_2 = mean squared crystal size, $(mm)^2$
μ_3 = mean cubed crystal size, $(mm)^3$
N = crystal number
M = mass of slurry in freezer, lbs

The weight fraction ice in the slurry is related to M, N, and μ_3 by

$$\epsilon = \frac{k' \rho_I N \mu_3}{M}$$

where $k' = \pi/6$ if the crystals are assumed spheres

ρ_I = ice density, mass/volume

The differential equations are as follows:

Salt balance

$$\dot{X}_s = \frac{W_s^o}{M(1 - \epsilon)}(X_s^o - X_s) + \frac{W_R(X_B - X_s)}{M(1 - \epsilon)} + \frac{X_s}{M(1 - \epsilon)}[W_s \epsilon + W_p' + k' \rho_I (\dot{\overline{\mu_3 N}})] \quad \text{E 5.5.1}$$

where $\dot{X}_s = dX_s/dt$

W_s^o = sea water feed rate, mass/time

W_s = freezer draw down rate (including recycle brine), mass/time

W_p' = water vapor removal rate, mass/time

M = freezer slurry inventory, mass

X_s^o = sea water salt concentration, mass fraction

The term $k' \rho_I \dot{\overline{\mu_3 N}}$ can be interpreted as the dynamic effect of the freezing on the composition change and is in fact equal to the rate of change of the ice in the system $d\epsilon M/dt$ as can be seen from the definition of ϵ.

Enthalpy balance

$$M\hat{C}_p \dot{T}_s + (1 - \epsilon)M\left(\frac{\partial h}{\partial X}\right)_{X_s} \dot{X}_s = W_s^o(h_1^o - h_1) - \epsilon W_s(h_s - h_1)$$

$$+ W_R(h_\ell^a - h_\ell) - W_p'(h_g - h_1) - h_s - h_1)k'\rho_I(\overline{\mu_3 N}) \qquad \text{E 5.5.2}$$

where $\dot{T}_s = dT_s/dt$

$\hat{C}_p$ = mean specific heat of the slurry, heat units/mass - ^oF

h_1^o = enthalpy of entering sea water, heat units/mass

h_ℓ^a = enthalpy of recycle brine, heat units/mass

h_1 = enthalpy of brine in freezer, heat units/mass

h_s = enthalpy of ice in freezer, heat units/mass

h_g = enthalpy of vapor leaving freezer, heat units/mass

$\left(\frac{\partial h}{\partial X}\right)_{X_s}$ = differential enthalpy of mixing at concentration X_s, heat units/mass--concentration units.

With the assumption that the brine leaves the freezer at equilibrium at the triple point, equation E 5.5.2 is not required.

Overall mass balance

$$\dot{M} = W_s^o + W_R - W_s - W_p' \qquad \text{E 5.5.3}$$

where $\dot{M} = dM/dt$

W_R = brine recycle rate, mass/time

Population balance equations

In addition to the preceding equations, population balance equations must also be written to describe the crystal growth which in turn influences the concentration and enthalpy equations through the terms involving μ_3 and N. In the population balance equations the nucleation rate is assumed to depend only on the surface of the exposed ice, and can be written as follows:

$$\frac{\dot{N}}{N} = \frac{B}{N} - \frac{aN}{2} - \frac{1}{\tau} \qquad \text{E 5.5.4}$$

where $\dot{N} \equiv dN/dt$

N = number of particles in the population

B = total nucleation rate, particles/unit time

a = an empirical agglomeration rate constant $(\text{time})^{-1}$

$\tau = M/W_s$, mean holding time of a particle in the population.

Mean crystal size

$$\dot{\mu}_1 = \frac{B}{N}\gamma_o - \mu_1\left(\frac{1}{\tau} + \frac{\dot{N}}{N}\right) \qquad \text{E 5.5.5}$$

where γ_o = crystal nucleus size.

Second moment

$$\dot{\mu}_2 = \frac{B}{N}\gamma_o^2 + aN\mu_1^2 - \mu_2\left(\frac{1}{\tau} + \frac{\dot{N}}{N}\right) \qquad \text{E 5.5.6}$$

Third moment

$$\dot{\mu}_3 = \frac{B}{N}\gamma_o^3 + 3aN\mu_1\mu_2 - \mu_3\left(\frac{1}{\tau} + \frac{\dot{N}}{N}\right) \qquad \text{E 5.5.7}$$

Suppose the nuclei production occurs only within a subcooled region of the freezer (i.e., some portion near the surface), and that the rate is independent of the amount of subcooling but depends on the surface area of ice in the region (secondary nucleation). If the vessel is well stirred, the surface area in the nucleation region will equal $\pi\mu_2 N$ times the fraction of the vessel occupied by the region, and the nucleation rate will be

$$B = \pi\mu_2 N \times \text{nucleation rate} = N\phi B_o$$

where B_o = (specific nucleation rate) $\times \pi$, number/unit area-time (if spherical crystals are assumed)

ϕ = fraction of the vessel occupied by nucleation zone

Pressure equations

In order to simulate the response of the freezer pressure to other dynamic quantities, the following equation has been derived

$$\left(V_T - \frac{M}{\rho_s}\right)\dot{P} = \frac{P}{\rho_s}\dot{M} + \frac{R}{18}\left[\frac{UA_F\Delta T}{hg - h_\ell} - W'_{pc}\right](T_v + 460) \qquad \text{E 5.5.8}$$

where $\dot{P} = dP/dt$ = change in freezer pressure with time, mm/hr

$\dot{M} = dM/dt$ = change in freezer mass contents with time, (cf equation E 5.5.4), mm/hr

V_T = total freezer vessel volume, ft^3

ρ_s = slurry density, lbm/ft^3

ΔT = freezer temperature driving force, ^oF

T_v = freezer vapor temperature, ^oF

W'_{pc} = freezer vapor production rate, corrected for sensible heat in the sea water feed, lbm/hr

V = effective freezer heat transfer coefficient, Btu/hr ft^2 ^oF

$hg - h_\ell$ = enthalpy change on condensing water vapor, Btu/lbm

R = gas constant, ft^3-mm Hg/lb mole ^oR

Equation E 5.5.8 is a dynamic statement of the perfect gas law which accounts for the change in vessel pressure due to changes in vapor spare volume. Momentum effects have been neglected.

Linear dynamic freezer equations

For the convenience of analog computer programming, several of the equations describing the freezer dynamics have been linearized about the steady state. The temperature equation, E 5.5.2 has been omitted since brine temperature changes will be small and can be neglected. The salt balance, E 5.5.1, the mass balance, E 5.5.4, and the pressure equation, E 5.5.8, have not been linearized since their simple form does not require it.

Population balance dynamics

The following definitions relate the time dependent variables to the steady state variables and the dynamic perturbations.

$$N = \bar{N} + \bar{N}y'$$

$$\mu_1 = \bar{\mu}_1 + \mu'_1$$

$$\mu_2 = \bar{\mu}_2 + \mu'_2$$

$$\mu_3 = \bar{\mu}_3 + \mu'_3$$

$$\epsilon = \bar{\epsilon}\,\epsilon'$$
$$X_s = \bar{X}_s + X_s'$$
$$P = \bar{P} + P'$$

where the overbars represent steady values, and the primed quantities are the perturbations assumed to be small enough so that all products and derivatives of higher order than one are vanishingly small. When these are substituted into the population equations and non-linear terms expanded in Taylor's series about the steady state, linear differential equations result with coefficients given in terms of the steady values. These equations are

Population size

$$\frac{dy'}{dt} = \overline{\phi B_o}\mu_2' - \frac{C_1}{\rho_s L}\overline{\mu_2}(18.45\,X_s' + P') + \left(\frac{\overline{W_s}}{M}\right)\left(\frac{M}{\bar{M}} - \frac{W_s}{\bar{W}_s}\right) - \frac{a\bar{N}}{2}y' \qquad \text{E 5.5.9}$$

Mean crystal size

$$\frac{d\mu_1'}{dt} = \overline{\phi B_o \gamma_o}\mu_2' - \frac{C_1}{\rho_s L}\overline{\mu_2\gamma_o}(18.45\,X_s' + P') - \left(\mu_1\frac{\overline{W_s}}{M}\right)\left(\frac{W_s}{\bar{W}_s} - \frac{M}{\bar{M}}\right) - \bar{\mu}_1\frac{dy'}{dt} - \left(\frac{\overline{W_s}}{M}\right)\mu_1' \qquad \text{E 5.5.10}$$

Second moment

$$\frac{d\mu_2'}{dt} = \left[\overline{\phi B_o \gamma_o^2} - \left(\frac{\bar{W}_s}{M}\right)\right]\mu_2' - \frac{C_1}{\rho_s L}\overline{\mu_2\gamma_o^2}\,(18.45\,X_s' + P') - \left(\mu_2\frac{\overline{W_s}}{M}\right)\left(\frac{W_s}{\bar{W}_s} - \frac{M}{\bar{M}}\right)$$
$$- \bar{\mu}_2\frac{dy'}{dt} + \left(a\overline{\mu_1^2 N}\right)y' + 2a\left(\overline{\mu_1 N}\right)\mu_1' \qquad \text{E 5.5.11}$$

Third moment

$$\frac{d\mu_3'}{dt} = \overline{[\phi B_o \gamma_o^3} + 3a\overline{N\mu_1}]\mu_2' - \frac{C_1}{\rho_s L}\overline{\mu_2 \gamma_o^3}(18.45\, X_s' + P') + 3a\overline{N\mu_2}\mu_1' - \overline{(\mu_3 \frac{W_s}{M})}(\frac{W_s}{\overline{W}_s} - \frac{M}{\overline{M}})$$

$$- \overline{\mu_3}\frac{dy'}{dt} - (\frac{\overline{W}_s}{M})\mu_3' + (3a\overline{\mu_1\mu_2 N})y'$$

E 5.5.12

Ice fraction

$$\epsilon' = 2 + y' + \frac{\mu_3'}{\overline{\mu}_3} - \frac{M}{\overline{M}}$$

E 5.5.13

Note that at the steady state all perturbations are zero and $W_s = \overline{W_s}$, $M = \overline{M}$ so that all time derivatives are zero, and $\epsilon' = 1$. When numerical values based on a steady state were assigned to the coefficients, it was determined that the coefficients of the term $(18.45\, X_s' + P')$ were very small except in equation E 5.5.9 and could be neglected. This indicates a negligible direct effect of brine composition and pressure on the mean size and second and third moments. There will be an interaction effect owing to the y' terms in these latter equations.

5.6 THE DYNAMIC MAIN HEAT EXCHANGER

The responses of both of the main heat exchangers are given in linear form by identification of the variables with the general result of Section 5.2.

5.6.1 THE FEED-PRODUCT EXCHANGER

The transient relationship is

$$\begin{matrix} tswf2 \\ tpf \end{matrix} = \frac{1}{22(1 + 10\,S)} \begin{bmatrix} 2 & 20 & -12 - 10\,S & 10 \\ 20 & 2 & -10 & 12 + 10\,S \end{bmatrix} X$$

$$\begin{matrix} tsw \\ tp \end{matrix}$$

$$(3.45)\left(-\frac{wf2}{.52 \times 10^5}\right)$$

$$(3.45)\left(\frac{-wp}{.52 \times 10^6}\right) \qquad \text{E 5.6.1}$$

S is the transform of 100 t (t in hours).

5.6.2 THE FEED-BRINE EXCHANGER

The transient relationship is

$$\begin{matrix} tswf1 \\ tbf \end{matrix} = \frac{1}{22(1 + 10\,S)} \begin{bmatrix} 2 & 20 & -12 - 10\,S & 10 \\ 20 & 2 & -10 & 12 + 10\,S \end{bmatrix} X$$

$$\begin{matrix} tsw \\ tb \end{matrix}$$

$$(4.09)\left(\frac{-wf1}{.77 \times 10^5}\right)$$

$$(4.09)\left(\frac{-wb}{.77 \times 10^6}\right) \qquad \text{E 5.6.2}$$

S is the transform of 100 t (t in hours).

5.6.3 NOTATION AND REFERENCE VALUES

TB = 25 = brine feed temperature, ^{o}F

TBF = 65.91 = brine discharge temperature, ^{o}F

TP = 32 = product temperature, ^{o}F

TPF = 66.55 = product discharge temperature, ^{o}F

TSW = 70 = sea water temperature, ^{o}F

TSWF1 = 29.09 = sea water discharge temperature, feed-brine exchanger, ^{o}F

TSWF2 = 35.45 = sea water discharge temperature from feed product exchanger, ^{o}F

WB = $.77 \times 10^{6}$ = brine feed rate, lbm/hr

WF1 = $.77 \times 10^{6}$ = sea water feed to feed-brine exchanger, ^{o}F

WF2 = $.52 \times 10^{6}$ = sea water rate to feed-product exchanger, lbm/hr

5.7 THE DYNAMIC MELTER

The melter equations have been derived to express the dynamics of the melter pressure and ice pack level as a function of the total vapor rate to the melter. Momentum and pressure-enthalpy effects were neglected, and the pressure variations were assumed to be those due to changes in the vapor spare volume caused by variations in the net total mass flow.

Applying the perfect gas law to the vapor volume results in the equation for the pressure change with time:

$$\frac{dP_M}{dt} = \frac{1}{(V_T - \frac{M_T}{\rho_s})}\left[\frac{P_M}{18\rho_s}\frac{dM_T}{dt} + \frac{RT'_v}{18}\left(W_{vi} - \frac{h_M A_M \Delta T}{\lambda_c}\right)\right] \qquad \text{E 5.7.1}$$

where V_T = total melter volume, ft^3

M_T = mass of ice pack, lbm

ρ_s = density of ice pack, lbm/ft^3

T'_v = vapor temperature, $^oR = T_v + 460$

W_{vi} = inlet vapor rate, lbm/hr

λ_c = enthalpy change on condensation, Btu/lbm

R = gas constant, 555 mm Hg-ft^3/lb mole ^oR

The term in square brackets represents the net change in vapor as the vapor volume changes when condensation occurs.

The mass of the ice pack M_T is given by a mass balance on the ice plus condensed water vapor as

$$\frac{dM_T}{dt} = W_I(1 + m) - W_M + \frac{h_M A_M \Delta T}{\lambda_M} \qquad \text{E 5.7.2}$$

where W_I = ice rate to the melter, lbm/hr

m = ratio of liquid to ice in slurry from washer, lbm water/lbm ice

W_M = rate of withdrawal of melter product, lbm/hr

λ_M = enthalpy change on melting, Btu/lbm

The temperature driving force, ΔT, is taken as T_v - 32 where

$$T_v = \frac{4839}{10.4926 - \log_{10} P_M} - 460 \ , \ ^oF \qquad \text{E 5.7.3}$$

and P_M = melter pressure in mm Hg.

Normally, the melter is under level control by sensing the pack level and regulating the liquid withdrawal rate, W_M. The controller equations can be represented as follows, assuming a two-mode controller:

$$\epsilon_M = M_T - \overline{M}_T \qquad \text{E 5.7.4}$$

$$\theta_c = k_c[\epsilon_M + \frac{1}{\tau_c} \int_o^t \epsilon_M dt] \qquad \text{E 5.7.5}$$

and

$$W_M = \overline{W}_M[1 + \frac{C_1}{\overline{W}_M} \theta_c] \qquad \text{E 5.7.6}$$

In these equations ϵ_M represents the error between the observed level M_T and the control point $\overline{M}_T$. This error is converted to a control signal by the action of the controller (E 5.7.5) having both proportional and reset action, the proportional band width given by k_c and the reset rate by $1/\tau_c$. The controller action in turn influences the valve through equation E 5.7.6 where $\overline{W}_M$ represents the design flow and C_1 represents the linear valve characteristic.

5.8 THE DYNAMIC WASH SEPARATOR

A total material balance together with an ice material balance gives the following relationship for the location of the bottom of the ice plug.

$$\frac{dB}{dt} = \frac{\alpha V_s - (1 - \epsilon_b)V_i}{(1 - \epsilon_b) - \alpha} \qquad \text{E 5.8.1}$$

where α = volume fraction ice in slurry
V_s = slurry velocity, ft/hr
ϵ_b = bed void fraction
V_i = ice velocity

The linearized version of this equation is

$$\frac{dB}{dt} = \frac{1}{.31}\left[\frac{1}{64.2\ A}(.19 + .976\ \epsilon)W_s - .5\ V_i\right] \qquad \text{E 5.8.2}$$

where A = washer area
V_i = ice velocity, a control variable
ϵ = perturbation value of slurry density, about .17
W_s = washer feed rate, lb/hr

451-332 O - 71 - 16

SECTION 6. THERMODYNAMIC AND RATE DATA

In this section are collected the thermodynamic, kinetic, and cost data utilized in the study.

6.1 THERMODYNAMIC DATA

6.1.1 WATER VAPOR--FUNDAMENTAL THERMODYNAMIC EQUATION

In the low pressure, low temperature range of interest, thermodynamic data for water vapor appear to be well represented by the fundamental equation

$$\ln(h - 852.14) = 2.212\ s + 0.2429 \ln p + 1.1619 \qquad \text{E 6.1.1}$$

where h = enthalpy, Btu/lbm
s = entropy, Btu/lbm-^{o}R
p = pressure, psia

This equation is fundamental in the sense that all other thermodynamic data can be derived from it via the relationship

$$dh = Tds + vdp \qquad \text{E 6.1.2}$$

Of interest in freezer modeling is the vapor enthalpy in terms of its temperature and pressure. This is found as follows: Differentiate equation E 6.1.1 partially to get T(s,p), i.e.,

$$T(s,p) = \left(\frac{\partial h}{\partial s}\right)_p \qquad \text{E 6.1.3}$$

or

$$T(s,p) = 7.0704 \exp(2.212\ s) p^{0.2429} \qquad \text{E 6.1.4}$$

Eliminating s from equations E 6.1.1 and E 6.1.4 then gives

$$h = 852.14 + 0.452\ T \qquad \text{E 6.1.5}$$

where T is ^{o}R. This equation agrees with the Keanan-Keyes data and must be augmented by 200 Btu/lbm to agree with the caustic data, which have a different reference state.

Note that the vapor enthalpy is a function only of temperature in the region of applicability of this equation. That this behavior is reasonable in the desired temperature and pressure range is confirmed by a quick glance at the Mollier diagram for water.

6.1.2 ENTHALPY, SATURATED WATER VAPOR

$$h\ \text{Btu/lbm} = 1268.2 + 2.008\ P - .0384\ P^2 \qquad \text{E 6.1.6}$$

for P in mm Hg. Also

$$h\ \text{Btu/lbm} = 1260.06 + .452\ T \qquad \text{E 6.1.7}$$

for T in ^{o}F.

6.1.3 ENTHALPY OF VAPORIZATION

$$\Delta h_{vap} = 1054.5 - .2091\ P \qquad \text{E 6.1.8}$$

6.1.4 ENTHALPY, AQUEOUS CAUSTIC SOLUTIONS

$$h \text{ Btu/lbm} = -223.3 + .833\ T + \frac{570}{C} \qquad \text{E 6.1.9}$$

for T in ^{o}F and C in weight fraction.

6.1.5 VAPOR PRESSURE, AQUEOUS CAUSTIC SOLUTIONS

$$\ln P = 25.3848 - 8.96\ C - 10838\left(\frac{1}{460 + T}\right) \qquad \text{E 6.1.10}$$

for P in mm Hg, C in weight fraction, and T in ^{o}F. This equation fits Colt laboratory data for commercial-grade caustic.

6.1.6 BRINE ENTHALPY

The brine enthalpies have been expressed in terms of empirical equations which were fitted to the h-T-x charts in the OSW Saline Water Conversion Data Book (Chart 12.30). These empirical formulas (also given in Section 4) are as follows:

For $32 < T \leq 90^{o}F$ and $0 \leq X \leq 0.08$, wt fract TDS

$$h_{\ell} = 200 + (T - 32) + (76.5 - 1.10\ T)X \text{ , Btu/lb} \qquad \text{E 4.5.6}$$

For $32 - 104\ X < T \leq 32$ and $0 \leq X \leq 0.08$

$$h_{\ell} = 200 - 1.395(32 - T) + 52.0\ X \text{ , Btu/lb} \qquad \text{E 4.5.7}$$

For brine at temperatures below the equilibrium freezing point at the given salt concentration, $0 \leq X \leq 0.08$

$$h = h_s + (250 + \frac{13,500}{32 - T})X \ , \quad \text{Btu/lb} \qquad \text{E 4.5.8}$$

where h_s = ice enthalpy

$$= h_o \exp -b(32 - T) \qquad \text{E 4.5.9}$$

and $h_o = 59.4$, $b = 0.01121$ $\Big\}$ $0 \leq T \leq 30$

$h_o = 200$, $b = 0.619$ $\Big\}$ $30 \leq T \leq 32$

6.2 MASS TRANSFER COEFFICIENT

In the absorber the mass transfer coefficient is taken as

$$MTC = 8.33 \exp[-8.82 + 0.148\ T] \qquad E\ 6.2.1$$

where MTC = $lb/hr\text{-}ft^2\text{-}\Delta X$

X = lb H_2O/lb NaOH

T = ^oF.

6.3 HEAT TRANSFER COEFFICIENTS

For the individual heat exchangers the heat transfer coefficients are given as functions of flow rate in the respective parts of Section 4. The design optimization is programmed to select optimum heat exchangers based on both pressure drop and heat exchanger area.

6.3.1 CONCENTRATOR

$$\text{Concentrator Heat Transfer Coefficient} = 400 \frac{\text{Btu}}{\text{hr-ft}^2\text{-}^\circ\text{F}}$$

6.3.2 ABSORBER

$$\text{Absorber Heat Transfer Coefficient} = 70 \frac{\text{Btu}}{\text{hr-ft}^2\text{-}^\circ\text{F}}$$

6.4 ESTIMATION OF PROCESS COSTS FOR OPTIMIZATION PROGRAM

In order to determine the optimum operating-design variables, the computer program minimizes an operating cost made up of energy costs plus amortized capital costs. The following is a summary of the formulas used to determine the operating costs for the different sections of the process.

6.4.1 CAPITAL EQUIPMENT COST ESTIMATION

Pumps. Pump (including electric motor drives) cost has been estimated from the following empirical formula as a function of the required horsepower.

For HP > 10

$$\log_{10}\left(\frac{\text{dollar cost}}{1000}\right) = 0.176 - 0.255 \log_{10} HP + 0.21(\log_{10} HP)^2 \qquad \text{E 6.4.1}$$

For HP $\leq$ 10

$$\log_{10}\left(\frac{\text{dollar cost}}{1000}\right) = 0.733(\log_{10} HP - 1) \qquad \text{E 6.4.2}$$

Individual pump horsepower has been estimated from the process head loss requirement by assuming a pump efficiency of 0.75 and a motor drive efficiency of 0.91 (overall combined efficiency of 0.68).

Vessels. The dollar cost per pound of carbon steel, unfired pressure vessels is a function of the total vessel weight, w, according to

$$\text{cost per pound} = 1.9658 - 0.7395 \log_{10} w + 0.07466(\log_{10} w)^2 \qquad \text{E 6.4.3}$$

The total weight in pounds for cylindrical steel vessels with dished heads can be approximated by

$$w = 136\ D(H + 0.8\ D)(t + x) \qquad \text{E } 6.4.4$$

where D = vessel diameter, feet
H = height of vessel shell, feet
t = shell thickness, inches
x = contents factor (0.15 for simple construction)

For estimating the freezer vessel cost, H is taken as the pool depth plus 6 feet to allow for inclusion of the absorber, concentrator tubes and ejector mixing zone. A factor of 1.1 was used to compute the added cost of the counter washer vessel to accommodate the scraper and drainage tubes. No vessel costs were included for the absorber-concentrators, since they are included in the freezer vessel.

Heat Exchangers. As Colt instructed, the following costs per unit surface have been used:

Feed-product-brine exchangers:	Sheets:	$\$2.10/ft^2$
NaOH heat exchangers:	Sheets:	$\$4.00/ft^2$
Absorber tube cost:		\$0.77/lineal ft
Concentrator tube cost:		\$2.20/lineal ft

Agitators. As Colt instructed, agitator cost was taken at \$45 per brake horsepower.

Ejector. The cost of the ejector has been estimated from the weight of the steel according to the vessel weight-cost relationships given previously. The weight was computed from the throat diameter assuming a mixing section angle of 8.5^{o} and a diffuser angle of 5^{o}. Throat length was taken as 4 times the throat diameter. Assuming 1/4-inch wall thickness, this gives for the ejector weight

$$\text{ejector weight} = 836\ A_1\ , \quad \text{pounds} \qquad \text{E } 6.4.5$$

where A_1 = throat area, ft^2.

The cost of the nozzle has been estimated from Colt information to correspond reasonably well with the formula

$$\text{nozzle cost} = 3.21\ W_v^{0.5}\ , \quad \text{dollars} \qquad \text{E } 6.4.6$$

where W_v = fresh water product rate, gallons/day.

6.4.2 COST INDEX RATIO

All capital costs have been adjusted for the current Chemical Engineering Plant Cost Index (1957--1959 = 100), by multiplying capital costs by the ratio (current cost index)/100. The current cost index for April 1971 is 128.

6.4.3 POWER AND STEAM COSTS

Electrical power costs have been estimated at 7 mils per KWH. Steam costs have been estimated at $30¢/10^6$ Btu.

6.4.4 CAPITAL EQUIPMENT OPERATING COST FACTOR

The contribution of capital cost to the operating cost can be estimated by multiplying the cost of the capital equipment by a factor which contains allowances for certain fixed charges. This factor has been

computed from the OSW procedure with slight modification by Colt as follows:

a) Essential plant cost. Based on cost of principal items of equipment (PIE).

			Σ
1)	Erection and assembly	0.30 (PIE)	
2)	Instruments	0.08 (PIE)	
3)	Equipment	1.00 (PIE)	
4)	Essential plant cost	1.38 (PIE)	1.38 (PIE)

b) Capital Investment

5)	Engineering, 5% of 4)	0.069 (PIE)	1.449 (PIE)
6)	Interest during construction, 9.5% of Σ	0.137 (PIE)	1.586 (PIE)

Therefore, capital investment = CPI = 1.586 (PIE)

c) Fixed operating costs

7) Supplies and maintenance, 0.0015% of CPI
8) Maintenance labor, 0.0015% of CPI
9) Payroll extra, 15% of 8)
10) G & A, 30% of 8) + 9)
11) Taxes and insurance, 0.006% of CPI

Fixed operating costs, 7) + . . . + 11) = $\frac{0.00374 \text{ CPI}}{100}$

d) Amortization rate. This rate has been calculated at 5% interest compounded annually for 25 years to give a fixed amortization rate of capital plus interest of 7.095% per year or 0.0215% per day (330 operating days).

e) Total fixed operating cost. The sum of c) and d)

$$= \frac{0.00374 \text{ CPI}}{100} + \frac{0.0215 \text{ CPI}}{100} = \frac{0.03124 \text{ CPI}}{100}$$

Since CPI = 1.586 PIE, then

$$\text{total fixed operating cost} = 1.586 \times \frac{.03124}{100}(\text{PIE}) = \frac{.0495}{100}(\text{PIE}), \text{ dollars/day.}$$

The operating cost to be minimized by the computer program is the quantity [Power cost + (0.0495)/100 (PIE)], dollars/day. Note that labor costs are not included.

U. S. GOVERNMENT PRINTING OFFICE : 1971 O - 451-332